OPTICAL SPECTROSCOPY OF

SOME SIMPLE FREE RADICALS

by

ALLAN SHI-CHUNG CHEUNG

B.Sc. (Hon.), University of Waterloo, 1977

A THESIS SUMITTED IN PARTIAL

FULFILMENT OF THE REQUIREMENTS

FOR THE DEGREE OF

DOCTOR OF PHILOSOPHY

in

THE FACULTY OF GRADUATE STUDIES

(Department of Chemistry)

We accept this thesis as conforming

to the required standard

THE UNIVERSITY OF BRITISH COLUMBIA

November 1981

In presenting this thesis in partial fulfilment of the requirements for an advanced degree at the University of British Columbia, I agree that the Library shall make it freely available for reference and study. I further agree that permission for extensive copying of this thesis for scholarly purposes may be granted by the head of my department or by his or her representatives. It is understood that copying or publication of this thesis for financial gain shall not be allowed without my written permission.

Department of _____CHEMISTRY_____

The University of British Columbia
2075 Wesbrook Place
Vancouver, B.C.
Canada V6T 1W5

Date _____Feb. 18, 1982_____

To my parents

Abstract

This thesis reports studies of the electronic spectra of some gaseous oxide molecules. The (0,0) band of the $C^4\Sigma^-$ - $X^4\Sigma^-$ electronic transition of VO has been recorded by intermodulated laser-induced fluorescence at a resolution of about 100 MHz over the range 17300 - 17427 cm^{-1}. The hyperfine structure caused by the ^{51}V nucleus ($I = 7/2$) is almost completely resolved. Internal hyperfine perturbations between the F_2 and F_3 electron spin components (where $N = J - \frac{1}{2}$ and $J + \frac{1}{2}$, respectively) occur in both electronic states; these are caused by hyperfine matrix elements of the type $\Delta J = \pm 1$. The $C^4\Sigma^-$ state has many local electronic-rotational perturbations, and also suffers from large spin-orbit perturbations by distant electronic states, for which it has been necessary to introduce a second spin-rotation parameter, γ_s, and the corresponding isotropic hyperfine parameter, b_s. The background theory for this new hyperfine parameter and the calculation of its matrix elements are described.

The $A^4\Pi$ - $X^4\Sigma^-$ electronic transition of VO in the near infra-red has been recorded at Doppler-limited resolution by Fourier transform spectroscopy, and rotational analyses performed for the (0,0) band at 1.05 μ and the (0,1) band in 1.18 μ. The hyperfine structure is prominent in the $^4\Pi_{5/2}$ - $X^4\Sigma^-$ subband, and in many of the spin satellite branches. As shown by the value of the Fermi contact hyperfine parameter in the $A^4\Pi$ its electron configuration is $(4s\sigma)^1 (3d\delta)^1 (4p\pi)^1$ in the single configuration approximation.

Laser-induced fluorescence spectra of gaseous FeO have proved that the bands whose P and R branches have been analysed rotationally by Harris and Barrow (and which are known to involve the ground state) are $\Omega' = 4$ -

$\Omega'' = 4$ transitions. The electron configuration $(4s\sigma)^1 (3d\delta)^3 (3d\pi)^2$ $^5\Delta_i$ is the only reasonable assignment for the ground state of FeO.

The rotational structure of the 000-000 band of the 2490 Å system of $^{15}NO_2$ $(2^2B_2 - \tilde{X}^2A_1)$ has been analysed from high dispersion grating spectrograph plates. The band is found to be slightly predissociated, exactly as in the $^{14}NO_2$ isotope, which suggests that it might be usable for laser separation of the isotopes of nitrogen.

TABLE OF CONTENTS

—

LIST OF TABLES

LIST OF FIGURES

ACKNOWLEDGEMENTS

Chapter 1

Introduction

Free radicals are molecular fragments or unstable molecules which usually possess one or more unpaired electrons. This definition of C.H. Townes and his coworkers (1) includes closed-shell unstable molecules such as CS, CF_2, etc. as well as open-shell stable molecules like O_2, NO_2, etc. Most spectroscopists would enlarge the definition to include any open-shell or paramagnetic species regardless of stability. In this thesis we shall be dealing with molecules with open-shell ground and excited electronic states.

Free radicals are of importance in almost every branch of chemistry, even though most branches are not directly concerned with their study. A chemical reaction involves the breaking and/or making of covalent bonds while the redistribution of electrons involved in either of these processes can result in species with open-shell electron configurations. Thus the intermediates in chemical reactions are often free radicals, which is why radicals are of such importance in chemistry. Radicals can undergo various types of reaction, such as decomposition, abstraction and combination, and consequently a wide variety of end products can result. A knowledge of these reaction pathways is important for both kinetic and photochemical studies, although for different reasons - whereas a kineticist determines reaction rates for individual steps involved in the total reaction, a photochemist is concerned with the way in which these intermediates, when formed in excited states, lose their excess energy. Nevertheless, the information provided by such studies is complementary in the sense that both indicate the reaction mechanism. An understanding of the processes involved in these complex gas phase reactions is also

essential to those interested in the chemistry of the upper atmosphere.

As a further example of the role played by radicals in gas phase reactions, it has been suggested that many reactions occurring in interstellar gas clouds proceed via free radical intermediates. The evidence for such reactions is supplied by the detection of absorption and emission signals by radioastronomers. The interstellar radicals detected so far have been mainly organic molecules, but in view of the high cosmic abundances of transition metals and oxygen, transition metal monoxides are possible interstellar molecules. These radicals are, therefore, of great astronomical significance, since in any case several of them are important constituents of the atmospheres of cool stars (2).

A rather different aspect of open-shell molecules arises from the presence of electron spin and/or orbital angular momenta within the molecules. Interactions between these angular momenta, although often making the analysis of the spectra more complicated, ultimately yield far more information about the electronic structure of the molecule than can be obtained for closed-shell systems.

An accurate determination of the parameters describing the intramolecular interactions is invaluable in evaluating theoretical models for the electronic structure: the experimental parameters are compared with those computed using ab initio wavefunctions. The magnetic hyperfine parameters are particularly useful in this respect since they are sensitive to the distribution of unpaired electrons, and hence provide a rigorous test for proposed wavefunctions. Measurements of this order of accuracy call for high resolution experimental techniques such as sub-Doppler laser spectroscopy (3), molecular beam methods (4), or microwave-optical double

resonance (5).

Our particular interest lies in high resolution studies giving information on the electronic structures of gas-phase radicals. The experiments described here employ the high resolution techniques of conventional grating spectroscopy and sub-Doppler laser spectroscopy in the visible region, and also Fourier transform spectroscopy in the near infrared region. The parameters obtained in these experiments are interpreted through an effective Hamiltonian which is restricted to operate only within the particular electronic and vibrational state from which the spectra arise.

Chapter 2 deals in detail with the theory of molecular energy levels, including the construction of an effective Hamiltonian. The derivation of the third order isotropic Fermi contact interaction (a higher order effect appearing in the energy levels of high multiplicity states) is detailed in chapter 3. Chapter 4 describes briefly the technique of laser induced fluorescence spectroscopy. Chapters 5, 6 and 7 describe studies of free radicals by means of different experimental techniques. Laser-induced fluorescence studies of the $C^4\Sigma^- - X^4\Sigma^-$ system of VO and the ground state of FeO are presented in chapters 5 and 6; chapter 7 is concerned with conventional grating spectroscopy of the $2^2B_2 - \tilde{X}^2A_1$ system of $^{15}NO_2$. Finally chapter 8 gives the analysis of the Fourier transform spectra of the $A^4\Pi(b) - X^4\Sigma^-$ system of VO.

Chapter 2

Theory of Molecular Energy Levels

of Free Radicals

A. Introduction

The energy levels of a molecule are given by the eigenvalues of the time-independent Schrodinger equation

$$H\Psi = E\Psi \qquad (2.1)$$

where H is the total Hamiltonian which may be written as

$$H = H_o + H_{rot} + H_{el} + H_{hfs} \qquad (2.2)$$

H_o represents the nonrelativistic Hamiltonian of the non-rotating molecule, i.e. the kinetic and potential energies of the electrons and nuclei other than the nuclear rotational energy, H_{rot} symbolizes the rotational motion of the nuclei, H_{el} contains magnetic terms that cause the electron spin fine structure and H_{hfs} includes all nuclear spin and nuclear moment terms that cause the hyperfine structure. Ψ is the eigenfunction associated with a stationary state and the eigenvalue E is the energy of this state.

It is impossible to solve Eq. (2.1) analytically. In practice, one chooses a convenient finite basis set ϕ_i and expands the eigenfunctions Ψ in terms of ϕ_i

$$\Psi = \sum_i a_i \phi_i \qquad (2.3)$$

This then reduces the solution of Eq. (2.1) to finding the roots of the secular determinant

$$| H_{ij} - E\delta_{ij} | = 0 \qquad (2.4)$$

where the quantities H_{ij} are the matrix elements of H, defined as

$$H_{ij} = \int \phi_i^* H \phi_j \, d\tau \tag{2.5}$$

The choice of basis set is, of course, arbitrary and any complete basis set would suffice provided the calculations are carried out to sufficient accuracy. However by making a wise choice of the initial basis set, H may be roughly partitioned into diagonal blocks (submatrices) between which there are only small off-diagonal matrix elements. In the general case the diagonal blocks refer to Born-Oppenheimer or adiabatic states.

This thesis is concerned with the rotational and spin structure of individual vibronic states. A convenient way to obtain the required energy level expression is illustrated in Fig. 2.1. In the first step degenerate perturbation theory is used to include matrix elements linking a particular vibronic state with nearby vibrational and/or electronic states. This leads to an effective Hamiltonian operator which operates only within the rotational sub-space of that vibronic state.
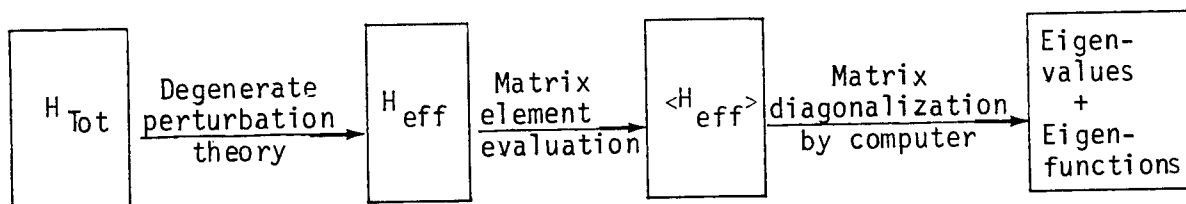
Fig. 2.1   The step-wise development of the theory employed in the analysis and interpretation of molecular spectra.

The second step in Fig. 2.1 is the evaluation of a matrix representation of the effective Hamiltonian. Irreducible tensor methods have been used in these evaluations because they are particularly convenient for dealing with coupling of three or more angular momenta.

The final step is the diagonalization of the Hamiltonian matrix and the determination of the eigenvalues and eigenfunctions. Electronic computers make this nowadays a routine matter.

In section B(i) the general Hamiltonian H_0 is discussed. This is followed by a description of the Born-Oppenheimer separation of nuclear and electronic motion in section B(ii). Section B(iii) is concerned with the eigenfunctions of the rotational Hamiltonian, H_{rot}. Sections B(iv) and B(v) derive the operators for the electron spin fine structure and the nuclear hyperfine structure from physical principles. Finally, B(vi) deals with the important concepts and derivation of an effective Hamiltonian operator.

Section C describes the evaluation of matrix elements of the effective Hamiltonian. In sections C(i) and (ii), some important results from the theory of angular momentum and some useful relationships in spherial tensor algebra are stated. These will be needed in the subsequent calculations. Hund's coupling cases(a) and (b), and their interconversion, are discussed in detail in section C(iii). Matrix element expressions are listed in section C(iv), for both case $(b_{\beta J})$ and case (a_β), in terms of Wigner's 3-j, 6-j and 9-j symbols. The absence of the third Euler angle in linear molecules, which leads to problems in the computation of matrix elements, is also discussed.

B. Hamiltonians and eigenfunctions

(i) The General Molecular Hamiltonian

A molecule is an assembly of nuclei and electrons, which is, in Carrington's words(1), "prepared to coexist in a certain configuration with considerable stability". To understand the energy levels of a molecule it is necessary to begin with the Hamiltonian operator corresponding to the total energy (2,3). It has been shown by Howard and Moss (4,5) that, starting from a relativistic many-body Hamiltonian, with terms correct to order c^{-2}, it is possible to obtain all the familiar energy level expressions used by experimental spectroscopists, and in addition, some not readily detectable new terms such as mass polarization and spin-vibration interactions. For our purpose, however, a non-relativistic many-body Hamiltonian, in which spin is added as an additional hypothesis, is adequate to describe the system. We therefore omit the relativistic effects, and define the potential energy of the Hamiltonian as depending only on the positions of the nuclei (Q) and the positions of the electrons (q). The Hamiltonian operator for the total energy of a molecule consisting of N nuclei and n electrons is then given by

$$H_o = \frac{1}{2m_e} \sum_e^n \underset{\sim}{P}_e^2 \qquad \text{(electron kinetic energy)}$$

$$+ \frac{1}{2} \sum_n^N \frac{\underset{\sim}{P}_n^2}{M_n} \qquad \text{(nuclear kinetic energy)}$$

$$+ V(q,Q) \qquad \text{(potential energy)} \qquad (2.6)$$

where

$$V(q,Q) = -\sum_a \sum_i \frac{Z_a e^2}{r_{ia}} \quad \text{(electron-nuclear attractions)}$$

$$+\sum_a^N \sum_{b>a}^N \frac{Z_a Z_b e^2}{r_{ab}} \quad \text{(nuclear-nuclear repulsions)} \quad (2.7)$$

$$+\sum_i^n \sum_{j>i}^n \frac{e^2}{r_{ij}} \quad \text{(electron-electron repulsions)}$$

In eq. (2.6) P_e and P_n denote the linear momenta of electron i (mass m_e) and nucleus n (mass M_n) respectively, and in eq. (2.7) e is the electron charge, $Z_a e$ is the charge on nucleus a and r_{xy} is the radius from particle x to particle y.

The magnetic interactions, such as electronic and nuclear dependent terms, are much smaller then the electrostatic interactions which characterized V, and for the present purpose may be neglected. They will be added later in a perturbation treatment.

(ii) Born-Oppenheimer Separation of Nuclear and Electronic Motion

Just as the classical problem of the relative motions of three bodies cannot be solved exactly, the quantum mechanical problem of finding the exact solutions of the full Schrödinger equation

$$H_o \Psi = \mathcal{E} \Psi \quad (2.8)$$

is also impossible for anything except the hydrogen atom. The approximation introduced by Born and Oppenheimer (6), in which the electronic part of the problem is solved first, forms a good basis for finding

approximate solutions. The total wavefunction Ψ is assumed to be expandable in a complete set of functions which are products of an electronic part $\psi_{ei}(q,Q)$ and a nuclear part $\psi_{vr}^{i}(Q)$, that is

$$\Psi_{evr}(q,Q) = \sum_{i} \psi_{ei}(q,Q) \psi_{vr}^{i}(Q) \qquad (2.9)$$

where $\psi_{ei}(q,Q)$ is an eigenfunction of the "electronic Hamiltonian"

$$H_e = \frac{1}{2m_e} \sum_e \underset{\sim}{P}_e^2 + V(q,Q) \qquad (2.10)$$

according to

$$H_e \psi_{ei}(q,Q) = E_e^i \, \psi_{ei}(q,Q) \qquad (2.11)$$

For eq. (2.9), which implies that the total energy $\mathcal{E}$ is the sum of the electronic energy, E_e, and the nuclear energy, E_{vr}, that is

$$\mathcal{E} = E_e + E_{vr} \qquad (2.12)$$

on substituting eq. (2.9) into eq. (2.8) one has

$$\left(\frac{1}{2m_e} \sum_e \underset{\sim}{P}_e^2 + V(q,Q) + \frac{1}{2} \sum_n \frac{\underset{\sim}{P}_n^2}{M_n}\right) \sum_i \psi_{ei}(q,Q) \psi_{vr}^{i}(Q) = \mathcal{E} \sum_i \psi_{ei}(q,Q) \psi_{vr}^{i}(Q) \qquad (2.13)$$

or

$$\sum_i \left\{ \psi_{vr}^{i}(Q)\left(\frac{1}{2m_e} \sum_e \underset{\sim}{P}_e^2\right)\psi_{ei}(q,Q) + \psi_{vr}^{i}(Q)\right.$$

$$V(q,Q)\psi_{ei}(q,Q) + \psi_{ei}(q,Q)\left(\frac{1}{2}\sum_n \frac{\underset{\sim}{P}_n^2}{M_n}\right)\psi_{vr}^{i}(Q)$$

$$+ \psi_{vr}{}^i(Q)\left(\frac{1}{2}\sum_n\frac{P_{\sim n}{}^2}{M_n}\right)\psi_{ei}(q,Q)+\sum_n\frac{1}{M_n}\left[P_n\psi_{ei}(q,Q)\right]\left[P_n\psi_{vr}{}^i(Q)\right]\right\} = \sum_i\psi_{ei}(q,Q)\psi_{vr}{}^i(Q)$$

$$(2.14)$$

Since the $\psi_{ei}(q,Q)$ are eigenfunctions of H_e, the first two terms give $\psi_{vr}{}^i(Q)E_{ei}(Q)\psi_{ei}(q,Q)$. Multiplying from the left by $\psi_{ek}{}^*(q,Q)$ and integrating over the electron coordinates q (which essentially picks out the state k from the electronic manifold) the equation becomes

$$\left\{\left(\frac{1}{2}\sum_n\frac{P_{\sim n}{}^2}{M_n}\right)+E_{ek}(Q)+\int\psi_{ek}{}^*(q,Q)\left(\frac{1}{2}\sum_n\frac{P_{\sim n}{}^2}{M_n}\right)\psi_{ei}(q,Q)dq\right\}$$

$$\psi_{vr}{}^k(Q)+\sum_{i\neq k}\left[\sum_n\int\psi_{ek}{}^*(q,Q)\left(\frac{P_{\sim n}}{M_n}\right)\psi_{ei}(q,Q)dq\cdot P_{\sim n}\right]\psi_{vr}{}^i(Q) = \mathcal{E}\psi_{vr}{}^k(Q) \quad (2.15)$$

Neglecting the cross-term which contains $\psi_{vr}{}^i(Q)$, eq. (2.15) is a new differential equation that defines the vibrational and rotational functions of the electronic state k. The equation has the form of a Schrödinger equation where the Hamiltonian consists of the nuclear kinetic energy, the electronic energy as an effective potential energy, and a small mass-dependent term which contributes a small electronic isotope effect.

The cross-terms neglected in eq. (2.15) are those which couple the electronic and vibrational motions in different electronic states. If the electronic states are degenerate (meaning that there are two or more orthogonal electronic functions corresponding to states of the same energy) severe breakdowns of the Born-Oppenheimer approximation can occur: these were first described for linear molecules by Renner (7), and for symmetric top molecules (possessing a 3-fold or

higher axis of symmetry) by Jahn and Teller (8). If the electronic states are non-degenerate the cross-terms give rise to the phenomenon of vibrational momentum coupling, which is one of the principal causes of the complexity of the electronic spectra of NO_2 and SO_2.

(iii) Rotational wavefunctions

The separation of vibration and rotation is in general difficult because certain combinations of vibrations produce motions indistinguishable from rotations, with accompanying vibrational angular momentum. This separation has been discussed in many excellent texts (9,10), and it is not necessary to repeat it here. The success of this separation depends of course on the magnitude of the vibration-rotation coupling terms. If these can be neglected one has essentially independent Hamiltonians which describe the vibrational and rotational motions separately. We restrict ourselves in this thesis to an extremely brief discussion of the rotational Hamiltonian and its eigenfunctions.

The classical rotational Hamiltonian (10) is

$$H_{rot} = \frac{J_x^2}{2I_x} + \frac{J_y^2}{2I_y} + \frac{J_z^2}{2I_z} \tag{2.16}$$

where J_x, J_y and J_z are the components of the rotational angular momentum $\underset{\sim}{J}$ along the principal axes of the molecule, and I_x, I_y and I_z are the principal moments of inertia (that is, where the axis system is chosen such that the off-diagonal elements of the moment of inertia tensor I vanish).

If the moments of inertia do not change during the rotational motion eq. (2.16) is known as the rigid rotator Hamiltonian. The corresponding Schrödinger equation

$$H_{rot} \psi_r = E_r \psi_r \qquad (2.17)$$

can only be solved analytically for spherical and symmetric tops. The motions of a rotating body (a 'top') are usually described by specifying the Euler angles (α, β, γ) (11) about the principal moments of inertia, which are angles describing how much the body has rotated from an initial reference configuration. The symmetric top eigenfunctions of eq. (2.17) are simply related to the elements of the Jth rank rotation matrix (12)

$$\psi_r = \psi_{JKM} = \left[\frac{2J+1}{8\pi^2} \right]^{\frac{1}{2}} D_{MK}^{(J)*} (\alpha, \beta, \gamma) \qquad (2.18)$$

where J is the rotational angular momentum quantum number, K is the projection of the rotational angular momentum vector on the molecule-fixed z-axis, M is its projection on the space-fixed Z-axis, and $D_{MK}^{(J)*}$ is an element of Wigner's rotation matrix. The choice of phase factor implicit in eq. (2.18) is equivalent to defining the matrix element of J_x, the component referred to the molecule-fixed x-axis, as real and positive (13).

The eigenfunctions of a rigid asymmetric top molecule (where no axes of symmetry higher than 2-fold are present) are more complicated than those just considered; they may nevertheless be expressed as

linear combinations of symmetric top wavefunctions (14)

$$\psi_{JK_{-1}K_1M} = \sum_K a_{JKM} \psi_{JKM} \qquad (2.19)$$

where a_{JKM} is an appropriate numerical coefficient, the subscript K_{-1} and K_1 are the values of the component K for the limiting prolate symmetric top and the limiting oblate symmetric top, respectively.

(iv) Electron Spin Fine Structure Hamiltonian

The effects of spin in molecular spectra arise from the interaction of each of the electron spin magnetic moments with:

(a) the magnetic moments generated by the orbital motions of the electrons (interaction with its own orbital motion being the most important); this is known as spin-orbit interaction.

(b) the magnetic moments generated by the rotational motions of the nuclei; this is called spin-rotation interaction.

(c) the spin magnetic moments of the other electrons which is known as spin-spin interaction.

Therefore the electron spin fine structure Hamiltonian operator, H_{el}, is the sum of these interactions,

$$H_{el} = H_{so} + H_{sr} + H_{ss} \qquad (2.20)$$

where H_{so}, H_{sr} and H_{ss} are respectively the energy operators for spin-orbit, spin-rotation and spin-spin interactions.

(a) Spin-orbit Interaction

An electron possesses an intrinsic spin angular momentum, $\underset{\sim}{s}$. This gives rise to a spin magnetic moment $\underset{\sim}{\mu}_m$, whose value is

$$\underset{\sim}{\mu}_m = \frac{-g\mu_B}{\hbar} \underset{\sim}{s} \qquad (2.21)$$

In this equation g is the relativistic "g-factor", 2.0023, μ_B is the unit of magnetic moment (the Bohr magneton, $e\hbar/2m$, which equals 9.274×10^{-24} JT^{-1} in SI units), and $\underset{\sim}{s}$ is the spin angular momentum such that

$$<\underset{\sim}{s}^2>^{\frac{1}{2}} = (s(s+1))^{\frac{1}{2}} \hbar \qquad (2.22)$$

According to Maxwell's equations (15) an electron moving with uniform linear velocity $\underset{\sim}{v}$ relative to a coordinate system where a static electric field $\underset{\sim}{E}$ exists, experiences a magnetic field, B, given by

$$\underset{\sim}{B} = \underset{\sim}{E} \wedge \frac{\underset{\sim}{v}}{c^2} \qquad (2.23)$$

as a result of its motion. Now electric field is the gradient of potential, so that if the electric field results from the presence of a charged nucleus we have

$$\underset{\sim}{E} = -\nabla V = -\left(\frac{\underset{\sim}{r}}{r}\right)\frac{dV}{dr} \qquad (2.24)$$

where $\dfrac{\underset{\sim}{r}}{r}$ is the unit vector from the position of the nucleus towards the position of the electron, and $\dfrac{dV}{dr}$ is the rate of change of the (Coulomb) potential of the nucleus with distance. Then

$$\underset{\sim}{B} = -\frac{1}{c^2 r}\left(\frac{dV}{dr}\right)\underset{\sim}{r} \wedge \underset{\sim}{v} \qquad (2.25)$$

The operator for the interaction energy of a magnetic dipole with a magnetic field is

$$H = -\underset{\sim}{\mu} . \underset{\sim}{B} .$$ (2.26)

This becomes the operator for the spin-orbit interaction, on substituting the values of $\underset{\sim}{\mu}$ and $\underset{\sim}{B}$; the result of the substitution is

$$H_{so} = \frac{-g\mu_B}{\hbar c^2 r} \left(\frac{dV}{dr}\right) \underset{\sim}{r} \wedge \underset{\sim}{v} . \underset{\sim}{s}$$ (2.27)

When the explicit meanings of $\underset{\sim}{r}$ and $\underset{\sim}{v}$ are considered, r becomes r_{en}, the distance of the electron from the nucleus, and v becomes v_{en}, the velocity of the electron with respect to the nucleus. For completeness the electron spin $\underset{\sim}{s}$ is written $\underset{\sim}{s}_e$. When the further relativistic correction introduced by Thomas (16) is included in the expression, $\underset{\sim}{v}_{en}$ equals $\frac{1}{2}\underset{\sim}{v}_e - \underset{\sim}{v}_n$. This 'Thomas precession' represents the fact that time appears to be slowed down for the fast-moving electron as seen by the nucleus, and it happens that it appears (to the nucleus) to be spinning only half as fast as if it were static. As a result we have

$$H_{so} = \frac{-g\mu_B}{\hbar c^2 r_{en}} \left(\frac{dV}{dr_{en}}\right) \underset{\sim}{r}_{en} \wedge (\frac{1}{2}\underset{\sim}{v}_e - \underset{\sim}{v}_n) . \underset{\sim}{s}_e$$ (2.28)

The spin-orbit interaction is additive for the various electrons and nuclei, so that for a molecule

$$H_{so} = \frac{-g\mu_B}{\hbar c^2} \sum_e \sum_n \frac{1}{r_{en}} \left(\frac{dV}{dr_{en}}\right) \underset{\sim}{r}_{en} \wedge (\frac{1}{2}\underset{\sim}{v}_e - \underset{\sim}{v}_n) . \underset{\sim}{s}_e$$ (2.29)

If eq. (2.29) is written as the difference of two terms, the second term may be taken as the interaction between the rotation of the nuclei, represented by $\underset{\sim}{v}_n$, and the electron spin: it is the spin-rotation interaction. The second term will be dropped at this point and considered again in the next section. The first term becomes recognisably the spin-orbit interaction when we substitute

$$\underset{\sim}{\ell}_{en} = \underset{\sim}{r}_{ev} \wedge m \underset{\sim}{v}_e \qquad (2.30)$$

as the orbital angular momentum vector operator for electron e moving around nucleus n:

$$H_{so} = \frac{-g\mu_B}{2\hbar mc^2} \sum_e \sum_n \frac{1}{r_{en}} \left(\frac{dV}{dr_{en}}\right) \underset{\sim}{\ell}_{en} \cdot \underset{\sim}{s}_e \qquad (2.31)$$

This may be approximated as

$$H_{so} = \sum_e a_e(r) \underset{\sim}{\ell}_e \cdot \underset{\sim}{s}_e , \qquad (2.32)$$

where
$$a_e(r) = \frac{-g\mu_B}{2\hbar mc^2} \sum_n \frac{1}{r_{en}} \left(\frac{dV}{dr_{en}}\right)$$

is a parameter for electron e, which sums over all n nuclei. Eq. (2.32) is the so-called "microscopic spin-orbit Hamiltonian" (17,18), describing the interaction of electron spins with the field due to electrons and nuclei, and containing spin-orbit, spin-other orbit and electronic screening effects. Using either eq. (2.31) or (2.32) the correct parametric dependence of the interactions is obtained but the interpretations

of the constants differ.

A convenient simple isotropic form of eq. (2.32),

$$H_{so} = A(r) \underset{\sim}{L} \cdot \underset{\sim}{S},$$ (2.33)

where $A(r)$ is an r-dependent parameter, is often used for the calculation of matrix elements diagonal in S. In eq. (2.33) $\underset{\sim}{L}$ is the total electronic orbital angular momentum of the molecule or radical,

$$\underset{\sim}{L} = \sum_i \underset{\sim}{\ell}_i$$ (2.34)

and $\underset{\sim}{S}$ is the total electronic spin angular momentum of the molecule or radical,

$$\underset{\sim}{S} = \sum_i \underset{\sim}{S}_i$$ (2.35)

The microscopic spin-orbit operator, $\sum_i a_i(r) \underset{\sim}{\ell}_i \cdot \underset{\sim}{S}_i$, is needed if matrix elements of the spin-orbit operator off-diagonal in S are to be calculated.

(b) Spin-Rotation Hamiltonian

The so-called spin-rotation interaction arise from two causes. One of these is the direct interaction of the electron spin with the magnetic field of the molecular rotation. It can be shown (18) that the second term in eq. (2.29) is equivalent to

$$\sum_{\alpha, \beta} \epsilon_{\alpha\beta} \underset{\sim}{N}_\alpha \underset{\sim}{S}_\beta$$ (2.36)

where the vector $\underset{\sim}{N}$ denotes the nuclear rotational angular momentum, and the coefficients $\varepsilon_{\alpha\beta}$ are complicated functions of the moments of inertia, the internuclear distances, and the average distances of the electrons to the various nuclei of the molecule.

Besides the direct coupling between electronic spin and molecular rotation, the combination of off-diagonal spin-orbit and orbit-rotation matrix elements, treated by second order perturbation theory, gives rise to much larger effective operators with the same angular momentum dependence (19,20). The two contributions cannot be distinguished, and are therefore added to produce the determinable spin-rotation coefficient $\varepsilon_{\alpha\beta}$.

Eq. (2.36) relates two non-commuting operators, $\underset{\sim}{N}$ and $\underset{\sim}{S}$, through the tensor ε, so that, strictly speaking, it should be written as the hermitian average:

$$H_{sr} = \frac{1}{2} \sum_{\alpha\beta} \varepsilon_{\alpha\beta} \left(\underset{\sim}{N}_\alpha \underset{\sim}{S}_\beta + \underset{\sim}{S}_\beta \underset{\sim}{N}_\alpha \right) \qquad (2.37)$$

(c) Spin-Spin Hamiltonian

Since electrons possesses magnetic moments, all the electrons of a molecule must interact with each other through Coulomb's law of magnetic interaction. This mechanism gives rise to the dipolar electron spin-spin interaction.

A spinning electron at a point j in space can be considered as a bar magnet with magnetic moment μ_j. The magnetic vector potential (15) that is produced at coordinate i is given by

$$A_i = \mu_j \wedge r_{ji}/r_{ji}^3 \qquad (2.38$$

By Maxwell's equations this corresponds to a magnetic field at point i

$$
\begin{aligned}
\underset{\sim}{B}_i &= \nabla \wedge \underset{\sim}{A}_i \\
&= \nabla \wedge (\underset{\sim}{\mu}_j \wedge \underset{\sim}{r}_{ji})/r_{ji}^{\,3}
\end{aligned}
\tag{2.39}
$$

The Hamiltonian for the interaction of a second electron placed at i
(with magnetic moment μ_i) and the electron at j (with magnetic moment
μ_j) is

$$
\begin{aligned}
H_{ss,ij} &= -\underset{\sim}{\mu}_i \cdot \underset{\sim}{B}_i \\
&= \frac{-g\mu_B^{\,2}}{\hbar^2} \left[\nabla \wedge \underset{\sim}{s}_j \wedge \underset{\sim}{r}_{ji}\left(\frac{1}{r_{ji}^{\,3}}\right) \right] \cdot \underset{\sim}{s}_i
\end{aligned}
\tag{2.40}
$$

Using the relations

$$
\nabla \left(\frac{1}{r}\right) = \frac{-\underset{\sim}{r}}{r^3}
\tag{2.41}
$$

and

$$
\nabla \wedge \nabla \wedge \underset{\sim}{V} = \nabla (\nabla \cdot \underset{\sim}{V}) - \nabla^2 \underset{\sim}{V}
\tag{2.42}
$$

for any vector $\underset{\sim}{V}$, this can be written

$$
H_{ss,ij} = \frac{g^2\mu_B^{\,2}}{\hbar^2} [\underset{\sim}{s}_i \cdot \underset{\sim}{s}_j) \nabla^2 - (s_i \cdot \nabla)(s_j \cdot \nabla)]\left(\frac{1}{r_{ji}}\right)
\tag{2.43}
$$

The first term of eq. (2.43) can be further simplified with Gauss' divergence theorem which gives

$$
\nabla^2\left(\frac{1}{r_{ji}}\right) = -4\pi \, \delta(r_{ji})
\tag{2.44}
$$

where $\delta(r_{ji})$ is a Dirac delta function. It is defined such that it picks out the square of the amplitude of the electron wavefunction for electron j at the coordinate origin, i.e. at the position of electron i

$$<\delta(r_{ji})> \quad = \quad |\psi_j(o)|^2 \tag{2.45}$$

Therefore, the first term becomes

$$H_{ss,ij} \text{ (contact)} = \frac{-g^2\mu_B^2}{\hbar^2} \; 4\pi \; | \; \psi_j(o)|^2 \; \underset{\sim}{s}_i \cdot \underset{\sim}{s}_j \tag{2.46}$$

The second term in eq. (2.43) is more involved, but, it can be shown that, after some algebra, it becomes

$$\frac{g^2\mu_B^2}{\hbar^2} \; \left\{ \frac{4\pi}{3} \; |\psi_j(o)|^2 + [(\underset{\sim}{s}_i \cdot \underset{\sim}{s}_j)r_{ji}^2 - 3(\underset{\sim}{s}_i \cdot \underset{\sim}{r}_{ji})(\underset{\sim}{s}_j \cdot \underset{\sim}{r}_{ji})]r_{ji}^{-5} \right\} \tag{2.47}$$

Finally, collecting terms and summing over all electrons, the spin-spin interaction Hamiltonian is

$$H_{ss} = \frac{g^2\mu_B^2}{\hbar^2} \; \sum_{i>j} \; \left\{ \frac{-8\pi}{3} \; |\psi(o)|^2 \; \underset{\sim}{s}_i \cdot \underset{\sim}{s}_j \right.$$

$$\left. + [(\underset{\sim}{s}_i \cdot \underset{\sim}{s}_j)r_{ji}^2 - 3(\underset{\sim}{s}_i \cdot \underset{\sim}{r}_{ji})(\underset{\sim}{s}_j \cdot \underset{\sim}{r}_{ji})]r_{ji}^{-5} \right\} \tag{2.48}$$

The first term turns out to give a constant contribution to the energy, and is included with the Born-Oppenheimer potential; the second term is the dipolar electron spin-spin interaction.

(v) Nuclear Spin Hyperfine Structure Hamiltonian

Hyperfine interactions, caused by non-zero nuclear spins, are the last terms we consider in the molecular Hamiltonian. Hyperfine structure results from the interaction of the magnetic and electric moments of the nuclei with the other electric and magnetic moments in the molecule. We shall write

$$H_{hfs} = H_{mag.\ hfs} + H_Q \qquad (2.49)$$

where $H_{mag.hfs}$ is the magnetic hyperfine Hamiltonian, which arises from the interaction of the nuclear-spin magnetic moments with other magnetic moments in the molecule, and H_Q is the electric quadrupole Hamiltonian, which arises when nuclei with spin $I \geq 1$ (which possess electric quadrupole moments) interact with the non-spherical electron charge distribution in the finite volume of each nucleus.

In molecules with electronic angular momentum, the magnetic hyperfine structure is usually much larger than that due to electric quadrupole moments. We begin by discussing the magnetic hyperfine Hamiltonian for a single spinning-nucleus.

(a) Magnetic hyperfine structure hamiltonian

The theory of magnetic hyperfine structure in diatomic molecules has been given by Frosch and Foley (21), who derived the Hamiltonian from the Dirac equation for the electron. An alternative and simplified derivation of the same hyperfine interaction expression is given by Dousmanis (22).

The mechanism giving rise to magnetic hyperfine structure is exactly

the same as the electron spin interaction, so with the replacement of one of the electron spin magnetic moments, $\underset{\sim}{\mu}_s$, by the nuclear spin magnetic moment, $\underset{\sim}{\mu}_I$,

$$\underset{\sim}{\mu}_I = g_n \mu_n \underset{\sim}{I} \qquad (2.50)$$

Eq. (2.48) becomes

$$H_{mag.hfs} = \frac{g_n^2 \mu_n^2}{\hbar^2} \underset{i>j}{\Sigma} \left\{ \frac{8\pi}{3} |\psi_i(o)|^2 \underset{\sim}{I}_i \cdot \underset{\sim}{s}_j \right.$$
$$\left. -[(\underset{\sim}{I}_i \cdot \underset{\sim}{s}_j) r_{ji}^2 - 3(\underset{\sim}{I}_i \cdot \underset{\sim}{r}_{ji})(\underset{\sim}{s}_i \cdot \underset{\sim}{r}_{ji})] r_{ji}^{-5} \right\} \qquad (2.51)$$

In this case the first term does not give a constant contribution; it is called the Fermi contact interaction and is a measure of the extent to which the unpaired electrons have non-zero probability amplitude at the spinning nucleus. For the amplitude to be non-zero an unpaired electron must occupy a molecular orbital derived from an atomic s orbital. Unlike the dipolar coupling, the Fermi contact interaction is isotropic, and is represented by a term of the form

$$\underset{i}{\Sigma} a_{c,i} \underset{\sim}{I} \cdot \underset{\sim}{s}_i \qquad (2.52)$$

where $a_{c,i}$ is the isotropic coupling constant.

The second term is the dipolar $(\underset{\sim}{I}, \underset{\sim}{s})$ interaction between the nuclear magnetic moment and the magnetic field produced at the nucleus by the valence electrons.

Eq. (2.51) gives the contact and dipolar parts of the magnetic inter-

action; on addition of the term $\sum_i a_i \underset{\sim}{I} \cdot \underset{\sim}{\ell}_i$ (23), which gives the inter-

action of the nuclear magnetic moment with the orbital angular momentum

of the unpaired electron or electrons, the total magnetic hyperfine

Hamiltonian is obtained as

$$H_{mag.hfs} = \sum_i a_i \underset{\sim}{I} \cdot \underset{\sim}{\ell}_i + \sum_i a_{c,i} \underset{\sim}{I} \cdot \underset{\sim}{s}_i$$

$$- \sum_i \frac{gg_n\mu_B\mu_n}{\hbar^2} [(\underset{\sim}{I} \cdot \underset{\sim}{s}_i)r^2 - 3(\underset{\sim}{I} \cdot \underset{\sim}{r})(\underset{\sim}{s}_i \cdot \underset{\sim}{r})]r^{-5} \tag{2.53}$$

It is usually sufficient to collect the sums over electrons into a

single parameter, giving

$$H_{mag,hfs} = a \underset{\sim}{I} \cdot \underset{\sim}{L} + b \underset{\sim}{I} \cdot \underset{\sim}{S} + c I_z S_z \tag{2.54}$$

where $\qquad a = \frac{gg_n\mu_B\mu_n}{\hbar^2} \left\langle \frac{1}{r_i^3} \right\rangle \tag{2.55}$

$$a_c = \frac{8\pi}{3} \frac{gg_n\mu_B\mu_n}{\hbar^2} |\psi(o)|^2 \tag{2.56}$$

$$c = \frac{3gg_n\mu_B\mu_n}{2\hbar^2} \left\langle \frac{(3\cos^2\theta - 1)}{\gamma^3} \right\rangle \tag{2.57}$$

and $\qquad b = a_c - \frac{1}{3}c \tag{2.58}$

The terms a, b and c are determinable coefficients in the magnetic hyper-

fine Hamiltonian; a is the nuclear spin-orbit interaction, b is a com-

bination of c with the Fermi contact interaction, a_c, and c is the dipo-

lar electron spin-nuclear spin interaction.

(b) Electric quadrupole Hamiltonian

Although the magnetic dipole interaction is responsible for the largest contribution to the observed hyperfine structure of a molecule in a multiplet electronic state, electric quadrupole effects are present whatever the multiplicity is, provided $I \geq 1$. These are caused by the interaction between the nuclear electric quadrupole moment and the electric field gradient produced by the surrounding electrons(24). The electrostatic interaction between a nucleus at point r_j and an electron at the point r_i is given by Coulomb's law as

$$H_c = \frac{-ze^2}{r_{ij}} = \frac{-ze^2}{|r_i - r_j|} \qquad (2.59)$$

Recalling that electrons are point charges but nuclei have a finite size for their electric charge distribution, we shall neglect any electronic charge lying within the nuclear radius, then $r_i > r_j$ and we can expand eq. (2.59) in ascending powers of r_j/r_i giving (25)

$$H_c = -ze^2 \sum_{k=0}^{\infty} \frac{r_j^k}{r_i^{k+1}} P_k(\cos \theta_{ij}) \qquad (2.60)$$

where $P_k(\cos \theta_{ij})$ is the Legendre polynomial of order k and θ_{ij} is the angle between r_j and r_i.

The first term in the summation of eq. (2.60) represents a monopole interaction and when summed over all electrons gives the familiar coulomb interaction. The second term represents a nuclear electric dipole interaction which, by application of parity and time reversal symmetry arguments (26), can be shown to be identically zero, as are the higher electric multipole moments of odd order. Finally, the term with k=2

corresponds to an electric quadrupole interaction. The separation of electric and nuclear coordinates in eq. (2.60) can be completed by applying the spherical harmonic addition theorem:

$$P_k(\cos\theta_{ij}) = \frac{4\pi}{2k+1} \sum_{q=-k}^{k} (-1)^q Y_q^k(\theta_i,\phi_i) Y_{-q}^k(\theta_j,\phi_j) \qquad (2.61)$$

where $Y_q^k(\theta,\phi)$ is the qth component of the spherical harmonic of order k, and the angles θ and ϕ are spherical polar coordinates. The electric quadrupole interaction then becomes

$$H_Q = e \sum_{q=-2}^{2} (-1)^q \left\{ \left(\frac{4\pi}{5}\right)^q r_j^2 Y_q^2(\theta_j,\phi_j) \right\} \left\{ \left(\frac{4\pi}{5}\right)^{\frac{1}{2}} \left(\frac{-ze}{r_i^3}\right) Y_{-q}^2(\theta_i,\phi_i) \right\}$$

$$= e \sum_q (-1)^q T_q^2(Q) T_{-q}^2(\nabla E) \qquad (2.62)$$

We observe that the above expression has the form of the scalar product of a nuclear electric quadrupole tensor and an electric field gradient tensor, each of rank two. (The properties of spherical tensors will be discussed in section (2.C)). Therefore:

$$H_Q = e\, T^2(Q) \cdot T^2(\nabla E) \qquad (2.63)$$

For a linear molecule the tensor $T^2(\nabla E)$ has one independent component, so that there is only one "quadrupole coupling constant" which will be defined in section (2.C).

(vi) Effective Hamiltonian and Degenerate Perturbation Theory

The analysis of molecular spectra using the true molecular eigen-functions is impractical, since it would require the diagonalization of an infinite matrix. Even if this matrix were suitably truncated the problem would still be very difficult to handle. Ideally a matrix re-presentation is required that contains no terms off-diagonal in vibra-tional or electronic state; although the matrix representation is still infinite it consists only of submatrices, each containing only elements pertaining to a single electronic-vibrational level. Eigenvalues can be obtained for the various submatrices, from which it is possible to determine the transition frequencies. The construction of such sub-matrices requires that the effects of all elements of the full Hamilto-nian that are off-diagonal in vibrational or electronic state be reduced to a negligible level. A simple practical way to set up these matrices employs an effective Hamiltonian that only operates within the manifold of a particular electronic-vibrational state. There are two commonly-used methods for deriving the effective Hamiltonian, namely contact transformations and perturbation theory.

In the contact transformation method (27) a carefully-chosen unitary transformation is applied to the Hamiltonian to eliminate specific off-diagonal elements; since this method has not been used in this thesis it will not be discussed further. The technique of degenerate perturba-tion theory has been used extensively in the next chapter and will therefore be discussed in more detail.

Messiah (25) has described the techniques of non-degenerate and degenerate perturbation theory most comprehensively, but a rather more

readable account of the derivation of an effective Hamiltonian has been given by Soliverez (28), using the formalism set up by Bloch (29).

The eigenfunctions $|i>$, of the total Hamiltonian which operates over all vector space, form a complete orthonormal set. We want a Hamiltonian that operates only within a particular manifold of the total Hilbert space. In other words we wish to project the effects of the total Hamiltonian operator onto a chosen vector space which is of dimension less than that of the total vector space, and hence to construct an effective Hamiltonian that operates only within this chosen vector space, and with the equivalent operator form within this manifold of the total Hamiltonian. The operator which brings about this projection of the total Hamiltonian is a projection operator, P_0.

Soliverez (28) shows that it is possible to set up an effective Hamiltonian which has the following properties:

(a) It operates only within a manifold of dimension less than that of the total vector space.

(b) Its eigenvalues are identical to those corresponding eigenvalues of the total Hamiltonian.

(c) Its eigenvectors are simply related to the corresponding eigenvectors of the total Hamiltonian.

(d) It can be expanded as a power series in terms of a perturbation V, and is Hermitian to all orders of the expansion.

We shall indicate briefly here how such a Hamiltonian is set up.

The total Hamiltonian of the system under study is split into two parts

$$H = H_0 + V \qquad (2.64)$$

where the eigenvalues and eigenvectors of H_0 are known:

$$H_0 |j>_0 = E_j |j>_0 \qquad (2.65)$$

and the eigenfunctions $|j>_0$ from a complete orthonormal set over all vector space.

V is a perturbation to this Hamiltonian and we are interested in its effects on the eigenvectors and eigenvalues of H_0. In particular, we are concerned with the eigenvectors spanning the particular manifold onto which the total Hamiltonian is projected; these will have a particular eigenvalue, E_0.

The projection operator is defined as

$$P_0 = \sum_i |i><i| \qquad (2.66)$$

where the eigenvectors $|i>$ span the manifold under consideration. It follows at once that

$$H_0 P_0 = P_0 H_0 = E_0 P_0 \qquad (2.67)$$

It is supposed that E_0 can be degenerate, and that the perturbation V lifts this degeneracy. The eigenvalues corresponding to the perturbed energy levels are given by

$$(H_0 + V) |k> = (E_0 + \Delta_k) |k> \qquad (2.68)$$

which can be rearranged to give

$$(H_0 - E_0) |k\rangle = (\Delta_k - V) |k\rangle \tag{2.69}$$

Δ_k are the shifts in the energy levels caused by the perturbation V. Using eq. (2.67) it can easily be shown that

$$P_0 V |k\rangle = \Delta_k P_0 |k\rangle = \Delta_k |k\rangle_0 \tag{2.70}$$

where the $|k\rangle_0$ are eigenfunctions of H_0, and in particular are those eigenfunctions $|i\rangle$ spanning the vector space under consideration.

There is a complementary projection operator Q_0 which follows from the closure relationship

$$\begin{aligned} Q_0 &= 1 - P_0 \\ &= \sum_\ell |\ell\rangle\langle\ell| \end{aligned} \tag{2.71}$$

where the eigenvectors $|\ell\rangle$ have been excluded from eq. (2.66) since they do not span the manifold we are interested in. Q_0 also has the property

$$Q_0 = \left(\frac{Q_0}{a}\right)(H_0 - E_0) = (H_0 - E_0)\left(\frac{Q_0}{a}\right) \tag{2.72}$$

where

$$\left(\frac{Q_0}{a}\right) = \sum_\ell \frac{|\ell\rangle\langle\ell|}{(E_0 - E_\ell)} \tag{2.73}$$

From eq. (2.69) and eq. (2.72) it follows that

$$Q_0 |k\rangle = \left(\frac{Q_0}{a}\right)(\Delta_k - V) |k\rangle \tag{2.74}$$

We are now able to find a relationship for $|k\rangle$ in terms of the un-perturbed eigenvectors $|k\rangle_0$:

$$|k\rangle = (P_0 + Q_0) |k\rangle$$
$$= |k\rangle_0 + \left(\frac{Q_0}{a}\right)(\Delta_k - V) |k\rangle \qquad (2.75)$$

The Δ_k terms can be eliminated from eq. (2.75) by repeated use of eq. (2.70) to give an expansion of $|k\rangle$ in terms of $|k\rangle_0$, V, P_0 and $\left(\frac{Q_0}{a}\right)$, that is substituting L.H.S. of eq. (2.75) into R.H.S. The eigenvectors for the perturbed and unperturbed Hamiltonians are thus related by an identity of general form

$$|k\rangle = U |k\rangle_0 \qquad (2.76)$$

where U is an operator involving V, P_0 and $\frac{Q_0}{a}$ which can be expanded as an infinite series in terms of these operators. Substitution of eq. (2.76) into eq. (2.70) leads to the following eigenvalue expression

$$P_0 V U |k\rangle_0 = \Delta_k |k\rangle_0 \qquad (2.77)$$

If we identify $(P_0 V U)$ with the effective Hamiltonian we see that it does possess the properties listed by Soliverez (28), although its hermitian nature has not been demonstrated. Note that the Δ_k's denote the energy shifts from an origin E_0. Eq. (2.77) is also particularly convenient in that it uses eigenfunctions of the unperturbed Hamiltonian as basis function and these are by definition known.

We can now return to the derivation of an effective molecular Hamiltonian. The basis functions $|k\rangle_0$ are taken to be the electronic-vibrational states of interest, which are eigenfunctions of H_0, and V is the perturbation that mixes them.

As described above (28,30) the total Hamiltonian is divided into two parts:

$$H = H_0 + \lambda V \qquad (2.78)$$

The parameter λ is a small number because V is assumed small compared to H_0.

The projection operators P_0 and Q_0 are given the more explicit definitions

$$P_0 = \sum_i |\ell_0 i\rangle\langle\ell_0 i| \qquad (2.79)$$

$$\left(\frac{Q_0}{a^n}\right) = \sum_{\ell \neq \ell_0} \sum_i \frac{|\ell i\rangle\langle\ell i|}{(E_o - E_\ell)^n} \qquad (2.80)$$

where ℓ_0 refers to the electronic-vibrational state of interest, ℓ refers to the electronic-vibrational states other than ℓ_0 and i refers to the set of quantum numbers within the manifold such as Σ, Ω or K etc.

The effective Hamiltonian is given by

$$H_{eff} = \lambda P_0 V U \qquad (2.81)$$

As has already been noted, U can be expanded as an infinite series

$$U = \sum_{n=0}^{\infty} \lambda^n U^n \qquad (2.82)$$

where U^n is given by the general formula

$$U^n = \sum_{n}{}' S^{K_1} V S^{K_2} V \ldots S^{K_n} V P_0 \qquad (2.83)$$

except that

$$U^0 = P_0 \qquad (2.84)$$

K_n can take the values 0, 1, 2 ...   such that

$$K_1 + K_2 + \ldots K_n = n$$
$$K_1 + K_2 + \ldots K_j \geq j \quad (j = 1,2 \ldots n-1) \qquad (2.85)$$

$\sum_{n}{}'$ is the condition that all K_i are non-negative. In addition

$$S^0 = -P_0$$
$$S^n = \left(\frac{Q}{a^n}\right) \quad \text{for } n \neq 0 \qquad (2.86)$$

As noted by Freed (31), certain terms in the expansion may be non-Hermitian, but by taking the Hermitian average of such terms the effective Hamiltonian is made Hermitian to all orders.

By the use of eq. (2.82) and (2.83), eq. (2.81) can be expanded as follows:

$$
\begin{aligned}
H_{eff} &= \lambda \, P_0 \, V \, U \\
&= \lambda \, P_0 \, V \, P_0 \\
&+ \lambda^2 \, P_0 \, V \, (Q_0/a) \, V \, P_0 \\
&+ \lambda^3 \{ P_0 \, V \, (Q_0/a) \, V \, (Q_0/a) \, V \, P_0 \\
&- [P_0 \, V \, (Q_0/a^2) \, V \, P_0 \, V \, P_0]^{\dagger} \} \\
&+ \lambda^4 \ldots
\end{aligned}
\tag{2.87}
$$

where the dagger means that the Hermitian average of the term in square brackets is to be taken. The coefficient of λ^n represents the nth order contribution to the effective Hamiltonian. The expansion of the effective Hamiltonian is expected to converge fairly rapidly, although the rate of convergence will depend on how the Hamiltonian was originally partitioned. In practice the total Hamiltonian is partitioned in such a way that the dominant interactions arise in first order of perturbation theory. Smaller interactions are included in the effective Hamiltonian by appealing to higher orders until the required precision of the eigenvalues, a limit usually imposed by experiment, is reached.

The effective Hamiltonian written in terms of operator equivalents will be considered in the next section after a brief discussion of angular momentum operators and some standard spherical tensor techniques.

C. Calculation of Matrix Elements

The concepts of angular momentum and rotational invariance play an important part in the analysis of molecular spectra. Using the general theory of angular momentum (11,12), expressions which depend only on the rotational properties of various operators and state vectors can be separated from quantities which are invariant under rotations.

It is worth noting that the structure of these expressions is primarily a function of the complexity of the system being studied such as, for instance, the number of angular momenta in the coupling scheme. When these ideas are to be carried out mathematically, spherical tensor algebra has proved extremely useful and also offers great physical insight.

It is not intended to give a through account of angular momentum and spherical tensor theory in this section ; the aim is merely to give some important results and useful relationships that will be called upon in subsequent calculations.

(i) <u>Angular Momenta</u>

Angular momentum operators are defined as those quantum mechanical operators that obey the commutation rules (11, 12)

$$[P_X, P_Y] = i\, P_Z \tag{2.88}$$

(and cyclic permutations of X, Y, Z) where P_X, P_Y and P_Z are cartesian components of the operator $\underset{\sim}{P}$. Since these components do not commute it is not possible to determine them all simultaneously. However, the angular momentum and the energy are both constants of the motion, so that

$$[P, H] = 0 \tag{2.89}$$

where H is the Hamiltonian operator. Because they commute P and H must possess simultaneous eigenfunctions. This is an important point because

matrix elements of the Hamiltonian operator can be calculated using the angular momentum eigenfunctions as basis functions. For this purpose it is convenient to write the Hamiltonian operator in terms of angular momentum operators and their components, rather than in terms of differential operators. The basis functions are defined in terms of quantum numbers relevant to the individual angular momenta rather than the explicit forms of the wavefunctions.

There are various kinds of angular momenta that can arise in a molecule. Firstly, there is the electronic orbital angular momentum $\underset{\sim}{L}$ which is the sum of the orbital angular momenta of each of the electrons

$$\underset{\sim}{L} = \sum_i \underset{\sim}{\ell_i} = \sum_i \underset{\sim}{r_i} \wedge \underset{\sim}{p_i} \qquad (2.90)$$

where $\underset{\sim}{r_i}$ and $\underset{\sim}{p_i}$ are respectively the position and momentum operators for the individual electrons. $\underset{\sim}{S}$ and $\underset{\sim}{I}$ are the electronic spin and nuclear spin angular momenta respectively. Finally we shall consider the angular momentum due to rotation of the nuclei, $\underset{\sim}{R}$. According to the rules of vector coupling[1] resultants $\underset{\sim}{J}$ and $\underset{\sim}{F}$ can be constructed:

$$\underset{\sim}{J} = \underset{\sim}{R} + \underset{\sim}{L} + \underset{\sim}{S} \qquad (2.91)$$

$$\underset{\sim}{F} = \underset{\sim}{J} + \underset{\sim}{I} \qquad (2.92)$$

---

[1] The possibility of different coupling schemes and the different sets of well-defined quantum numbers that emerge will be dealt with in section C (iii).

$\underset{\sim}{J}$ is the total angular momentum in the absence of nuclear spins, while $\underset{\sim}{F}$ is the grand total angular momentum. A partial sum

$$\underset{\sim}{N} = \underset{\sim}{J} - \underset{\sim}{S} \tag{2.93}$$

will also be considered. Conservation of angular momentum applies to the total angular momentum ($\underset{\sim}{F}$ or $\underset{\sim}{J}$) but not necessarily to the component angular momenta. This is equivalent to saying that only the conserved angular momenta possess well defined eigenfunctions. In general, for any conserved angular momentum $\underset{\sim}{P}$ we have the well known relations

$$\underset{\sim}{P}^2 \mid P \; M_p > \; = P(P+1)\hbar^2 \mid P \; M_p > \tag{2.94}$$

$$P_Z \mid P \; M_p > \; = M_p \, \hbar \mid P \; M_p > \tag{2.95}$$

P is the quantum number of the angular momentum $\underset{\sim}{P}$, and can take integral or half-integral non-negative values. M_p is the quantum number referring to the projection of the operator $\underset{\sim}{P}$ along the Z-axis (as yet undefined) and takes the (2P+1) values P, P-1, ..., -P. The symbol $\hbar$ is Planck's constant divided by 2π; however in what follows it will be assumed that the angular momenta are dimensionless, and the $\hbar$ units will be mainly dropped.

It is possible to define two new operators P_+ and P_- for which

$$P_+|PM_p> \; = (P_X+iP_Y)|PM_p>$$
$$= \exp(i\phi) \, [P(P+1)-M_p(M_p+1)]^{\frac{1}{2}} \, |PM_p+1> \tag{2.96}$$

$$P_-|PM_p> \; = (P_X-iP_Y)|PM_p>$$
$$= \exp(i\phi) \, [P(P+1)-M_p(M_p-1)]^{\frac{1}{2}} \, |PM_p-1> \tag{2.97}$$

where P_+ and P_- are called raising and lowering or shift operators, as they raise and lower by unity the projection quantum number M_p. In eqs. (2.96) and (2.97) ϕ is an arbitrary phase angle: the commutation relationships of eq. (2.88) do not fix the magnitude of ϕ. Condon and Shortley (24) take $\phi=0$ which fixes the relative phases of the $(2P+1)$ states $| P\ M_p \rangle$ of different M_p. This phase convention is used throughout this thesis.

It is well known that the operator P_z is the "generator of infinitesimal rotations about the z-axis"(32), because by successive infinitesimal rotations about this axis it is possible to generate an operator for rotation through a finite angle α about this z-axis. This operator will be called $D(\alpha)$, and defined as

$$D(\alpha) = 1 - \frac{i\alpha}{\hbar}\ P_z - \frac{\alpha^2}{4\hbar^2}\ P_z{}^2 + \ldots$$
$$= \exp\left(\frac{-i\alpha}{\hbar}\ P_z\right) \tag{2.98}$$

In general, for a rotation of a physical system in which the coordinates of points after rotation are related to the original coordinates by the Euler angles α,β,γ (11).

$$D(\alpha,\beta,\gamma) = \exp(-i\alpha P_z/\hbar)\exp(-i\beta Py/\hbar)\exp(-i\gamma P_z/\hbar) \tag{2.99}$$

The matrix elements of this rotation operator are defined as

$$\langle P\ M_p|\ D(\alpha,\beta,\gamma)\ |\ P\ M_p{}'\rangle = D^{(P)}_{M_p M_p{}'}(\alpha,\beta,\gamma) \tag{2,100}$$

Unfortunately the phase conventions used by various authors (Rose (33),

Brink and Satchler (12), and Edmonds (11)) differ; the definitions for $D(\alpha,\beta,\gamma)$ given by Rose will be followed in this thesis.

It has been stated in section B(iii) that the rotation matrix elements $D^{(P)}_{M_p M_p'}(\alpha,\beta,\gamma)$ are the eigenfunctions of a symmetric top, and it can also be shown that they are eigenfunctions of the angular momentum operators (11); therefore the angular momentum eigenfunctions $|P\ M_p>$ in general can be defined in terms of rotation matrix elements.

(ii) Irreducible Spherical Tensors

An irreducible spherical tensor operator of rank k will be defined as consisting of (2k+1) functions $T^k_q(\underset{\sim}{P})$ (q = -k, -k+1, ..., k) which transform under the 2k+1 - dimensional representation of the rotation group according to

$$D(\alpha\beta\gamma)\ T^k_q(\underset{\sim}{P})D^{-1}(\alpha\beta\gamma) = \sum_{q'} T^k_{q'}(P)\ D^{(k)}_{q'q}(\alpha\beta\gamma) \qquad (2.101)$$

This means that under a coordinate rotation $D(\alpha\beta\gamma)$ the operator $T^k_q(\underset{\sim}{P})$ is transformed into linear combinations of the 2k+1 operators $T^k_q(P)$, where the expansion coefficients are the elements of the Wigner rotation matrices, $D^{(k)}_{q'q}(\alpha\beta\gamma)$. This definition can be shown (32) to be equivalent to Racah's original expression (34).

$$[J\pm,\ T^k_q(\underset{\sim}{P})] = T^k_{q\pm1}(\underset{\sim}{P})\ [(k\mp q)(k\pm q+1)]^{\frac{1}{2}} \qquad (2.102)$$

and

$$[J_z,\ T^k_q(\underset{\sim}{P})] = q\ T^k_q(\underset{\sim}{P}) \qquad (2.103)$$

which are the alternative definitions of irreducible tensor operators.

A simple illustration of Racah's expressions is provided by the set of angular momentum operators; for instance, if k=1 then the spherical components $T_q^1(\underset{\sim}{P})$ are related to the cartesian components of a vector $\underset{\sim}{P}$ (a vector is a first rank tensor) according to

$$T_{\pm 1}^1(\underset{\sim}{P}) = \mp \frac{1}{\sqrt{2}} (P_X \pm i\, P_Y) \tag{2.104}$$

$$T_0^1(\underset{\sim}{P}) = P_Z \tag{2.105}$$

Angular momentum operators are vectors, and can therefore be written in spherical tensor form. Tensor operators of rank 2 or more can also arise in the Hamiltonian operators, for instance, the dipolar spin-spin interaction operator and the electric quadrupole operator both involve second rank tensors.

We choose to write all the terms in the Hamiltonian operator in spherical tensor notation. We are then able to use the extremely useful, and powerful, spherical tensor technique in the calculation of matrix elements. Products of spherical tensor operations can be treated without much difficulty, which is of particular value when products of matrix elements are to be written in an equivalent operator form. Some particular equations that will be of importance are as follows; these and other standard expressions can be found in standard texts on angular momentum (11, 12, 32, 33, 35).

(a) Tensor product of two tensor operators

$$T_q^k(\underset{\sim}{A},\underset{\sim}{B}) = (2k+1) \underset{q_1 q_2}{\Sigma} (-1)^{-k_1+k_2-q} \begin{pmatrix} k_1 k_2 k \\ q_1 q_2 q \end{pmatrix} T_{q_1}^{k_1}(\underset{\sim}{A})\, T_{q_2}^{k_2}(\underset{\sim}{B})$$

with $\qquad |k_1-k_2| \leq k \leq |k_1+k_2|$ $\qquad\qquad$ (2.106)

(b) Scalar product of two tensor operators of the same rank

$$T^k(\underset{\sim}{A}) \cdot T^k(\underset{\sim}{B}) = \sum_{q=-k}^{k} (-1)^q \, T_q^k(\underset{\sim}{A}) \, T_{-q}^k(\underset{\sim}{B}) \qquad (2.107)$$

(c) Wigner-Eckart Theorem

$$\langle P \, M_p \mid T_q^k(P) \mid P' M_p' \rangle = (-1)^{P-M_p} \begin{pmatrix} P & k & P' \\ -M_p & q & M_p' \end{pmatrix} \langle P \| T^k(P) \| P' \rangle \qquad (2.108)$$

The symbol $\langle P \| T^k(P) \| P' \rangle$ is called a reduced matrix element because it contains no reference to a coordinate system. It is the Wigner-Eckart theorem that enables terms which depend on the orientation of the coordinate system, mainly terms involving M_p, to be factored out. In this thesis Edmonds' definition (11) of reduced matrix elements is used, which implies explicitly $\langle P \| T(\underset{\sim}{P}) \| P' \rangle = [P(P+1)(2P+1)]^{\frac{1}{2}} \, \delta_{pp'} \qquad (2.109)$

(d) Relation between tensor operators in different coordinate systems - these systems can be transformed into each other by means of rotations through the appropriate Euler angles. If p and q are the components of the tensor in the two different coordinate systems,

$$T_p^k(\underset{\sim}{A}) = \sum_{q=-k}^{k} D_{pq}^{(k)*}(\alpha\beta\gamma) \, T_q^k(\underset{\sim}{A}) \qquad (2.110)$$

where $D_{pq}^{(k)*}(\alpha\beta\gamma)$ is the complex conjugate of the (p,q) element of the kth rank rotation matrix $D^{(k)}(\alpha\beta\gamma)$. The phase convention implicit in eq. (2.110) is that adopted by Brink and Satchler, and Rose (opposite to Edmonds).

The symbol $\begin{pmatrix} J_1 & J_2 & J_3 \\ m_1 & m_2 & m_3 \end{pmatrix}$ in equations (2.106) and (2.108) is the

Wigner 3-j symbol, which is a coefficient relating the eigenvectors corresponding to the angular momenta $\underset{\sim}{J_1}$ and $\underset{\sim}{J_2}$ to those corresponding to the angular momentum $\underset{\sim}{J_3}$ that results from coupling $\underset{\sim}{J_1}$ with $\underset{\sim}{J_2}$

$$|J_1 J_2 J_3 m_3\rangle = \sum_{m_1} \sum_{m_2} |J_1 m_1\rangle |J_2 m_2\rangle (-1)^{J_1 - J_2 - m_3}$$

$$(2J_3 + 1)^{\frac{1}{2}} \begin{pmatrix} J_1 & J_2 & J_3 \\ m_1 & m_2 & -m_3 \end{pmatrix}$$

$$(2.111)$$

Wigner 3-j symbols are simply related to the Clebsch-Gordan coefficients that arise in the coupling of two angular momenta. We shall also have occasion to use Wigner's 6-j and 9-j symbols, which are needed to describe the coupling of three and four angular momenta, respectively. Wigner symbols are used here because they have greater symmetry than the corresponding Clebsch-Gordan and Racah coefficients; in addition, they are easier to manipulate.

The symmetry properties of these symbols are given in standard texts (11,12). The relations of particular relevance in subsequent calculations are those by which 3-j (and 6-j) symbols can be reexpressed in terms of 6-j (and 9-j) symbols; a product of two 3-j symbols can be contracted in the following manner

$$\begin{pmatrix} J_1 & \ell_2 & \ell_3 \\ m_1 & \mu_2 & -\mu_3 \end{pmatrix} \begin{pmatrix} \ell_1 & J_2 & \ell_3 \\ -\mu_1 & m_2 & \mu_3 \end{pmatrix} = (-1)^P \sum_{J_3} (2J_3 + 1)$$

$$(2.112)$$

$$\begin{pmatrix} J_1 & J_2 & J_3 \\ m_1 & m_2 & m_3 \end{pmatrix} \begin{pmatrix} \ell_1 & \ell_2 & J_3 \\ \mu_1 & -\mu_2 & m_3 \end{pmatrix} \begin{Bmatrix} J_1 & J_2 & J_3 \\ \ell_1 & \ell_2 & \ell_3 \end{Bmatrix}$$

where $P = \ell_1 + \ell_2 + \ell_3 + \mu_1 + \mu_2 + \mu_3$, and the last collection of symbols in braces is a 6-j symbol. Similarly, by the use of the Biedenharn-Elliot relationship (11), a product of two 6-j symbols can be rewritten

$$\begin{Bmatrix} J_1 & J_2 & J_{12} \\ J_3 & J_{123} & J_{23} \end{Bmatrix} \begin{Bmatrix} J_{23} & J_1 & J_{123} \\ J_4 & J & J_{14} \end{Bmatrix} = \sum_{J_{124}} (-1)^S (2J_{124}+1)$$

(2.113)

$$\begin{Bmatrix} J_3 & J_2 & J_{23} \\ J_{14} & J & J_{124} \end{Bmatrix} \begin{Bmatrix} J_2 & J_1 & J_{12} \\ J_4 & J_{124} & J_{14} \end{Bmatrix} \begin{Bmatrix} J_3 & J_{12} & J_{123} \\ J_4 & J & J_{124} \end{Bmatrix}$$

where $S = J_1 + J_2 + J_3 + J_4 + J_{12} + J_{23} + J_{14} + J_{123} + J_{124} + J$

A product of four or five 3-j symbols summed over appropriate indices can be contracted as follows:

$$\sum_{defghi} \begin{pmatrix} B & E & H \\ b & e & h \end{pmatrix} \begin{pmatrix} C & F & I \\ c & f & i \end{pmatrix} \begin{pmatrix} A & D & G \\ a & d & g \end{pmatrix} \begin{pmatrix} D & E & F \\ d & e & f \end{pmatrix} \begin{pmatrix} G & H & I \\ g & h & i \end{pmatrix}$$

$$= \begin{pmatrix} A & B & C \\ a & b & c \end{pmatrix} \begin{Bmatrix} A & B & C \\ D & E & F \\ G & H & I \end{Bmatrix}$$

(2.114)

$$\sum_{dfgi} \begin{pmatrix} C & F & I \\ c & f & i \end{pmatrix} \begin{pmatrix} A & D & G \\ a & d & g \end{pmatrix} \begin{pmatrix} D & E & F \\ d & e & f \end{pmatrix} \begin{pmatrix} G & H & I \\ g & h & i \end{pmatrix}$$

(2.115)

$$= \sum_B (2B+1) \begin{pmatrix} A & B & C \\ a & b & c \end{pmatrix} \begin{pmatrix} B & E & H \\ b & e & f \end{pmatrix} \begin{Bmatrix} A & B & C \\ D & E & F \\ G & H & I \end{Bmatrix}$$

The symbols containing a 3 x 3 array of letters are Wigner 9-j symbols.

In this section, only the properties of irreducible spherical tensors have been discussed. The transformation from cartesian tensors $T_{(i)}$

to irreducible spherical tensors is considered in Appendix I.

In the next section, we will consider different Hund's coupling cases and the different sets of well-defined quantum numbers that are implied. After that we can calculate the matrix elements we require by applying irreducible spherical tensor techniques.

(iii) Hund's Coupling Cases

Provided we use basis functions that are combinations of eigenfunctions of the appropriate angular momentum operators, we have essentially complete freedom of choice in how to set up these combinations when we calculate matrix elements of the Hamiltonian. Sometimes it may be advantageous to use a basis where the calculation of the matrix elements is easy but the matrix itself is far from diagonal, since digital computers make the diagonalizations routine. At other times we may wish to use a basis that gives the most nearly diagonal representation, since the diagonal elements will already be a good approximation to the observed energy level pattern. The basis giving the most nearly diagonal representation depends on the relative magnitudes of the couplings of the various angular momenta.

In all known cases, coupling between the nuclear spin and other angular momenta by hyperfine interactions is much smaller than other couplings, so it is reasonable to begin the considerations by excluding nuclear spin. Hund investigated the various coupling schemes for electronic motion and showed that there are five possibilities, known as Hund's couplings cases (a) to (e) (36). Light diatomic and symmetric triatomic molecules (free radicals), such as described in this thesis,

normally belong to either case (a) or case (b), although case (c) is occasionally met.

Figure 2.2 illustrates coupling schemes (a) and (b). Case (a) applies when the spin-orbit interaction is quite large relative to the rotational energy. The orbital angular momentum $\underset{\sim}{L}$ (which results from the circulation of the electrons around the internuclear axis) precesses about this axis, and L_z, the projection of $\underset{\sim}{L}$ onto the internuclear z-axis, remains a constant of the motion but $\underset{\sim}{L}$ itself is not conserved. $\underset{\sim}{S}$ is coupled strongly to $\underset{\sim}{L}$ by the spin-orbit interaction. The quantum numbers Σ and Λ refer to the projections of $\underset{\sim}{S}$ and $\underset{\sim}{L}$ along the internuclear axis, respectively. $\underset{\sim}{L}$ and $\underset{\sim}{S}$ are coupled to the nuclear rotational angular momentum, $\underset{\sim}{R}$, to produce the total angular momentum excluding nuclear spin, $\underset{\sim}{J}$:

$$\underset{\sim}{R} + \underset{\sim}{L} + \underset{\sim}{S} = \underset{\sim}{J} \tag{2.116}$$

The quantum number for the projection of $\underset{\sim}{J}$ along the molecular axis is called Ω, and is given by

$$\Lambda + \Sigma = \Omega \tag{2.117}$$

The basis set in this case is completely defined in terms of the above-mentioned quantum numbers;

$$| \eta \Lambda ; S \Sigma ; J \Omega > \tag{2.118}$$

The symbol η refers to the other electron coordinates needed to describe the electronic state fully.

(i)   case (a)

$\Omega = \Lambda + \Sigma$

$| \, \eta \, \Lambda \, S \, \Sigma \, J \, \Omega >$
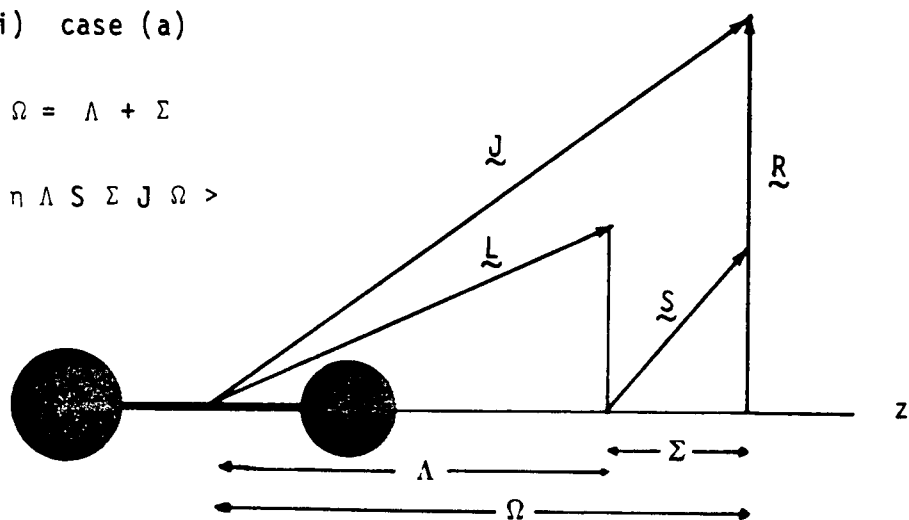
(ii)   case (b)

$\underset{\sim}{N} + \underset{\sim}{S} = \underset{\sim}{J}$

$| \, \eta \, \Lambda \, N \, (K) \, S \, J >$
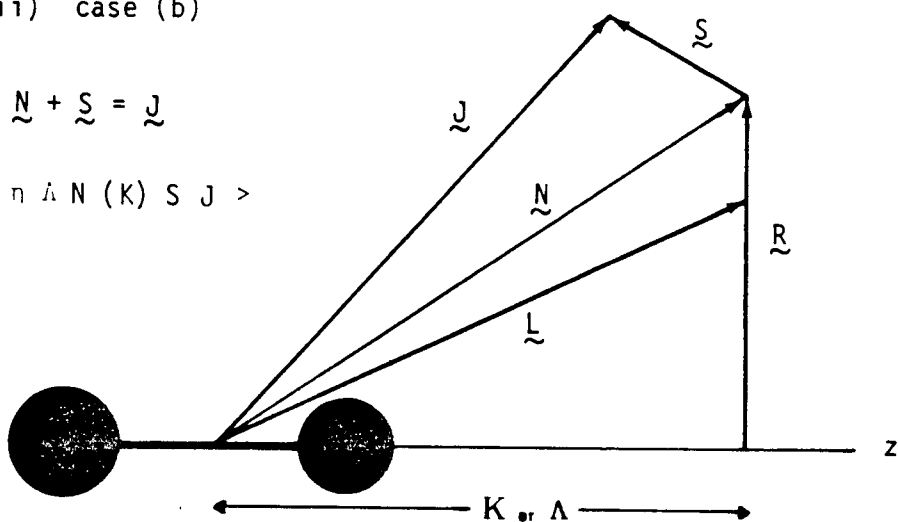
Fig. 2.2   Hund's coupling cases (a) and (b)

The case (b) scheme is important when spin-orbit coupling is small, so that there is no reason for $\underset{\sim}{S}$ to be coupled to the internuclear axis. $\underset{\sim}{L}$ has the same significance as for case (a); however in case (b) no distinction is made between the angular momenta for the motions of the nuclei and the electrons in obtaining the total rotational angular momentum of the molecule, $\underset{\sim}{N}$. Formally one can write

$$\underset{\sim}{R} + \underset{\sim}{L} = \underset{\sim}{N} \qquad (2.119)$$

This is then coupled with $\underset{\sim}{S}$ to form the total angular momentum excluding nuclear spin $\underset{\sim}{J}$:

$$\underset{\sim}{N} + \underset{\sim}{S} = \underset{\sim}{J} \qquad (2.120)$$

The quantum numbers Ω and Σ are undefined in this scheme; the only 'good' projection quantum number is K, corresponding to the component of $\underset{\sim}{N}$ along the z axis. K is called Λ for a linear molecule, where $\underset{\sim}{R}$ is perpendicular to the molecular axis so that the projection of $\underset{\sim}{N}$ along the axis is due to the electron orbital motion only. The basis set for case (b) takes the form

$$| \, \eta \, \Lambda \, ; \, N \, K \, S \, J > \qquad (2.121)$$

The transformation of basis functions from case (b) to case (a) is given by Brown and Howard (13):

$$| \, \eta \, \Lambda; \, N \, K \, S \, J > = \sum_{\Sigma,\Omega} (-1)^{N - S + \Omega}(2N + 1)^{\frac{1}{2}}\begin{pmatrix} J & S & N \\ \Omega & -\Sigma & -K \end{pmatrix} | \, \eta \, \Lambda \, ; \, S \, \Sigma; \, J \, \Omega>$$

$$(2.122)$$

Case (a$_\alpha$)

$\Lambda + \Sigma + I_z = \Omega_F$

$|\, \eta\ \Lambda\ S\ \Sigma\ I\ I_z\ F\ \Omega_F >$

Case (a$_\beta$)

$\underset{\sim}{J} + \underset{\sim}{I} = \underset{\sim}{F}$

$|\, \eta\ \Lambda\ S\ \Sigma\ J\ \Omega\ I\ F >$
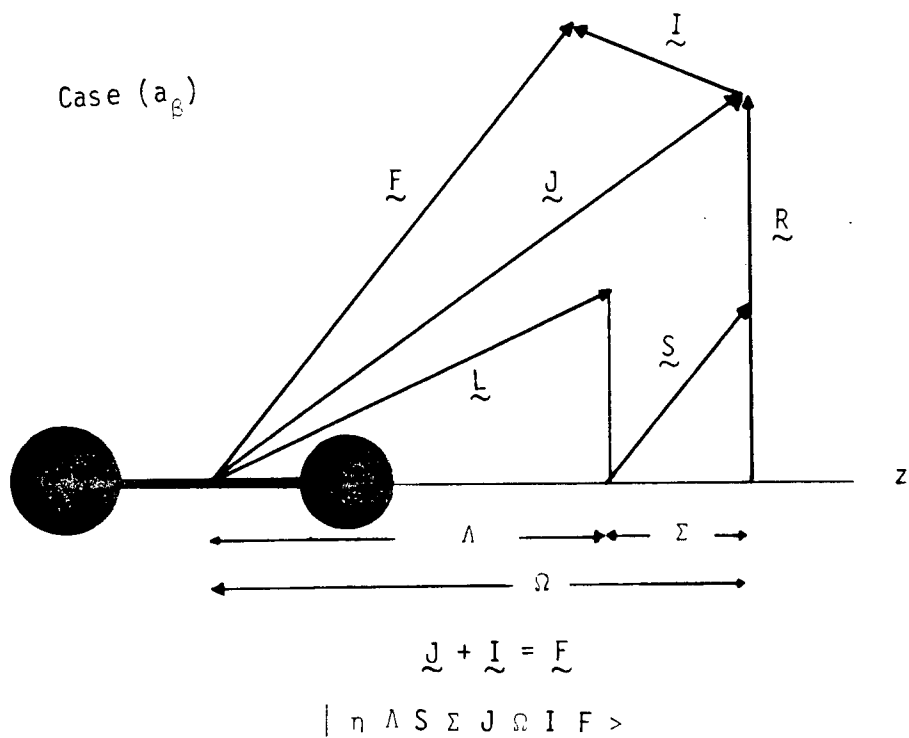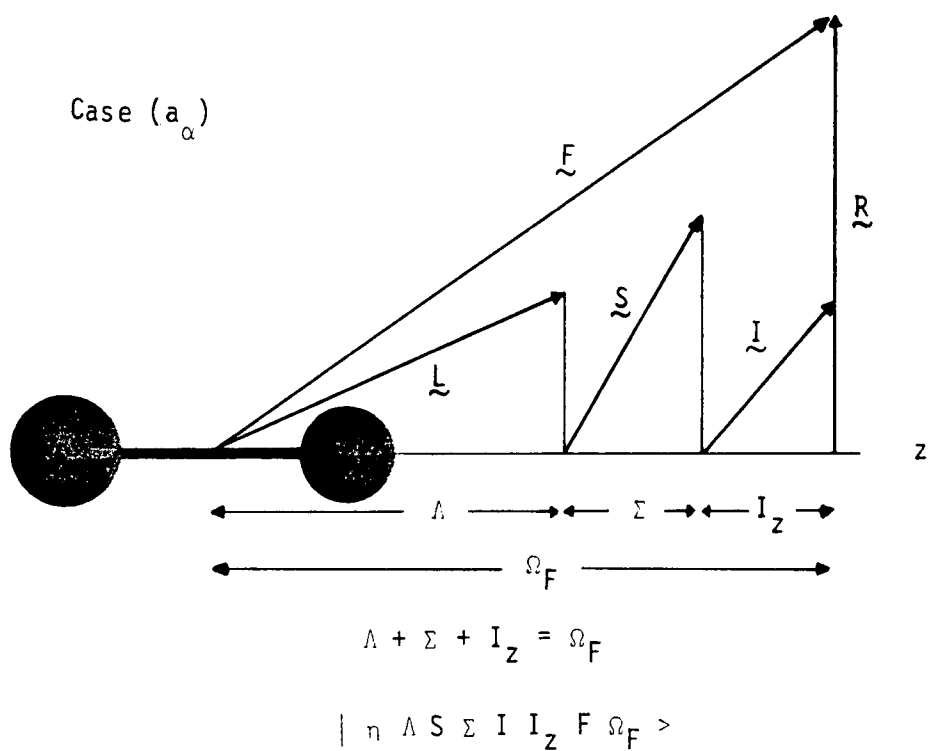
Fig. 2.3a Molecular coupling schemes including nuclear spin
Case (a$_\alpha$) and Case (a$_\beta$)

Case $(b_{\beta S})$

$$\underset{\sim}{I} + \underset{\sim}{S} = \underset{\sim}{G} \quad \& \quad \underset{\sim}{G} + \underset{\sim}{N} = \underset{\sim}{F}$$

$$| \eta \Lambda \, (I \, S) \, G \, N \, F >$$

Case $(b_{\beta N})$

$$\underset{\sim}{N} + \underset{\sim}{I} = \underset{\sim}{F_1} \quad \& \quad \underset{\sim}{F_1} + \underset{\sim}{S} = \underset{\sim}{F}$$

$$| \eta \Lambda \, (N \, I) \, F_1 \, S \, F >$$
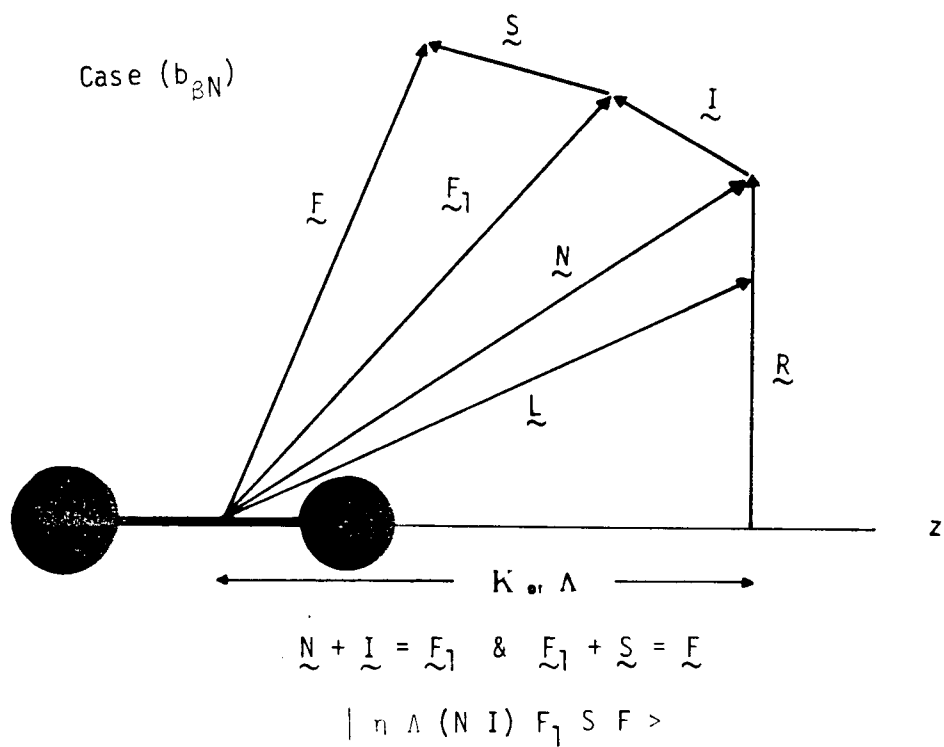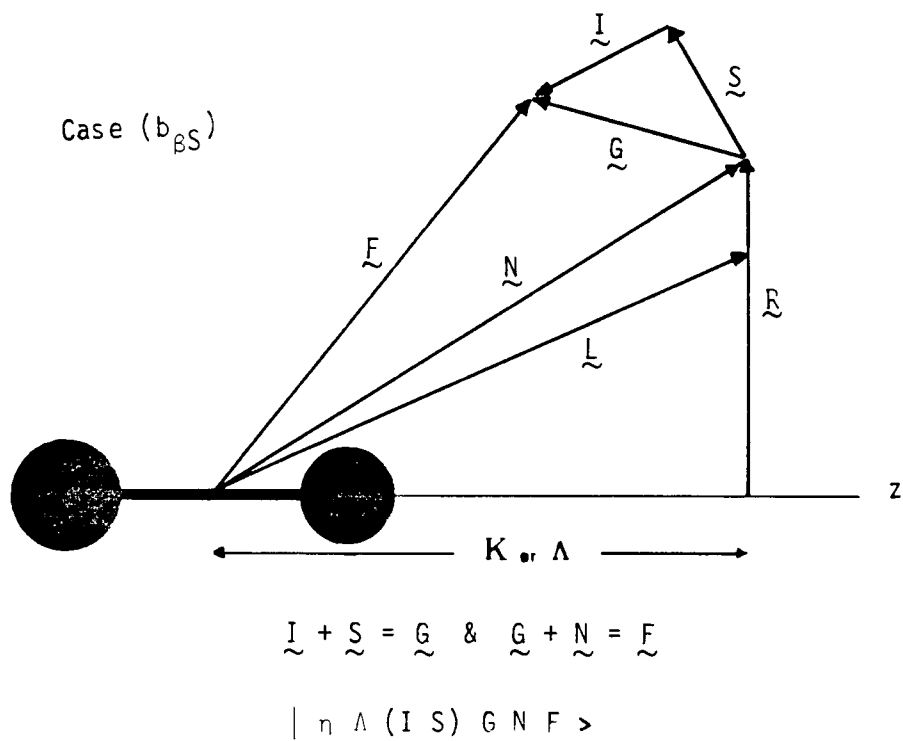
Fig. 2.3b Molecular coupling schemes Case $(b_{\beta S})$ and Case $(b_{\beta N})$

$$\underset{\sim}{N} + \underset{\sim}{S} = \underset{\sim}{J} \quad \& \quad \underset{\sim}{J} + \underset{\sim}{I} = \underset{\sim}{F}$$

$$| \ \eta \ \Lambda \ (N \ S) \ J \ I \ F >$$
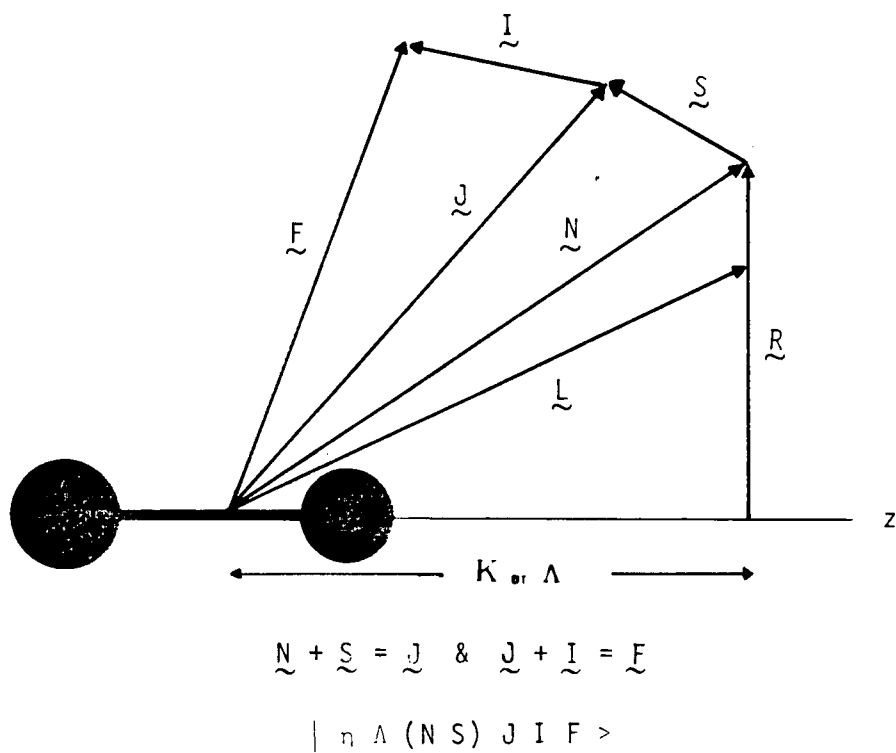
Fig. 2.3c Molecular coupling scheme   Case $(b_{\beta J})$

We now consider the couplings involving nuclear spin angular momentum. It will be assumed that only one spinning nucleus is present. The nuclear spin may be coupled with varying strength to the several molecular angular momenta, providing additional coupling possibilities. The commonly expected coupling schemes are shown in Fig. 2.3 . They are classified according to Hund's scheme, with the subscript α indicating that the nuclear spin is most strongly coupled to the molecular axis (as is $\underset{\sim}{S}$ in Hund's case (a)) and a subscript β indicating that the nuclear spin is not coupled to the molecular axis but to some other angular momentum (as in case (b)). For Hund's case (a), one may expect the nuclear spin to be coupled either to the molecular axis (case (a_α)) or to J (case (a_β)). Fig. 2.3a. However, for Hund's case (b), where the electron spin is not coupled to the molecular axis, it is very unlikely that the nuclear spin will be coupled to the molecular axis since the interaction of its small nuclear magnetic moment with the molecular fields should be considerably less than that between the electron moment and the molecular fields. Hence only the various (b_β) cases are expected to occur. The vector models and basis sets for different coupling schemes are written explicitly in Fig.2.3 b & c. Case ($b_{\beta N}$) where the nuclear spin is coupled to the molecular rotation more strongly than the electron spin is, is also not expected to occur. Case ($b_{\beta S}$) is found when the Fermi contact interaction $a_c \underset{\sim}{I}.\underset{\sim}{S}$ is larger than any of the electron spin interactions, but case ($b_{\beta J}$) is the most common situation.

iv) <u>Matrix Elements in case $(b_{\beta J})$ and (a_β) coupling</u>

Quantum mechanical calculations for systems having symmetry may usually be divided fairly completely into two parts. One part consists of deriving as much information as possible from the symmetry alone. The other is the evaluation of certain integrals, the estimation of parameters, or the solution of equations which have no symmetry or for which symmetry considerations can provide no information. The irreducible tensor methods described above are designed to separate these two parts and then to provide a well developed and consistent way of calculating matrix elements involving the angular momentum operators. Since the free radicals discussed in this thesis are diatomic and triatomic, matrix elements for both Hund's cases (a_β) and $(b_{\beta J})$ are given. Case (a) expressions are particularly useful in dealing with diatomic or linear free radicals.

In the derivation, we follow Brown and Howard's procedures (13). They do not use Van Vleck's reversed angular momentum method (18) but instead evaluate matrix elements directly in space-fixed (p) components, rather than in a molecule-fixed coordinate system (q). Operators that are naturally defined in the molecule-fixed axis system, such as the electron orbital angular momentum $\underset{\sim}{L}$, are referred back from the space-fixed axis system by the use of the rotation matrix eq. (2.110). In this way the anomalous commutation relations are completely avoided and spherical tensor methods can be applied in their standard form.

Matrix elements in the case $(b_{\beta J})$ coupling scheme will be presented first. The details of the derivations are mainly omitted, but as an

illustration the matrix elements of the dipolar hyperfine interaction
are derived in Appendix II. The rotational Hamiltonian for a near-
prolate asymmetric top can be written in the familiar cartesian form
of eq. (2.16), where the I^r association (10) of the inertial angular
momentum axes has been made:

$$H_{rot} = A N_z^2 + B N_x^2 + C N_y^2 \qquad (2.123)$$

The equivalent irreducible tensor form of H_{rot} is

$$H_{rot} = \sum_{k=0}^{2} T^k(B) \cdot T^k(\underset{\sim}{N},\underset{\sim}{N}) \qquad (2.124)$$

where the $T^k(B)$ are irreducible tensors of rank k. There are only three
distinct non-zero components, namely $T_0^0(B)$, $T_0^2(B)$ and $T_2^2(B) = T_{-2}^2(B)$
(Appendix I). $T^k(N,N)$ is an irreducible tensor operator of kth rank
obtained by coupling $T^1(N)$ with itself, according to eq. (2.106).
The matrix elements of the rotational Hamiltonian H_{rot} in eq. (2.124) are
given by

$$< \eta\, N\, K'\, S\, J\, I\, F \mid H_{rot} \mid \eta\, N\, K\, S\, J\, I\, F >$$

$$= \sum_{k=o}^{2} \sum_{q} (-1)^{N-K'} T_q^k(B) \begin{pmatrix} N & k & N \\ -K' & q & K \end{pmatrix} < N||T^k(\underset{\sim}{N},\underset{\sim}{N})||N > \qquad (2.125)$$

where the reduced matrix elements are

$$< N||T^k(\underset{\sim}{N},\underset{\sim}{N})||N > = (-1)^k [(2k+1)]^{\frac{1}{2}} [N(N+1)(2N+1)]$$

$$\begin{Bmatrix} N & N & 1 \\ k & 1 & N \end{Bmatrix} \qquad (2.126)$$

The quartic centrifugal distortion terms for an asymmetric top can be described by an operator of the form (37)

$$H_{cd} = -\Delta_N (N^2)^2 - \Delta_{NK} N^2 N_z^2 - \Delta_K N_z^4 - \delta_N N^2 2(N_x^2 - N_y^2)$$

$$- \delta_K \{ (N_x^2 - N_y^2) N_z^2 + N_z^2 (N_x^2 - N_y^2) \}. \qquad (2.127)$$

This expression is valid provided that the effective Hamiltonian is soundly based (i.e. there are no strong interactions between vibrational states) and that the molecule is not an accidental symmetric top. When cast in irreducible form the general expression for H_{cd} is

$$H_{cd} = - \sum_{k=0}^{4} \sum_{k_1,k_2} T^k(\Delta_{k_1 k_2}) \cdot T^k(N^4_{k_1 k_2}) \qquad (2.128)$$

$T^k(N^4_{k_1 k_2})$ is an irreducible tensor operator formed by coupling the vector $T^1(N)$ with itself four times

$$T^k_p(N^4_{k_1 k_2}) = (-1)^{p+k_1-k_2} (2k+1)^{\frac{1}{2}} \sum_{p_1,p_2} T^{k_1}_{p_1}(\underline{N},\underline{N}) T^{k_2}_{p_2}(\underline{N},\underline{N}) \begin{pmatrix} k_1 & k_2 & k \\ p_1 & p_2 & -p \end{pmatrix}$$

$$(2.129)$$

The five determinable centrifugal distortion parameters can be chosen in several different ways; eq. (2.127) represent just one such choice. The matrix elements of the centrifugal distortion Hamiltonian are

$$< \eta \, N \, K \, S \, J \, I \, F \mid H_{cd} \mid \eta \, N \, K \, S \, J \, I \, F >$$
$$= -\Delta_N \, N^2(N+1)^2 - \Delta_{NK} N(N+1) K^2 - \Delta_K K^4 \qquad (2.130)$$

and

$$< \eta \, N \, K \pm 2 \, S \, J \, I \, F \mid H_{cd} \mid \eta \, N \, K \, S \, J \, I \, F >$$

$$= \{ - \delta_N \, N(N+1) - \frac{1}{2} \delta_K \, [K^2 + (K \pm 2)^2] \}$$

$$\qquad (2.131)$$

$$[N(N+1) - K(K \pm 1)]^{\frac{1}{2}} \, [N(N+1) - (K \pm 1)(K \pm 2)]^{\frac{1}{2}}$$

The electron spin fine structure Hamiltonian consists of spin-orbit, spin-rotation and spin-spin dipolar interactions. We will first consider the spin-orbit interaction for a non-linear molecule. The spin-orbit Hamiltonian takes the general form

$$H_{so} = \underset{\sim}{L}^+ \cdot \underset{=}{A}^{so} \cdot \underset{\sim}{S} \qquad (2.132)$$

where $\underset{=}{A}^{so}$ is a 3x3 matrix containing the spin-orbit coupling coefficients. Since molecules do not possess spherical symmetry, L is far from being a good quantum number. This makes it necessary to consider the product $\underset{\sim}{L}^+ \cdot \underset{=}{A}^{so}$ as a vector $\underset{\sim}{V}$ (19). The interaction Hamiltonian is therefore a scalar product of this vector with $\underset{\sim}{S}$, or, in irreducible tensor notation,

$$H_{so} = T^1(\underset{\sim}{V}) \cdot T^1(\underset{\sim}{S}) \qquad (2.133)$$

The matrix elements (38) are

$$< \eta' \, N' \, K' \, S \, J \, I \, F \mid H_{so} \mid \eta \, N \, K \, S \, J \, I \, F >$$
$$= (-1)^{N+S+J} [S(S+1)(2S+1)]^{\frac{1}{2}} \, [(2N+1)(2N'+1)]^{\frac{1}{2}}$$

$$\begin{Bmatrix} J & S & N' \\ 1 & N & S \end{Bmatrix} (-1)^{N'-K'} \sum_q \begin{pmatrix} N' & 1 & N \\ -k' & q & K \end{pmatrix} < \eta' \mid T^1(\underset{\sim}{V}) \mid \eta > \qquad (2.134)$$

The spin-rotation Hamiltonian in cartesian tensor notation (39) is

$$H_{sr} = \frac{1}{2} \sum_{\alpha,\beta} \varepsilon_{\alpha\beta} (N_\alpha S_\beta + S_\beta N_\alpha) \qquad (2.135)$$

where α and β run separately over the molecule-fixed coordinates. In irreducible tensor notation, this Hamiltonian is

$$H_{sr} = \frac{1}{2} \sum_{k=0}^{2} [T^k(\varepsilon) \cdot T^k(N,S) + T^k(N,S) \cdot T^k(\varepsilon)] \qquad (2.136)$$

in which $T^k(N,S)$ is the tensor operator obtained by coupling the two first rank tensors $T^1(N)$ and $T^1(S)$ in a manner defined in eq. (2.106). $T^k(\varepsilon)$ is an irreducible tensor (k= 0,1,2) and in general all nine components can be non-zero; these components are usually defined in the molecule fixed inertial axis system. The relationships between these nine components and $\varepsilon_{\alpha\beta}$, van Vleck's spin-rotation parameters (18) as extended by Raynes (40)), and Curl and Kinsey's parameters (41) are given by Bowater et al (39).

The matrix elements of the spin-rotation Hamiltonian are given by the expression

$$< \eta\, N'\, K'\, S\, J\, I\, F \mid H_{sr} \mid \eta\, N\, K\, S\, J\, I\, F >$$

$$= \sum_{k=0}^{2} (2k+1)^{\frac{1}{2}} [S(S+1)(2S+1)]^{\frac{1}{2}} [(2N+1)(2N'+1)]^{\frac{1}{2}}$$

$$(-1)^{J+S+N'} \begin{Bmatrix} N & S & J \\ S & N' & 1 \end{Bmatrix} \cdot \frac{1}{2} [(-1)^k [N(N+1)(2N+1)]^{\frac{1}{2}}$$

$$\begin{Bmatrix} 1 & 1 & k \\ N' & N & N \end{Bmatrix} + [N'(N'+1)(2N'+1)]^{\frac{1}{2}} \begin{Bmatrix} 1 & 1 & k \\ N & N' & N' \end{Bmatrix}]$$

$$\sum_{q} (-1)^{N'-K'} \begin{pmatrix} N' & k & N \\ -K' & q & K \end{pmatrix} T_q^k(\varepsilon) \qquad (2.137)$$

The spin-spin dipolar interaction given in eq. (2.48) can be expressed in tensor notation either as the tensor product (32)

$$H_{ss} = -\sqrt{30}g^2 \, \mu_B^2 \sum_{i>j} R_{ij}^{-3} \, T_0^0(T^2(T^1(\underset{\sim}{s}_i), T^1(\underset{\sim}{s}_j)), C^2) \tag{2.138}$$

or the scalar product

$$H_{ss} = \sqrt{10} \, g^2 \, \mu_B^2 \sum_{i>j} R_{ij}^{-3} \, T^1(\underset{\sim}{s}_i) . T^1(\underset{\sim}{s}_j, \, C^2) \tag{2.139}$$

where R_{ij} is the distance between the unpaired electrons and $C_q^2(\theta, \phi)$ is closely related to the second rank spherical harmonic,

$$C_q^2(\theta, \phi) = \left(\frac{4\pi}{5}\right)^{\frac{1}{2}} Y_q^2(\theta, \phi) \tag{2.140}$$

θ and ϕ are the spherical polar angles defining the position of one electron relative to the other.

The matrix elements of the spin-spin interaction are

$$< \eta \, N' \, K' \, S \, J \, I \, F \mid H_{ss} \mid \eta \, N \, K \, S \, J \, I \, F > = -\sqrt{6} \, g^2 \, \mu_B^2$$

$$(-1)^{S+J+N} \begin{Bmatrix} J & S & N' \\ 2 & N & S \end{Bmatrix} \sum_{i>j} < S \mid\mid T^2(\underset{\sim}{s}_i, \underset{\sim}{s}_j) \mid\mid S >$$

$$\sum_q (-1)^{N'-K'} [(2N+1)(2N'+1)]^{\frac{1}{2}} \begin{pmatrix} N' & 2 & N \\ -K' & q & K \end{pmatrix} T_q^2(C) \tag{2.141}$$

where the reduced matrix element $\sum_{i>j} < S \mid\mid T^2(\underset{\sim}{s}_i, \underset{\sim}{s}_j) \mid\mid S >$ has the value listed in ref. (42) and Appendix III for different spin multiplicities. The components

$$T_q^2(C) = <\eta \mid \frac{C^2}{R^3}(\theta,\phi) \mid \eta> \qquad (2.142)$$

are the parameters describing the dipolar interaction.

The nuclear spin terms consist of two kinds of interactions, namely the magnetic hyperfine and the electric quadrupole. We shall confine ourselves with the case in which only one of the nuclei has non-zero spin. Thus the magnetic hyperfine interactions in eq. (2.54) can be written as (39)

$$H_{mag.hfs} = a\ T^1(\underline{I}).T^1(\underline{L}) + a_c\ T^1(\underline{I}).T^1(\underline{S})$$
$$\qquad (2.143)$$
$$-\frac{10^{\frac{1}{2}}}{R^3}\ g\mu_B g_N \mu_N\ T^1(\underline{I}).T^1(\underline{S},C^2)$$

where the third term is the nuclear spin-electron spin dipolar interaction and R is distance between the unpaired electron and the nucleus with spin I. The matrix elements of $H_{mag.hfs}$ are

$$< \eta\ N´\ K´S\ J´\ I\ F \mid H_{mag.hfs} \mid \eta\ N\ K\ S\ J\ I\ F >$$

$$= (-1)^{J+I+F} \begin{Bmatrix} F & I & J´ \\ 1 & J & I \end{Bmatrix} [\ I(I+1)(2I+1)(2J+1)(2J´+1)]^{\frac{1}{2}}$$

$$\Bigg[\quad [\ (2N+1)(2N´+1)]^{\frac{1}{2}}\ (-1)^{N´+S+J+1} \begin{Bmatrix} N´ & J´ & S \\ J & N & 1 \end{Bmatrix}$$

$$\sum_q (-1)^{N´-K´} \begin{pmatrix} N´ & 1 & N \\ -K´ & q & K \end{pmatrix} < \eta \mid T_q^1(\underline{L}) \mid \eta > .\ a$$

$$+ \delta_{N'N} \, \delta_{K'K} \, [S(S+1)(2S+1)]^{\frac{1}{2}} \, (-1)^{N+S+J'+1} \begin{Bmatrix} S & J' & N \\ J & S & 1 \end{Bmatrix} a_c$$

$$- (30)^{\frac{1}{2}} g \mu_B g_N \mu_N \, [S(S+1)(2S+1)(2N+1)(2N'+1)]^{\frac{1}{2}}$$

$$\begin{Bmatrix} N' & N & 2 \\ S & S & 1 \\ J' & J & 1 \end{Bmatrix} \sum_q (-1)^{N'-K'} \begin{pmatrix} N' & 2 & N \\ -K' & q & K \end{pmatrix} T_q^2(C) \Bigg] \qquad (2.144)$$

where the quantities $\langle n|T_q^1(L)|n\rangle \cdot a$ and a_c are experimentally determinable parameters. The components $T_q(C)$ are the parameters describing the dipolar interaction. In general, there are five independent components of $T^2(C)$ but for a planar molecule these are reduced to three (39). A detailed derivation of the nuclear spin-electron spin dipolar interaction matrix elements is worked out in Appendix II.

If the nucleus has a spin greater than $\frac{1}{2}$, we must include the nuclear quadrupole interaction. The operator for this interaction has been written in tensor notation in eq. (2.63). The matrix elements of H_Q are given by (39)

$$\langle n \, N' \, K' \, S \, J' \, I \, F \mid H_Q \mid n \, N \, K \, S \, J \, I \, F \rangle$$

$$= \frac{eQ}{2} \begin{pmatrix} I & 2 & I \\ -I & 0 & I \end{pmatrix}^{-1} (-1)^{J+I+F} \begin{Bmatrix} I & J' & F \\ J & I & 2 \end{Bmatrix}$$

$$(-1)^{N'+S+J} \begin{Bmatrix} N' & J & S \\ J & N & 2 \end{Bmatrix} [(2J+1)(2J'+1)(2N+1)(2N'+1)]^{\frac{1}{2}}$$

$$\sum_q (-1)^{N'-K'} \begin{pmatrix} N' & 2 & N \\ -K' & q & K \end{pmatrix} T_q^2(\nabla E) \qquad (2.145)$$

where the electric quadrupole moment Q is defined by

$$\frac{1}{2} Q = <\text{II}| T_0^2 (Q) | \text{I I} >$$

$$= \begin{pmatrix} \text{I} & 2 & \text{I} \\ -\text{I} & 0 & \text{I} \end{pmatrix} < \text{I} || T^2 (Q) || \text{I} > \qquad (2.146)$$

and $T^2(\nabla E)$ is the electric field gradient tensor.

Finally, the interaction of the nuclear spin with the magnetic field of the molecular rotation gives rise to an operator

$$H_{IN} = c_I T^1(\underset{\sim}{I}) \cdot T^1(\underset{\sim}{N}) \qquad (2.147)$$

where c_I is the nuclear spin-rotational coupling parameter. The matrix elements are

$$< \eta \, N \, K \, S \, J' \, I \, F \, | \, H_{IN} \, | \, \eta \, N \, K \, S \, J \, I \, F >$$

$$= (-1)^{J+I+F} \begin{Bmatrix} F & I & J' \\ 1 & J & I \end{Bmatrix} (-1)^{N+S+J+1} \begin{Bmatrix} S & N & J' \\ 1 & J & N \end{Bmatrix}$$

$$[I(I+1)(2I+1) \ (2J+1)(2J'+1) \ N(N+1)(2N+1)]^{\frac{1}{2}} \ c_I$$

$$(2.148)$$

This completes the matrix element expressions for case $(b_{\beta J})$ coupling. For non-linear molecules all three Euler angles are needed to specify the orientation of the molecule, but this is a problem for linear molecules because the orientation round the molecular axis is undefined so that one of the Euler angles is missing. The 'absence' of the third Euler angle leads to problems later on in the theoretical treatment when one comes to

compute and use matrix elements, since much of the theory, and in particular irreducible tensor methods, require there to be three rotational coordinates. Hougen (43) and later Watson (44), have provided a solution to this problem by introducing the third Euler angle as a redundant coordinate in an isomorphic Hamiltonian.

Consider a linear molecule which is modified by the addition of an off axis, nearly massless particle, which is bound to the molecule, but which does not affect the motion of the nuclei and electrons of the molecule. The missing third Euler angle must be restored in order to specify the orientation of this non-linear pseudo-molecule. The visualization of such a molecular system immediately suggests that the formalism developed earlier will be applicable to linear molecules. This isomorphic Hamiltonian can be handled in the normal way, except that only certain of its eigenvalues and eigenfunctions are acceptable, the other solutions being a consequence of the redundancy introduced into the Hamiltonian.

Linear molecules or free radicals where Λ and S are greater than zero have first order spin-orbit effects. The diagonal elements in Hund's coupling case (a) are then a closer approximation to the energy level pattern. We now discuss the operators and matrix elements for linear molecules or free radicals in case (a_β) coupling.

First of all, the rotational kinetic energy and centrifugal distortion energy are described by the operators (45)

$$H_{rot} = B \, T^2(\underset{\sim}{R}) \tag{2.149}$$

and

$$H_{cd} = - D\, T^2(\underset{\sim}{R}) \cdot T^2(\underset{\sim}{R}) \tag{2.150}$$

where

$$\underset{\sim}{R} = \underset{\sim}{J} - \underset{\sim}{L} - \underset{\sim}{S}$$

Their matrix elements are respectively,

$$< \eta\, \Lambda\, S\, \Sigma'\, J\, \Omega'\, I\, F \mid H_{rot} \mid \eta\, \Lambda\, S\, \Sigma\, J\, \Omega\, I\, F >$$

$$= B \Bigg\{ \delta_{\Sigma'\Sigma}\, \delta_{\Omega'\Omega}\, [J(J+1) - \Omega^2 + S(S+1) - \Sigma^2 + < L_x^2 + L_y^2 >]$$

$$-2 \sum_{q=\pm 1} (-1)^{J-\Omega'+S-\Sigma'} \begin{pmatrix} J & 1 & J \\ -\Omega' & q & \Omega \end{pmatrix} \begin{pmatrix} S & 1 & S \\ -\Sigma' & q & \Sigma \end{pmatrix}$$

$$[J(J+1)(2J+1)\, S(S+1)(2S+1)]^{\frac{1}{2}} \Bigg\} \tag{2.151}$$

and

$$< \eta\, \Lambda\, S\, \Sigma'\, J\, \Omega'\, I\, F \mid H_{cd} \mid \eta\, \Lambda\, S\, \Sigma\, J\, \Omega\, I\, F >$$

$$= -D \Bigg\{ \delta_{\Sigma'\Sigma}\, \delta_{\Omega'\Omega}\, \Bigg[[J(J+1) - \Omega^2 + S(S+1) - \Sigma^2]^2$$

$$+ 4 \cdot \sum_{q=\pm 1} \sum_{\Omega'',\Sigma''} \begin{pmatrix} J & 1 & J \\ -\Omega & q & \Omega'' \end{pmatrix}^2 \begin{pmatrix} S & 1 & S \\ -\Sigma & q & \Sigma'' \end{pmatrix}^2$$

$$[J(J+1)(2J+1)\, S(S+1)(2S+1)\ ] \Bigg]$$

$$-2 \sum_{q=\pm 1} (-1)^{J-\Omega'+S-\Sigma'} \begin{pmatrix} J & 1 & J \\ -\Omega' & q & \Omega \end{pmatrix} \begin{pmatrix} S & 1 & S \\ -\Sigma' & q & \Sigma \end{pmatrix}$$

$$[J(J+1)(2J+1)\, S(S+1)(2S+1)]^{\frac{1}{2}}\, [2J(J+1) - (\Omega')^2$$
$$- \Omega^2 + 2S(S+1) - (\Sigma')^2 - \Sigma^2]$$

$$+ 4 \sum_{q=\pm 1} \sum_{\Omega''\Sigma''} (-1)^{\Omega'+\Sigma'+\Omega''+\Sigma''} \begin{pmatrix} J & 1 & J \\ -\Omega' & q & \Omega'' \end{pmatrix} \begin{pmatrix} S & 1 & S \\ -\Sigma' & q & \Sigma'' \end{pmatrix} \begin{pmatrix} J & 1 & J \\ -\Omega'' & q & \Omega \end{pmatrix} \begin{pmatrix} S' & 1 & S \\ -\Sigma'' & q & \Sigma \end{pmatrix}$$

$$[J(J+1)(2J+1) \ S(S+1)(2S+1)] \Bigg\} \tag{2.152}$$

The spin fine structure Hamiltonian consists of three different contributions.

$$H_{so} = A \ T_0^1(\underset{\sim}{L}) \ T_0^1(\underset{\sim}{S}) \qquad \text{represents the spin-orbit} \\ \text{interactions} \tag{2.153}$$

$$H_{ss} = \frac{2}{3} \sqrt{6} \ \lambda \ T_0^2(\underset{\sim}{S} , \underset{\sim}{S}) \qquad \text{the spin-spin interaction} \tag{2.154}$$

$$H_{sr} = \gamma T^1(\underset{\sim}{J} - \underset{\sim}{S}) \cdot T^1(\underset{\sim}{S}) \qquad \text{the spin-rotation interaction} \tag{2.155}$$

where A, λ and γ are spin-orbit, spin-spin and spin-rotation parameters respectively. Their matrix elements are

$$< \eta \ \Lambda \ S \ \Sigma \ J \ \Omega \ I \ F \ | \ H_{so} \ | \ \eta \ \Lambda \ S \ \Sigma \ J \ \Omega \ I \ F > = A \Lambda \Sigma \tag{2.156}$$

$$< \eta \ \Lambda \ S \ \Sigma \ J \ \Omega \ I \ F \ | \ H_{ss} \ | \ \eta \ \Lambda \ S \ \Sigma \ J \ \Omega \ I \ F > = \frac{2}{3} \lambda \ [3\Sigma^2 - S(S+1)] \tag{2.157}$$

$$< \eta \ \Lambda \ S\Sigma' \ J\Omega' \ I \ F \ | \ H_{sr} \ | \ \eta \ \Lambda \ S \ \Sigma \ J \ \Omega \ I \ F >$$
$$= \gamma \Bigg\{ \delta_{\Sigma'\Sigma} \ \delta_{\Omega'\Omega} \ [\ \Omega\Sigma - S(S+1)] + \sum_{q=\pm 1} (-1)^{J-\Omega'-S-\Sigma'}$$

$$\begin{pmatrix} J & 1 & J \\ -\Omega' & q & \Omega \end{pmatrix} \begin{pmatrix} S & 1 & S \\ -\Sigma' & q & \Sigma \end{pmatrix} [J(J+1)(2J+1) \ S(S+1)(2S+1)]^{\frac{1}{2}} \Bigg\} \tag{2.158}$$

The magnetic hyperfine interaction terms appropriate to Hund's case (a_β) coupling are

$$H_{mag.hfs} = a \ T_{q=0}^1(\underset{\sim}{I}) \cdot T_{q=0}^1 (\underset{\sim}{L}) + a_c \ T^1(\underset{\sim}{I}) \cdot T^1(\underset{\sim}{S})$$
$$+ \frac{1}{3}(6)^{\frac{1}{2}} c \ T_0^2 (\underset{\sim}{I} , \underset{\sim}{S}) \tag{2.159}$$

where a and c are the hyperfine parameters defined by Frosch and Foley (21) and a_c is the Fermi contact parameter. The matrix elements are given by

$$
< n \Lambda S \Sigma' J' \Omega' I F \mid H_{mag.hfs} \mid n \Lambda S \Sigma J \Omega I F >
$$

$$
= (-1)^{J+I+F} \begin{Bmatrix} F & J & I \\ 1 & I & J' \end{Bmatrix} [I(I+1)(2I+1)(2J+1)(2J'+1)]^{\frac{1}{2}}
$$

$$
\sum_q (-1)^{J'-\Omega'} \begin{pmatrix} J' & 1 & J \\ -\Omega' & q & \Omega \end{pmatrix} \left[a \Lambda \, \delta_{\Sigma'\Sigma} \, \delta_{\Omega'\Omega} \right.
$$

$$
+ a_c (-1)^{S-\Sigma'} \begin{pmatrix} S & 1 & S \\ -\Sigma' & q & \Sigma \end{pmatrix} [S(S+1)(2S+1)]^{\frac{1}{2}}
$$

$$
+ \frac{1}{3} (30)^{\frac{1}{2}} c (-1)^q (-1)^{S-\Sigma'} \begin{pmatrix} S & 1 & S \\ -\Sigma' & q & \Sigma \end{pmatrix} \begin{pmatrix} 1 & 2 & 1 \\ -q & 0 & q \end{pmatrix}
$$

$$
\left. [S(S+1)(2S+1)]^{\frac{1}{2}} \right] \tag{2.160}
$$

In a linear molecule, the charge distribution is symmetric around the molecular axis; the electric quadrupole interaction becomes

$$
H_Q = e \, T_0^2(Q) \cdot T_0^2(\nabla E) \tag{2.161}
$$

and the matrix elements are

$$\langle \eta_. \Lambda S \Sigma J' \Omega I F \mid H_Q \mid \eta_. \Lambda S \Sigma J \Omega I F \rangle$$

$$= \frac{1}{4} e q_0 Q \begin{pmatrix} I & 2 & I \\ -I & 0 & I \end{pmatrix}^{-1} \quad (-1)^{J+I+F} \begin{Bmatrix} F & J & I \\ 2 & I & J' \end{Bmatrix}$$

$$[(2J+1)(2J'+1)]^{\frac{1}{2}} \quad (-1)^{J'-\Omega} \begin{pmatrix} J' & 2 & J \\ -\Omega' & 0 & \Omega \end{pmatrix} \qquad (2.162)$$

where $q_0 = e q = e \langle \nabla E_{zz} \rangle$ which is the expectation value of the zz component of the electric field gradient tensor at the nucleus produced by the electrons.

Chapter 3

High Order Spin Contributions to the

Isotropic Hyperfine Hamiltonian in High

Multiplicity Σ Electronic States

A. Introduction

The nuclear hyperfine structure of an open-shell molecule is dominated by interactions between the nuclear spin magnetic moments and the electron spin and orbital magnetic moments (1). The two principal interactions between an electron spin $\underset{\sim}{S}$ and a nuclear spin $\underset{\sim}{I}$ are the isotropic, or Fermi contact, interaction, which has the operator form $\underset{\sim}{I} \cdot \underset{\sim}{S}$ (2), and the dipolar interaction, with operator form $[3(\underset{\sim}{I} \cdot \underset{\sim}{r})(\underset{\sim}{S} \cdot \underset{\sim}{r}) - (\underset{\sim}{I} \cdot \underset{\sim}{S})r^2]r^{-5}$, which corresponds to the interaction between the two particles treated as tiny bar magnets whose separation is given by the vector $\underset{\sim}{r}$. The Fermi contact interaction is proportional to $\psi^2(0)$, the probability of finding the electron at the nucleus, and is therefore particularly large when unpaired electrons occupy σ m.o.'s derived from s atomic orbitals in the l.c.a.o. description. When the unpaired electrons possess orbital angular momentum their orbital magnetic moments also interact with the nuclear spin magnetic moments, producing an operator of the form $\underset{\sim}{I} \cdot \underset{\sim}{L}$ (1,3). The much smaller hyperfine effects that are familiar in closed shell molecules, and which do not depend on the presence of unpaired electrons, are of course still present in open-shell molecules; these include electric quadrupole interactions for nuclei with $I \geqslant 1$, nuclear spin-rotation interactions and couplings between two or more nuclei.

So far the hyperfine structure in gaseous open-shell molecules has only been studied extensively for doublet and triplet electronic states. States of quartet and higher multiplicity are quite rare, and high resolution spectra have only been obtained for such states in diatomic molecules; as a result not much information on their hyperfine structure is available (4). The aim of this chapter is to point out that higher

order magnetic hyperfine interactions are required for a full description of states of quartet and higher multiplicity, and that the largest of these is a third-order cross term between the spin-orbit interaction and the isotropic hyperfine operator. A second independently-determinable isotropic hyperfine parameter arises, whose existence is required by group theory arguments.

Recent sub-Doppler optical spectra of the $C^4\Sigma^-$ state of VO (4) have shown the need for this second isotropic parameter, and it should obviously be included in accurate work on all Σ states where $S \geqslant 3/2$. There is a close parallel between the new hyperfine parameter and the second spin-rotation interaction parameter, originally introduced for $^4\Sigma$ states by Hougen (6), and discussed in more detail by Brown and Milton (7); it will be shown that the mechanisms for their appearance are very similar, and that their qualitative effects on the level structure are analogous.

B. Isotropic hyperfine interaction in the third-order effective Hamiltonian

When unseen electronic states are causing perturbations that affect every level of a vibronic state whose structure is to be analysed, it is often convenient to set up an effective Hamiltonian (8) which has matrix elements acting only within the state of interest. All the parameters determined by least squares are effective, but the problem of determining them is separated from the problem of interpreting them. A convenient procedure for setting up the effective Hamiltonian, based on degenerate perturbation theory, has been described by Miller (9). The Hamil-

tonian is divided into a zero-order part that is independent of the spin contributions, and a perturbing Hamiltonian, which for the purposes of this work can be taken as (7)

$$V = H_{rotation} + H_{spin-orbit} + H_{spin-spin} + H_{spin-rotation}$$
$$+ H_{magnetic\ hfs} \qquad (3.1)$$

The effective Hamiltonian consists of the zero-order part, plus additional terms, which, up to third order, from eq. (2.87), read

$$H_{eff}{}^{(1)} = P_0 V P_0$$

$$H_{eff}{}^{(2)} = P_0 V (Q_0/a) V P_0 \qquad (3.2)$$

$$H_{eff}{}^{(3)} = P_0 V (Q_0/a) V (Q_0/a) V P_0$$
$$- \frac{1}{2}[P_0 V (Q_0/a^2) V P_0 V P_0 + P_0 V P_0 V (Q_0/a^2) V P_0]$$

where the perturbing Hamiltonian V is that part of the total Hamiltonian giving matrix elements off diagonal in vibronic state, and

$$P_0 = \sum_k |1_0 k><1_0 k|$$
$$(Q_0/a^n) = \sum_{1 \neq 1_0} \sum_k \frac{|1k><1k|}{(E_0-E_1)^n} \qquad (3.3)$$

In eq. (3.3) the symbol 1 refers to any vibronic state, including the state of interest (which is given the special symbol 1_0), and k stands for all the rotational and spin quantum numbers for the sub-levels making up a vibronic state .

Since this study is concerned with hyperfine effects in Σ electronic states we shall write the perturbing Hamiltonian as

$$V = B(\underset{\sim}{J}-\underset{\sim}{S})^2 + \sum_i a_i \underset{\sim}{l}_i \cdot \underset{\sim}{s}_i + \tfrac{2}{3}\lambda(3S_z^2 - \underset{\sim}{S}^2) + \gamma(\underset{\sim}{J}-\underset{\sim}{S}) \cdot \underset{\sim}{S}$$

$$+ \sum_i b_i \underset{\sim}{I} \cdot \underset{\sim}{s}_i + \sum_i c_i I_z s_{iz} \tag{3.4}$$

where the terms correspond to the way in which eq. (3.1) is written. All the coefficients in eq. (3.4) are assumed to be functions of internuclear distance, and it is further assumed that i electrons are present, but only one spinning nucleus, which has spin I.

When the additional terms in the effective Hamiltonian, eq. (3.2), are computed, the largest of the higher order terms are centrifugal distortion corrections to the rotational energy and the spin energies, and corrections to all of the main parameters resulting from transformation of off-diagonal elements of the spin-orbit interaction. For the hyperfine structure the largest corrections can be shown, by order-of-magnitude considerations, to be cross-terms between the spin-orbit interaction and the isotropic hyperfine interaction, because in general the spin-orbit parameters a_i for the various electrons are larger than the rotational constant B, and the isotropic hyperfine parameters b_i are larger than the dipolar parameters c_i when s electrons are considered. From here on we can omit the spin-spin and spin-rotation interactions (the terms in λ and γ, respectively) because they are very much smaller than the effects of the spin-orbit interaction.

Qualitative arguments based on perturbation theory show that the first cross-terms that give additional hyperfine interactions in Σ electronic states arise in third order. For instance, if the off-diagonal elements of V are treated directly by second order perturbation theory, and the spin-orbit and isotropic hyperfine operators are approximated as $\underset{\sim}{L}\cdot\underset{\sim}{S}$ and $\underset{\sim}{S}\cdot\underset{\sim}{I}$ respectively, the second order cross-term essentially has the form

$$\langle 1_0 k | \underset{\sim}{L}\cdot\underset{\sim}{S} | 1k'\rangle\langle 1k' | \underset{\sim}{S}\cdot\underset{\sim}{I} | 1_0 k''\rangle / \Delta E_{1_0 1}$$

using the notation of eq. (3.3). Even without writing explicit matrix elements it can be seen that this is equivalent to the results of having an effective operator $H_{eff}^{(2)}$ of the type $\underset{\sim}{L}\cdot\underset{\sim}{I}$ acting within the state of interest, 1_0. An operator $\underset{\sim}{L}\cdot\underset{\sim}{I}$, or $\underset{\sim}{I}\cdot\underset{\sim}{L}$, must have zero matrix elements within a Σ electronic state, because the value of Λ is zero. In third order one of the cross-terms given by perturbation theory has the form

$$\langle 1_0 k | \underset{\sim}{S}\cdot\underset{\sim}{L} | 1k'\rangle\langle 1k' | \underset{\sim}{L}\cdot\underset{\sim}{S} | 1'k''\rangle\langle 1'k'' | \underset{\sim}{S}\cdot\underset{\sim}{I} | 1_0 k'''\rangle / \Delta E^2$$

which has the same effect as if an operator $H_{eff}^{(3)}$ of the type $\underset{\sim}{S}\cdot\underset{\sim}{I}$ (or $\underset{\sim}{I}\cdot\underset{\sim}{S}$) were acting within the state of interest, 1_0. It will be shown below that this third order effective operator $H_{eff}^{(3)}$ contains a part which is exactly equivalent to the first order isotropic hyperfine interaction, and a part which has a slightly different dependence on the spin quantum numbers; in qualitative terms the difference between the two parts is connected to the relationship between k and k'''. The first part of $H_{eff}^{(3)}$ is incorporated into the first order hyperfine interaction,

but the second part gives the new hyperfine effect which appears for states with $S \geqslant 3/2$.

The exact form of this third-order interaction is most easily derived using spherical tensor algebra. We choose a Hund's case (a_β) basis, $|n\Lambda S\Sigma J\Omega IF\rangle$, because it is an advantage to have as many of the electronic angular momenta as possible with well-defined eigenvalues for their molecule-fixed z-components. The symbols in this basis are well-known; n stands for the vibronic state, and the others are all familiar diatomic molecule quantum numbers (10). Translating the operators of eq. (3.4) into spherical tensor form, we have

$$H_{\text{spin-orbit}} = \sum_i T^1(a_i l_i) \cdot T^1(s_i)$$

$$H_{\text{isotropic hfs}} = \sum_i b_i T^1(I) \cdot T^1(s_i)$$

$$(3.5)$$

Their matrix elements, in Hund's case (a_β), are

$$\langle n\Lambda S\Sigma J\Omega IF|H_{\text{spin-orbit}}|n'\Lambda'S'\Sigma'J\Omega IF\rangle = \sum_q (-1)^q (-1)^{S-\Sigma} \begin{pmatrix} S & 1 & S' \\ -\Sigma & q & \Sigma' \end{pmatrix}$$

$$\times \sum_i \langle S||T^1(s_i)||S'\rangle\langle n\Lambda|T^1_{-q}(a_i l_i)|n'\Lambda'\rangle \qquad (3.6)$$

$$\langle n\Lambda S\Sigma J\Omega IF|H_{\text{isotropic hfs}}|n'\Lambda S'\Sigma'J'\Omega'IF\rangle = (-1)^{I+J'+F} \begin{Bmatrix} F & J & I \\ 1 & I & J' \end{Bmatrix}$$

$$\times [I(I+1)(2I+1)(2J+1)(2J'+1)]^{\frac{1}{2}} \sum_q (-1)^{J-\Omega} \begin{pmatrix} J & 1 & J' \\ -\Omega & q & \Omega' \end{pmatrix} \qquad (3.7)$$

$$\times (-1)^{S-\Sigma} \begin{pmatrix} S & 1 & S' \\ -\Sigma & q & \Sigma' \end{pmatrix} \sum_i \langle S||T^1(s_i)||S'\rangle\langle n\Lambda S|b_i|n'\Lambda S'\rangle$$

The final terms in each of these expressions are parameters that in principle can be evaluated experimentally, and can be computed by __ab initio__ methods. Both expressions obey the selection rule $\Delta S = 0, \pm 1$, as a result of the microscopic form of the electron spin operators; in addition the isotropic hyperfine operator is diagonal in Λ, but the spin-orbit operator follows $\Delta \Lambda = 0, \pm 1$.

When we substitute the matrix elements of eq. (3.6) into the expression for $H_{eff}^{(3)}$ given in eq. (3.2) we get nine terms, because there are three parts to $H_{eff}^{(3)}$, and three ways of permuting the operators of eq. (3.6) remembering that $H_{spin-orbit}$ must be taken twice. There is no need to write out any of these terms because the substitution is entirely straightforward. Many common factors occur in all nine because they are constructed similarly, and closer examination shows that they can be collapsed to five different types of term, which must be evaluated separately. Table 3.1 summarizes the properties of these five types.

It is apparent that the quantum numbers S and Σ for the distant perturbing electronic states occur in the matrix elements of the third order effective Hamiltonian, but they must not appear explicitly in the final expressions because the effective Hamiltonian is assumed to act only within the vibronic state of interest. It is therefore necessary to use relationships between the Wigner coefficients to sum over these quantum numbers as far as possible, and to cast them into the form of an experimental parameter or parameters. We follow Brown and Milton (7), who encountered a similar problem in their discussion of higher order spin-rotation interactions in multiplet Σ states, and solved it by applying the relation in eq. (2.112).

Table 3.1 The five types of term contributing to the third-order isotropic hyperfine interaction.

	Initial state	Operator	First intermediate state	Operator	Second intermediate state	Operator	Final state	Energy denominator
1	$S\Lambda$	s.o.	$S'\Lambda'$	iso	$S'\Lambda'$	s.o.	$S\Lambda$	$(E_0-E_1)(E_0-E_2)$
		s.o.	$S'\Lambda'$	iso	$S\Lambda'$	s.o	$S\Lambda$	
		s.o.	$S\Lambda'$	iso	$S'\Lambda'$	s.o.	$S\Lambda$	
2	$S\Lambda$	s.o.	$S'\Lambda'$	s.o.	$S'\Lambda'$	iso	$S\Lambda$	$(E_0-E_1)(E_0-E_2)$
		iso	$S'\Lambda'$	s.o.	$S'\Lambda'$	s.o.	$S\Lambda$	
3	$S\Lambda$	s.o.	$S\Lambda'$	s.o.	$S'\Lambda$	iso	$S\Lambda$	$(E_0-E_1)(E_0-E_2)$
		iso	$S'\Lambda$	s.o.	$S\Lambda'$	s.o.	$S\Lambda$	
4	$S\Lambda$	s.o.	$S'\Lambda'$	s.o.	$S\Lambda$	iso	$S\Lambda$	$(E_0-E_1)^2$
5	$S\Lambda$	iso	$S\Lambda$	s.o.	$S'\Lambda'$	s.o.	$S\Lambda$	$(E_0-E_2)^2$

The operators are s.o. = spin-orbit and iso = isotropic hyperfine (see eq (3.6))

For example, in the terms of type 1 from Table 3.1 we have the product

$$\begin{pmatrix} S & 1 & S' \\ -\Sigma & q & \Sigma' \end{pmatrix} (-1)^{S'-\Sigma'} \begin{pmatrix} S' & 1 & S'' \\ -\Sigma' & q' & \Sigma'' \end{pmatrix} (-1)^{S''-\Sigma''} \begin{pmatrix} S'' & 1 & S \\ -\Sigma''-q & \Sigma''' \end{pmatrix}$$

where the single and double primes on S and Σ refer to the intermediate

states, and Σ''' refers to the final state. After two applications of

eq. (2.112) this product becomes

$$(-1)^{S''-S-q} \sum_{k,K} (2k+1)(2K+1) \begin{Bmatrix} S & S & K \\ 1 & k & S'' \end{Bmatrix} \begin{pmatrix} S & S & K \\ \Sigma & -\Sigma'''-q' \end{pmatrix} \begin{pmatrix} 1 & k & K \\ -q & q+q' & -q' \end{pmatrix}$$

$$\times \begin{Bmatrix} S'' & S & k \\ 1 & 1 & S' \end{Bmatrix} \begin{pmatrix} 1 & 1 & k \\ -q & -q' & q+q' \end{pmatrix}$$

In this expression k and K are tensor indices that arise in the successive

applications of eq. (2.112). It will be seen that nowhere do the inter-

mediate state Σ values (Σ' and Σ'') appear.

Eventually the general matrix element of the third order effective

Hamiltonian can be obtained as

$$\langle \eta \Lambda S \Sigma J \Omega I F | H_{iso}{}^{(3)} | \eta \Lambda S \Sigma''' J''' \Omega''' I F \rangle = (-1)^{J'''+I+F} \begin{Bmatrix} F & J & I \\ 1 & I & J''' \end{Bmatrix}$$

$$\times [I(I+1)(2I+1)]^{\frac{1}{2}} [(2J+1)(2J'''+1)]^{\frac{1}{2}} \sum_{q'} (-1)^{J-\Omega} \begin{pmatrix} J & 1 & J''' \\ -\Omega & q' & \Omega''' \end{pmatrix} \sum_k (-1)^{S-\Sigma} \begin{pmatrix} S & K & S \\ -\Sigma & q' & \Sigma''' \end{pmatrix}$$

$$\times \sum_{\substack{k \\ (q)}} \sum_{\substack{S'\Lambda' \\ S''}} (-1)^{S'-S}(-1)^{q}(2k+1)(2K+1) \begin{pmatrix} 1 & 1 & k \\ -q & -q' & q+q' \end{pmatrix} \begin{pmatrix} 1 & k & K \\ q & -q-q' & q' \end{pmatrix} \begin{Bmatrix} 1 & k & K \\ S & S & S'' \end{Bmatrix}$$

$$x \sum_i \langle n\Lambda | T^1_{-q}(a_i \underset{\sim}{l_i}) | n'\Lambda' \rangle \langle n'\Lambda' | T^1_q(a_i \underset{\sim}{l_i}) | n\Lambda \rangle \langle S'' || T^1(\underset{\sim}{s_i}) || S \rangle$$

$$x \left[\sum_i \langle S || T^1(\underset{\sim}{s_i}) || S' \rangle \langle S' || T^1(\underset{\sim}{s_i}) || S'' \rangle \begin{Bmatrix} 1 & 1 & k \\ S & S'' & S' \end{Bmatrix} (E^0_{n\Lambda S} - E^0_{n'\Lambda'S'})^{-1} \right.$$

$$x \; (E^0_{n\Lambda S} - E^0_{n''\Lambda'S''})^{-1} \{ \langle n\Lambda'S' | b_i | n''\Lambda'S'' \rangle (-1)^{1+k+K} + \langle n''\Lambda S'' | b_i | n\Lambda S \rangle [1+(-1)^{K+1}] \}$$

$$- \; [S(S+1)(2S+1)]^{\frac{1}{2}} \sum_i \langle S || T^1(\underset{\sim}{s_i}) || S'' \rangle \begin{Bmatrix} 1 & 1 & k \\ S & S'' & S \end{Bmatrix} (E^0_{n\Lambda S} - E^0_{n''\Lambda'S''})^{-2}$$

$$x \; \langle n\Lambda S | b_i | n\Lambda S \rangle x \frac{1}{2} [1+(-1)^{K+1}] \right] \tag{3.8}$$

The separate contributions of the five terms from Table 3.1 can be distinguished in the bracket forming the second half of eq. (3.8).

The triangle rules from the 3-j symbols limit the values that k and K can assume, such that k can be 0, 1 and 2, and K is then restricted, according to the value of k, to

$$\begin{array}{cccc} k = & 0 & 1 & 2 \\ K = & 1 & 0,1,2 & 1,2,3 \end{array}$$

It is evident that the coefficients $1+(-1)^{K+1}$ in eq. (3.8) cause most of it to vanish for even K values, and only the term with coefficient $(-1)^{1+k+K}$ coming from the type 1 terms in Table 3.1 is left. However it can be shown, by arguments similar to those used by Brown and Milton (7), that this also vanishes for K even. The procedure, in essence, is to prove, by the Biedenharn-Elliot relationship (eq. 2.113), that the terms with q=1 and -1 in the sum over q in eq. (3.8) differ by a factor $(-1)^{1+K}$; therefore they are equal and opposite for even K. The q=0 term is easily shown to be zero for even K, so that the whole sum vanishes. One of the steps in the proof requires the equality

$$<n\Lambda|T_q^1(a_i\underset{\sim}{1}_i)|n'\Lambda'> = <n'\Lambda'|T_{-q}^1(a_i\underset{\sim}{1}_i)|n\Lambda> \qquad (3.9)$$

which therefore limits the results to $\Lambda=0$, i.e. Σ states only.

The value of K can be 1 or 3 only, in consequence. Consider K=1 first. The two 3-j symbols involving k in eq. (3.8) can be contracted:

$$\sum_q \begin{pmatrix} 1 & 1 & k \\ -q & -q' & q+q' \end{pmatrix} \begin{pmatrix} 1 & k & 1 \\ q & -q-q' & q' \end{pmatrix} = \sum_q \begin{pmatrix} 1 & 1 & k \\ q & q' & -q-q' \end{pmatrix}^2 \qquad (3.10)$$

and, using the orthogonality properties of 3-j symbols [11], become

$$\sum_q \begin{pmatrix} 1 & 1 & k \\ q & q' & -q-q' \end{pmatrix}^2 = \frac{1}{3} \qquad (3.11)$$

The general matrix element reduces to

$$\langle n\Lambda S\Sigma J\Omega IF|H_{iso}^{(3)},K=1|n\Lambda S\Sigma'''J'''\Omega'''IF\rangle=(-1)^{J'''+I+F}\begin{Bmatrix}F&J&I\\1&I&J'''\end{Bmatrix}[I(I+1)(2I+1)]^{\frac{1}{2}}$$

$$\times\sum_{q'}(-1)^{J-\Omega}\begin{pmatrix}J&1&J'''\\-\Omega&q'&\Omega'''\end{pmatrix}(-1)^{S-\Sigma}\begin{pmatrix}S&1&S\\-\Sigma&q'&\Sigma'''\end{pmatrix}\Bigg\{\sum_{\substack{S'\Lambda'\\S''}}\sum_{k=0}^{2}(-1)^{S''-S}(-1)^q(2k+1)$$

$$\times\sum_i\langle n\Lambda|T_{-q}^1(a_i\underset{\sim}{l}_i)|n'\Lambda'\rangle\langle n'\Lambda'|T_q^1(a_i\underset{\sim}{l}_i)|n\Lambda\rangle\sum_i\langle S||T^1(\underset{\sim}{s}_i)||S''\rangle$$

$$\times\begin{Bmatrix}1&k&1\\S&S&S''\end{Bmatrix}\Bigg[\sum_i\langle S||T^1(\underset{\sim}{s}_i)||S'\rangle\langle S'||T^1(\underset{\sim}{s}_i)||S''\rangle\begin{Bmatrix}1&1&k\\S&S''&S'\end{Bmatrix}(E_{n\Lambda S}^0-E_{n'\Lambda'S'}^0)^{-1}$$

$$\times(E_{n\Lambda S}^0-E_{n''\Lambda'S''}^0)^{-1}\{\langle n\Lambda'S'|b_i|n\Lambda'S''\rangle(-1)^{k+1}+2\langle n''\Lambda S''|b_i|n\Lambda S\rangle\}\qquad(3.12)$$

$$-[S(S+1)(2S+1)]^{\frac{1}{2}}\sum_i\langle S||T^1(\underset{\sim}{s}_i)||S''\rangle\begin{Bmatrix}1&1&k\\S&S''&S\end{Bmatrix}(E_{n\Lambda S}^0-E_{n''\Lambda'S''}^0)^{-2}\langle n\Lambda S|b_i|n\Lambda S\rangle\Bigg]\Bigg\}$$

which can be seen, by comparison with eq. (3.7), to be exactly similar in form to the normal isotropic hyperfine matrix elements. For K=1 the third order spin-orbit interaction therefore gives a higher order contribution to the Fermi contact parameter.

The final remaining term in eq. (3.8) has K=3 and k=2. Using eq. (2.112) again, the pair of 3-j symbols involving k in eq. (3.8) can be recast into the form

$$\begin{pmatrix} 3 & 1 & 2 \\ q' & q & -q-q' \end{pmatrix} \begin{pmatrix} 1 & 1 & 2 \\ -\dot{q} & -q' & q'+q \end{pmatrix} = (-1)^{q-\acute{q}}(5) \begin{pmatrix} 3 & 1 & 2 \\ q'-q' & 0 \end{pmatrix} \begin{pmatrix} 1 & 1 & 2 \\ q & -q & 0 \end{pmatrix} \begin{Bmatrix} 3 & 1 & 2 \\ 1 & 1 & 2 \end{Bmatrix} \quad (3.13)$$

$$= (-1)^{q'} \begin{pmatrix} 3 & 1 & 2 \\ q' & -q' & 0 \end{pmatrix} (-1)^{q} \begin{pmatrix} 1 & 1 & 2 \\ q & -q & 0 \end{pmatrix} \quad (3.14)$$

where we have substituted the value

$$\begin{Bmatrix} 3 & 1 & 2 \\ 1 & 1 & 2 \end{Bmatrix} = \frac{1}{5} \quad (3.15)$$

It turns out that the 3-j symbol with q' in it is important when we carry out the transformation from case (a_β) coupling to case $(b_{\beta J})$, so that it must not be incorporated into the sum over distant states comprising the experimental parameter. The K=3 term then becomes

$$\langle n\Lambda S\Sigma J\Omega IF|H_{iso}^{(3)},K=3|n\Lambda S\Sigma'''J'''\Omega'''IF\rangle = (-1)^{J'''+I+F} \begin{Bmatrix} F & J & I \\ 1 & I & J''' \end{Bmatrix} [I(I+1)(2I+1)]^{\frac{1}{2}}$$

$$\times [(2J+1)(2J'''+1)]^{\frac{1}{2}} \sum_{q'} (-1)^{J-\Omega} \begin{pmatrix} J & 1 & J''' \\ -\Omega & q' & \Omega''' \end{pmatrix} (-1)^{S-\Sigma} \begin{pmatrix} S & 3 & S \\ -\Sigma & q' & \Sigma''' \end{pmatrix}$$

$$\times (-1)^{q'} \begin{pmatrix} 3 & 1 & 2 \\ q' & -q' & 0 \end{pmatrix} \left[35 \sum_{S'\Lambda'S''} \sum_{q} (-1)^{S'-S} \begin{pmatrix} 1 & 1 & 2 \\ q & -q & 0 \end{pmatrix} \langle n\Lambda|T_q^1(a_i l_i)|n'\Lambda'\rangle \right.$$

$$\times \langle n'\Lambda'|T_{-q}^1(a_i l_i)|n\Lambda\rangle \sum_i \langle S||T^1(s_i)||S'\rangle \begin{Bmatrix} 1 & 2 & 3 \\ S & S & S'' \end{Bmatrix} [\sum_i \langle S||T^1(s_i)||S'\rangle$$

$$x \; <S'||T^1(\underset{\sim i}{s})||S''> \; \begin{Bmatrix} 1 & 1 & 2 \\ S & S'' & S' \end{Bmatrix} \; (E^0_{n\Lambda S} - E^0_{n'\Lambda'S'})^{-1} \; (E^0_{n\Lambda S} - E^0_{n''\Lambda'S''})^{-1}$$

$$\{<n\Lambda'S'|b_i|n''\Lambda S''> + 2<n''\Lambda S''|b_i|n\Lambda S>\} \; -[S(S+1)(2S+1)]^{\frac{1}{2}} \sum_i <S||T^1(\underset{\sim i}{s})||S''>$$

$$\begin{Bmatrix} 1 & 1 & 2 \\ S & S'' & S \end{Bmatrix} \; (E^0_{n\Lambda S} - E^0_{n''\Lambda'S''})^{-2} \; <n\Lambda S|b_i|n\Lambda S> \Big] \tag{3.16}$$

Eq. (3.6) represents a new type of hyperfine interaction matrix element, which, as can be seen from the properties of the second 3-j symbol, is non-vanishing for electronic states where $S \geq 3/2$. The form of eq. (3.16) is somewhat similar to the isotropic hyperfine matrix element given in eq. (3.6); the differences are that the reduced spin matrix element appears in another place, and that the simple matrix element of b_i is replaced by the complicated expression between the large brackets which becomes the experimental parameter.

Our definition of the new experimental parameter has been chosen with the analogy between it and Brown and Milton's second spin-rotation parameter γ_S (7) in mind. Not surprisingly, since the mechanisms for their appearance are similar, the analogy between the two parameters is very close. To make the analogy as close as possible we name the new parameter b_S, and define it as

$$b_S = -4(3/35)^{\frac{1}{2}}[(2S-2)(2S-1)2S(2S+1)(2S+2)(2S+3)(2S+4)]^{-\frac{1}{2}}t \tag{3.17}$$

where t is the complicated expression in large brackets in eq. (3.16). The reason for the peculiar numerical factor will become apparent when we consider the matrix elements in case $(b_{\beta J})$ coupling in the next Section.

Table 3.2 Matrix elements of the third order isotropic hyperfine interaction in a Hund's case (a_β) basis

$$\langle \eta\Lambda S \Sigma J\Omega I F | H_{iso}^{(3)} | \eta\Lambda S\Sigma J\Omega I F\rangle = -b_S \frac{\Omega\Sigma[F(F+1)-I(I+1)-J(J+1)][3S(S+1)-5\Sigma^2-1]}{2J(J+1)}$$

$$\langle \eta\Lambda S \Sigma J\Omega I F | H_{iso}^{(3)} | \eta\Lambda S\Sigma,J-1,\Omega I F\rangle = b_S \frac{\Sigma(J^2-\Omega^2)^{\frac{1}{2}}[(F+I+J+1)(I+J-F)(F+J-I)(F+I-J+1)]^{\frac{1}{2}}[3S(S+1)-5\Sigma^2-1]}{2J(4J^2-1)^{\frac{1}{2}}}$$

$$\langle \eta\Lambda S \Sigma J\Omega I F | H_{iso}^{(3)} | \eta\Lambda S,\Sigma\pm1,J,\Omega\pm1,I F\rangle = -b_S \frac{[J(J+1)-\Omega(\Omega\pm1)]^{\frac{1}{2}}[S(S+1)-\Sigma(\Sigma\pm1)]^{\frac{1}{2}}}{4J(J+1)}$$

$$\times \ [F(F+1)-I(I+1)-J(J+1)][S(S+1)-5\Sigma(\Sigma\pm1)-2]$$

$$\langle \eta\Lambda S \Sigma J\Omega I F | H_{iso}^{(3)} | \eta\Lambda S,\Sigma\pm1,J-1,\Omega\pm1,I F\rangle = \pm b_S \frac{[(J\mp\Omega)(J\mp\Omega-1)]^{\frac{1}{2}}}{4J(4J^2-1)^{\frac{1}{2}}} [S(S+1)-\Sigma(\Sigma\pm1)]^{\frac{1}{2}}$$

$$\times \ [(F+I+J+1)(I+J-F)(F+J-I)(F+I-J+1)]^{\frac{1}{2}}[S(S+1)-5\Sigma(\Sigma\pm1)-2]$$

The phase choice for the rotational wave functions follows that of Brown and Howard (14) or Carrington, Dyer and Levy (19), based on Condon and Shortley's conventions (20).

On substituting eq. (3.17) into eq. (3.16), and writing explicit expressions for the Wigner coefficients, the matrix elements of the third order isotropic hyperfine interaction in case (a_β) coupling can be obtained; they are listed in Table 3.2.

C. Transformation to case $(b_{\beta J})$ coupling

Of the various $^4\Sigma$ states known, only two, those in GeF (12) and SnH (13), show marked departures from case (b) coupling. Therefore, despite the logical preference among diatomic spectroscopists for calculating energy levels in a Hund's case (a) basis, it is instructive to look at the form of the matrix elements in case (b) coupling, because the diagonal elements show directly how the parameter affects the level structure in a real situation.

With the case (b) functions given in terms of case (a) functions (14) by

$$|N\Lambda SJ> = \sum_{\Sigma,\Omega} (-1)^{N-S+\Omega} (2N+1)^{\frac{1}{2}} \begin{pmatrix} J & S & N \\ \Omega & -\Sigma & -\Lambda \end{pmatrix} |\Lambda S\Sigma J\Omega> \qquad (3.18)$$

we obtain

$$<N\Lambda SJIF|H_{iso}^{(3)}, K=3|N'\Lambda'SJ'IF> = t.(-1)^{I+J'+F} \begin{Bmatrix} F & J & I \\ 1 & I & J' \end{Bmatrix} [I(I+1)(2I+1)]^{\frac{1}{2}}$$

$$\times \sum_{\Sigma,\Omega} \sum_{\Sigma'\Omega'} (-1)^{N-S+\Omega+N'-S+\Omega'} [(2N+1)(2N'+1)]^{\frac{1}{2}} \begin{pmatrix} J & S & N \\ \Omega & -\Sigma & -\Lambda \end{pmatrix} \begin{pmatrix} J' & S & N' \\ \Omega' & -\Sigma' & \Lambda' \end{pmatrix}$$

$$[(2J+1)(2J'+1)]^{\frac{1}{2}} \tag{3.19}$$

$$x \sum_{q'} (-1)^{J-\Omega} \begin{pmatrix} J & 1 & J' \\ -\Omega & q' & \Omega' \end{pmatrix} (-1)^{S-\Sigma} \begin{pmatrix} S & 3 & S \\ -\Sigma & q' & \Sigma' \end{pmatrix} (-1)^{q'} \begin{pmatrix} 3 & 1 & 2 \\ q' & -q' & 0 \end{pmatrix}$$

(where we have replaced the triple primes of eq. (3.16) by single primes).
After some rearrangement (which by happy chance eliminates virtually all
the phase factors) we can contract the sum over the product of five 3-j
symbols to an expression involving a 9-j symbol (15); remembering that
Λ and Λ' are restricted to the value 0 we finally get

$$<NSJIF|H_{iso}^{(3)},K=3|N'SJ'IF> = \frac{1}{4}(35/3)^{\frac{1}{2}}b_S \cdot (-1)^{I+J'+F} \begin{Bmatrix} F & J & I \\ 1 & I & J' \end{Bmatrix}$$

$$x \; [I(I+1)(2I+1).(2J+1)(2J'+1).(2N+1)(2N'+1).(2S-2)(2S-1)2S(2S+1)(2S+2)$$

$$(2S+3)(2S+4)]^{\frac{1}{2}} \quad (-1)^N \begin{pmatrix} N & 2 & N' \\ 0 & 0 & 0 \end{pmatrix} \begin{Bmatrix} N & N' & 2 \\ S & S & 3 \\ J & J' & 1 \end{Bmatrix} \tag{3.20}$$

which is the desired result. These 9-j symbols are unfortunately not
listed in standard tabulations (16), and give very cumbersome algebraic
expressions, but vast amounts of cancelling occur in the evaluation of
actual matrix elements, so that quite simple expressions are finally ob-
tained. Our algebraic forms for the 9-j symbols are given in ref. (5).

We do not list general forms for the matrix elements of eq. (3.20), but give merely the diagonal elements for a $^4\Sigma$ state. It is useful to include the diagonal elements of the isotropic hyperfine interaction b $\underline{I}\cdot\underline{S}$ in these expressions:

$$F_1(J=N+\tfrac{3}{2}): \quad \tfrac{3}{2}C[b-b_SN/(2N+3)]/(2N+3)$$

$$F_2(J=N+\tfrac{1}{2}): \quad \tfrac{1}{2}C[b(2N+9)+3b_S\{(3N+2)+3/(2N+3)\}]/[(2N+1)(2N+3)]$$

$$F_3(J=N-\tfrac{1}{2}): \quad -\tfrac{1}{2}C[b(2N-7)+3b_S\{(3N+1)+3/(2N-1)\}]/[(2N-1)(2N+1)]$$

$$F_4(J=N-\tfrac{3}{2}): \quad -\tfrac{3}{2}C[b-b_S(N+1)/(2N-1)]/(2N-1)$$

(3.21)

where

$$C=F(F+1)-I(I+1)-J(J+1)$$

(3.22)

It can be seen how when N is large, so that similar powers of N can be cancelled, these expressions simplify so that there is one effective b parameter for the F_1 and F_4 levels and another effective b parameter for the F_2 and F_3 levels:

$$F_1 \text{ and } F_4: b_{eff}\cong b-\tfrac{1}{2}b_S; \quad F_2 \text{ and } F_3: b_{eff}\cong b+\tfrac{9}{2}b_S$$

(3.23)

The 3-j symbol and its phase factor in eq. (3.20), if the values of Λ and Λ' are left unspecified, are actually $(-1)^{N-\Lambda}\begin{pmatrix} N & 2 & N \\ -\Lambda & q & \Lambda' \end{pmatrix}$, which, when the normalization factor $[(2N+1)(2N'+1)]^{\tfrac{1}{2}}$ is included, is the reduced matrix element of the second rank rotation matrix (17):

$$\langle N\Lambda | | D^{(2)*}_{\cdot q}(\omega) | | N'\Lambda' \rangle = (-1)^{N-\Lambda}[(2N+1)(2N'+1)]^{\frac{1}{2}} \begin{pmatrix} N & 2 & N' \\ -\Lambda & q & \Lambda' \end{pmatrix} \tag{3.24}$$

This suggests that it is possible to devise an equivalent operator, acting within the manifold of a given vibrational level of a multiplet Σ electronic state, which has the same matrix elements as eq. (3.20) but which gives a different perspective on how the new hyperfine interaction operator is constructed.

After some experimentation the equivalent operator was found to be

$$H_{iso}^{(3)}, K=3 \equiv \sum_{i>j} T^1(\underset{\sim}{I}) \cdot T^1[T^3\{T^1(\underset{\sim}{S}), T^2(\underset{\sim}{s_i}, \underset{\sim}{s_j})\}, C^2]/r_{ij}^3 \tag{3.25}$$

where i and j are electrons, r_{ij} is their separation and C^2 is related to the spherical harmonic giving their relative polar coordinates,

$$C_q^2 = (4\pi/5)^{\frac{1}{2}} Y_{2q}(\theta,\phi) \tag{3.26}$$

The matrix elements of eq. (3.25) are identical to those of eq. (3.20) except that they are given in terms of a parameter $T_0^2(C)$, which must be expressed in terms of b_S, according to

$$b_S = (3/10) T_0^2(C)/(14)^{\frac{1}{2}} \tag{3.27}$$

The derivation of the matrix elements of eq. (3.25) is interesting because it involves a number of widely-occurring electron spin reduced matrix elements, several of which appear not to have been given in general form (though some explicit expressions have been given by Brown and Merer (18).

In order to interpret the parameter b_S according to eq. (3.16), or to obtain expressions for the Λ-doubling parameters, o, p and q, in terms of the spin-orbit matrix elements for high multiplicity states (18), it is useful to have these general forms. Accordingly the derivation of the matrix elements of eq. (3.25) is given in Appendix III.

The operator form of eq. (3.25) shows exactly how the effective operator for the new third-order cross-term is constructed. In Cartesian tensor notation it consists of a sum of terms of the type $I_\alpha S_\beta S_\gamma S_\delta$; the advantage of the spherical tensor form is readily appreciated.

Exactly similar expressions to eq. (3.21) are found to hold for Brown and Milton's γ_S parameter (7). The transformation of the case (a) matrix given in ref. (7) to case (b) coupling is rather more messy than the transformation of eq. (3.19) to eq. (3.20) because now there is only a partial sum over the index q´ (which cannot take the value zero since the spin-uncoupling operator is $-2B(J_x S_x + J_y S_y)$ rather than $-2B \underset{\sim}{J} \cdot \underset{\sim}{S}$ so that the q´=0 component is missing). After some algebra we find

$$\langle NSJ|H^{(3)}_{spin\text{-}rotation}, K=3|N´SJ\rangle = \tfrac{1}{4}(2/3)^{\frac{1}{2}} \gamma_S [(2N+1)(2N´+1) \cdot J(J+1)(2J+1)]^{\frac{1}{2}}$$

$$\times \; [(2S-2)(2S-1)2S(2S+1)(2S+2)(2S+3)(2S+4)]^{\frac{1}{2}}$$

$$\times \sum_{z=2,4} (2z+1) \begin{pmatrix} 3 & z & 1 \\ -1 & 0 & 1 \end{pmatrix} (-1)^N \begin{pmatrix} N & z & N´ \\ 0 & 0 & 0 \end{pmatrix} \begin{Bmatrix} N & N´ & z \\ S & S & 3 \\ J & J & 1 \end{Bmatrix} \qquad (3.28)$$

As explained in ref. (5) the matrix elements are more easily obtained by an algebraic transformation of the case (a) matrix rather than directly from eq. (3.28) because of the complexity of the 9-j symbols. Corresponding to eq. (3.21) we have

$$F_1(J=N+\tfrac{3}{2}): \quad \tfrac{3}{2}[\gamma-\gamma_S(N+1)/(2N+3)]N$$

$$F_2(J=N+\tfrac{1}{2}): \quad \tfrac{1}{2}[\gamma(N-3)+3\gamma_S N(3N+5)/(2N+3)]$$

$$F_3(J=N-\tfrac{1}{2}): \quad -\tfrac{1}{2}[\gamma(N+4)+3\gamma_S(N+1)(3N-2)/(2N-1)]$$

$$F_4(J=N+\tfrac{3}{2}): \quad -\tfrac{3}{2}[\gamma-\gamma_S N/(2N-1)](N+1)$$

$$(3.29)$$

which simplifies for high N to

$$F_1 \text{ and } F_4: \gamma_{eff} \cong \gamma-\tfrac{1}{2}\gamma_S; \quad F_2 \text{ and } F_3: \gamma_{eff} \cong \gamma+\tfrac{9}{2}\gamma_S \qquad (3.30)$$

The points we make in this section are (i) that by choosing the numerical factor as in eq. (3.17) we can define the new hyperfine parameter b_S so that eqs. (3.23) and (3.30) have exactly the same form, and (ii) that the case (b) expressions show how the third order isotropic hyperfine term and the third-order spin-rotation term both act in the same way, which is to give the F_1 and F_4 levels different effective parameters from the F_2 and F_3 levels in a $^4\Sigma$ state. In addition it is possible to derive the form of the effective operator, acting entirely within the manifold of the Σ electronic state, which is equivalent to the third-order isotropic hyperfine term.

D. Conclusion

This chapter gives the background theory for the new hyperfine parameter b_S which had to be introduced by Cheung et al (5) to explain the

hyperfine structure of the $C^4\Sigma^-$ state of VO measured by sub-Doppler laser-induced fluorescence. The new parameter is a third-order cross-term between the spin-orbit interaction and the familiar isotropic hyperfine interaction, and, like the corresponding spin-rotation effect (7), must be included in accurate work on all electronic Σ states of quartet and higher multiplicity. The new effect will be especially large if there are nearby states that interact strongly through the spin orbit operator with the state of interest; therefore it will probably be more important in the excited electronic states of high multiplicity molecules than in their ground states, since ground states are often well separated from other interacting electronic states.

The new term in b_S is in fact required for all electronic states of quartet and higher multiplicity, not just Σ states. The reason is that no approximations have been made in its derivation which limit the value of Λ (or K for polyatomic molecules), so that eqs. (3.16) and (3.17) for case (a) coupling, or eqs. (3.20) and (3.24) for case (b) coupling, are entirely general. The only restriction to Σ electronic states is in eq. (3.9), which was invoked to prove that the terms involving the tensor ranks K=0 and 2 vanish for $\Lambda=0$. We have not investigated the consequences of not invoking eq. (3.9), but qualitatively it seems that the K=2 terms should give rise to a higher order contribution to one of the other hyperfine operators, probably a $\underset{\sim}{I}\cdot\underset{\sim}{L}$, which is non-vanishing when $\Lambda\neq0$

Chapter 4

Laser Induced Fluorescence Spectroscopy

A. Introduction

The advent of high power monochromatic tunable laser sources has stimulated important advances in optical spectroscopy as documented by several recent reviews (1 - 4).

Laser induced fluorescence (which will be taken here to mean the process whereby a molecule absorbs laser light at one wavelength and emits some fraction of the energy as light at the same and other wavelengths) is a much more sensitive technique than absorption spectroscopy (5). The ratio of $(S/N)_{abs}$ and $(S/N)_{fluor}$, where S/N means signal-to-noise ratio, is proportional to the noise equivalent power of the detector, NEP, and the fourth power of the fluorescence wavelength. As the fluorescence wavelength decreases, fluorescence detection is increasingly favored. In regions where photomultipler tubes can be used, the NEP drops considerably and fluorescence detection becomes even more favorable. Consequently, most laser experiments done in those regions use fluorescence detection techniques.

The highest resolution in optical spectroscopy is achieved by eliminating the Doppler broadening of atomic and molecular spectral lines. The high intensity of laser light has led to the development of a variety of new nonlinear spectroscopic techniques which permit Doppler-free observations of a simple gas sample. Saturated absorption spectroscopy or Lamb dip spectroscopy (6,7) was the earliest developed and perhaps the most widely used of these methods; here the spread of atomic velocities along the direction of observation is effectively reduced by velocity-selective bleaching and probing with two counter-propagating monochromatic laser beams. Saturated fluorescence spectros-

copy (8) and in particular the sensitive technique of intermodulated fluorescence (9) extended the potential of this method to optically very thin fluorescent samples.

In this chapter, various effects related to laser experiments will be discussed; they include (i) non-linear interactions of molecules with a very intense laser beam to produce saturation effects, (ii) observation of excitation spectra (which are essentially absorption spectra provided no radiationless process is occurring) by monitoring the total fluorescence, and (iii) the use of saturation effects to study atomic or molecular lines without Doppler broadening. Moreover, the experimental techniques of intermodulated fluorescence and resolved fluorescence will also be considered; the former yields line positions to very high precision (1 part in 10^8), while the latter gives relationships between lines which permit unambiguous rotational assignment.

B. Saturation of Molecular Absorption Lines

In light absorption experiments at "conventional" low power levels Beer's law states that the absorbed power is a constant fraction of the incident power. This linear relationship holds only if the incident power is low. In contrast, intense coherent light sources, which are capable of supplying very high power densities, and hence a very strong optical electric field, can generate a wealth of non-linear phenomena as a result of the dielectric polarization of the absorbing medium by the intense field.

The order of magnitude of the optical electric field $\underset{\sim}{\varepsilon}$ required to produce non-linear effects can be obtained from Heisenberg's uncertainty

principle

$$\mu\varepsilon \cdot \tau \gtrsim \hbar \qquad (4.1)$$

In this expression μ is the electric dipole matrix element for the transition, τ the relaxation time and $\hbar$ (= Planck's constant h, divided by 2π) $\sim 10^{-34}$ J.s. A laser power of 1 W through a cross-section of 0.1 cm^2 (typical beam size) gives a power density of 10^5 Wm^{-2} and produces an electric field of $\varepsilon \sim 10^4$ NC^{-1}, so that a power of 1 μW gives $\varepsilon \sim 10$ NC^{-1} (since power density is proportional to the square of the electric field). Therefore, a laser power of 10^{-6} to 1 W is adequate to observe non-linear effects in molecules with $\mu = 1$ D and a relaxation time of 10^{-5} to 10^{-8} s. A rotational relaxation time of this magnitude is typical at a gas pressure of 10^{-3} to 1 torr (10).

Let us consider the behavior of an isolated system with two energy levels, E_1 and E_2, under the action of an electromagnetic field. The behaviour of the system, that is its wavefunction Ψ, is described by the time-dependent Schrödinger equation,

$$i\hbar \frac{\partial \Psi}{\partial t} = H\Psi \qquad (4.2)$$

where H is the total hamiltonian of the system, composed of the unperturbed hamiltonian H_0 and the energy of the quantum system-field interaction, or, more specifically in this case, the electric dipole interaction between particle and field, which has the form

$$H' = -\mu \cdot \varepsilon$$
$$H = H_0 + H'$$
$$= H_0 - \mu \cdot \varepsilon \cos \omega t \qquad (4.3)$$

In eq. (4.3) μ is the component of the molecular dipole moment along the direction of the field, ε is the strength of the electric field of the light wave, and ω its frequency.

The wavefunction Ψ can be expressed in term of eigenfunctions of the H_0 operator,

$$\Psi = \sum_n a_n(t)\phi_n \tag{4.4}$$

i.e. as a superposition of the wavefunctions ϕ_n of the quantum system without a light field, where ϕ_n is defined as

$$i\hbar \frac{\partial\phi_n}{\partial t} = H_0 \phi_n \tag{4.5}$$

Then the equation to determine the coefficients in the expansion is

$$\frac{d}{dt} a_n = -\frac{i}{\hbar} \sum_k H'_{nk} a_k \exp\left[\frac{i}{\hbar}(E_n - E_k)t\right] \tag{4.6}$$

from eq. (4.2).

In a two-level system, $n = 1$ and 2, and the single transition frequency is $\omega_0 = (E_2 - E_1)/\hbar$. Eq. (4.6) gives a pair of coupled equations for $a_1(t)$ and $a_2(t)$

$$\frac{da_1}{dt} = \frac{i}{2} K \varepsilon a_2 \{\exp[i(\omega-\omega_0)t] + \exp[-i(\omega+\omega_0)t]\}$$

$$\frac{da_2}{dt} = \frac{i}{2} K \varepsilon a_1 \{\exp[-i(\omega-\omega_0)t] + \exp[i(\omega+\omega_0)t]\} \tag{4.7}$$

where $K = 2\mu_{12}/\hbar$, in which μ_{12} is the dipole matrix element between the states 1 and 2. As long as the Rabi frequency $\omega_1 = K\varepsilon$ is very much

less than ω_0, we may neglect the high-frequency terms, $\exp[\ i(\omega+\omega_0)t]$, in the rotating wave approximation; then eq. (4.7) gives

$$\frac{d^2a_2}{dt^2} + i(\omega-\omega_0)\ \frac{da_2}{dt} + \left(\frac{K\epsilon}{4}\right)^2 a_2 = 0 \qquad\qquad (4.8)$$

The general solution to eq. (4.8) is

$$a_2(t) = [A\ \exp(i\Omega t/2) + B\ \exp(-i\Omega t/2)]\ \exp(-i\Delta t/2) \qquad (4.9)$$

$$a_1(t) = -\ \frac{1}{K\epsilon}[(\Delta-\Omega)A\ \exp(i\Omega t/2) + (\Delta+\Omega)B\ \exp(-i\Omega t/2)]\ \exp(i\Delta t/2)$$

with $\Delta = \omega-\omega_0$ and $\Omega = [\Delta^2 + (K\epsilon)^2]^{\frac{1}{2}}$; the constants A and B are determined from the initial condition of the system.

Assuming that the molecule is initially in the lower state 1, $a_1(t_0) = \exp(i\theta)$ (i.e. one multiplied by an arbitrary phase factor) and $a_2(t_0) = 0$. This gives the coefficient

$$a_1(t) = \left[\cos\frac{\Omega}{2}(t-t_0) - i\frac{\Delta}{\Omega}\sin\frac{\Omega}{2}(t-t_0)\right]\exp[i\theta + i\Delta(t-t_0)/2]$$

$$\qquad\qquad (4.10)$$

$$a_2(t) = i\frac{K\epsilon}{\Omega}\sin\left[\frac{\Omega(t-t_0)}{2}\right]\exp[i\theta - i\Delta(t-t_0)/2]$$

The squares of the coefficients which correspond to relative populations of the two states are

$$N_1(t) = |a_1(t)|^2 = \frac{\Delta^2}{\Omega^2} + \frac{(K\epsilon)^2}{\Omega^2}\cos^2\frac{\Omega}{2}(t-t_0)$$

$$\qquad\qquad (4.11)$$

$$N_2(t) = |a_2(t)|^2 = \frac{(K\epsilon)^2}{\Omega^2}\sin^2\frac{\Omega}{2}(t-t_0)$$

In a gas at low pressure, the coherent oscillation of the molecular dipole moment is interrupted by collisions between molecules and by the

life time of the eigenstate.

The effect of collisions can be incorporated in this treatment by averaging eq. (4.11) over a Poisson distribution of dephasing collisions with relaxation time τ. The probability that the molecule has survived under coherent interaction with the field in the interval $t = t_0$ is

$$dN(t) = \frac{1}{\tau} \exp[-(t-t_0)/\tau] \, dt \qquad (4.12)$$

The transition probability for an ensemble of molecules in the gas is then obtained by taking an average over t_0, to give

$$<|a_2|^2> = \frac{1}{\tau} \int_{-\infty}^{t} |a_2(t,t_0)|^2 \exp[-(t-t_0)/\tau] \, dt_0$$

$$= \frac{1}{2} \frac{(K\varepsilon)^2}{(\omega-\omega_0)^2 + \tau^{-2} + (K\varepsilon)^2} \qquad (4.13)$$

This average increases monotonically with the intensity of the radiation field and approaches 0.5 as the limit $\varepsilon \to \infty$. This means that a very intense field will eventually equalize populations between upper and lower levels of a transition.

The power absorbed, which is the observable in this system, can be obtained as

$$\Delta P = \frac{dW}{dt} = \frac{(N_1-N_2) \, \hbar\omega \, (K\varepsilon)^2}{2\tau \, [(\omega-\omega_0)^2 + \tau^{-2} + (K\varepsilon)^2]}$$

where N_1 and N_2 are the numbers of molecules in the states 1 and 2, respectively. The power flow per unit area in SI units

$$P = \frac{1}{2} \epsilon_0 . c \, \varepsilon^2 \qquad (4.14)$$

where ϵ_0 is the dielectric constant and c is the speed of light.

As $\epsilon \to \infty$, ΔP becomes a constant, the power absorption coefficient of a gas of two-level molecules is given by

$$\alpha = \frac{\Delta P}{P} = \frac{(N_1 - N_2) \, 2\hbar\omega K^2}{\epsilon_0 \tau \, [(\omega - \omega_0) + \tau^{-2} + (K\epsilon)^2]} \to 0 \qquad (4.15)$$

and the medium saturates. With $\omega = \omega_0$, this can be rewritten as the phenomenological expression

$$\alpha = \frac{\alpha_0}{1 + I/I_S} \qquad (4.16)$$

where all the appropriate factors are incorporated into α_0 and I_S. The saturation parameter I_S is the power per unit area that a wave on resonance must carry in order to reduce the population difference to one-half its unsaturated value (11).

With a moderate intensity $(I < I_S)$, we have

$$\alpha = \alpha_0 \left(1 - \frac{I}{I_S} + \ldots\right) \qquad (4.17)$$

A similar derivation, by the use of density-matrix equations, is discussed by Letokhov and Chebotayev (3). Saturation of Doppler-broadened absorption lines has been considered by Shimoda and Shimizu (10).

C. Saturated Fluorescence Spectroscopy

A Doppler-broadened spectral line is a sum of a great number of much narrower lines corresponding to molecules with different thermal

velocity, $\underset{\sim}{v}$. This is why the Doppler effect on spectral lines is often called inhomogeneous broadening. A coherent light wave of wave vector $\underset{\sim}{k}$ interacts only with particles it resonates with, that is, with particles for which the Doppler shift in the absorption frequency, $\underset{\sim}{k}.\underset{\sim}{v}$, compensates precisely for the detuning of the field frequency, ω, with respect to the transition frequency, ω_0, of a fixed molecule, (Fig. 4.1)

$$\omega_0 = \omega + \underset{\sim}{k}.\underset{\sim}{v} \tag{4.18}$$

The excitation of particles with a certain velocity changes the equilibrium distribution of particle velocities in each level of the transition. In the lower level there is a lack of particles whose velocity complies with the resonance condition, that is, a hole appears in the velocity distribution, an effect i known as Bennett hole burning (12), Fig.4.2. By contrast, in the upper level there is an excess of particles with resonance velocities or a peak in the velocity distribution. The hole depth and peak height depend on the degree of absorption saturation by the light field. The width of the hole determines the homogeneous line width, which can be thousands of times less than the Doppler width.

E_2

ω

$\omega_0 = (E_2 - E_1)/\hbar$

E_1
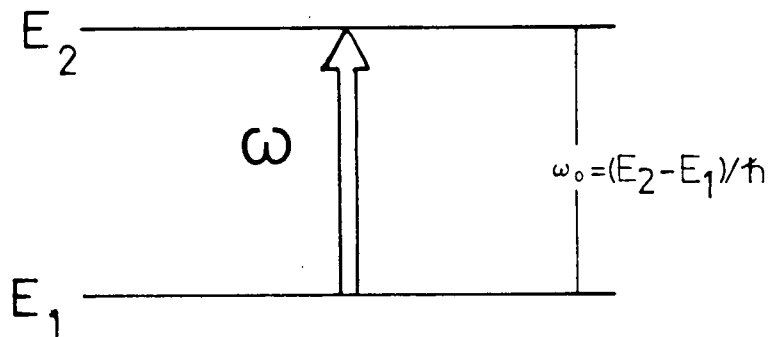
Fig. 4.1   Two level system
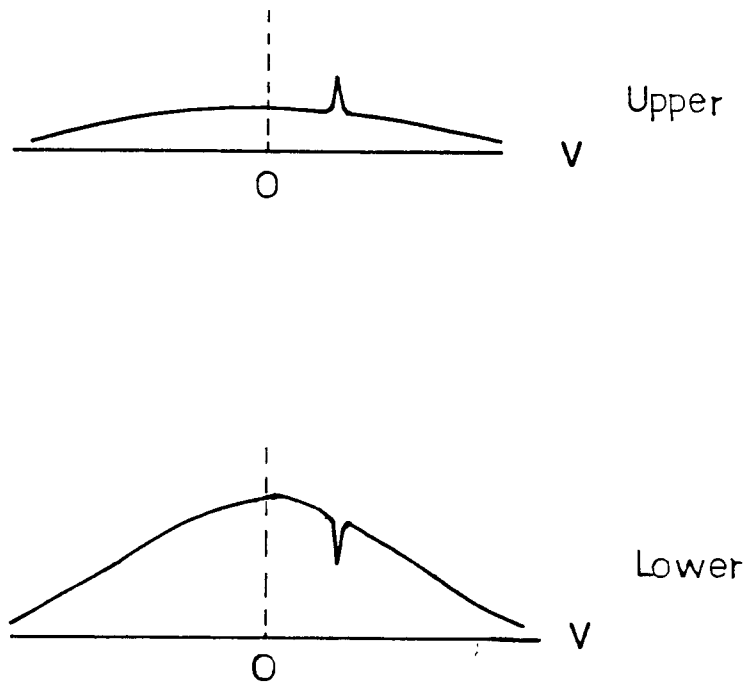
Fig. 4.2   Molecular velocity distributions for both upper and lower

levels under the action of a laser wave of frequency ω.

A related phenomenon known as the Lamb dip (7) forms the basis for many experiments in saturation spectroscopy (6). Although Lamb has shown, in his gas-laser theory (7), that the interaction of a Doppler-broadened line with a standing wave produces this phenomenon, in fact, the light wave need not be a standing wave: a strong travelling wave is sufficient to produce the same effect (9). Also this signal can be detected by monitoring the total fluorescence, which is just a constant fraction of the total absorbed power.

Consider the situation that two strong travelling waves from the same laser source pass through a cell in opposite directions. A photo-multiplier tube is mounted next to the cell so that fluorescence light

from the cell, perpendicular to the laser propagation direction, can be monitored, Fig. 4.3.
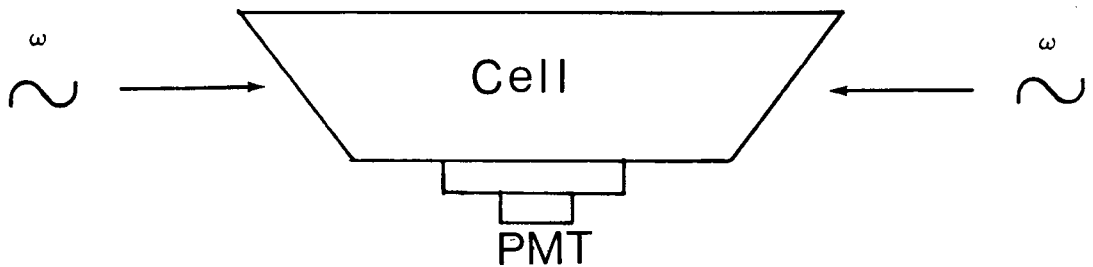
Fig. 4.3 Lamb dip experiment

Each travelling wave burns its own hole in the velocity distribution. Because these two waves run in opposite directions, there arise two holes symmetrical about the centre of the Doppler profile, fig. 4.4a In this case, the total fluorescence intensity is the sum of the contributions from each beam. As the laser frequency is tuned near to the centre of the Doppler profile, the two holes get closer and closer; also because of the gaussian distribution of the molecular velocities, the total fluorescence intensities increases. When the laser frequency is tuned to the centre of the Doppler profile, those two holes coincide and the travelling light wave interacts with only one group of particles, Fig. 4.4b. This results in a resonant decrease of absorbed power, which in turn, decreases the total fluorescence intensity, Fig. 4.5. This

effect is known as a 'Lamb dip'. Experimental observations of this effect were reported in (6,8).

(a)   (b)
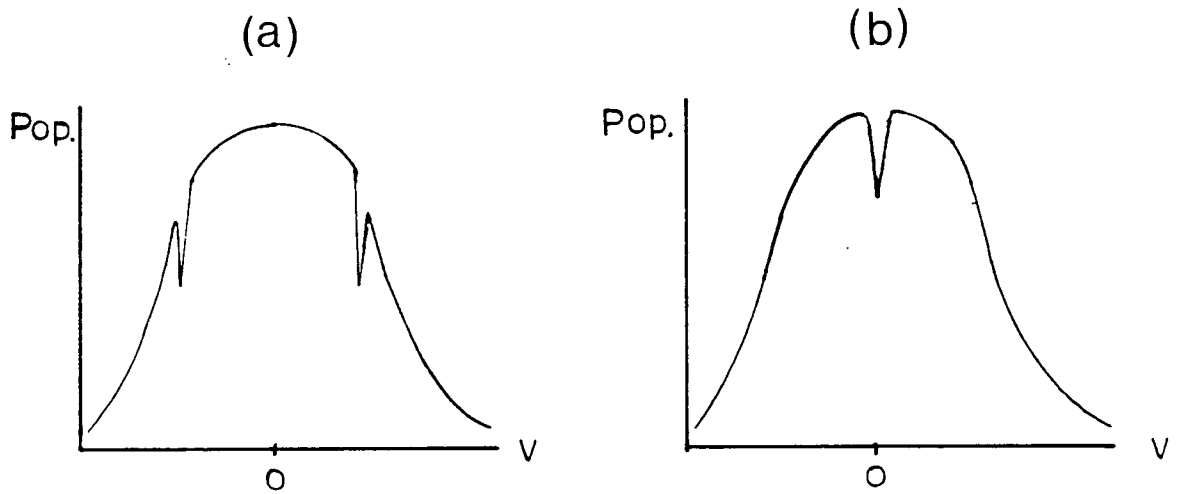
Fig. 4.4 Velocity distribution curves
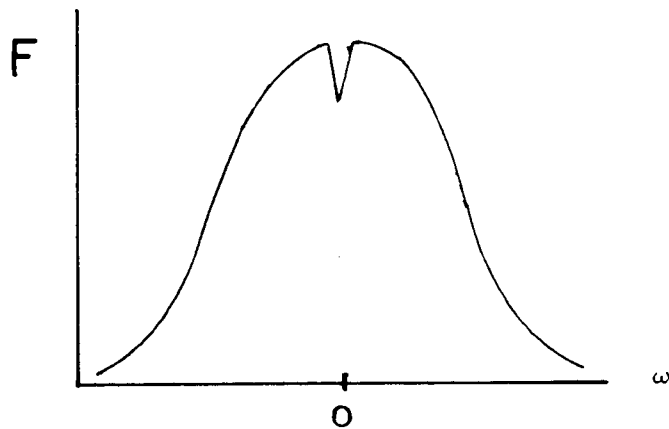
Fig. 4.5 Total fluorescence intensity vs laser frequency

D. <u>Intermodulated Fluorescence Spectroscopy</u>

The decrease in fluorescence intensity from the Lamb dip phenomenon has been used to detect saturation peaks and is particularly useful when the total absorption is small. Sorem and Schawlow (9) developed a sensitive modulation method for isolating a small change in fluorescence intensity.

Consider an experimental set up as Fig. 4.6. The molecules are exposed to light of two oppositely-directed beams from the same laser which are chopped at different frequencies, ω_1 and ω_2. The modulated fluorescence signal is detected by phase sensitive detection with reference signal set at the sum frequency, $\omega_1 + \omega_2$.
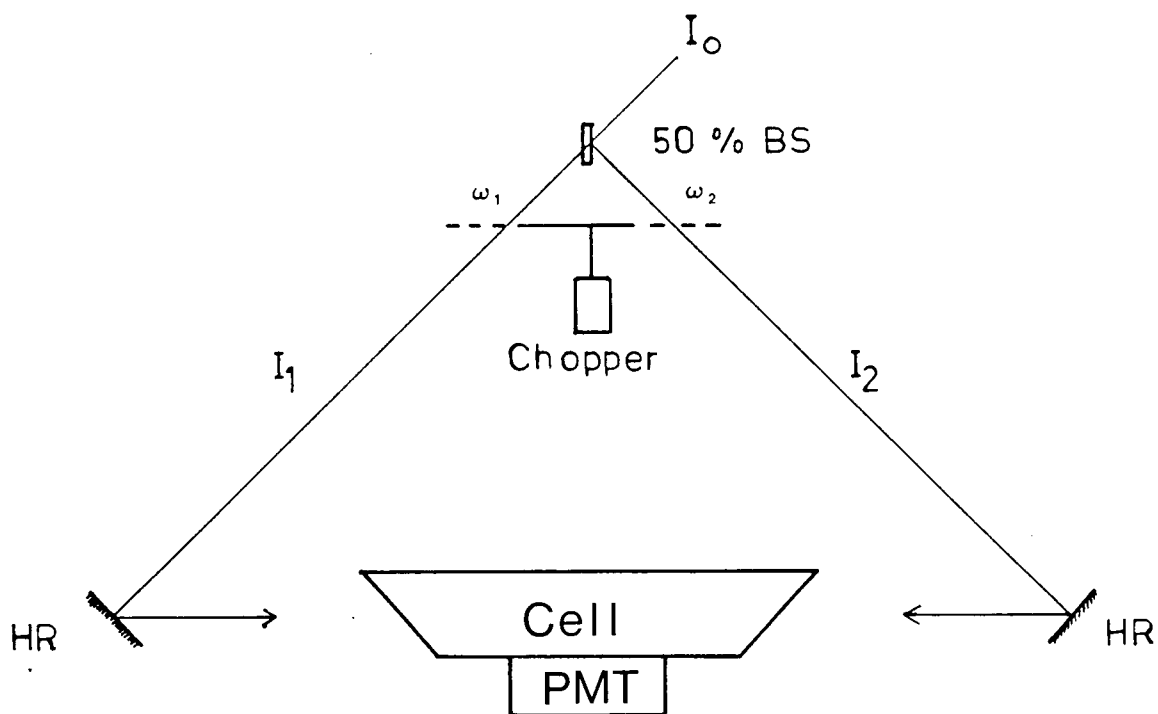
Fig. 4.6. Experimental set up for intermodulated fluorescence

The basic concepts behind this saturated fluorescence technique can be understood in terms of a very simple two level model. In the limit of the Doppler width being much greater than the homogeneous linewidth and $I < I_S$, from eq. (4.17) the absorption coefficient at frequency ω is given by

$$\alpha = \alpha_0 \left(1 - \frac{I}{I_S}\right) \qquad (4.18)$$

The total power of the beam is AI where A is the cross-section of the beam and the transmittance is given by AI exp$[-\alpha L]$ where L is the sample length. Since the fluorescence power, F, is some fraction of the absorbed power,

$$F = KAI \left\{1 - \exp[-\alpha L]\right\} \qquad (4.19)$$

where K is a proportionality constant. When $\alpha L < 1$, the exponential term in eq. (4.19) becomes $1-\alpha L$, such that

$$F = KAI\alpha L \qquad (4.20)$$

Since the beams are modulated at ω_1 and ω_2, the powers contained in beams 1 and 2 are

$$I_1 = \frac{1}{2} I_0 \cos \omega_1 t,$$
$$I_2 = \frac{1}{2} I_0 \cos \omega_2 t, \text{ respectively,}$$

with
$$I = I_1 + I_2$$
$$= \frac{1}{2} I_0 (\cos \omega_1 t + \cos \omega_2 t) \qquad (4.21)$$

where I_0 is the total power before splitting. Substituting eq. (4.17)

and eq. (4.19) into eq. (4.20) with rearrangement gives

$$F = \frac{1}{2} KALI_0 \alpha_0 \{ \cos \omega_1 t + \cos \omega_2 t$$

$$-\frac{I_0}{2I_S} [1 + \cos (\omega_1 + \omega_2)t + \cos (\omega_1 - \omega_2)t$$

$$+ \frac{1}{2} \cos 2\omega_1 t + \frac{1}{2} \cos 2\omega_2 t]\} \qquad (4.22)$$

Therefore the fluorescence power at the sum frequency $\omega_1 + \omega_2$ is

$$F (\omega_1 + \omega_2) = - \frac{KALI_0^2 \alpha_0}{4I_S} \cos (\omega_1 + \omega_2)t \qquad (4.23)$$

It should be noted that there will also be narrow resonant terms modulated at the frequencies ω_1, ω_2, $\omega_1 - \omega_2$ and zero, but that each of these will be accompanied by a large background because of low frequency amplitude noise in the laser power. Equations (4.22) and (4.23) show that the ratio of the power at the reference frequency to the d c fluorescence background is independent of $\alpha_0 L$. Comparing to a similar calculation for the saturated absorption (13) shows that this ratio is proportional to $\alpha_0 L$ in the limit of $\alpha_0 L < 1$. Thus this method, which is called intermodulated fluorescence, has a strong advantage for experimentalists working with very weak transitions, very low particle densities, or a poorly populated lower state.

This technique has been employed by a few workers in spectroscopy to study hyperfine splittings (9,14 - 16). The highest resolution achievable by this method, where the signals have a full width at half maximum (FWHM) of a few hundred kilohertz is obtained when the gas pressure is less than 0.1 torr. The signal suffers from sizeable pressure broadening if the pressure is substantially higher than 0.1 torr.

E. Resolved Fluorescence Spectroscopy

Heavy molecules with high spin multiplicity always exhibit severely blended spectra in the optical region. The overlap of different subbands or hot bands makes the analysis difficult simply because it is no longer possible to recognize the patterns of branch structure, and some "lines" have unexpected intensity due to the blending of many lines. In addition, rotational perturbations by different electronic states cause shifts and splittings of the lines. Under such circumstances, the rotational analysis would be completely impossible without some knowledge of the quantum numbers involved in the individual lines or their relationship to other lines. Resolved fluorescence is of very great value in solving this problem.

If a molecule is irradiated with laser light having the wavelength of a single rotational line, the absorbing molecules will be brought into the upper state of this particular absorption line only. The excited molecules can then emit light, falling to different rotational levels in the ground state according to the selection rules for electronic transitions (17) with emission of radiation, and giving rise to other fluorescence wavelengths besides the exciting wavelength.

The first step in the experiment is to tune the laser to a particular line of an electronic transition. Fluorescence, induced by the pump laser, is monitored, perpendicular to the laser propagation direction, by a monochromator with a photomultipler tube. A resolved fluorescence spectrum is obtained by scanning the monochromator.

There are two important pieces of information concerning the line assignment that can be obtained from a resolved fluorescence spectrum:

i) the ΔJ selection rule for the line which is excited by the laser.

When a single energy level is optically excited the fluorescence

spectrum consists of two or three lines. If λ_L is the exciting wave-

length, one of the lines in the fluorescence spectrum will always appear

at λ_L. If only two lines appear and the other line is at a shorter

wavelength, the exciting line belongs to an P branch; if the other line

is at a longer wavelength the exciting line belongs to an R branch.

A Q line may appear, in between the RP doublet, depending on the select-

ion rules and the type of transition. When a Q line is being excited in a

parallel transition, most of the intensity is re-emitted in the P and R

lines, Fig. 4.7.
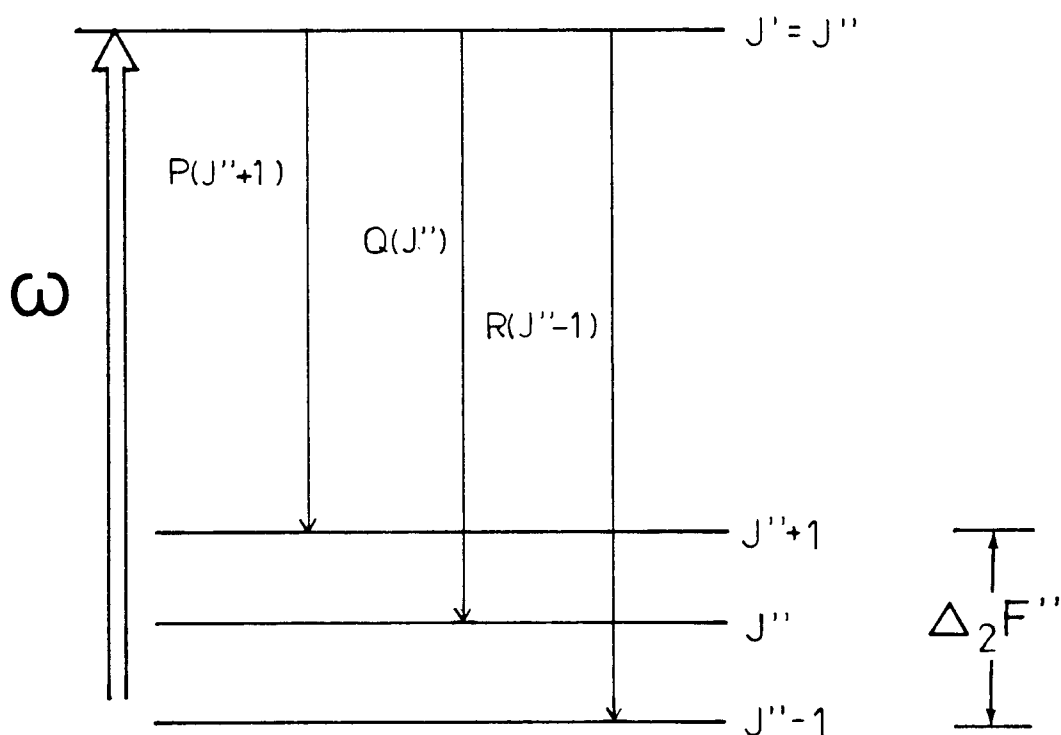
Fig. 4.7   Origin of induced fluorescence lines

ii) The separation between $P(J''+1)$ and $R(J''-1)$ fluorescence lines, called $\Delta_2 F''(J'')$, is given for a linear molecule by

$$\Delta_2 F''(J'') = (4B''_v - 6D''_v)(J'' + \tfrac{1}{2}) - 8D''_v(J'' + \tfrac{1}{2})^3 \qquad (4.24)$$

where B" and D" are the effective rotational and centrifugal distortion constants for the lower state (17). Measurement of the various separations allows the assignment of the J numberings to be made and simultaneously gives a rough B''_v value for this ground state. In an actual case, because the resolution of the monochromator is an order of magnitude lower than that of the laser excitation spectrum, it is often not possible to identify exactly which line in a crowded excitation spectrum goes with the line being excited, to within 1 cm^{-1}. It may be necessary to determine this by measuring the resolved fluorescences for various lines in the range indicated by the first experiment.

Furthermore, the excited molecules can also emit to different vibrational levels of the lower state. We could thus obtain in fluorescence a progression with v' = constant but different v" in the lower state, each band consisting of a P line, an R line and possibly a Q line. Vibrational assignment of the upper state can sometimes be made by counting the minima in the intensity pattern of a vibrationally resolved fluorescence spectrum (18); the number of minima corresponds to the number of nodes in the vibrational wavefunction.

Combining the powerful techniques of intermodulated and resolved fluorescence, it becomes possible in principle to analyse any spectrum of any complexity - for instance high resolution spectra where small

hyperfine splittings are present can be analysed to give the details
of the electron spin and hyperfine coupling constant with great precis-
ion, and perturbed electronic band systems can be unambiguously
assigned no matter how fearsome the perturbations may be.

Chapter 5

Laser Spectroscopy of VO; Analysis of
the Rotational and Hyperfine Structure
of the $C^4\Sigma^-$ - $X^4\Sigma^-$ (0,0) Band

A. Introduction

Vanadium monoxide, VO, is an important constituent of the atmospheres of cool red stars, its band systems being used for the spectral classification of stars of spectral types M7-M9 (1). There are three band systems of VO in the visible and near infra-red. Near 1.05 μ is the A-X system discovered by Kuiper, Wilson and Cashman (2), and later studied in the laboratory by Lagerqvist and Selin (3); following recent Fourier transform work by Cheung, Taylor and Merer (4) this is assigned as $A^4\Pi - X^4\Sigma^-$, where the $A^4\Pi$ state has quite small spin-orbit coupling. At 7900 Å is the $B^4\Pi - X^4\Sigma^-$ system (5,6) where the $B^4\Pi$ state is extensively perturbed by an unseen $^4\Sigma^-$ state (4), and near 5700 Å is the $C^4\Sigma^- - X^4\Sigma^-$ system (6-9) whose detailed analysis is described in this chapter.

A partial rotational analysis of bands of the C-X system was first performed by Lagerqvist and Selin (8). Their spectra were obtained using an arc between vanadium electrodes, which gives a very high temperature, and correpondingly wide lines. Their line assignments were correct, but they were only able to analyse parts of the R_2, R_3, P_2 and P_3 branches, and they suggested that the transition was possibly $^2\Delta - ^2\Delta$. The ground state was later established as $\sigma\delta^2\ ^4\Sigma^-$ by the e.s.r. work of Kasai (10), and shortly afterwards Richards and Barrow (6), reinvestigating the B-X and C-X systems, found that the two systems contain lines of different widths as a result of hyperfine structure in the ground state caused by the ^{51}V nucleus, which has I=7/2. Richards and Barrow could not resolve the hyperfine structure in their furnace spectra, but they discovered a very unusual internal hyperfine perturb-

ation in the ground state. What happens is that the F_2 and F_3 levels ($J=N\pm\frac{1}{2}$) with the same N value happen to cross near N=15 because of the particular values of the rotational and electron spin parameters. Matrix elements of the hyperfine Hamiltonian of the type $\Delta N=0$, $\Delta J=\pm 1$ act between them, and cause an avoided crossing of the hyperfine levels making up the two rotational levels. At medium resolution the perturbation appears as a small doubling of the lines near $N''=15$, and the minimum separation, which is related to the isotropic hyperfine parameter b (11), was found to be consistent with the e.s.r. work.

The hyperfine structures of the R_1, R_4, P_1 and P_4 lines were resolved by Hocking, Merer and Milton (12) in high resolution grating emission spectra. The hyperfine patterns give the difference of the b parameters in the C and X states, and it was found that there are sizeable hyperfine splittings in the C state as well. Another internal hyperfine perturbation, similar to that in the ground state, was discovered at $N'=5$ in the $C^4\Sigma^-$ state. A rough value could be obtained for the isotropic parameter b, but the dipolar interaction parameter c could not be extracted from their Doppler-limited spectra.

In this chapter we describe an analysis of the $C^4\Sigma^- - X^4\Sigma^-$ (0,0) band from sub-Doppler spectra recorded by the technique of intermodulated fluorescence (13). The line width is limited by pressure broadening effects to about 100 MHz, but this is sufficient for the hyperfine structure to be essentially completely resolved, barring the region at the R_2 head. Except for the places where the upper state suffers from electronic perturbations the lines can be fitted by least squares with

a standard deviation of better than 0.0008 cm^{-1}. Accurate values for the rotational, electron spin and nuclear spin constants have been obtained for both states.

B. Experimental Details

VO was prepared in a flow system by passing $VOCl_3$ mixed with argon through a 2450 MHz electrodeless discharge operating at 75 W. The mixture was pumped through a stainless steel fluorescence cell fitted with quartz windows, and VO fluorescence was excited by light from a Coherent Inc. Model CR-599-21 tunable dye laser. The strongest fluorescence occurred when the microwave discharge was a purplish pink colour with a pale blue 'tail'; the fluorescence induced by excitation of the $C^4\Sigma^- - X^4\Sigma^-$ (0,0) band (at 5738 Å) was a yellow orange colour.

Spectra of VO were recorded at sub-Doppler resolution by intermodulated fluorescence (13). Figure 5.1 illustrates the optical arrangement for this experiment. A Coherent Radiation CR-10 Ar^+ laser operating at 514.5 nm with 2.2 W output is used to pump a Coherent Radiation CR-599-21 dye laser with rhodamine 6 G dye. Dye laser output is typically 30 mW single frequency ($\Delta\nu_{FWHM} \sim 3x10^{-5}$ cm^{-1}), and is monitored using a 1.5 GHz free spectral range (FSR) spectrum analyzer, a 299-MHz FSR fixed length semiconfocal Fabry-Perot interferometer, and an I_2 cell. I_2 fluorescence excited by the dye laser is detected perpendicular to the laser propagation direction by an RCA IP28 photomultiplier tube (PMT 1) operated at -870 VDC. The dye laser beam was split by a 50-50% beam splitter (B S), and the resulting two beams were chopped mechanically at 582 Hz and 784 Hz. The laser power was about 15 mW in each beam, and the fluorescence signal was recorded through a sharp-cut yellow filter using an RCA C31025C (PMT 2). A narrow-band electrical filter selected the sum of the chopper frequencies, and the intermodulated signal was extracted with a Princeton Applied Research model 128A
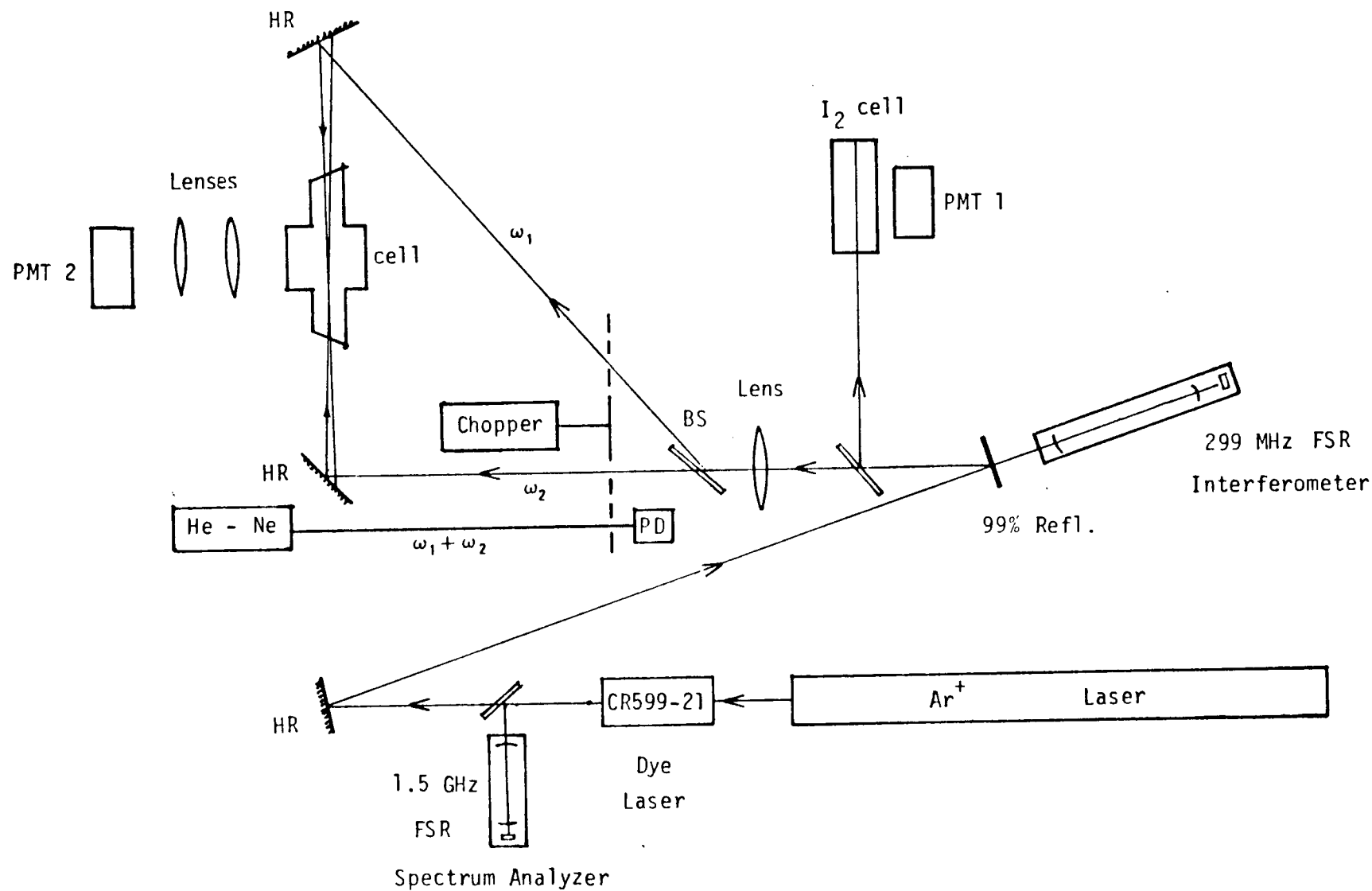
Fig. 5.1 Experimental set up for intermodulated fluorescence spectroscopy.

lock-in-amplifier. All the necessary electronics were connected as in Fig. 5.2 to minimize the ground loop problem. The results were displayed on a three-pen chart recorder. As the laser frequency was scanned one pen plotted the intermodulated signal, the second pen gave frequency markers spaced at 299 MHz intervals from the semi-confocal Fabry-Perot interferometer, and the third pen recorded the fluorescence spectrum of I_2 for absolute calibration. This system is similar to that used by Field et al (14) in their intermodulated fluorescence experiments, except that we use a narrow band electrical filter rather than a second lock-in-amplifier (15).

For intensity reasons we were not able to run the microwave discharge such that the total pressure in the fluorescence cell was less than about 1 mm Hg if we were to record intermodulated fluorescence. As a result the linewidths in our spectra are pressure broadened, and were never less than about 80 MHz even though the laser linewidth is 1-2 MHz. For the weaker high N lines we had to increase the total pressure; the linewidths rose to about 130 MHz, but fortunately these lines are only rarely blended so that the only adverse effect was lower precision in their calibration.

We encountered no problems with relative calibration of the spectra over a 1 cm^{-1} scan of the dye laser; for example the ground state hyperfine combination differences in the P_2 and P_3 lines were routinely reproduced to within ±0.0005 cm^{-1} (15 MHz); this is because the interferometer markers are sharp compared to the VO lines, and because the temperature of the room (which affects the positions of the markers
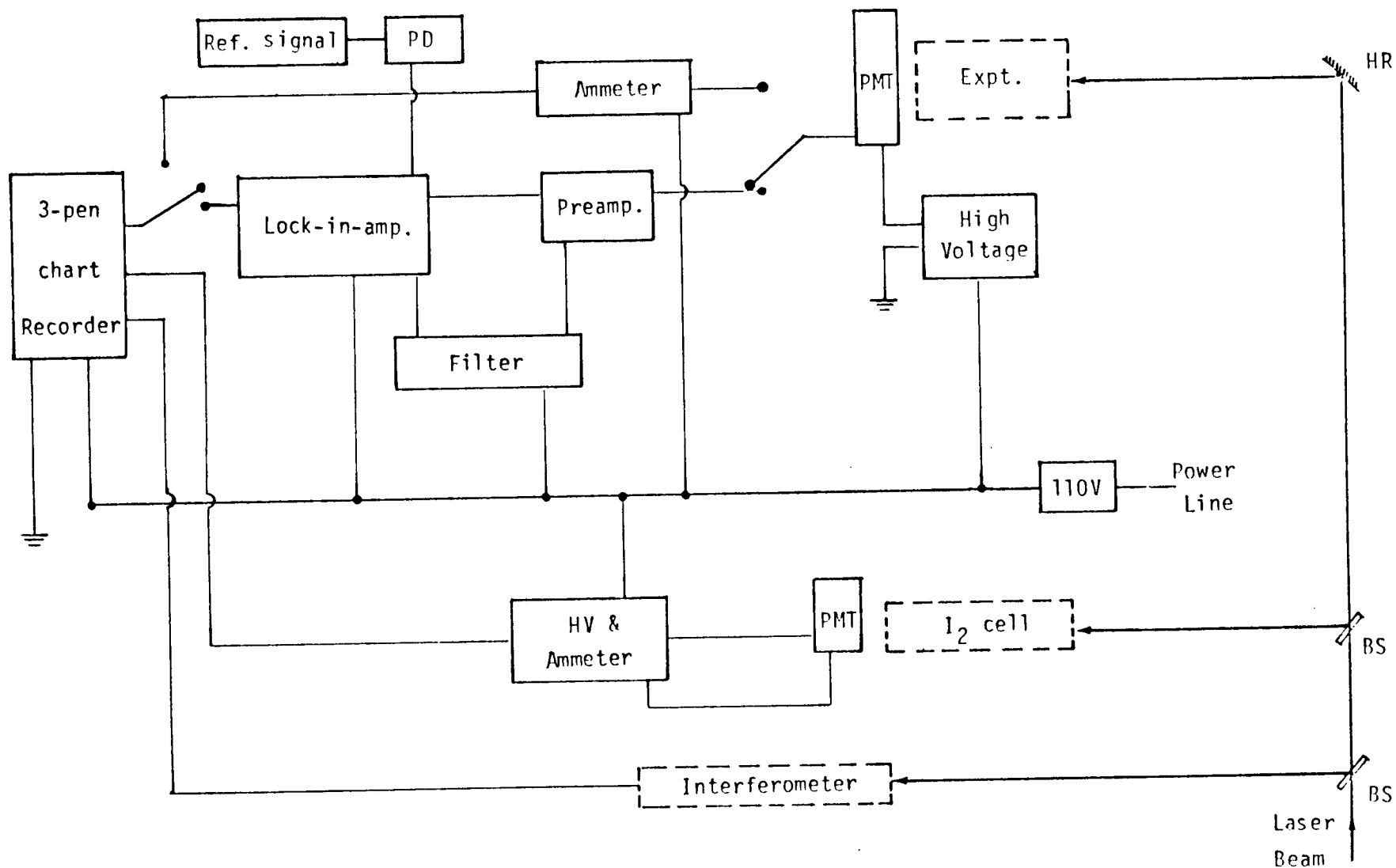
Fig. 5.2 Schematic diagram for intermodulated fluorescence detection system.

though not their spacing) remained sufficiently constant during the few minutes required for a scan. However the absolute calibration was always much less certain. As explained we used Doppler-limited I_2 fluorescence lines, excited by a portion of the laser beam picked off by a beam-splitter. The wavenumbers of the I_2 lines have been listed to 0.0001 cm^{-1} (3 MHz) by Gerstenkorn and Luc (16), but, since the I_2 lines are about 1 GHz wide because of unresolved hyperfine structure, their absolute uncertainty is about 0.002 cm^{-1} (60 MHz). Fortunately the VO spectrum is sufficiently dense near the band head that we were able to establish the relative shifts of the "ladders" of interferometer markers between successive 1 cm^{-1} laser scans, using lines duplicated in the overlap regions. In this way we could plot a calibration graph for the I_2 lines relative to the interferometer markers over ranges of up to 10 cm^{-1}. This gave us the marker spacing with great accuracy, and enabled us to use 40-50 I_2 lines to establish the absolute calibration of the "ladder". The calibration graphs consisted of a scatter of points, one for each I_2 line, spread randomly over ±0.002 cm^{-1} along a straight line. This procedure is very laborious, but we consider it worthwhile because it improves the standard deviation in a least squares fit to the line positions by nearly a factor of two: the final standard deviation for 1300 low N lines calibrated in this way was 0.00076 cm^{-1} (23 MHz).

C. Rotational and hyperfine energy level expressions

Since this work on VO is the first detailed study of the hyperfine structure in a $^4\Sigma$ electronic state, we did not know at first which terms to include in the Hamiltonian. After some experimentation we found it necessary to vary 12 parameters for each electronic state. The Hamiltonian was taken (17,18) as

$$H = H_{rot} + H_{el} + H_{hfs} + H_{el,c.d.} + H^{(3)}_{s.o.} \qquad (5.1)$$

where

$$
\begin{aligned}
H_{rot} &= B\underset{\sim}{N}^2 - D\underset{\sim}{N}^4 \\
H_{el} &= \gamma\underset{\sim}{N}\cdot\underset{\sim}{S} + \tfrac{2}{3}\lambda(3S_z^2 - \underset{\sim}{S}^2) \\
H_{hfs} &= b\underset{\sim}{I}\cdot\underset{\sim}{S} + cI_zS_z + \frac{e^2Qq(3I_z^2 - I^2)}{4I(2I-1)} + c_I\underset{\sim}{I}\cdot\underset{\sim}{N} \\
H_{el,c.d.} &= \gamma_D(\underset{\sim}{N}\cdot\underset{\sim}{S})\underset{\sim}{N}^2 + \tfrac{1}{3}\lambda_D[(3S_z^2 - \underset{\sim}{S}^2)\underset{\sim}{N}^2 + \underset{\sim}{N}^2(3S_z^2 - \underset{\sim}{S}^2)]
\end{aligned}
\qquad (5.2)
$$

which are basically described in chapter 2, and $H^{(3)}_{s.o.}$ represents third-order spin-orbit contributions to the parameters γ and b, which are described later. The rotational energy, given by H_{rot}, requires no explanation; the terms in H_{el} are the electron spin-rotation interaction and the electron spin-spin dipolar interaction, while the terms in H_{hfs} are the direct electric and magnetic hyperfine interactions. The terms in b and c are the determinable coefficients in the magnetic hyperfine Hamiltonian for a $^4\Sigma$ state; c is the dipolar electron spin-nuclear spin interaction, and b is a combination of c with the Fermi contact interaction, a_c. A more fundamental way of writing these I,S magnetic hyperfine terms (19), which is convenient for the calculation

of matrix elements, is

$$H_{mag.hfs} = a_c \underset{\sim}{I} \cdot \underset{\sim}{S} + c(I_z S_z - \tfrac{1}{3}\underset{\sim}{I} \cdot \underset{\sim}{S}) \tag{5.3}$$

The electric quadrupole interaction (e^2Qq) and the nuclear spin-rotation interaction (c_I) are familiar from microwave spectra of singlet states (18,20), while the centrifugal distortion corrections to H_{el} should be self-explanatory.

In the $^4\Sigma$ states of VO under discussion the electron spin-spin interaction (λ) is large compared to the hyperfine effects, so that the basis giving the most nearly diagonal representation is case $(b_{\beta J})$ coupling (11,18) where

$$\underset{\sim}{N} + \underset{\sim}{S} = \underset{\sim}{J} \; ; \; \underset{\sim}{J} + \underset{\sim}{I} = \underset{\sim}{F} \tag{5.4}$$

The basis functions are then $|N\Lambda SJIF\rangle$, where Λ can be suppressed because it is equal to zero. However the matrix elements in case $(b_{\beta J})$ coupling are much more complicated algebraically than those in case (a_β) coupling so that the use of case $(b_{\beta J})$ is logical for VO only because of the internal hyperfine perturbations mentioned in the Introduction. The matrix elements responsible for the internal hyperfine perturbations are off-diagonal in both basis sets, but in case (a_β) the spin-uncoupling is also off-diagonal. The spin-uncoupling matrix elements, which arise from the x and y components of the operator $-2B \underset{\sim}{J} \cdot \underset{\sim}{S}$, are very much larger than the internal hyperfine perturbation elements, and we found that they gave trouble with the energy ordering

of the eigenvalues in the regions of the internal hyperfine perturbations. This led to disaster in our attempts to fit the line positions by least squares, so that we returned to case $(b_{\beta J})$, though not without misgivings. In retrospect a two step diagonalization starting from case (a_β) might have saved much lengthy algebra: the first step would have been essentially a numerical transformation to case $(b_{\beta J})$, and the second step would have completed the diagonalization.

We quickly discovered that it was necessary to use a full matrix treatment for a correct description of the magnetic hyperfine effects; for instance the $\Delta N=\pm 2$, $\Delta J=\pm 1$ elements of the dipolar interaction have a significant effect on the course of the energy levels at the internal hyperfine perturbations. Therefore the only simplification we have made was to omit the $\Delta J=\pm 2$ elements of the electric quadrupole interaction, after calculating that these were less than 1 MHz. The matrix elements of the terms in B, D, γ and γ_D are diagonal in case $(b_{\beta J})$:

$$\langle NSJIF|H_{rot + spin-rot}|NSJIF\rangle = BN(N+1)-DN^2(N+1)^2$$
$$-\tfrac{1}{2}[N(N+1)+S(S+1)-J(J+1)][\gamma+\gamma_D N(N+1)]$$

(5.5)

Matrix elements of the other terms in eq. (5.2) are most conveniently calculated using spherical tensor formalism as shown in chapter 2 (19,21). For electronic Σ states of any multiplicity, where a single spinning nucleus is present, we have

$$\langle N'SJIF|H_{spin\text{-}spin}|NSJIF\rangle = \frac{2}{3}\lambda(-1)^{N+S+J} \begin{Bmatrix} J & S & N' \\ 2 & N & S \end{Bmatrix} \tag{5.6}$$

$$\times[S(S+1)(2S+1)(2S-1)(2S+3)]^{\frac{1}{2}} (-1)^{N'} \begin{pmatrix} N' & 2 & N \\ 0 & 0 & 0 \end{pmatrix}[(2N+1)(2N'+1)]^{\frac{1}{2}}$$

$$\langle N'SJ'IF|H_{mag.hfs}|NSJIF\rangle = (-1)^{J+I+F} \begin{Bmatrix} F & I & J' \\ I & J & I \end{Bmatrix} \frac{[(2J+1)(2J'+1)\ I(I+1)}{(2I+1)]^{\frac{1}{2}}}$$

$$\times\left[(-1)^{N+S+J'+1} \begin{Bmatrix} S & J' & N \\ J & S & 1 \end{Bmatrix} [S(S+1)(2S+1)]^{\frac{1}{2}} a_c \right. \tag{5.7}$$

$$-\frac{1}{3}c[30(2N+1)(2N'+1)\ S(S+1)(2S+1)]^{\frac{1}{2}} \begin{Bmatrix} N' & N & 2 \\ S & S & 1 \\ J' & J & 1 \end{Bmatrix} \frac{(-1)^{N'}}{} \begin{pmatrix} N' & 2 & N \\ 0 & 0 & 0 \end{pmatrix}$$

$$+(-1)^{N+S+J+1} \begin{Bmatrix} N & J' & S \\ J & N & 1 \end{Bmatrix} [N(N+1)(2N+1)]^{\frac{1}{2}} c_I \left. \right]$$

where a_c (the true Fermi contact interaction) is $b + \frac{1}{3}c$, and

$$\langle N'SJ'IF|H_{quadrupole}|NSJIF\rangle = \frac{1}{4}e^2Qq \begin{pmatrix} I & 2 & I \\ -I & 0 & I \end{pmatrix}^{-1}(-1)^{J+I+F} \begin{Bmatrix} F & I & J' \\ 2 & J & I \end{Bmatrix} \tag{5.8}$$

$$\times(-1)^{N'+S+J} [(2J+1)(2J'+1)\ (2N+1)(2N'+1)]^{\frac{1}{2}} \begin{Bmatrix} S & N' & J' \\ 2 & J & N \end{Bmatrix}(-1)^{N'} \begin{pmatrix} N' & 2 & N \\ 0 & 0 & 0 \end{pmatrix}$$

It is straight-forward to obtain explicit expressions except for the dipolar term $c(I_z S_z - \frac{1}{3}\underset{\sim}{I}\cdot\underset{\sim}{S})$, where the 9-j symbol is not listed in standard tabulations (22), and the algebraic expressions given by

Mizushima (23) contain various small but important errors. For complete-
ness we list the corrected forms of the relevant 9-j symbols in Appen-
dix IV. Our phase choice in eqs. (5.5)-(5.8) corresponds to that of
Bowater, Brown and Carrington, where $\underset{\sim}{N}$ is treated as a space-fixed
operator (19), and the order of coupling the vectors in eq. (5.4) is
also the same as theirs.

The third-order spin-orbit contributions will be unfamiliar since
they only occur for $S \geqslant \frac{3}{2}$, that is for electronic quartet states or worse.
In this study we have had to use the third-order contribution to the
spin-rotation interaction, γ_S, introduced by Brown and Milton (25),
and the corresponding correction to the isotropic hyperfine interaction,
which we call b_S (26). The term in γ_S has a complicated history. The
original formulae for $^4\Sigma$ states derived by Budó (27) and Kovács (28)
accounted nicely for Nevin's data for O_2^+ (29), but not for the data on
GeH (30) and SiF (31). Hougen (32) attempted to find the source of
the discrepancy, and extended the theory to include the second spin-
rotation parameter required by group theory arguments for a $^4\Sigma$ state in
the general case. Later work by Martin and Merer (33) showed that the
original SiF spectrum has been misassigned, and that there were no dis-
crepancies, but their theoretical treatment was still incomplete.
Finally Brown and Milton (25) gave a full discussion of the higher
order spin dependence of the spin-rotation interaction in $^4\Sigma$ states.
Their conclusion was that the single spin-rotation term in γ given in
eq. (5.2) will usually suffice, except in cases where very high resolut-
ion is available, or where another nearby electronic state interacts

strongly by spin-orbit coupling; in this case a second spin-rotation term will be needed. This second term results from a third order interaction where the spin-uncoupling operator $-2B(J_x S_x + J_y S_y)$ is taken with the spin-orbit operator $\sum_i a_i l_i \cdot s_i$ twice: the matrix elements in case (a), with Σ and Ω taken as signed quantities, are

$$
\begin{aligned}
\langle S\Sigma, J\Omega | H_{sr}^{(3)} | S\Sigma \pm 1, J\Omega \pm 1 \rangle = &-\tfrac{1}{2}\gamma_S [S(S+1)-5\Sigma(\Sigma \pm 1)-2] \\
&\times [J(J+1)-\Omega(\Omega \pm 1)]^{\frac{1}{2}} [S(S+1)-\Sigma(\Sigma \pm 1)]^{\frac{1}{2}}
\end{aligned}
\tag{5.9}
$$

The experimental parameter γ_S is a complicated function of the spin-orbit matrix elements, the energy separation to the interacting states and the differences ΔB between the B values of the interacting states and the state of interest.

Barrow (34) has reported that the $C^4\Sigma^-$ and $X^4\Sigma^-$ states of VO both require two spin-rotation parameters (presumably in Hougen's formalism). The present work confirms this conclusion, although we have used Brown and Milton's definitions for the parameters. These states of VO are the first $^4\Sigma$ states known where two γ's are definitely needed.

The high precision of our data has required that we consider the corresponding effect in the isotropic hyperfine Hamiltonian. The mechanism for its appearance is entirely analogous: instead of the spin-uncoupling operator $-2B(J_x S_x + J_y S_y)$ we take the isotropic hyperfine operator $\sum_i b_i \underset{\sim}{I} \cdot \underset{\sim}{s_i}$ with the spin-orbit operator twice (26). The result is as if there were an effective operator

$$
H_{iso}^{(3)} = \sum_{i>j} T^1(\underset{\sim}{I}) \cdot T^1(T^3(T^1(\underset{\sim}{S}), T^2(\underset{\sim}{s_i} \cdot \underset{\sim}{s_j})), T^2(C))
\tag{5.10}
$$

acting within the manifold of the $^4\Sigma$ state of interest. As given in ref. (25), the matrix elements of eq. (5.10) in case $(b_{\beta J})$ coupling for $\Lambda = 0$ are

$$\langle N'SJ'IF|H_{iso}^{(3)}|NSJIF\rangle = \frac{1}{4}(-1)^{J+I+F} \begin{Bmatrix} F & I & J' \\ I & J & I \end{Bmatrix} [(2J+1)(2J'+1).I(I+1)(2I+1)]^{\frac{1}{2}}$$

$$\times(-1)^{N'}\begin{pmatrix} N' & 2 & N \\ 0 & 0 & 0 \end{pmatrix} [(2N+1)(2N'+1)]^{\frac{1}{2}} \begin{Bmatrix} N' & N & 2 \\ S & S & 3 \\ J' & J & 1 \end{Bmatrix} \qquad (5.11)$$

$$\times[35(2S-2)(2S-1)2S(2S+1)(2S+2)(2S+3)(2S+4)/3]^{\frac{1}{2}}b_S$$

The experimental parameter $T_0^2(C)$, which would result from eq. (5.10), has been put equal to $\frac{10}{3}(14)^{\frac{1}{2}} b_S$, in order to define a parameter b_S which is as similar as possible to Brown and Milton's γ_S.

Calculation of the explicit matrix elements from eq. (5.11) in case $(b_{\beta J})$ coupling was a long process because the 9-j symbols give uncompromisingly intractable algebraic expressions. For reference they are included in Appendix IV. No doubt there are simpler forms for the 9-j symbols with $N'=N$, but we have not tried to search for them. The final matrix elements, on the other hand, are quite simple because of extensive cancelling.

Another approach to the matrix elements of these third-order terms is to set up the matrices in case (a_β) coupling and transform them algebraically to case $(b_{\beta J})$ using the eigenvectors of the case (a_β) rotational matrices. This is no real advantage for the hyperfine term

because the case (a_β) matrices are already quite complicated, having elements of the type $\Delta\Omega=0,\pm1$, $\Delta J=0,\pm1$; we did however transform the diagonal blocks in this way in order to check the calculation of the 9-j symbols. On the other hand the spin-rotation term has a simple matrix representation in case (a) coupling, consisting only of the elements given in eq. (5.9), but a fearsome form in case (b):-

$$\langle N'SJIF|H^{(3)}_{spin-rot}|NSJIF\rangle = \frac{1}{4}[(2N+1)(2N'+1).J(J+1)(2J+1)]^{\frac{1}{2}}$$

$$\times[2(2S-2)(2S-1)2S(2S+1)(2S+2)(2S+3)(2S+4)/3]^{\frac{1}{2}} \gamma_S \qquad (5.12)$$

$$\times \sum_{x=2,4} (2x+1)\begin{pmatrix} 3 & x & 1 \\ -1 & 0 & 1 \end{pmatrix} (-1)^{N'} \begin{pmatrix} N' & x & N \\ 0 & 0 & 0 \end{pmatrix} \begin{Bmatrix} N' & N & x \\ S & S & 3 \\ J & J & 1 \end{Bmatrix}$$

Accordingly we converted eq. (5.9) to case (b) algebraically using a Wang transformation followed by the similarity transformation

$$\underset{\sim}{H}^{(b)} = \underset{\sim}{S}^{-1}\underset{\sim}{H}^{(a)}\underset{\sim}{S} \qquad (5.13)$$

If the $H^{(a)}_{11}$ element corresponds to $|\Omega|=3/2$ and the $H^{(b)}_{11}$ element to F_3 or F_4, the eigenvector matrix $\underset{\sim}{S}$, given by

$$\underset{\sim}{S} = \begin{bmatrix} c & -s \\ s & c \end{bmatrix} \qquad (5.14)$$

has elements for a $^4\Sigma^-$ state as follows:-

e levels (F_1 and F_3): $\quad c = \frac{1}{2}[3(J-\frac{1}{2})/J]^{\frac{1}{2}}, \quad s = -\frac{1}{2}[(J+\frac{3}{2})/J]^{\frac{1}{2}}$

f levels (F_2 and F_4): $\quad \frac{1}{2}[(J-\frac{1}{2})/(J+1)]^{\frac{1}{2}}, \quad -\frac{1}{2}[3(J+\frac{3}{2})/(J+1)]^{\frac{1}{2}}$ $\qquad$ (5.15)

The two third-order terms have quite similar effects on the energy level structure. Table 5.1 gives the algebraic forms of the matrix elements we have used. It can be seen that when similar powers of N are cancelled, the spin-rotation and isotropic hyperfine energies follow the same type of expression:

$$F_1 \text{ and } F_4 \ (J=N+\tfrac{3}{2}): \quad E_{sr} + E_{iso} \cong \pm\tfrac{3}{2}N(\gamma-\tfrac{1}{2}\gamma_S) \ \pm\tfrac{3}{2}C(b-\tfrac{1}{2}b_S)/2N$$

$$F_2 \text{ and } F_3 \ (J=N+\tfrac{1}{2}): \quad E_{sr} + E_{iso} \cong \pm\tfrac{1}{2}N(\gamma+\tfrac{9}{2}\gamma_S) \ \pm C(b+\tfrac{9}{2}b_S)/2N$$

$\qquad$ (5.16)

where

$$C = F(F+1) - J(J+1) - I(I+1) \qquad (5.17)$$

The result is that the F_1 and F_4 levels have different effective γ and b parameters from the F_2 and F_3 levels.

The energy level calculations based on the matrix elements of Table 5.1 require that two 16 x 16 matrices be set up and diagonalized for each F value. One of these matrices has basis functions extending from N=F+5 to N=F-5 in steps of 2, and the other has basis functions from N=F+4 to N=F-4, also in steps of 2. Unfortunately the structures of the two matrices are not the same, and there are problems with missing levels at low F values: the complete 16x16 matrices first appear for F=5. We have reduced the general forms of the matrix elements

Table 5.1 Matrix elements of the spin and hyperfine Hamiltonian

for a $^4\Sigma$ state in a case $(b_{\beta J})$ basis.

Diagonal elements

$F_1(J=N+\tfrac{3}{2})$: $\tfrac{3}{2}\gamma N + [-\tfrac{3}{2}\gamma_S N(N+1)-2\lambda N + c_I CN + \tfrac{3}{2}C\{b + \dfrac{c-b_S N}{2N+3}\} - \dfrac{e^2 Qq XN}{2I(2I-1)(N+1)(2N+3)}]/(2N+3)$

$F_2(J=N+\tfrac{1}{2})$: $\tfrac{1}{2}\gamma(N-3) + [\tfrac{3}{2}\gamma_S N(3N+5) + 2\lambda(N+3)]/(2N+3)$

$+ [c_I C\{2N(N+1) + (N-3)\} + \tfrac{1}{2}C\{b(2N+9) + 3b_S(3N+2+ \dfrac{3}{2N+3}) + c(\dfrac{6}{2N+3} + 7)\}$

$- \dfrac{e^2 Qq X(N+3)(2N-3)}{2I(2I-1).N(2N+3)}]/[(2N+1)(2N+3)]$

$F_3(J=N-\tfrac{1}{2})$: $-\tfrac{1}{2}\gamma(N+4) + [-\tfrac{3}{2}\gamma_S(N+1)(3N-2) + 2\lambda(N-2)]/(2N-1)$

$+ [c_I C\{2N(N+1)-(N+4)\} - \tfrac{1}{2}C\{b(2N-7) + 3b_S(3N+1+ \dfrac{3}{2N-1}) + c(\dfrac{6}{2N-1} - 7)\}$

$- \dfrac{e^2 Qq X(N-2)(2N+5)}{2I(2I-1).(N+1)(2N-1)}]/[(2N-1)(2N+1)]$

$F_4(J=N-\tfrac{3}{2})$: $-\tfrac{3}{2}\gamma(N+1) + [\tfrac{3}{2}\gamma_S N(N+1) - 2\lambda(N+1) + c_I C(N+1) - \tfrac{3}{2}C\{b - \dfrac{c+b_S(N+1)}{2N-1}\}$

$- \dfrac{e^2 Qq X(N+1)}{2I(2I-1).N(2N-1)}]/(2N-1)$

$X = \tfrac{3}{4}C(C+1)-I(I+1)J(J+1)$, $C = F(F+1)-J(J+1)-I(I+1)$, and $b = a_c-c/3$

The rotational Hamiltonian has only diagonal elements, equal to $BN(N+1)-DN^2(N+1)^2$

Off-diagonal elements

$\langle N-2\ J\ F|H|NJF\rangle = \left\{[3(J-\tfrac{1}{2})(J+\tfrac{3}{2})]^{\tfrac{1}{2}}/(2N-1)\right\} [2\lambda + \{5(J+\tfrac{1}{2})(J-N+1)-2\}\gamma_S$

$+\left\{cC + \dfrac{3e^2 Qq\ X}{I(2I-1)(2J-1)(2J+3)} + \tfrac{1}{2}b_S C\{2(5N+3)(J-N+1)-\tfrac{5}{2}\}\right\}/\{2J(J+1)\}]$

where X and C have been defined in the diagonal elements

Table 5.1 Continued.

$$\langle N\ J\text{-}1\ F|H|NJF\rangle = [(F+J+I+1)(J-F+I)(F+J-I)(F-J+I+1)]^{\frac{1}{2}}\ [R(N)/4J]\ [b-c_I + b_S Q(N)$$

$$+\ \frac{\{N(N+1)+J^2-19/4\}}{(2N-1)(2N+3)}\ \left\{c\ +\ 3e^2Qq\ \frac{\{F(F+1)-I(I+1)-(J-1)(J+1)\}}{4I(2I-1)(J-1)(J+1)}\right\}\ ]$$

where $R(N)$ and $Q(N)$ are given by

$J=N+\frac{3}{2}$: $R(N)= [3N/(N+1)]^{\frac{1}{2}}$; $Q(N)= -(4N+3)/(4N+6)$

$J=N+\frac{1}{2}$: $[(2N-1)(2N+3)/\{N(N+1)\}]^{\frac{1}{2}}$ $[12N(N+1)-3]/[2(2N-1)(2N+3)]$

$J=N-\frac{1}{2}$: $[3(N+1)/N]^{\frac{1}{2}}$ $-(4N+1)/(4N-2)$

$$\langle N\text{-}2\ J+1\ F|H|NJF\rangle = -\frac{3}{4}[(F+N+I+\frac{1}{2})(N-F+I-\frac{1}{2})(F+N-I-\frac{1}{2})(F-N+I+\frac{3}{2})/\{N(N-1)\}]^{\frac{1}{2}}\ \times$$

$$[c\ +\ 3e^2Qq\ \frac{\{F(F+1)-I(I+1)-(N-\frac{3}{2})(N+\frac{1}{2})\}}{I(2I-1)(2N-3)(2N+1)}\ -\ b_S\{10N(N-1)+1\}]\ /(2N-1)^2$$

$$\langle N\text{-}2\ J\text{-}1\ F|H|NJF\rangle = [(F+J+I+1)(J-F+I)(F+J-I)(F-J+I+1)]^{\frac{1}{2}}\ [W(N)/\{8J(2N-1)\}]\ \times$$

$$[c\ +\ 3e^2Qq\ \frac{\{F(F+1)-I(I+1)-(J-1)(J+1)\}}{4I(2I-1)(J-1)(J+1)}\ -b_S+\frac{5}{2}b_S\cdot\delta_{J,N-\frac{1}{2}}\ ]$$

where $\delta_{J,N-\frac{1}{2}}$ is the Kronecker delta, and $W(N)$ is given by

$J=N+\frac{1}{2}$: $W(N)= [3(N-1)(2N-1)(2N+3)/N]^{\frac{1}{2}}$

$J=N-\frac{1}{2}$: $4[(N+1)(N-2)]^{\frac{1}{2}}$

$J=N-\frac{3}{2}$: $[3N(2N-1)(2N-5)/(N-1)]^{\frac{1}{2}}$

to algebraic expressions, rather than programming the computer to call subroutines for the Wigner angular momentum coupling coefficients, in order to save computing time; immense amounts of cancelling occur in the calculation of the algebraic expressions from the Wigner coefficients, and even without this it takes 20 seconds of CPU time on the University's Amdahl 470 V/8 computer for one least squares iteration to N=25 using the algebraic expressions.

D. Analysis of the spectrum

(i) General description of the band

The (0,0) band of the $C^4\Sigma^-$ - $X^4\Sigma^-$ system of VO is quite strongly red-degraded, and has two well-marked heads at 17426.4 cm^{-1} (R_1 and R_4) and 17424.2 cm^{-1} (R_2 and R_3). The spectrum is very crowded down to about 17400 cm^{-1}, with typical line densities of the order of 50 per wavenumber. To the red of this the band opens out and the rotational lines become well separated; the eight hyperfine components of each line resulting from the I=7/2 spin of the ^{51}V nucleus are clearly resolved, and the lines can readily be assigned to their respective electron spin components by their distinctive hyperfine patterns. Some typical hyperfine patterns are illustrated in Fig. 5.3. The hyperfine patterns of the F_1 and F_4 branches are three times as wide as those of the F_2 and F_3 branches, as can be understood from the diagonal matrix elements of the hyperfine Hamiltonian given in Table 5.1.

There is no problem with the rotational assignments in the tail of the band because the constants given by Barrow (34) usually reproduce

the line positions to within 0.2 cm^{-1}. We have recorded the band out to 17288 cm^{-1} (the P(41) group), where the branches have nearly died out. All four electron spin components suffer from rotational perturbations by other electronic states, which mainly appear as discontinuities in the branch structure; we have found extra lines in only two of the perturbations, though Lagerqvist and Selin (8) have identified extra lines in various higher N perturbations in their arc spectra.

The assignment of the hyperfine F quantum numbers is easy for the F_1 and F_4 electron spin components because the hyperfine structure follows the Landé interval-type pattern described by eq. (5.17) and the diagonal elements of Table 5.1: the hyperfine patterns open out at the high F side, and the higher F lines have greater intensity. For the F_2 and F_3 branches the internal hyperfine perturbations cause the patterns to be irregular over the complete range of N values we have studied, even though the maxima in the internal perturbations are at $N'=5$ and $N''= 15$. It can be seen in Fig. 5.3 how the most intense hyperfine lines (which have the highest F values) are clustered together, in contrast to the patterns for the F_1 and F_4 branches. The reason is that the F_2 and F_3 spin components of the ground state are only 0.5 cm^{-1} apart at N=30, and the hyperfine matrix elements between them, which are F-dependent and of the order of 0.1 cm^{-1}, are able to reverse the Landé patterns.

(ii) Internal hyperfine perturbations

As the F_2 and F_3 branches are followed to lower N values extra lines induced by the hyperfine perturbations start to appear at N=21.
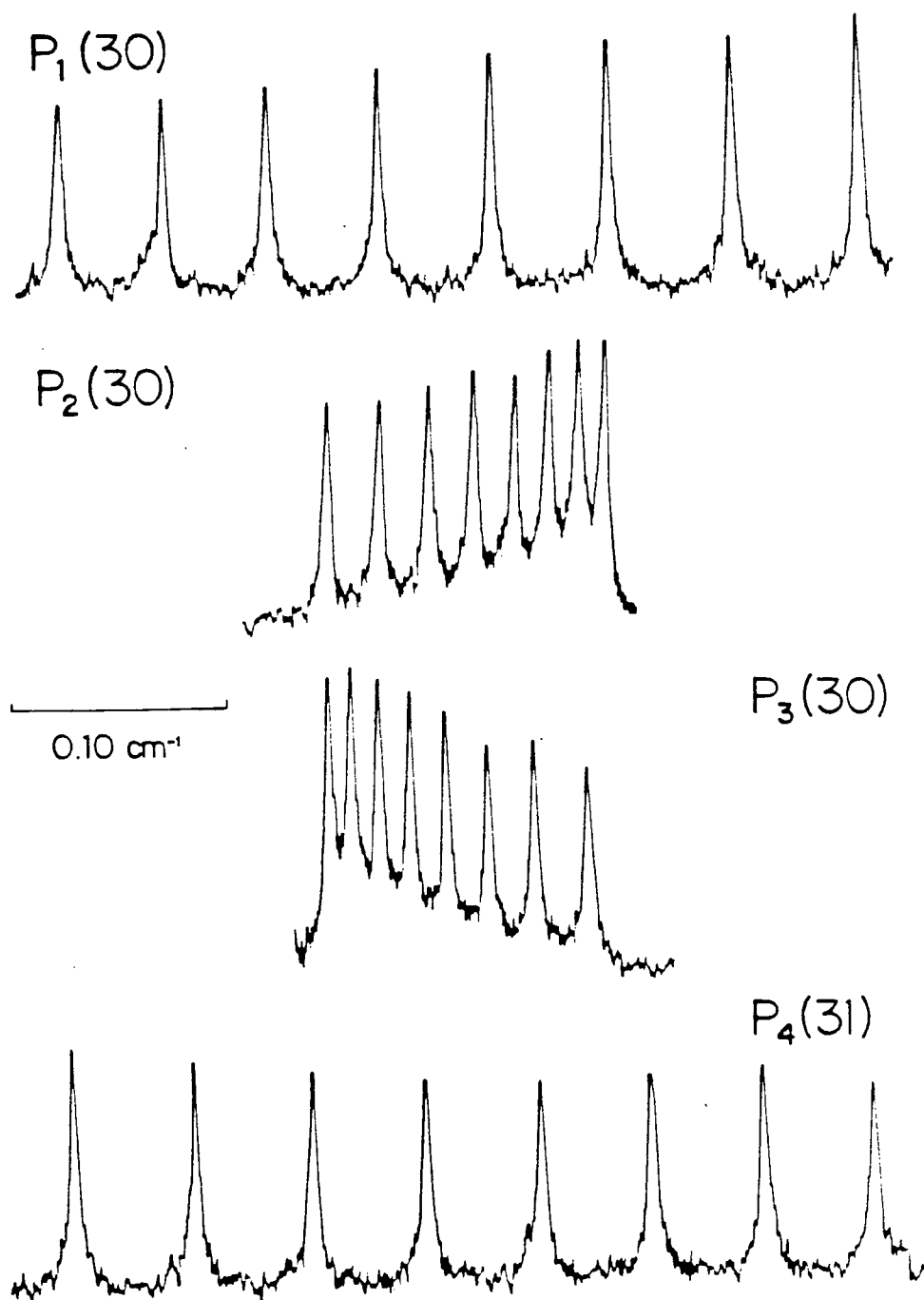
Fig. 5.3 Hyperfine structures of lines from the four electron spin
components of the VO $C^4\Sigma^- - X^4\Sigma^-$ (0,0) band.

These extra lines, though not resolved into individual hyperfine components, had been observed by Richards and Barrow (9) and Hocking, Merer and Milton (12). The patterns of hyperfine lines become very complicated because the F order of the hyperfine components inverts at an internal hyperfine perturbation, producing a kind of band-head in the hyperfine structure for both the main lines and the extra lines. The perturbation-induced extra lines can be seen for about five N values on each side of the maximum, so that the effects of the upper and lower state internal perturbations run into each other and produce extra lines over the complete range N=4-21. These lines have proved to be very valuable in determining the spin and hyperfine constants, as will be described in Section F.

The internal hyperfine perturbations are best understood from plots of the energy levels against N. Fig. 5.4 shows the quartet electron spin structure of the ground state with the hyperfine effects omitted. The F_1 and F_4 levels cross near N=10, but their J values differ by 3 units, so that they do not interact. The F_2 and F_3 levels cross in zero order near N=15, but must avoid each other because of the $\Delta F = \Delta N = 0$, $\Delta J = \pm 1$ matrix elements of the hyperfine Hamiltonian. The avoided crossing is shown magnified in Fig. 5.5 with the hyperfine structure drawn in. Only seven of the eight hyperfine components of each level actually avoid each other. The reason is that the range of F values is different in the two levels; $F_2(J=N+\frac{1}{2})$ has F=N-3 to N+4 while $F_3(J=N-\frac{1}{2})$ has F=N-4 to N+3. Hyperfine components with F=N-3 to N+3 occur in both electron spin levels, and therefore perturb each other, but the F=N+4 component of F_2 and the F=N-4 component of F_3 pass through the avoided
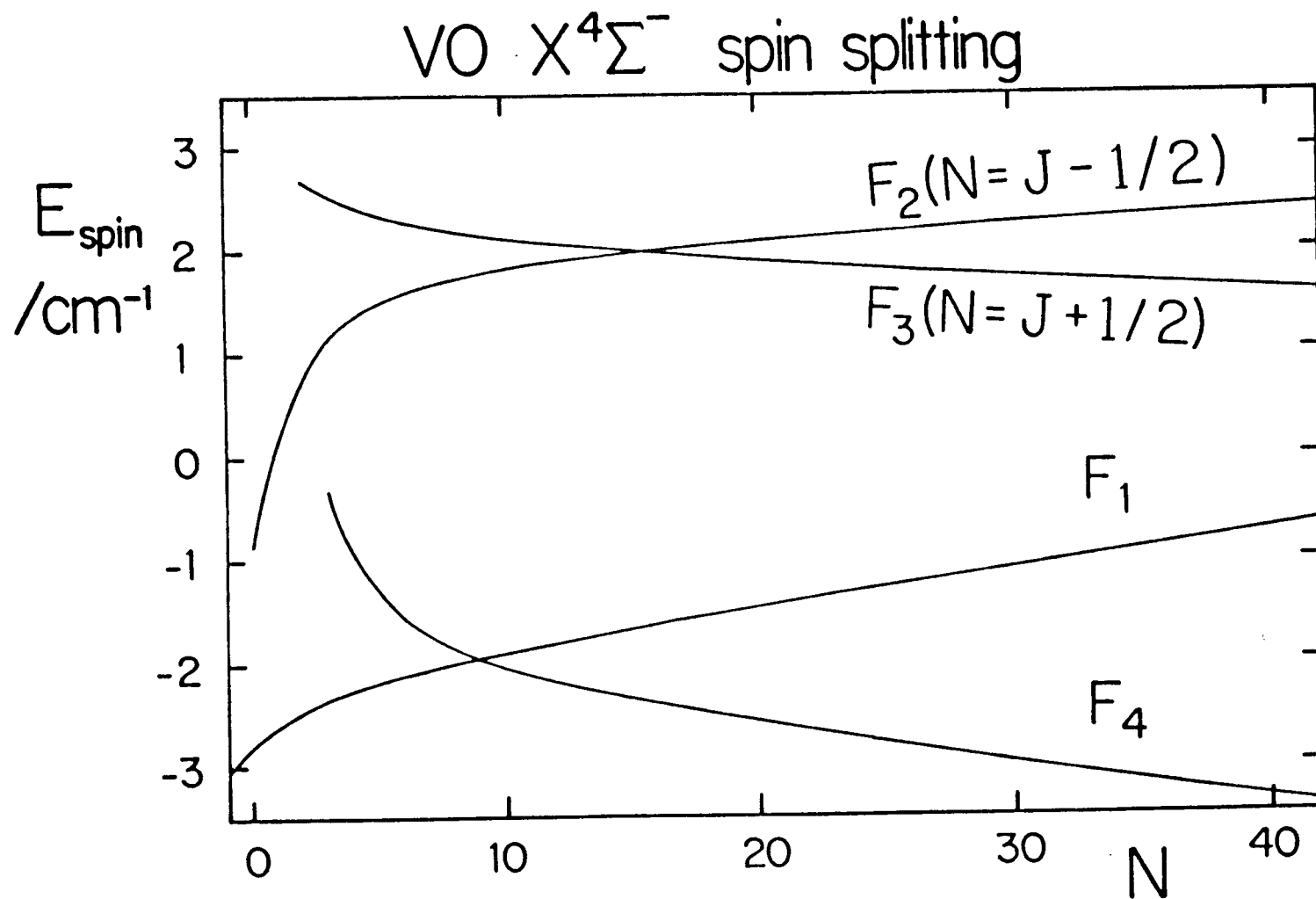
Fig. 5.4 Electron spin fine structure of the VO $X^4\Sigma^-$ $v = 0$ level plotted as a function of N. The rotational and hyperfine structures are not shown.
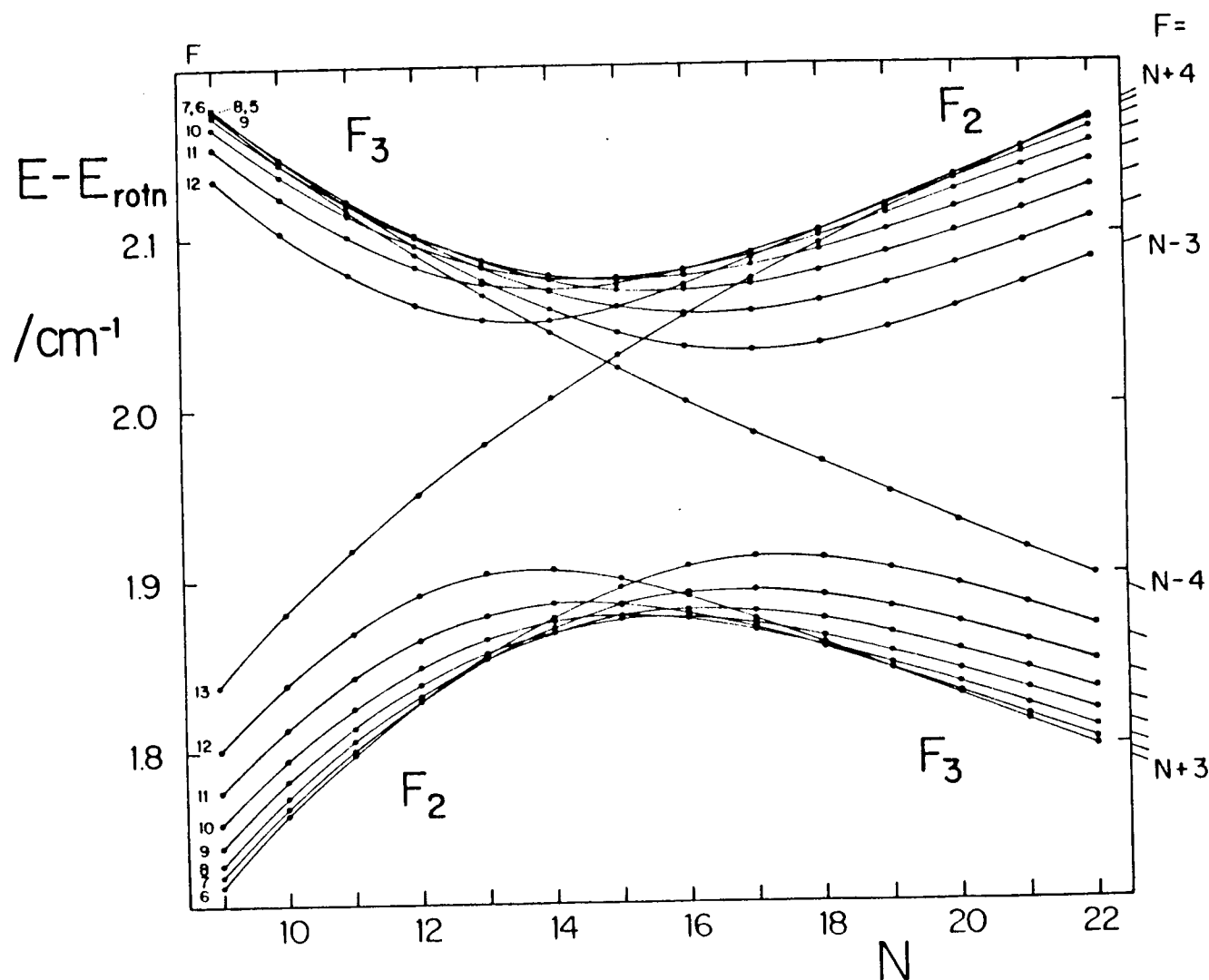
Fig. 5.5 Calculated hyperfine energy level patterns for the F_2 and F_3 electron spin components of the $X^4\Sigma^-$ $v = 0$ state of VO in the range $N'' = 9 - 22$. The calculations are from the final least squares fit to the ground state hyperfine structrues, and levels with the same values of $F''-N''$ are connected.

crossing region unaffected. They give rise to the isolated strong lines in the centres of some of the hyperfine patterns which are very characteristic, as can be seen in Fig. 5.6.

Figure 5.6 shows the P_3 lines for $N'' = 15-18$. This is almost the only region where the perturbed lines are not overlapped by other branch structure. The $P_3(18)$ line has most of its intensity in the short wavelength components (left hand side), which are the zero order P_3 transitions. The intensity transferred to the induced lines (on the right) depends on two factors, the separation of the zero-order hyperfine components, and the value of F. For $P_3(18)$ the two factors approximately balance for F=15-18, but the higher F components, which are starting to form a hyperfine 'head', are much weaker. The central unperturbed F=14 line (F=N-4) is very distinct.

With decreasing N the intensity of the P_3 lines is progressively transferred to the long wavelength components, and the 'heads' in the hyperfine structure become very pronounced. As might be expected from Fig. 5.5 the effects pass through a maximum at $N''=15$. An interesting effect of the reversal of the hyperfine energy order at the perturbation is that the different hyperfine 'branches' (with the same value of F-N) have their minimum separation and most nearly equal intensities at different N values: for instance the F=N+3 hyperfine components have minimum separation at N=14, but the F=N-3 components have minimum separation at N=17. This caused us some difficulty in the early stages of the least squares fitting, because we needed to establish the exact parentage of a hyperfine component in order to match it with an eigenvalue from the diagonalization.

Internal hyperfine perturbations in VO, $X^4\Sigma^-$
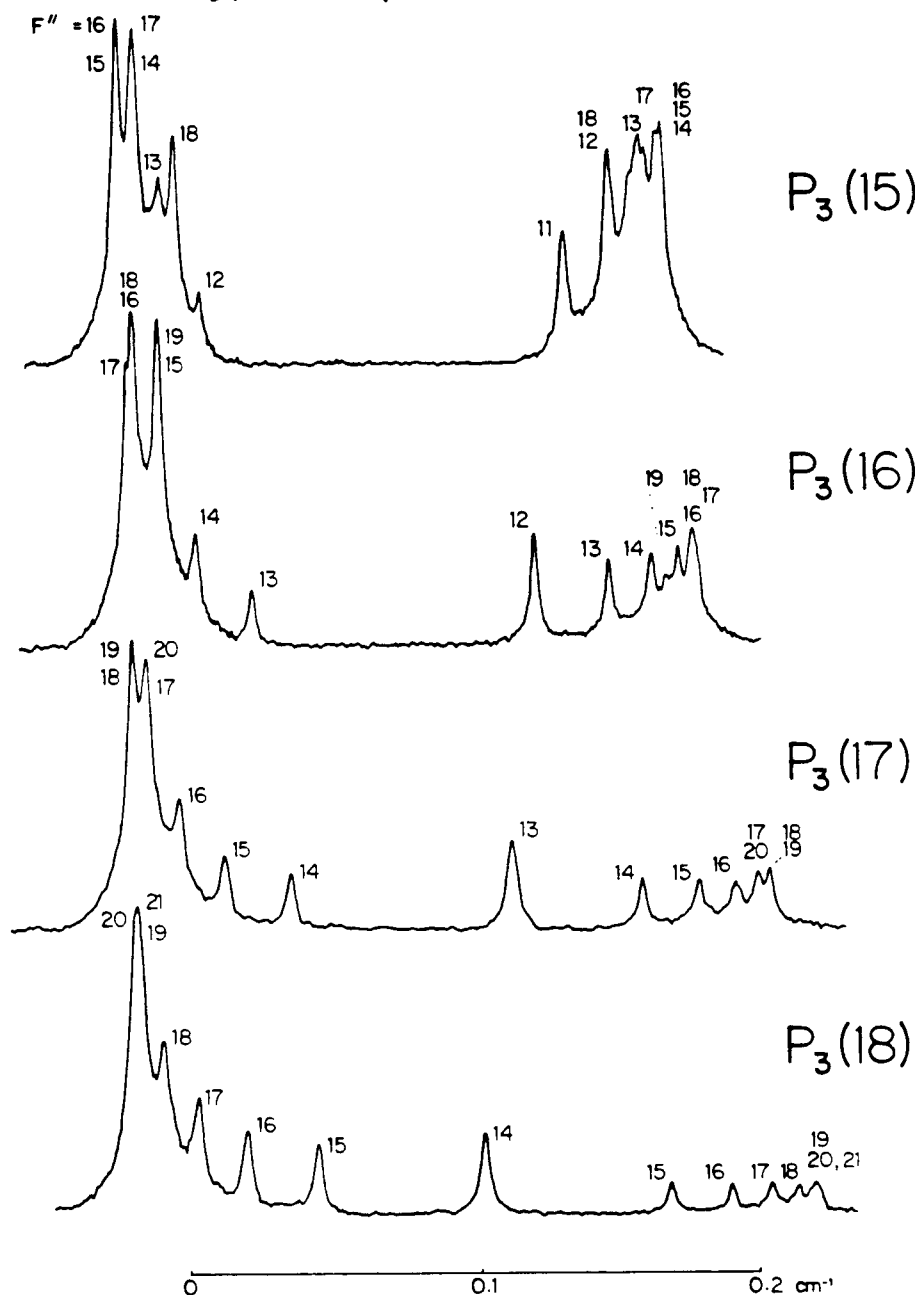
Fig. 5.6 The P_3 branch lines of the $C^4\Sigma^- - X^4\Sigma^-$ (0,0) band in the region n" = 15-18, showing the hyperfine patterns near the ground state internal hyperfine perturbation. The F" quantum numbers for the hyperfine components are marked.

Below $N''=15$ the patterns are unfortunately blended because the upper state spin splittings are smaller than the ground state perturbation doublings; also other branches interfere. Figure 5.7 shows the P_2 and P_3 lines for $N''=11-14$. At this stage the N values are low enough for the energy 'spread' of the hyperfine structure of the $F_2''(N)$ and $F_3''(N)$ levels to be noticeably different, as can be seen in Fig. 5.5. This difference governs many of the features of the low N hyperfine patterns, and results from the factors $(2N+9)$ and $(2N-7)$, respectively, in the diagonal elements of $b\underline{I}.\underline{S}$ for the F_2 and F_3 components. The result in the spectrum is that the F_2 branches are very open while the F_3 branches begin to collapse into sharp spikes where the hyperfine structure is often not fully resolved. The factor $(2N-7)$ for the F_3 levels in fact causes the hyperfine energy order to invert between $N=3$ and 4.

The upper state has a similar hyperfine perturbation centred near $N'=5$. The energy level pattern is shown in Fig. 5.8. Parts of this pattern are anomalous because the N values are so low that the full complement of eight hyperfine components is not present. Also the inversion of the hyperfine energy order for the lower set of interacting components does not occur: the reason is that the inversion in the F_3 components between $N=3$ and 4 cancels the inversion caused by the fact that they turn into F_2 levels at the perturbation. The only seeming irregularity in the lower set is that the $F=N+3$ components lie above the $F=N+2$ for $N'=4$ and 5.

The P_2 and P_3 branches in the region $N''=5-8$ are shown in Fig. 5.9. The P_2 lines are more than 0.5 cm^{-1} to the blue of the P_3 lines with the
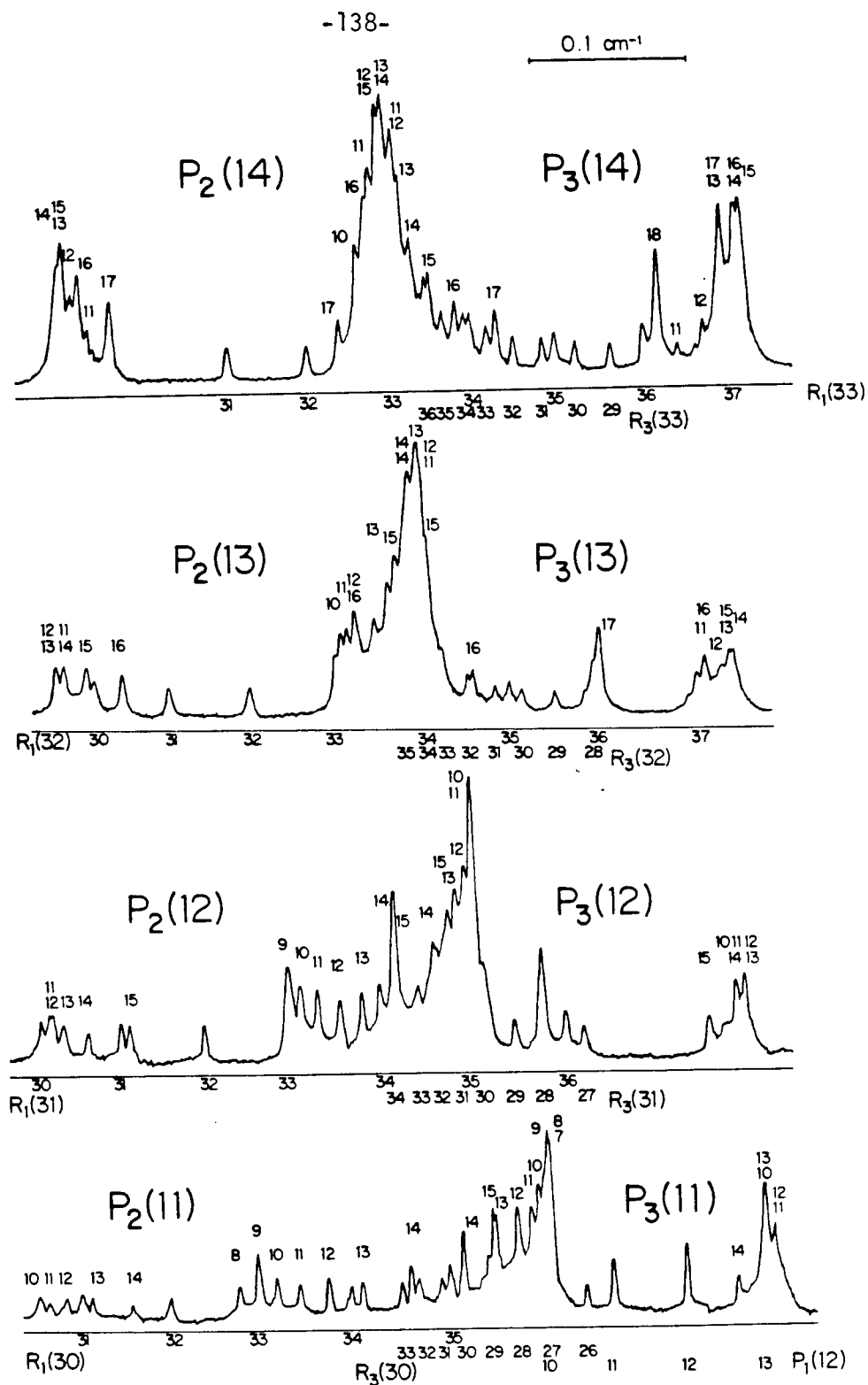
Fig. 5.7 The P_2 and P_3 branch lines of the VO $C^4\Sigma^- - X^4\Sigma^-$ (0,0) band in the range N''= 11-14. Numbers above the spectra are F'' values for the hyperfine components of the P_2 and P_3 lines; other lines belonging to overlapping branches are indicated below the spectra.
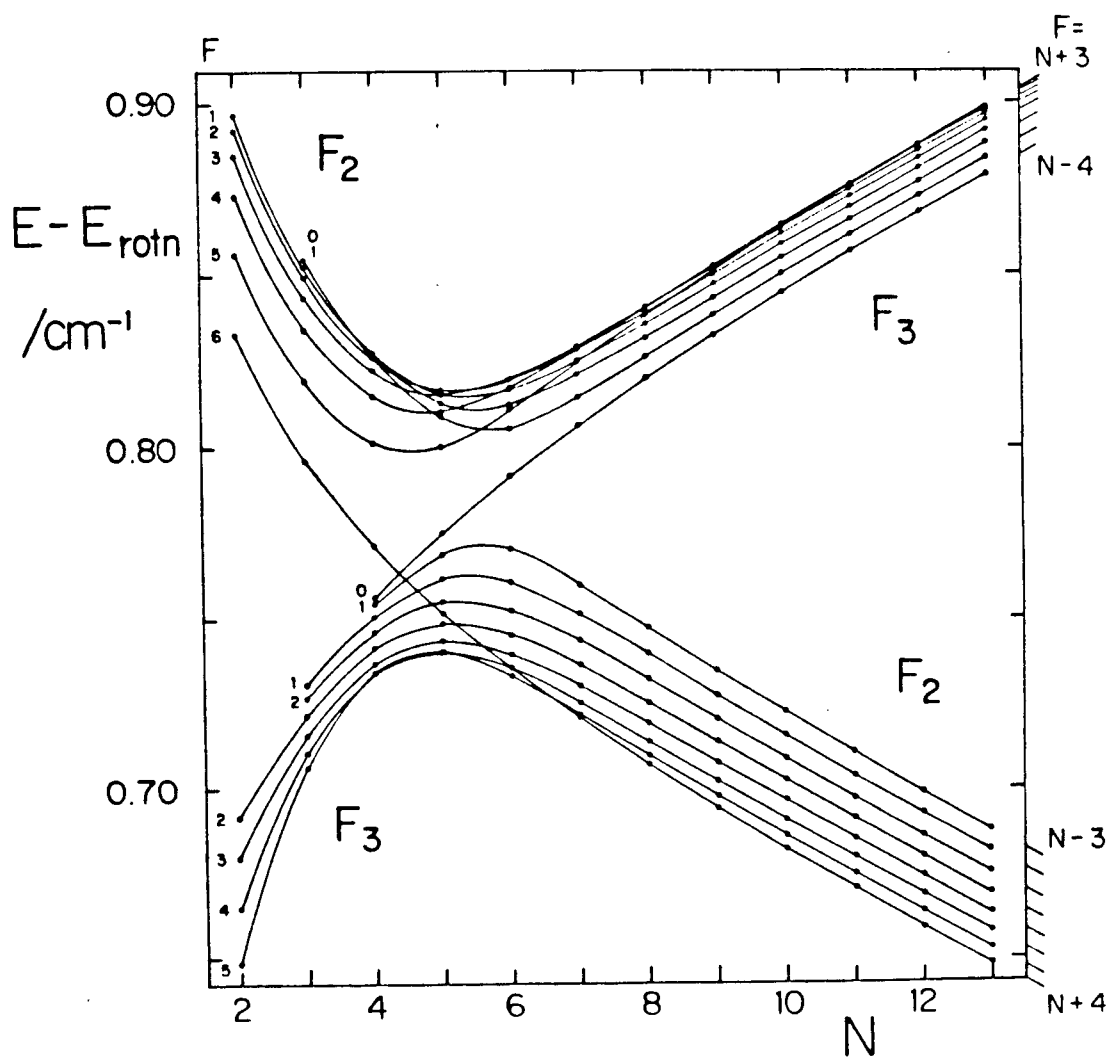
Fig. 5.8 Calculated hyperfine energy level patterns for the F_2 and F_3 electron spin components of the $C^4\Sigma^-$ v=0 state of VO in the region of the internal hyperfine perturbation (N' = 2-13). Levels with the same values of F'-N' are connected.
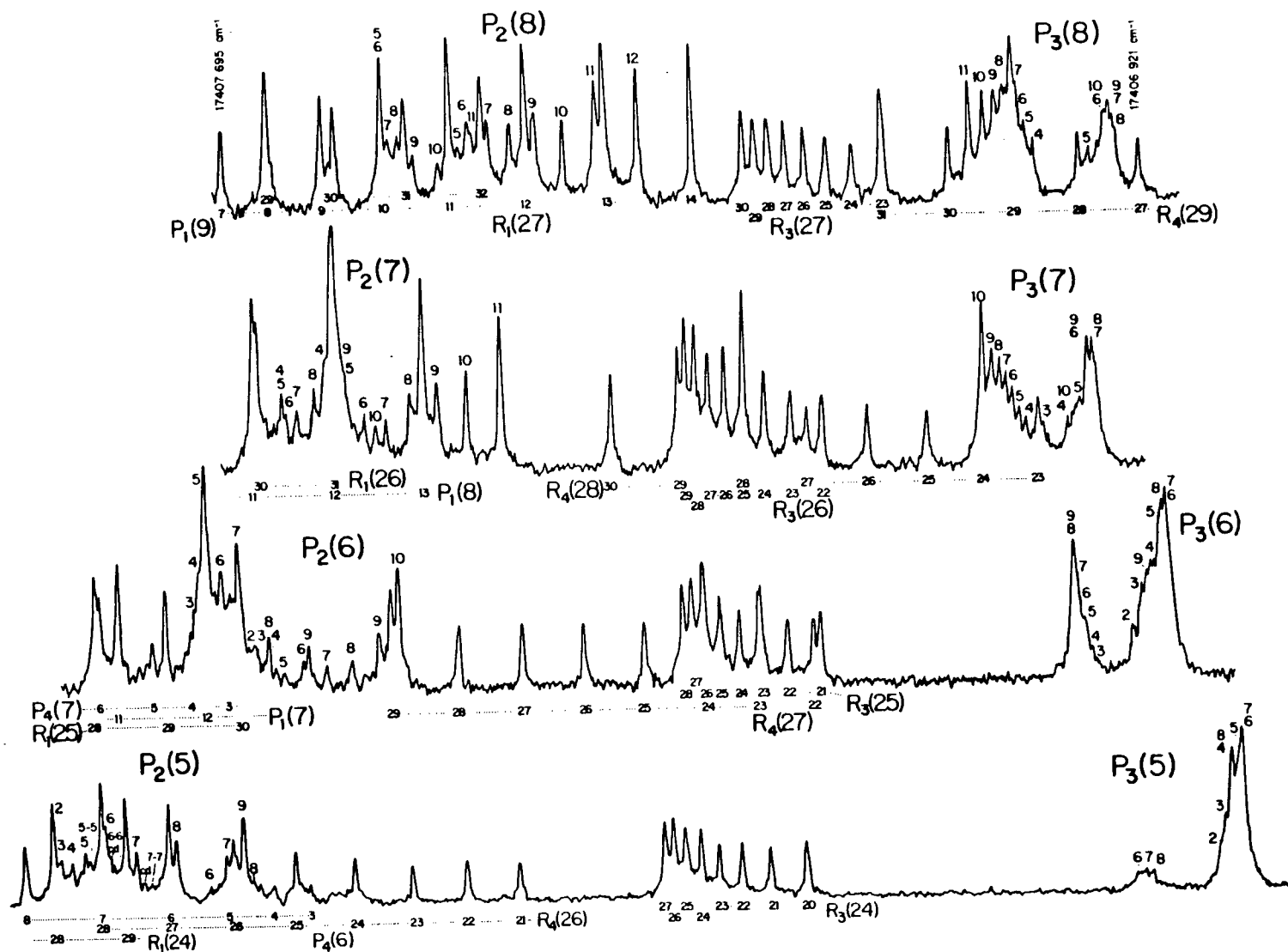
Fig. 5.9 The P_2 and P_3 branch lines of the VO $C^4\Sigma^- - X^4\Sigma^-$ (0,0) band in the region N" = 5-8 ; the F" quantum numbers of the hyperfine components are marked above the spectra. Overlapping high-N R lines and low-N P_1 and P_4 lines are indicated below the spectra. All four tracings are to the same scale.

same N'' value, reflecting the large spin splitting in the ground state, and their appearance is altogether different because of the different overall hyperfine energy 'spread' described above. The P_3 lines are only partially resolved even at our resolution of 100 MHz, and it is fortunate that the induced lines in the P_2 branches are so well resolved, otherwise it would not be possible to follow the upper state hyperfine energy pattern. The hyperfine assignments are very difficult to make in this region, because the line positions depend critically on the spin and hyperfine constants of both states; this was in fact the last region of the band to be assigned.

(iii) <u>The band centre</u>

The centre of the band contains R lines with N''=15-20 (corresponding to the ground state internal hyperfine perturbation) together with the very low N lines. The R lines confirm the hyperfine patterns given by the P lines, but blending limits their usefulness. The low N lines on the other hand are very interesting because they carry most of the information about the dipolar $\underset{\sim}{I},\underset{\sim}{S}$ interaction and the quadrupole constants. Often they are quite difficult to assign because the hyperfine patterns are fragmentary, and detailed calculations of the energy levels are needed.

Typical patterns are shown in Fig. 5.10. The upper tracing, which covers the region just to the blue of the band origin, shows the $P_2(1)$, $R_3(2)$ and $Q_{ef}(\tfrac{1}{2})$ lines, superimposed on the perturbed $R_2(17)$ and $R_3(17)$ lines. The line strengths in our spectra are such that hyperfine components with F''≤2 are usually not seen. However in the range F''=3-7 we
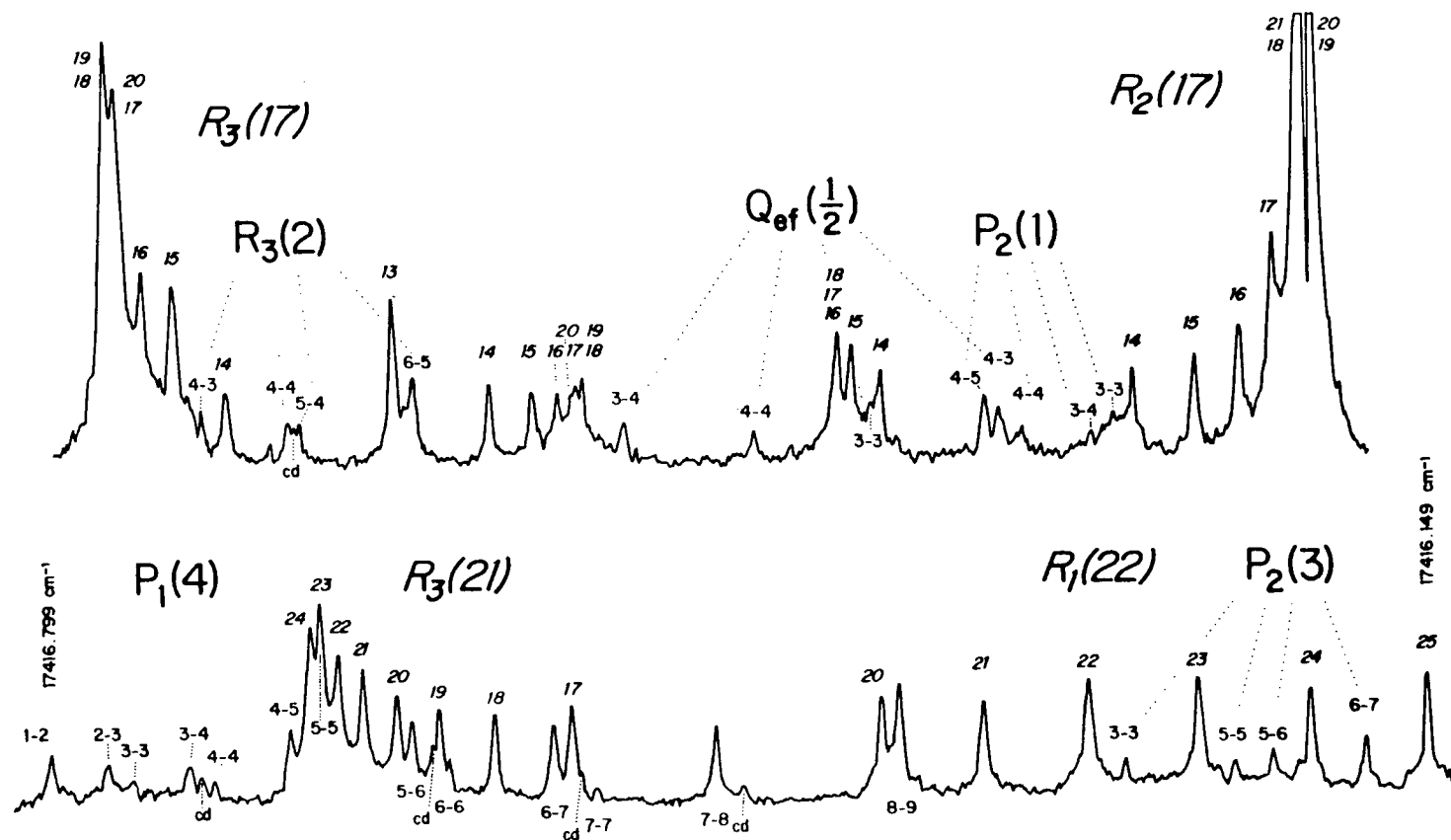
Fig. 5.10 Two regions of the VO $C^4\Sigma^- - X^4\Sigma^-$ (0,0) band near the band origin. Low-N lines are marked in roman type with hyperfine quantum numbers indicated as F'-F"; high-N lines are marked in italic type with only the F" quantum numbers of the hyperfine components indicated. Cross-over signals (centre dips) are marked 'cd' . The two tracings are at the same scale.

frequently observe lines with $\Delta F \neq \Delta J$, and, where lines with a common lower level lie within the same Doppler profile, we observe centre dips. These two effects are well-known in sub-Doppler spectroscopy, particularly for I_2(35), and require no further explanation. The advantage of the additional lines that arise is that they give direct hyperfine combination differences, which break the correlation between the upper and lower state hyperfine constants resulting from the parallel selection rules of the electronic transition. For example, in the line $Q_{ef}(\frac{1}{2})$ (or $^PQ_{12}(0)$, to give it its case (b) designation) we observe all four of the possible hyperfine components, and therefore obtain directly the separations of the F=3 and F=4 components of the two combining $J=\frac{1}{2}$ levels. An energy level diagram illustrating this is given in Fig. 5.11.

The lower tracing of Fig. 5.10 shows the $P_1(4)$ and $P_2(3)$ lines, against the background of $R_3(21)$ and $R_1(22)$. The $P_1(4)$ line has particularly clear $\Delta F = \Delta J$ hyperfine components, and also centre dips between them and the case (b) allowed $\Delta F = \Delta J = -1$ components. An interesting centre dip involves the strong $F'=7-F''=8$ component and the unobserved $F'=8-F''=8$ component; this centre dip is quite weak, because the strength of a centre dip is proportional to the square root of the product of the strengths of the two contributing transitions (35).

Altogether about forty $\Delta F \neq \Delta J$ hyperfine components have been identified in the low N lines. We had not anticipated them in our original least squares programme for fitting the observed transitions, and had to include them as special cases. Similarly we had not anticipated that the Q branches would be so comparatively strong. Twelve hyperfine components belonging to four Q lines have been assigned; the observed Q
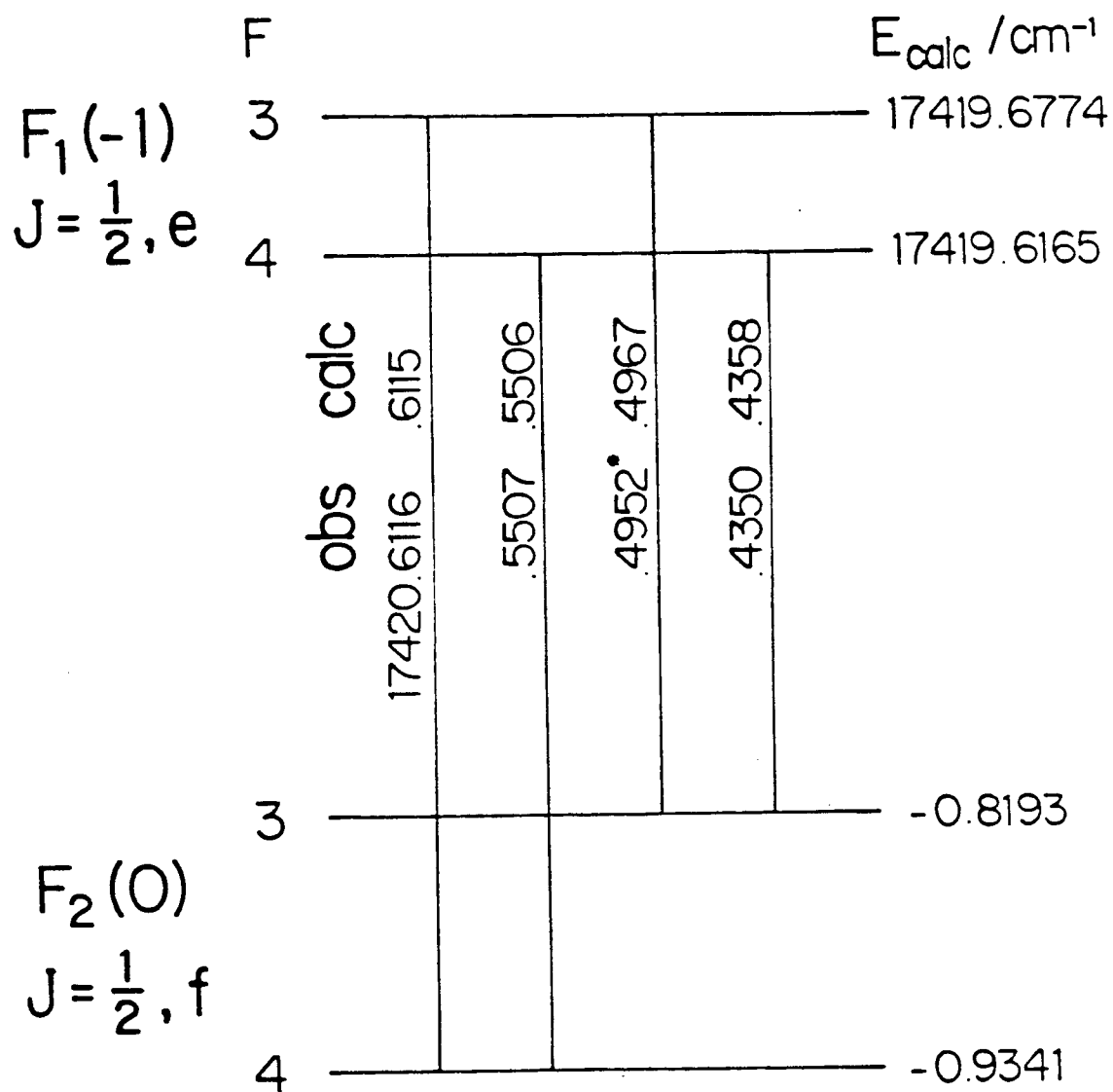
Fig. 5.11 Energy level diagram indicating the assignment of the four

hyperfine components of the line $Q_{ef}^{(\frac{1}{2})}$.

lines are $Q_{ef}(\frac{1}{2})$ and $Q_{fe}(\frac{1}{2})$, which form the Λ-doubling components of the $Q(J=\frac{1}{2})$ line of the $^4\Sigma^-_{\frac{1}{2}} - {}^4\Sigma^-_{\frac{1}{2}}$ sub-band in a case (a) description, and the corresponding first Q lines of the $^4\Sigma^-_{3/2} - {}^4\Sigma^-_{3/2}$ sub-band, $Q_{ef}(\frac{3}{2})$ and $Q_{fe}(\frac{3}{2})$.

At these low J values the case (b) description of the levels and transitions breaks down, and some apparently impossible lines arise. The $Q(\frac{1}{2})$ lines are good examples: $Q_{ef}(\frac{1}{2})$ and $Q_{fe}(\frac{1}{2})$ become ${}^PQ_{12}(0)$ and ${}^RQ_{21}(-1)$, respectively.

We have kept the case (b) notation for the main branches since they show no discontinuities when followed down from high N. This breakdown in notation for a $^4\Sigma$ state in fact only happens when the $\Omega=\frac{1}{2}$ component in case (a) corresponds to the F_1 and F_2 levels, that is when the spin-spin parameter λ is greater than the rotational constant B(33); both the $C^4\Sigma^-$ and $X^4\Sigma^-$ states of VO have $\lambda > B$.

The inner band head formed by the R_2 and R_3 branches is very complex because it contains many extra lines caused by the internal hyperfine perturbations, together with overlapping R_1 and R_4 lines. Nevertheless all the features have been assigned with the aid of computer calculations. The assigned lines of the band are listed in Appendix VI, Table I.

E. Electronic perturbations in the $C^4\Sigma^-$ state

Nine electronic perturbations have been found in the $C^4\Sigma^-$ v=0 level. Seven of these are shown in Fig. 5.12, which is a plot of the energy levels against $J(J+1)$; two others, at $F_2(74)$ and $F_3(85)$, which
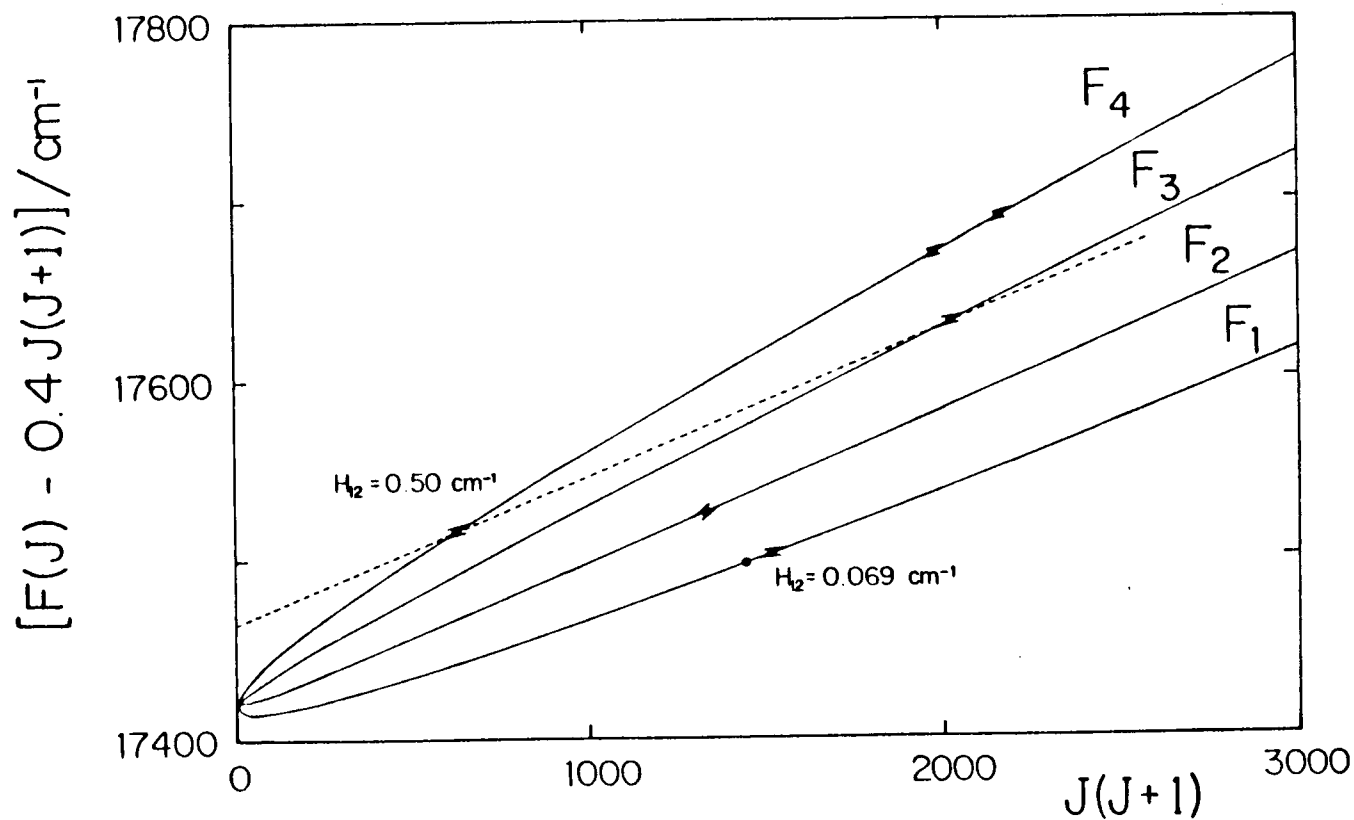
Fig. 5.12 Rotational energy levels of the $C^4\Sigma^-$ v = 0 state of VO (with scaling as indicated) plotted

against J(J+1). Dots indicate rotational perturbations, and the perturbation matrix elements,

H_{12}, are given where they can be determined. The dashed line is probably a component of a $^2\Pi$

state (see text) with B_{eff}= 0.482 cm^{-1} .

were discovered by Lagerqvist and Selin (8) lie beyong the range of the figure. The figure also includes the perturbation matrix elements where they can be determined from the induced extra lines. The only regularity we can recognize is that the perturbations at $F_4(26)$ and $F_3(45)$ are caused by the two Λ-components of an orbitally-degenerate state, which could possibly be $^2\Pi$, as we now show.

(i) The $F_4(26)$ perturbation

The perturbation at $F_4(26)$ is particularly annoying because the perturbing state has almost the same B value as $C^4\Sigma^-$; its effects therefore do not die away rapidly to zero on either side of the maximum of the avoided crossing. It can be shown that the perturbation shift at the origin of $C^4\Sigma^-$ is still 0.006 cm^{-1}, so that since we can determine the line positions to better than 0.0005 cm^{-1} we must allow for the effects of the perturbation over the complete range of F_4 levels. The details of how this was done are given in Section F.

We can assign the perturbations at $F_4(26)$ and $F_3(45)$ to the same perturbing state because it is possible to interpret the $F_4(26)$ perturbation in detail from the laser spectra. Ignoring the hyperfine structure initially, we fitted the upper state term values with $N'=24-28$ (including the single observed 'extra' level) to the eigenvalues of the Hamiltonian matrix

$$\underset{\sim}{H} = \begin{bmatrix} T_C + B_C N(N+1) & H_{12} \\ H_{12} & T_{pert} + B_{pert} N(N+1) \end{bmatrix} \quad (5.18)$$

It was necessary to fix B_C (for the $C^4\Sigma^-$ state) at an effective value for this N range calculated from preliminary least squares work, and to assume that the perturbation matrix element can be treated as constant over such a small N range. The results are given in Table 5.2. The fit is good, and the parameter T_C comes out to within 0.1 cm^{-1} of the C state origin; also the perturbation matrix element H_{12} is given to an accuracy of $\pm0.005_5$ cm^{-1}.

Eq. (5.18) assumes that the rotational energy of the perturbing state is proportional to $N(N+1)$; however the N range of the fit is so small that we can convert the results, without loss of accuracy, to the case where the energy of the perturbing state is linear in $J(J+1)$. When this is done it is found that B_{pert} agrees to within 0.0007 cm^{-1} with what is obtained if the $F_4(26)$ and $F_3(45)$ perturbations are assumed to be caused by the same perturbing state. This is excellent agreement, and unambiguously proves a connection between the two perturbations. Because the F_4 and F_3 levels have different e/f symmetries the perturbing state must have rotational levels with double parity (i.e. it must be orbitally-degenerate); the two perturbations are therefore caused by different Λ-components of a perturbing orbitally-degenerate state.

Extrapolation of the vibrational structures of the $B^4\Pi$ and $A^4\Pi$ states (34) rules them out as candidates for the perturbing state. Of course a third $^4\Pi$ state could be responsible, though we see no evidence for such a state in our Fourier transform spectra, which extend down to 6000 cm^{-1}: the emission transition to $X^4\Sigma^-$ would be spin and orbitally allowed. On the other hand the hyperfine structure suggests that

Table 5.2 Analysis of the $C^4\Sigma^-$, $F_4(26)$ perturbation.

	Upper state energy levels			
N'	with F = N-1 (cm^{-1})		Obs-calc (cm^{-1})	
24	17716.011		-0.003	
25	17740.641		0.003	
26	17766.039	17767.084	0.000	-0.000
27	17793.169		0.002	
28	17820.725		-0.001	

Least squares results: (1σ)

T_c =   17420.055   ± 0.018 cm^{-1}

B_c =   0.49336   (fixed)

T_{pert} =   17447.313   ± 0.020

B_{pert} =   0.4550   ± 0.0003

H_{12} =   0.496   ± 0.005$_5$

the perturbing state has only moderate spin-orbit coupling, so that a possible candidate would be a $^2\Pi$ state from the same electron configuration as $A^4\Pi$ (probably $4s\sigma^1 3d\delta^1 4p\pi^1$).

The sum of hyperfine energies of the doubled $F_4(26)$ levels is found to be linear in $F(F+1)$, so that the perturbing state must follow case (a_β) or ($b_{\beta J}$) coupling; also the spacing of its hyperfine levels is found to be almost exactly the same as that of $C^4\Sigma^-$, $F_4(26)$. If we write the hyperfine energy expression for a rotational level (N,J) as

$$E_{hfs} = T_0 + kF(F+1) \qquad (5.19)$$

where k is a function of N, J and the hyperfine constants, the deperturbed values are

$$k(C^4\Sigma^-, N=26, J=24\tfrac{1}{2}) = 0.000234 \text{ cm}^{-1},$$
$$k(\text{perturbing}, J=24\tfrac{1}{2}) = 0.000205 \text{ cm}^{-1} \qquad (5.20)$$

Now case ($b_{\beta J}$) states have wider hyperfine spacings at high J than case (a_β) states for the same hyperfine parameters, as can be seen from the diagonal elements of $b\underset{\sim}{I}.\underset{\sim}{S}$: the case ($b_{\beta J}$) expression

$$\langle N\Lambda SJIF|b\underset{\sim}{I}.\underset{\sim}{S}|N\Lambda SJIF\rangle = \frac{-b[N(N+1)-S(S+1)-J(J+1)][F(F+1)-I(I+1)-J(J+1)]}{4J(J+1)}$$

$$(5.21)$$

has essentially an extra factor of J compared to the case (a_β) expression (11,36)

$$\langle J\Omega S\Sigma\Lambda I F|b\underset{\sim}{I}.\underset{\sim}{S}|J\Omega S\Sigma\Lambda I F\rangle = b\Omega\Sigma\frac{[F(F+1)-I(I+1)-J(J+1)]}{2J(J+1)} \tag{5.22}$$

Therefore the comparatively large value of k for the orbitally-degenerate perturbing state indicates a considerable tendency to case $(b_{\beta J})$ coupling, or in other words that it has comparatively small spin-orbit coupling. This is what we expect for a $^2\Pi$ state from the same configuration as $A^4\Pi$ (where $A \simeq 30$ cm^{-1}), but not what we expect for a $^2\Pi$ state from the same configuration as $B^4\Pi$ (where $A \simeq 70$ cm^{-1}). If the perturbing state is indeed a component of the $^2\Pi$ state corresponding to $A^4\Pi$, the positive sign of the hyperfine parameter k suggests that it is the F_1 component, though its magnitude is only a quarter of what we calculate for case $(b_{\beta J})$ coupling, indicating that the spin-uncoupling is only quite partial[1].

---

[1] The argument runs as follows. The hyperfine parameter b for $A^4\Pi$ is known to be virtually identical to that of $X^4\Sigma^-$, namely 0.027$_3$ cm^{-1}. The $^2\Pi$ state from the same configuration as $A^4\Pi$ should, in first approximation, have a b-value three times as large, because the isotropic hyperfine operator is strictly $\underset{i\ electrons}{\Sigma\ b_i\ \underset{\sim}{I}.\underset{\sim}{s}_i}$ rather than $b\underset{\sim}{I}.\underset{\sim}{S}$. Therefore from eq. (5.21) we calculate, for case $(b_{\beta J})$ coupling,

$$k(^2\Pi, F_1, J=24\tfrac{1}{2}) = 0.00084\ \mathrm{cm}^{-1}$$
$$K(^2\Pi, F_2, J=24\tfrac{1}{2}) = -0.00080\ \mathrm{cm}^{-1}$$

Further evidence that the spin-uncoupling has not progressed very far comes from the spin-orbit matrix elements given by Kovács (37): in pure case (b) coupling

$$\langle ^2\Pi, F_1|H_{s.o.}|^4\Sigma^-, F_4\rangle = 0$$

so that no perturbation would have been observed.

(ii) The $F_1(37)$ perturbation

The very small perturbation at $F_1(37)$ has been reported already (38). It forms an instance where an avoided crossing occurs within the hyperfine structure of a single rotational level, and the analysis can be carried out by treating the hyperfine structure as a fragment of rotational branch structure. Two regions of the spectrum are shown in Fig. 5.13. The lower tracing is the $P_1(27)$ line near 17353 cm^{-1}, which is unperturbed and shows the Landé-type pattern; the lower state F values are given underneath. The upper tracing shows two lines, the $P_1(38)$ and $P_3(38)$ lines. The $P_1(38)$ line consists of 13 components, rather than eight, and the intensity pattern is anomalous. The $P_3(38)$ line has been included to give the intensity scale; nevertheless its hyperfine pattern is found to be irregular as well, as a result of the internal hyperfine perturbation in the ground state described earlier.

Intensity considerations allow the F" quantum numbers to be assigned to the components of $P_1(38)$, as given in Fig. 5.3. It is evident there has to be a perturbation within the hyperfine structure of the $F_1(37)$ rotational level of the upper state. The lower state rotational-hyperfine energies can be calculated from the rotational constants got by fitting the ground state combination differences The upper state term values can then be obtained by combining these with the line positions, as in Table 5.3. When the upper state energy levels are plotted against F(F+1), the classic pattern of an avoided crossing (41) emerges (see Fig. 5.14): there are two sets of energy levels which have minimum separation where the intensities of the corresponding lines are equal, and the averaged energy levels are
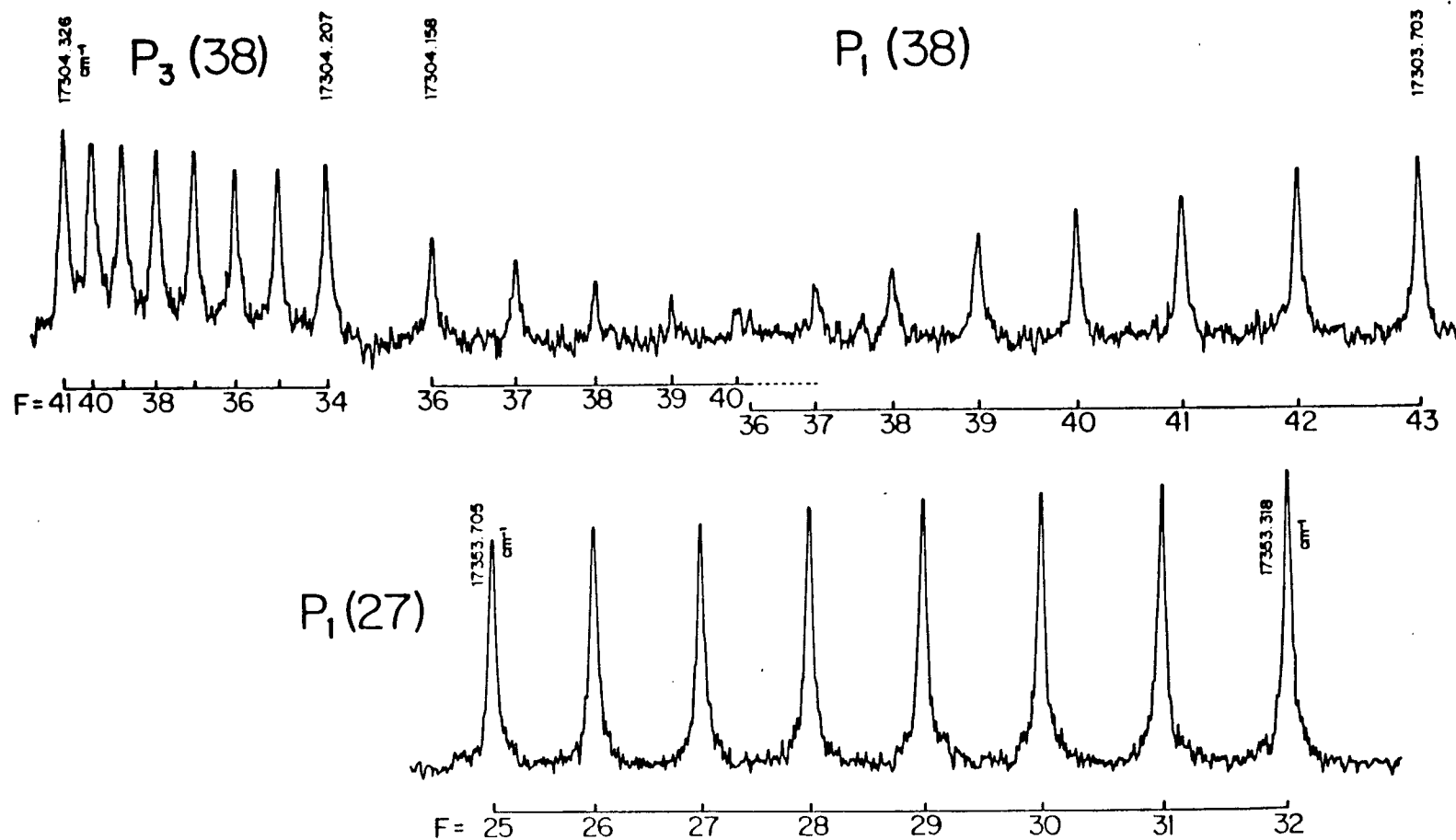
Fig. 5.13 Two regions of the intermodulated fluorescence spectrum of the $C^4\Sigma^-$ – $X^4\Sigma^-$ (0,0) band of VO. Upper tracing: the $P_3(38)$ and perturbed $P_1(38)$ lines. Lower tracing: the unperturbed $P_1(27)$ line.
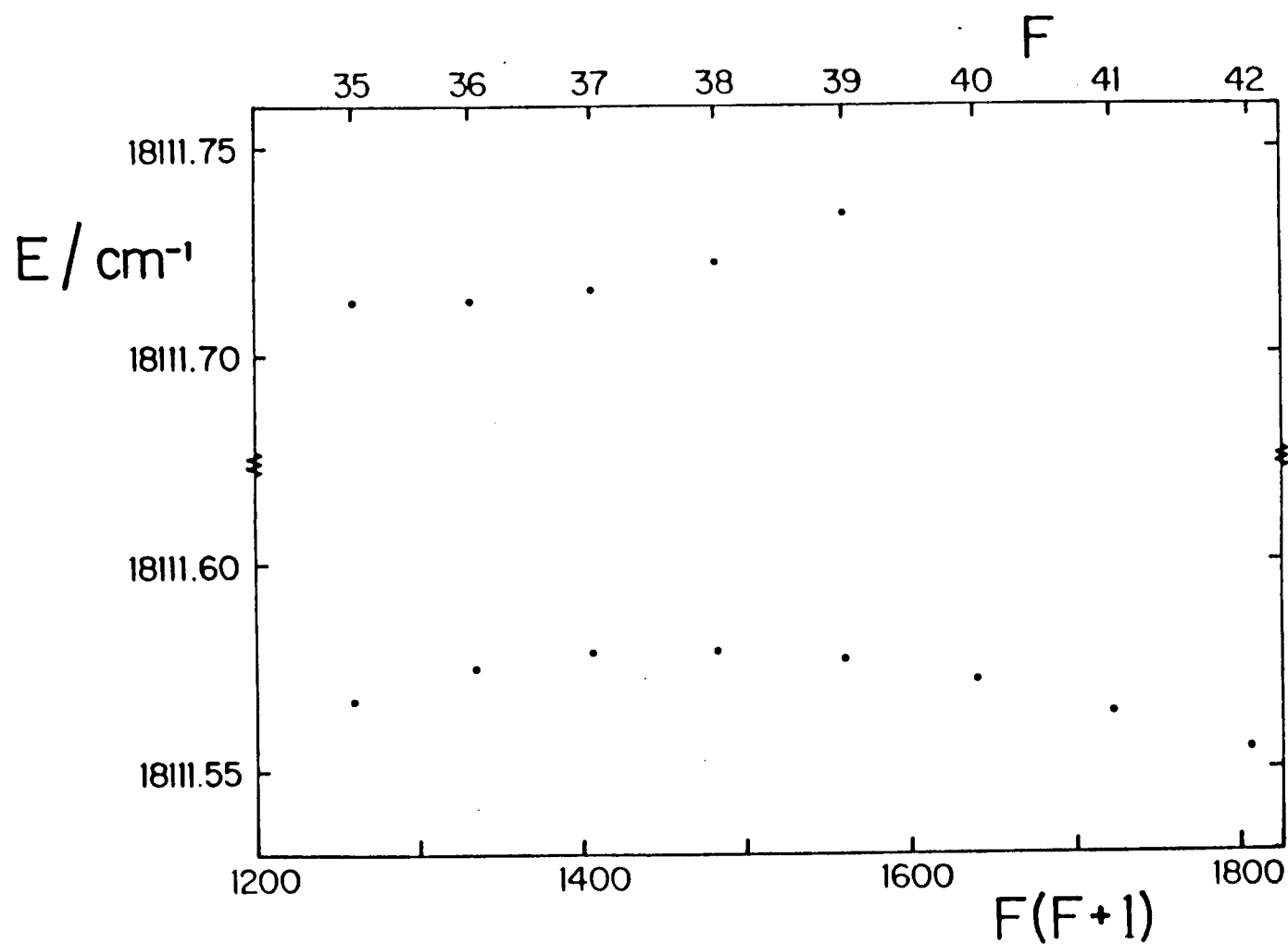
Fig. 5.14 Upper-state term values (cm^{-1}) of the hyperfine levels of the perturbed $F_1(37)$ rotational level of the $C^4\Sigma^-$, v=0 state of VO plotted against F(F+1).

Table 5.3 Analysis of the $C^4\Sigma^-$, $F_1(37)$ perturbation.

F'	$P_1(38)$ lines			$R_1(36)$ lines			$F_1'(37)$ levels		10^4(O-C)	
	lower	upper	$F_1"(38)$ energy	lower	upper	$F_1"(36)$ energy	lower	upper	lower	upper
35	17304.0117	4.1577	807.3564	17385.7700*	5.9101	725.6015	18111.3674	1.5129	1	2
36	3.9807	4.1195	7.3933	5.7339	5.8716	5.6383	1.3731	1.5114	0	0
37	3.9451	4.0824	7.4314	5.6984	5.8360	5.6764	1.3757	1.5131	-1	-3
38	3.9044	4.0479	7.4708	5.6587	5.8034	5.7158	1.3749	1.5190	-1	0
39	3.8601	4.0173	7.5115	5.6131		5.7565	1.3706	1.5281	-2	1
40	3.8116		7.5534	5.5654		5.7986	1.3645		6	
41	3.7585		7.5968	5.5116		5.8420	1.3545		-3	
42	3.7031		7.6414	5.4568		5.8869	1.3441		1	

Values in cm^{-1}; * means blended line. Allowance has been made in the averaging for an absolute calibration shift of 0.0007 cm^{-1} between the $P_1(38)$ and $R_1(36)$ lines.

Least squares results:

$C^4\Sigma^-$: $T_o^{(1)}$ = 18111.6888 ± 0.0020 cm^{-1} (1σ)

k_1 = -0.000178 ± 0.000001$_2$

pert : $T_o^{(2)}$ = 18111.1122 ± 0.0032

k_2 = 0.000241 ± 0.000002

H_{12} = 0.0685 ± 0.0001$_1$

Standard deviation = 0.00028 cm^{-1}

linear in $F(F+1)$. The perturbation matrix element is very small, but analysis is nonetheless possible because the k parameters are very different for the two interacting levels.

We have now disentangled the $R_1(36)$ lines from the strong overlapping $P_2(17)$ lines and can refine the parameters reported previously (38). The effect of averaging the $R_1(36)$ amd $P_1(38)$ data has been to improve the standard deviation of the least squares. fit considerably. The results are given in Table 5.3. The model used was a simple 2x2 matrix for each F value, akin to eq. (5.18):

$$H = \begin{bmatrix} T_o^{(1)} + k_1 F(F+1) & H_{12} \\ & \\ H_{12} & T_o^{(2)} + k_2 F(F+1) \end{bmatrix} \quad (5.23)$$

Nothing was held fixed in the least squares treatment, and the accuracy of the model and the fit must be assessed by comparing the observed and calculated k values for $C^4\Sigma^-$, $F_1(37)$:

$$k(C^4\Sigma^-, N=37, J=38\tfrac{1}{2})_{calc} = -0.000185 \text{ cm}^{-1}$$
$$\quad (5.24)$$
$$k(C^4\Sigma^-, N=37, J=38\tfrac{1}{2})_{obs} = -0.000178\pm0.00004 \text{ cm}^{-1} (3\sigma)$$

The perturbing state has a lower B value than $C^4\Sigma^-$, which means that further perturbations in the other spin components of $C^4\Sigma^-$ might be expected at lower N values. We have not identified any such perturbations, and can unfortunately say nothing about the nature of the perturbing state except that its hyperfine splitting is large. An

interesting effect of the perturbation is that the hyperfine structures of the levels within about four units of N on either side of the avoided crossing are noticeably irregular; this reflects the fact that the unperturbed level separations show a strong dependence on F.

A second small perturbation occurs in the F_1 component at N=36. The F_2 component is also perturbed at this position. Unfortunately extra lines do not occur and we can say nothing about these perturbations except that they appear to be unrelated to each other or to the other perturbations described.

F. Least squares fitting of the line positions

It has been a formidable problem achieving a least squares fit to the observed data that reflects their precision adequately. We discovered at an early stage that a full matrix treatment of the hyperfine structure was required, and the only approximation we have made has been to omit the $\Delta J=\pm 2$ elements of the electric quadrupole interaction; these are the only elements which do not add to matrix elements of the magnetic interactions, and in any case are calculated to be very small. We also quickly found that the absolute calibration of the isolated lines in the tail of the band was less precise than that of the crowded lines in the head of the band where the overlapping of VO lines between successive 1 cm^{-1} scans of the laser permits several scans to be calibrated at once (see Section B).

However, the main difficulty has been the fact that the $C^4\Sigma^-$ F_4 levels are shifted by electronic perturbations throughout the N range

of our spectra; also we cannot trust the other $C^4\Sigma^-$ spin components not to have been shifted similarly after about $N'= 25$. When we attempted to fit the raw data we were unable to obtain a satisfactory converged fit unless we restricted ourselves to $N<20$, and even then the upper state centrifugal distortion parameter D was unrealistically low ($\sim 6.2\times10^{-7}$ cm^{-1}, compared to the Kratzer relation value of 6.62×10^{-7} cm^{-1}). After some experimenting with higher order terms we realised that it would be necessary to allow for the effects of the state crossing the F_4 levels at $N=26$, and not to attempt to fit the upper state beyond $N'=25$; the ground state $\Delta_2 F''$ combination differences, although less precisely determined because of calibration problems, could be included for the full range of our data, to $N=40$.

(i) Deperturbation of the $C^4\Sigma^-$ F_4 level positions

The 'deperturbation' procedure obviously depends critically on the nature of the perturbing state (hence the detailed discussion in the previous Section). To summarize, we are certain that the perturbing state is orbitally-degenerate, has an effective rotational energy expression

$$E_{pert} = 0.482 \ J(J+1) \ cm^{-1} \qquad (5.25)$$

and that the interaction matrix element $<J_{pert}=24 \ |H| \ C^4\Sigma^-, \ N=26, \ J=24 >$ is 0.496 ± 0.006 cm^{-1}. It seems unlikely that Δ states, or states with $2S+1>4$ will be important, so that we are restricted to $^2\Pi$ and $^4\Pi$ states. Provisionally we favour $^2\Pi$ because we might expect to see a perturbing

$^4\Pi$ state directly in emission to the ground $^4\Sigma^-$ state, and particularly because of arguments based on the hyperfine structure. Fortunately, as can be seen from the tables of Kovács (37), the matrix elements between $^4\Sigma^-$, F_4 and $\underline{any}$ component of $^2\Pi(a)$ or $^4\Pi(a)$ are essentially independent of J, inasfar as matrix elements of $B\underset{\sim}{L}$ can be neglected compared to those of $\sum_i a_i \underset{\sim}{l}_i$; the single exception is $^4\Pi_{5/2}$, but this is ruled out by hyperfine arguments since the hyperfine splittings of the perturbing state are either much too big or of the wrong sign.

We can therefore take the interaction matrix element as being in-dependent of J, and can calculate the downward shifts caused in the $^4\Sigma^-$ F_4 levels according to eq. (5.18), with the zero order perturbing state energy written as in eq. (5.25). The shifts are given in Table 5.4, where they are seen to rise from 0.0060 cm^{-1} at N=3 to 0.0300 cm^{-1} at N=22. For the final least squares work we raised the F_4 levels by the amount from Table 5.4 in excess of 0.0060 cm^{-1}; the quantity 0.0060 cm^{-1} is thus incorporated into the effective λ parameter for $C^4\Sigma^-$. Similar corrections should be needed in the F_3 levels (as Fig. 5.12 shows), but it is easy to prove that they are an order of magnitude smaller. We have not included them specifically, so that they are taken up in the effective spin and centrifugal distortion parameters.

The principal justification of this deperturbation procedure is that it works - it removes the systematic trends in the least squares residuals for the rotational structure, and it makes the centrifugal distortion parameters more realistic: for instance the upper state D value, determined from levels up to N'=24 only, rises to 6.44 x 10^{-7}

Table 5.4 Calculated perturbation shifts in the VO $C^4\Sigma^-$ v=0 F_4 level

N	$\Delta\nu/cm^{-1}$	N	$\Delta\nu/cm^{-1}$	N	$\Delta\nu/cm^{-1}$
3	0.0060	10	0.0082	17	0.0139
4	0.0062	11	0.0087	18	0.0156
5	0.0065	12	0.0093	19	0.0177
6	0.0067	13	0.0099	20	0.0204
7	0.0071	14	0.0107	21	0.0243
8	0.0074	15	0.0116	22	0.0300
9	0.0078	16	0.0126	23	0.0393

cm^{-1}, compared to the Kratzer relation value[2] of 6.62×10^{-7} cm^{-1}. We emphasize that the ground state rotational constants are unaffected: they are determined principally from the $\Delta_2 F''$ measurements up to N=40. Similarly the hyperfine constants of both states are unaffected; a least squares fit of the uncorrected data up to N=6 gives essentially the same hyperfine constants as the deperturbed data up to N=24, though the precision of the latter is greater.

(ii) Least squares results

The least squares fitting was carried out in two steps. In a first step all the lines to N''=23 and the high N $\Delta_2 F''$'s up to N=40 were fitted simultaneously. This gives a good determination of the spin and rotational constants, though the lower accuracy of the high N $\Delta_2 F''$'s affects the statistics for the hyperfine constants. In a second step the ground state rotational constants were held fixed, and only the more accurately calibrated data up to N''=23 were fitted. The spin and hyperfine constants do not change, but their standard errors improve considerably.

---

[2] Anomalous D values in apparently unperturbed excited states of transition metal oxides are not uncommon. For instance the $A^6\Sigma^+$ v=1 state of MnO (24) has a D value three times higher than expected, and many of the upper levels of the 'orange system' of FeO have unusually large D values (A.S-C. Cheung, A.M. Lyyra and A.J. Merer, work in progress).

The model used was the full matrix of Table 5.1 in each case. The only constraints applied were that λ_D and b_S were set to zero for the ground state, and that the nuclear spin-rotation parameters c_I were fixed. It was found that convergence was very slow with the c_I parameters floating, but that the difference $\Delta c_I = c_I' - c_I''$ was well determined and remained constant in successive iterations. Accordingly, since the apparent nuclear spin-rotation interaction, $c_I \underset{\sim}{I} \cdot \underset{\sim}{N}$, arises principally from second-order spin-orbit effects (18), as does the electron spin-rotation interaction $\gamma \underset{\sim}{S} \cdot \underset{\sim}{N}$, we made the arbitrary choice

$$\frac{c_I(C^4\Sigma^-)}{c_I(X^4\Sigma^-)} = \frac{\gamma(C^4\Sigma^-)}{\gamma(X^4\Sigma^-)} \qquad (5.26)$$

Effectively this portions out the contributions to Δc_I from the two states in the ratio of the two γ's, on the assumption that the spin-orbit terms are similar.

The results are given in Table 5.5. The error limits for the spin and rotational constants are 3σ values, taken from the first fit, including the $\Delta_2 F''$'s, where the overall standard deviation, normalized to unit weight, is 0.00092 cm^{-1} (28 MHz). The error limits for the hyperfine constants are from the second fit, using only the 1363 lines up to $N''=23$, where the normalized standard deviation is 0.00076 cm^{-1} (23 MHz).

G. Hyperfine parameters

The electron spin resonance spectrum of VO, $X^4\Sigma^-$, in an argon matrix at 4 K has been measured by Kasai (10). He derived values for the iso-

Table 5.5 Rotational, spin and hyperfine constants for the $C^4\Sigma^-$ and $X^4\Sigma^-$ states of VO.

	$C^4\Sigma^-$, v=0		$X^4\Sigma^-$, v=0	
T_o	17420.1025_7	$\pm 0.0001_7$	0.0	
B	0.493789_6	$\pm 0.000003_3$	0.546383_3	$\pm 0.000002_9$
$10^7 D$	6.44	± 0.03	6.50_9	$\pm 0.01_4$
γ	-0.018444	± 0.000069	0.022516	± 0.000066
λ	0.7469_7	± 0.0003	2.0308_7	$\pm 0.0002_4$
$10^7 \gamma_D$	5.43	± 0.50	0.56	± 0.32
$10^6 \lambda_D$	-4.3	± 0.5	0.0	fixed
$10^5 \gamma_S$	-23.1	± 1.4	-1.0	± 1.5
b	-0.00881	± 0.00003	0.02731	± 0.00004
c	-0.00114	± 0.00009	-0.00413	± 0.00008
e^2Qq	0.00139	± 0.00023	0.00091	± 0.00088
$10^6 c_I$	-3.9	fixed	4.7	fixed
$10^5 b_S$	4.5	± 1.8	0.0	fixed

Values in cm^{-1}; error limits are three standard deviations; $\sigma = 0.00076 \ cm^{-1}$.

The bond lengths (r_o) are: $C^4\Sigma^-$ 1.6747 Å, $X^4\Sigma^-$ 1.5920 Å.

tropic and dipolar interactions which are closely similar to our gas phase values. With the conversions

$$b = a_c - \frac{1}{3}c = A_\perp = A_{iso} - A_{dip}; \quad c = A_\parallel - A_\perp = 3A_{dip} \qquad (5.27)$$

the values are

$$
\begin{aligned}
b &= 0.02731 \quad 0.00004 \ cm^{-1} \ (gas) \\
&= 0.02792 \quad 0.00002 \ cm^{-1} \ (matrix)
\end{aligned}
\qquad (5.28)
$$

$$
\begin{aligned}
\text{and} \quad c &= -0.00413 \quad 0.00008 \ cm^{-1} \ (gas) \\
&= -0.00408 \quad 0.00003 \ cm^{-1} \ (matrix)
\end{aligned}
\qquad (5.29)
$$

There is excellent agreement for the dipolar constant c, but there is a small though definite difference between the gas and matrix values of the isotropic parameter. As pointed out by Kasai (10), these parameters provide strong evidence for the ground state electron configuration $4s\sigma^1$ $3d\delta^2$: the sign of b for transition metal d electron radicals is negative because of spin polarization effects unless s electrons are also present (39), and c will be negative also. The parameter c is a sum over the valence electrons of the terms

$$c_i = 3g\mu_B g_I \mu_N \langle n | r^{-3} \cdot \frac{1}{2}(3\cos^2\theta - 1) | n \rangle \qquad (5.30)$$

where r is the distance between an electron carrying spin angular momentum and the vanadium nucleus.

If we make the approximation that the states n closely resemble V atomic orbitals, the sum becomes

$$c = 3 \times (2/3) g \mu_B g_I \mu_N \langle 3d\delta | r^{-3} \cdot \tfrac{1}{2}(3\cos^2\theta - 1) | 3d\delta \rangle \qquad (5.31)$$

where the factor 2/3 arises because only the two $3d\delta$ electrons, out of the three valence electrons, give non-vanishing average values of $3\cos^2\theta - 1$. For atomic-like orbitals the average value expression is (18,20)

$$\langle n\ell m | r^{-3} \cdot \tfrac{1}{2}(3\cos^2\theta - 1) | n\ell m \rangle = \tfrac{1}{2}\langle \ell m | 3\cos^2\theta - 1 | \ell m \rangle \langle n\ell | r^{-3} | n\ell \rangle$$
$$= -\frac{[3m^2 - \ell(\ell+1)]}{(2\ell-1)(2\ell+3)} \langle r^{-3} \rangle_{n\ell} \qquad (5.32)$$

which, for the ground state of VO, gives c in cm^{-1} units as

$$c = -\tfrac{4}{7} g \mu_B g_I \mu_N \langle r^{-3} \rangle_{3d} / hc \qquad (5.33)$$

The observed value $c = -0.00413 \ \text{cm}^{-1}$ therefore gives

$$\langle r^{-3} \rangle_{3d} = 3.0 \times 10^{24} \ \text{cm}^{-3} \qquad (5.34)$$

which is 85% of the value given by the Hartree-Fock calculations of Freeman and Watson (40) for the free V atom.

It is interesting that this simple model also accounts for the value of the ground state electric quadrupole parameter e^2Qq. Assuming that only the two $3d\delta$ electrons are responsible for the quadrupole parameter we find

$$e^2Qq = -(4.803 \times 10^{-10} \text{esu})^2 \times 0.27 \times 10^{-24} \text{cm}^2 \times 2 \times -\tfrac{4}{7} \langle r^{-3} \rangle_{3d} / hc \qquad (5.35)$$

from which the experimental value $e^2Qq = 0.00091$ cm^{-1} gives

$$<r^{-3}>_{3d} = 2.5 \times 10^{24} \text{ cm}^{-3} \qquad (5.36)$$

However the error limits on e^2Qq are so very large that the agreement in the values of $<r^{-3}>_{3d}$ is probably mainly fortuitous.

It is not so easy to apply these agreements to the $C^4\Sigma^-$ excited state because the $4s\sigma$ electron has been replaced by a $4p\sigma$ electron. As expected the isotropic parameter b is negative because of spin polarization, and the dipolar parameter c is much smaller than in the ground state. The decrease of c on electronic excitation can be understood from the model given in eq. (5.30). For the $C^4\Sigma^-$ state the expression becomes

$$c = \frac{3}{2}g\mu_B g_I \mu_N [\frac{2}{3}<r^{-3}.(3\cos^2\theta-1)>_{3d\delta} + \frac{1}{3}<r^{-3}.(3\cos^2\theta-1)>_{4p\sigma}] \qquad (5.37)$$

It is not easy to obtain independent estimates of $<r^{-3}>_{4p}$, but with the very crude approximation that $<r^{-3}>_{3d}=<r^{-3}>_{4p}$, we obtain

$$c = g\mu_B g_I \mu_N(-\frac{4}{7}<r^{-3}>_{3d} + \frac{2}{3}<r^{-3}>_{4p})/hc \qquad (5.38)$$
$$= -0.171 g\mu_B g_I \mu_N <r^{-3}>_{3d}/hc = -0.00126 \text{ cm}^{-1}$$

Somewhat surprisingly, this number agrees, almost to within the experimental error, with our observed values. The upper state quadrupole parameter does not fit this model.

As for the other two hyperfine parameters, b_S and c_I, we have difficulty determining the parameters separately for the two electronic states,

though the difference between the parameters on electronic excitation is well determined. This is a consequence of the selection rule $\Delta F = \Delta N$, which applies except at the lowest N values; obviously, direct measurements of the hyperfine level separations will be needed to break the correlation.

We estimate that the measured difference $\Delta c_I = c_I' - c_I''$ is accurate to about 10%, or, in figures

$$\Delta c_I = c_I' - c_I'' = (-8.6 \pm 0.9) \times 10^{-6} \text{ cm}^{-1} \tag{5.39}$$

The standard deviation in the least squares fit was improved by about 2% when we included the c_I terms, though as explained above we had to fix the c_I parameters in the ratio of the γ parameters in the final least squares fitting. The symptom showing that the c_I terms were needed was that the least squares residuals for the hyperfine structures of all four electron spin components showed a systematic trend from positive to negative with increasing F; the effect is only about 0.002 cm^{-1}, but it disappeared at once on inclusion of the c_I terms.

The third-order cross term b_S is well determined for the $C^4\Sigma^-$ state provided we set b_S'' equal to zero. This is not an unreasonable approximation because the value of b_S reflects the positions of nearby electronic states coupled through spin-orbit interaction, and we know that the $C^4\Sigma^-$ state suffers many local perturbations. Also the related parameter γ_S is essentially undetermined for the ground state but well-determined for the $C^4\Sigma^-$ state. It is unfortunately not simple to interpret the parameter b_S, so that all we can do is point out the need to include

b_S in precise work on excited electronic states of quartet and higher multiplicity.

H. Discussion

This analysis of the $C^4\Sigma^- - X^4\Sigma^-$ (0,0) band of VO at sub-Doppler resolution is the most detailed account so far of an electronic band involving quartet states. The most interesting aspects are the internal hyperfine perturbations in the two electronic states, which we can fit in detail using the complete $^4\Sigma$ spin and hyperfine Hamiltonian.

Electronic perturbations are unfortunately widespread in the $C^4\Sigma^-$ state, which means that we cannot obtain a fit to the higher N data that does justice to their precision. In fact we have had to apply corrections to all the F_4 levels of the $C^4\Sigma^-$ state to allow for the comparatively large perturbation at N = 26. Without these corrections the least squares results show systematic residuals even at low N, and the centrifugal distortion parameters are unrealistic. The final fit was performed with 'deperturbed' data only up to N' = 24, plus ground state Δ_2F'' combination differences to N = 40. The upper state term values beyond N = 24 are calculated from this fit to within about 0.1 cm^{-1}, as can be seen from Fig. 5.15. This figure shows the residuals for the R branch lines up to N' = 42, calculated using the final constants of Table 5.5. The chaotic courses of all four spin components are readily appreciated.

The $C^4\Sigma^-$ state also suffers from 'global' perturbations affecting all levels, besides the local rotational perturbations. These require the introduction of a second spin-rotation parameter γ_S, following the formalism of Brown and Milton (25). This parameter is a third-order

spin-orbit effect, and gives evidence for a close-lying electronic state that interacts strongly through the spin-orbit operator. We have also had to introduce the corresponding isotropic hyperfine parameter b_S (26), which arises in similar fashion as a cross-term between the $\underset{\sim}{I}.\underset{\sim}{S}$ hyperfine operator and the spin-orbit interaction. The parameters γ_S and b_S only occur for states of quartet and higher multiplicity.

The magnetic hyperfine constants for the two states have been accurately determined. For the ground state there is good agreement with the e.s.r. values of Kasai (10), inasfar as the gas phase and matrix values can be compared. The magnetic constants for the upper state show clearly that its electron configuration is $3d\delta^2 4p\sigma^1$. The electric quadrupole parameters are unfortunately not well determined, though there appears to be consistency between the ground state electric quadrupole and magnetic dipole parameters, which involve roughly the same averages over electron coordinates.

The electron spin-spin parameters λ for the two states have been accurately determined, despite the parallel selection rules, because of the observation of Q branches at low N values. The Q lines essentially permit an exact determination, according to the $^4\Sigma$ relation

$$4\lambda - 2\gamma = F_2(N) + F_3(N) - F_1(N) - F_4(N) \qquad (5.40)$$

(which follows from Table 5.1) because they can be combined with the main branch R and P lines to provide the separations $F_2(N) - F_1(N)$ and $F_4(N) - F_3(N)$. Less precise values could still have been obtained without the Q branch measurements because the low N line positions are quite sensi-
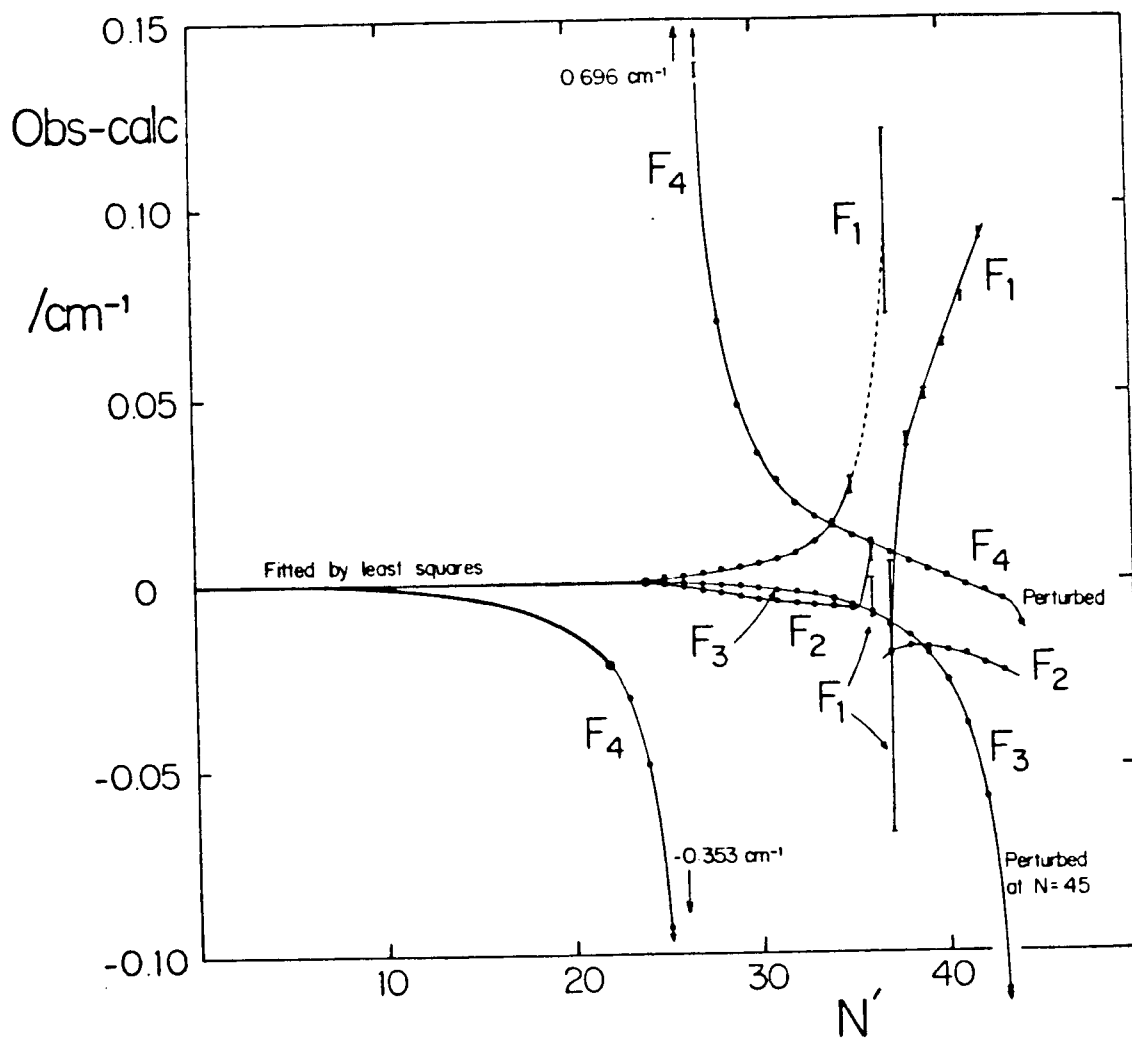
Fig. 5.15 Residuals (obs-calc) for the R branch lines of the VO

$C^4\Sigma^- - X^4\Sigma^-$ (0,0) band, as compared to the positions predicted

from the constants of Table 5.5, plotted against N'. 'Raw' data

have been used, so that the R_4 lines from N' = 9-22,.which were

deperturbed for the least squares treatment (thick lines) have

non-zero residuals. Vertical bars indicate the spread of the

hyperfine structure.

tive to the exact values of the two λ parameters.

The low N energy levels of VO $X^4\Sigma^-$, v=0 will be of interest to astronomers concerned with the detection of VO in interstellar space and to spectroscopists concerned with microwave and far infra-red studies of the ground state. We therefore list the ground state rotational and hyperfine energy levels (as calculated from the constants of Table 5.5) up to N" = 5 in Table 5.6. The experimental ground state hyperfine combination differences, between levels with the same F value in the F_2 and F_3 electron spin components over the range N" = 8-20, are listed in Table 5.7.

To summarize, the VO $C^4\Sigma^-$ - $X^4\Sigma^-$ electronic transition provides 'textbook' examples of the effects of electron spin and hyperfine structure in a quartet state in case $(b_{\beta J})$ coupling; it is frustrating that electronic perturbations prevent the higher N lines from being fitted to an accuracy that matches their precision.

Table 5.6 Rotational and hyperfine energy levels of the $X^4\Sigma^-$ v=0 state of VO for N ≥ 5, calculated from the constants of Table 5.5. Values in cm^{-1}.

N	J		F=J-7/2	F=J-5/2	F=J-3/2	F=J-1/2	F=J+1/2	F=J+3/2	F=J+5/2	F=J+7/2
0	F_1	1.5					-2.8982	-2.8391	-2.7595	-2.6576
1	F_1	2.5			-1.6426	-1.6160	-1.5759	-1.5220	-1.4541	-1.3716
	F_2	1.5					1.2592	1.2536	1.2434	1.2264
	F_3	0.5[a]							-3.1255	-2.9492
2	F_1	3.5	0.6665	0.6766	0.6969	0.7273	0.7681	0.8194	0.8814	0.9545
	F_2	2.5			4.0231	4.0275	4.0340	4.0425	4.0527	4.0642
	F_3	1.5					5.9068	5.9379	5.9782	6.0269
	F_4	0.5[a]							-0.8199	-0.9343
3	F_1	4.5	4.0522	4.0685	4.0930	4.1258	4.1670	4.2167	4.2751	4.3424
	F_2	3.5	7.6362	7.6389	7.6442	7.6525	7.6638	7.6785	7.6967	7.7190
	F_3	2.5			9.0674	9.0741	9.0835	9.0948	9.1070	9.1187
	F_4	1.5					6.2261	6.2351	6.2490	6.2694
4	F_1	5.5	8.5121	8.5326	8.5599	8.5943	8.6357	8.6842	8.7401	8.8035
	F_2	4.5	12.2171	12.2219	12.2294	12.2396	12.2531	12.2703	12.2918	12.3183
	F_3	3.5	13.3492	13.3505	13.3531	13.3565	13.3601	13.3632	13.3647	13.3636
	F_4	2.5			10.0328	10.0224	10.0072	9.9875	9.9638	9.9369
5	F_1	6.5	14.0522	14.0756	14.1050	14.1405	14.1820	14.2297	14.2838	14.3443
	F_2	5.5	17.8219	17.8279	17.8364	17.8476	17.8621	17.8803	17.9032	17.9318
	F_3	4.5	18.7437	18.7449	18.7463	18.7475	18.7479	18.7468	18.7430	18.7354
	F_4	3.5	15.1594	15.1529	15.1400	15.1208	15.0955	15.0643	15.0275	14.9855

[a] Note: $F_3(1)$, $J = \frac{1}{2}$ and $F_4(2)$, $J = \frac{1}{2}$ must be treated as $F_1(-1)$ and $F_2(0)$, respectively, since $\lambda > B$.

Table 5.7 Gronud state hyperfine combination differences, $F_2(N)-F_3(N)$, in cm^{-1}, for the $X^4\Sigma^-$, v=0 state of VO in the range N=8-20.

N	F=N+3	F=N+2	F=N+1	F=N	F=N-1	F=N-2	F=N-3
8	-0.4193	-0.4606	-0.4896	-0.5101			
9	-0.3325	-0.3770	-0.4066	-0.4272	-0.4411	-0.4510	-0.4559
10	-0.2638	-0.3103	-0.3411	-0.3629	-0.3735	-0.3804	
11	-0.2091	-0.2581	-0.2871	-0.3057	-0.3163		
12	-0.1699	-0.2190	-0.2461	-0.2615	-0.2692	-0.2700	-0.2677
13	-0.1484	-0.1947	-0.2184	-0.2300	-0.2330	-0.2287	-0.2213
14	0.1455	-0.1829	-0.2021	-0.2080	-0.2056	-0.1958	-0.1795
15	0.1589	0.1854	0.1977	-0.1993	-0.1909	-0.1750	-0.1501
16	0.1813	0.1992	0.2045	0.2001	-0.1859	-0.1628	-0.1281
17	0.2101	0.2197	0.2195	0.2104	0.1913	0.1631	-0.1202
18		0.2413	0.2400	0.2248	0.2040	0.1723	0.1252
19			0.2619	0.2466	0.2222	0.1888	0.1406
20				0.2694	0.2438	0.2095	0.1618

The tabulated values are observed quantities corresponding to the differences between the calculated hyperfine levels with the same F value shown in Fig 5.3.

Chapter 6

Laser-Induced Fluorescence and Discharge
Emission spectra of FeO; Evidence for a
$^5\Delta_i$ Ground State

A. Introduction

Ferrous oxide, FeO, is probably the most important of the diatomic oxide molecules whose spectra have so far defied detailed interpretation. It is of interest in astrophysics, as well as molecular spectroscopy, because of the high cosmic abundances of both iron and oxygen. The difficulties with FeO have been its low dissociation energy (which means that it is quite difficult to prepare in discharge systems), its involatility, and the tremendous complexity of its spectrum.

Considerable argument has surrounded the nature of the ground state of FeO. Quite recently Engelking and Lineberger[1] have interpreted the photoelectron spectrum of FeO$^-$ in terms of a $^5\Delta$ ground state for FeO, with a vibrational frequency of 970 ± 60 cm^{-1}, and De Vore and Gallaher [2] identified a band at 943.4 ± 2.0 cm^{-1} in infrared emission experiments on FeO, but it is now clear, from the matrix isolation work of Green et al. [3], that FeO has a ground-state vibrational frequency of about 875 cm^{-1}. This number is also found for the lower state of the well-known electronic band system in the orange region [4-6], which must therefore involve the ground state. The orange band system is unusually complex [7,8], but has been found to contain a few surprisingly simple parallel bands consisting of single P and R branches [4-6], apparently of type $^1\Sigma$-$^1\Sigma$. Harris and Barrow [6] recognize that the bands must be more complex than this, since theoretical predictions give, variously, $^5\Delta$[9,10] and $^5\Sigma^+$ [11] for the ground state.

The purpose of this chapter is to report new emission and laser-induced fluorescence spectra of FeO which prove that the simple bands in the orange system are $\Omega' = 4 - \Omega'' = 4$ bands. This provides strong evidence that the ground state is $^5\Delta_i$, since $\Omega = 4$ components do not arise in the other possible candidate states, $^5\Sigma^+$, $^5\Pi$, and $^7\Sigma^+$. This identification agrees also with Weltner's report (12) that matrix isolated FeO gives no ESR spectrum under conditions where orbitally nondegenerate species normally give strong signals.

B. Experimental Details

Emission spectra of FeO were excited by a 2450-MHz electrodeless discharge in a mixture of flowing argon, oxygen, and ferrocene (dicyclopentadienyl iron) at low pressure. The discharge is unfortunately not very stable, and gives mainly CO spectra if the buildup of solid rust-like products becomes excessive, because these interfere with the transmission of the microwave power. As a result, photographic exposures longer than 1 hr were often unsatisfactory, but this time was sufficient to give good spectra in the region 5500 - 6300 Å using Kodak IIa-D plates in a 7-m Ebert-mounted plane grating spectrograph. The temperature of the emitting molecules, as estimated from the development of rotational branch structure, is about 500°C.

Laser-induced fluorescence of FeO was produced using a Coherent Inc. CR-599-21 tunable dye laser operating with rhodamine 6G, and pumped by an argon ion laser. The optical arrangement for this experiment was the same as in chapter 5. The laser beams were sent through the end of the flame of the microwave discharge system described above, and observed at right angle to the stream of molecules. Broadband and single frequency laser excitation spectra, and Sub-Doppler intermodulated fluorescence spectra (13) of certain regions of the 5819Å band were recorded, as well as resolved fluorescence spectra.

The photographic "survey" spectra were measured on a Grant automatic comparator, and reduced to vacuum wavenumbers using a four-term polynomial. Calibration spectra were provided by an iron-neon hollow cathode lamp, for which the wavelengths have been listed by Crosswhite (14). The laser spectra were calibrated by means of the iodine spec-

trum atlas of Gerstenkorn and Luc (14), with the correction of 0.0056 cm^{-1} to give absolute wavenumbers applied.

C. Results

Harris and Barrow (6) have identified three bands involving the level v" = 0 of the state which appears also in the matrix isolation experiments of Green et al. (3); they occur at 5583, 5819 and 5911 Å. The 5583- and 5911 Å bands lie in crowded spectral regions where blending is severe, but the 5819-Å band is in a comparatively clear region and we have selected it for study. Its head is illustrated in Fig. 6.1. The band is a very strongly red-degraded parallel band, and the assignments of the P and R lines are those of Harris and Barrow (6).

A feature of this band is that where small rotational perturbations occur they usually appear as two lines of equal intensity. Because this implies that there are several exact coincidences of perturbed and perturbing levels if the states involved have Ω = 0 (as postulated by Harris and Barrow (6) we suspected that there could be Λ-doubling present which is not resolved in the grating spectra. Sub-Doppler intermodulated fluorescence spectra of the unperturbed line R(15) at a resolution of about 75 MHz showed at once that this is true (see Fig. 6.2); in this figure the line is seen to consist of two equally intense closely spaced components separated by about 120 MHz.

Given that $\Omega' = \Omega" \neq 0$, we searched for possible Q lines in the grating spectra, because the J numbering of the first Q line would give the Ω value. Quite a number of lines occur in the expected region, but a branch could be picked out. Its numbering was established by plotting the line positions against n(n + 1), where n is an arbitrary running number, and choosing the best straight line. The result gave Ω = 4.

The Q(4) line of the 5819-Å band runs into the R(10) line in Fig. 6.1 because of the strong exposure; the lines are seen resolved in the sub-Doppler spectrum shown in Fig. 6.2b.

In view of the fact that there are many weak background lines underlying the 5819-Å band which could easily be mistaken for Q lines (see Fig. 6.1) confirmation was sought from rotationally resolved laser-induced fluorescence experiments. These turned out to be absolutely conclusive and leave no doubt about the Q branch and its numbering. Some of the patterns observed are illustrated in Fig. 6.3. As expected, excitation at the wavelength of the first line, Q(4), gives only Q(4) and P(5) emission, while higher J lines of the Q branch give R-, Q-, and P-branch emission. Excitation of the R-branch lines gives consistent patterns, and somewhat surprisingly, weak Q-branch emission can even be seen when the line R(16) is excited. In the end it was possible to follow the Q branch on the grating spectra from its first line, Q(4), up to Q(26), where it becomes lost in the background of weak lines. The assigned lines of the 5819-Å band and the other bands we have studied are listed in Appendix VI Table II.

Figure 6.1 also shows the head region of the 6180-Å band. This band was shown by Harris and Barrow (6) to have the same Ω'' value as the 5819-Å band, but with $v'' = 2$ rather than $v'' = 0$. Quite a strong Q branch can be seen, which can be numbered unambiguously by means of the $\Delta_1 F''$ combination differences for the level $v'' = 2$. Again the first line is $J = 4$, which is consistent with the laser-induced fluorescence experiments described above. Similar Q branches have been identified in the 5583- and 5866-Å bands ($v'' = 0$ and 1).
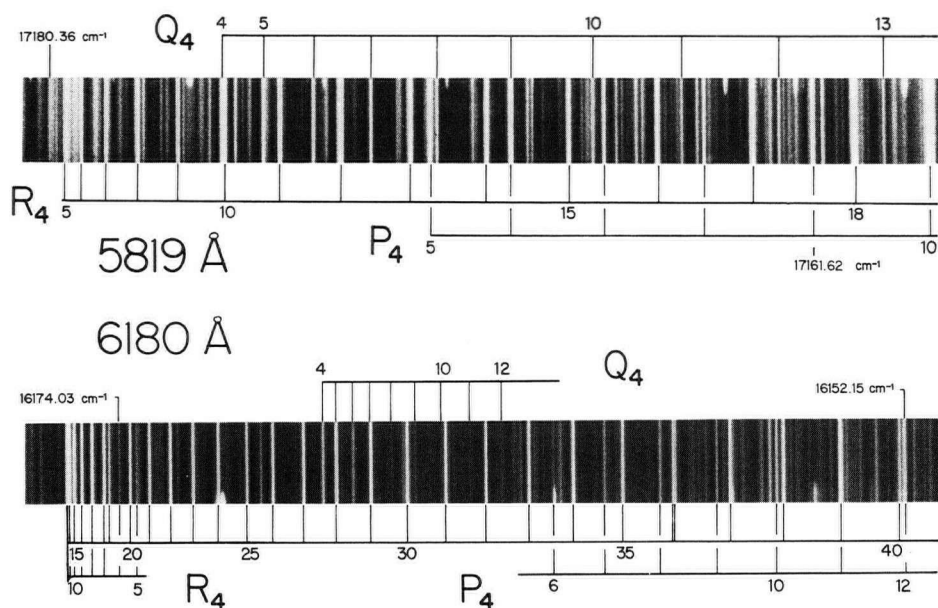
Fig 6.1 Head of the 5819-Å band of FeO. Lower print: head of the 6180-Å band of FeO.
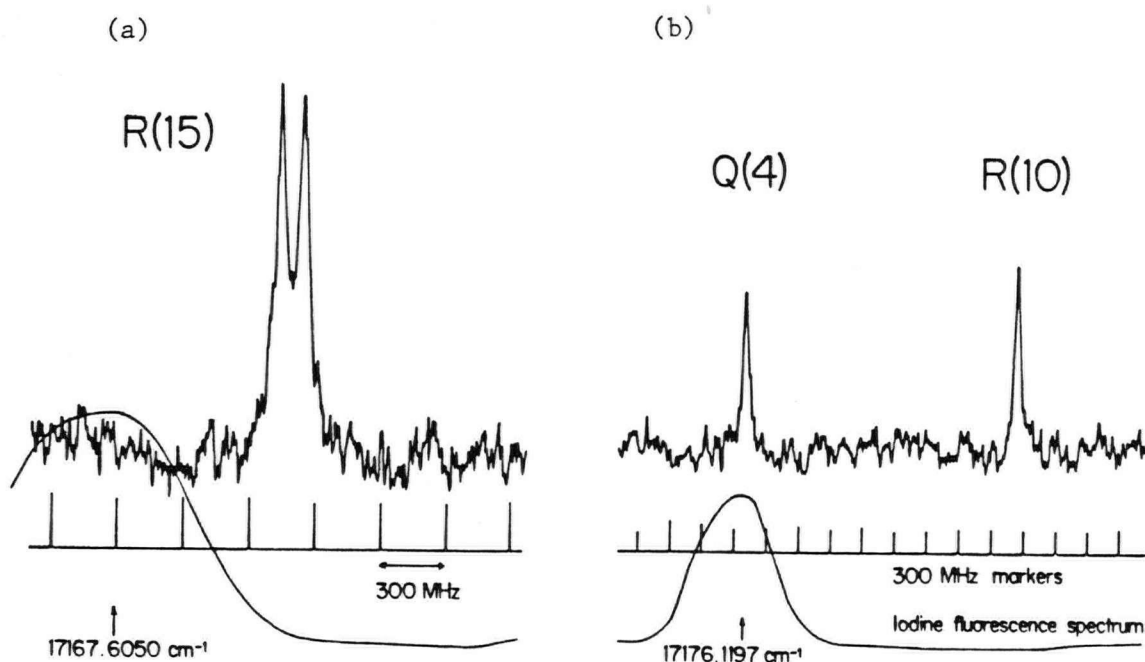
Fig 6.2 Two regions of the intermodulated fluorescence spectrum of FeO: (a) The twoΛ components of the R(15) line of the 5819-Å band. (b) The Q(4) and R(10) lines of the 5819-Å band; the Λ doubling is not resolved for these lines.
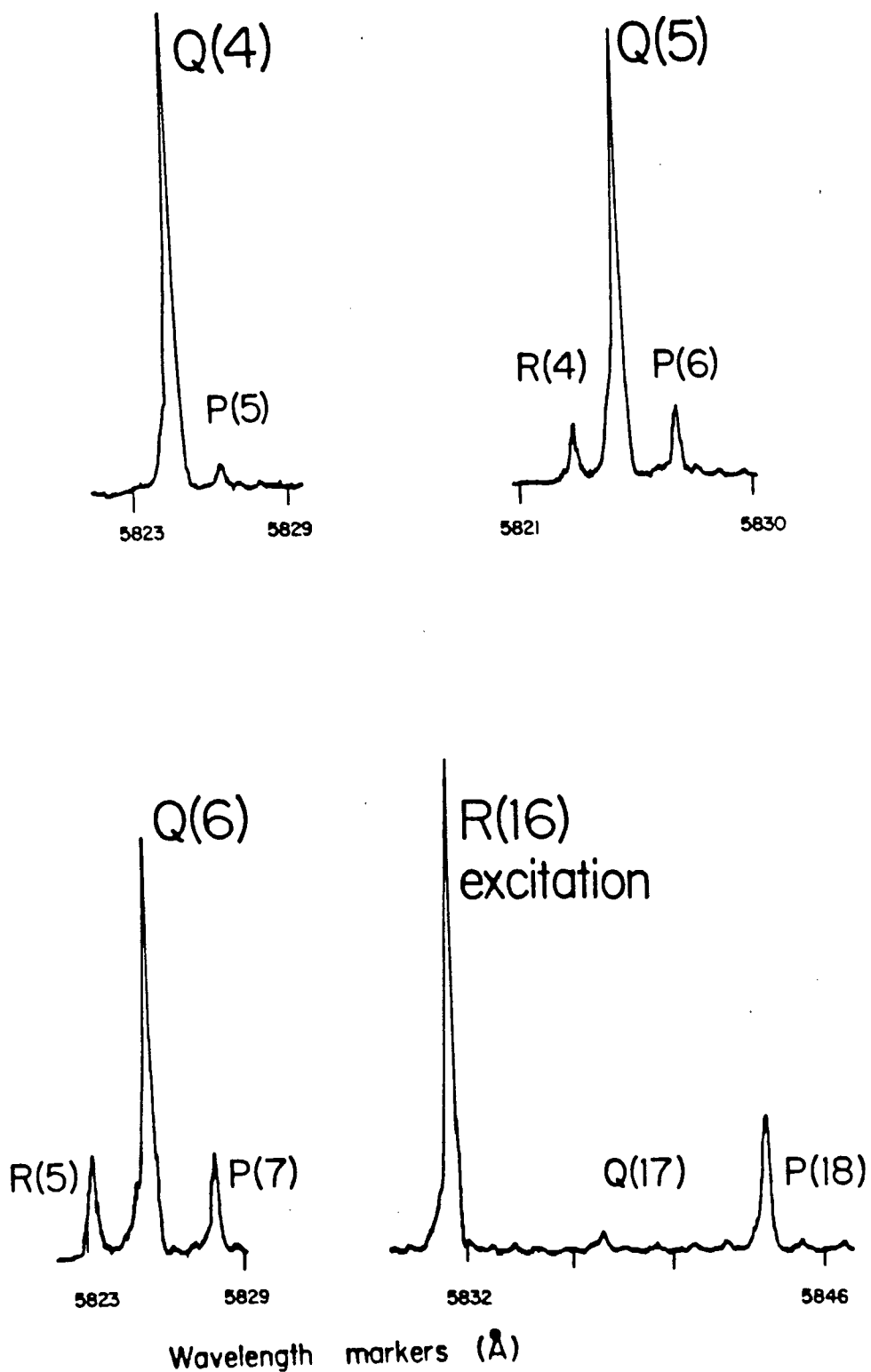
Fig 6.3 Resolved fluorsecence spectra of FeO produced by excitation of various lines of the 5819-Å band: excitation of Q(4),Q(5), Q(6) and R(16). The intensity of the excited line is anomalously high as a result of scattered laser light.

D. Discussion

The work presented here proves that the comparatively simple bands analyzed by Barrow and his co-workers (5,6) have $\Omega'' = 4$. Some of these bands (including the 6180-Å band illustrated in Fig. 6.1) form a lower-state progression which gives vibrational constants (6) that are almost identical to those obtained from the infrared spectrum of matrix-isolated FeO by Green et al. (3), viz.,

$$\text{Gas:} \quad \omega_e = 880.61 \text{ cm}^{-1}, \quad \omega_e x_e = 4.64 \text{ cm}^{-1};$$

$$\text{Matrix:} \quad \omega_e = 880.2 \text{ cm}^{-1} \quad \omega_e x_e = 3.47 \text{ cm}^{-1}. \tag{6.1}$$

Therefore the ground state of FeO contains an $\Omega = 4$ spin-orbit component.

The ground electron configurations of the transition oxides immediately before FeO are known (15,16) to be (Appendix V)

$$
\begin{array}{lll}
\text{TiO} & (4s\sigma)^1(3d\delta)^1 & {}^3\Delta_r \\[4pt]
\text{VO} & (4s\sigma)^1(3d\delta)^2 & {}^4\Sigma^- \\[4pt]
\text{CrO} & (4s\sigma)^1(3d\delta)^2(3d\pi)^1 & {}^5\Pi_r \\[4pt]
\text{MnO} & (4s\sigma)^1(3d\delta)^2(3d\pi)^2 & {}^6\Sigma^+
\end{array}
\tag{6.2}
$$

where the energy order of $4s\sigma$ and $3d\delta$ is not certain. In FeO the extra electron could go into the next unoccupied m.o., $3d\sigma$, giving a ${}^7\Sigma^+$ ground state, or into the $4s\sigma$ or $3d\delta$ m.o.'s, giving ${}^5\Sigma^+$ or ${}^5\Delta$ as the ground state. Theoretical computations (9-11) are divided between ${}^5\Sigma^+$ and ${}^5\Delta$, through the CI calculations of Bagus and Preston (9) con-

clude that the ground state is not $^5\Sigma^+$. The fact that there is an

$\Omega = 4$ component in the ground state is only consistent with $^5\Delta$, where

the Ω values run from 0 to 4; the highest Ω values in $^5\Sigma^+$ and $^7\Sigma^+$

states are 2 and 3, respectively.

It is interesting that the $^5\Delta$ state under discussion, which comes

from the configuration $(4s\sigma)^1(3d\delta)^3(3d\pi)^2$, must be inverted, with its

$\Omega = 4$ component as the lowest in energy. This is probably the reason

why the matrix-isolation vibrational constants (3) agree so exactly

with the gas-phase constants (5,6) because at the low temperature of

the matrix only the $\Omega = 4$ component is likely to be appreciably popu-

lated, assuming spin-orbit intervals of about 100 cm^{-1} (by analogy with

TiO (17), where there is also an unpaired 3dδ electron). The other

Ω components of the $^5\Delta$ state will have slightly different effective

vibrational frequencies because of the variation of the spin-orbit

coupling with vibration.

The subbands so far analyzed carry no direct information about the

spin-orbit coupling of the ground state. For a start the subbands are

all parallel-polarized ($\Omega' = \Omega''$), and as yet only one spin component

has been identified. However, these $\Omega = 4$ subbands, though prominent

in the spectrum, account for only a small fraction of the total

emission intensity, and subbands involving the other spin components

must also be present. The prominence of the $\Omega = 4$ subbands probably

results from the fact that the Λ-doubling is unresolved, so that their

lines have apparently twice the strength of other lines belonging to

subbands in the same region with resolved Λ-doubling; this effect is

also pronounced for the $\Omega = 3$ subbands of the $A^5\Pi - X^5\Pi$ system of CrO (18).

In the CrO spectrum the five subband heads form a regular series, which is obvious in low-dispersion spectra, but the same is not true in the FeO spectrum. It appears that there are extensive interactions between two or more excited electronic states in FeO which produce an almost random distribution of Ω substates, as if the spin coupling were case (c).

Because the Ω value of each band has to be determined individually in the FeO spectrum, it will be a lengthy process assembling data for all five spin-orbit components of the ground state. At present even the bond length is not accurately given by the available B value for $^5\Delta_4$ because of the spin-uncoupling. In principle, it would be possible to use the difference between the apparent centrifugal distortion constant for the $^5\Delta_4$ component and the value given by the Kratzer relation to estimate the spin-orbit separations and then correct the B value for spin-uncoupling. In practice we find that the error limits on $D_{apparent}(^5\Delta_4)$ are too large for this approach to succeed. A least-squares fitting of the Δ_2F'''s we have measured gives

$$B_{apparent}(^5\Delta_4) = 0.51089 \pm 0.00003_5 \text{ cm}^{-1} \text{ (1}\sigma\text{)} \qquad (6.3)$$
$$D_{apparent}(^5\Delta_4) = 6.6_0 \times 10^{-7} \pm 0.2_3 \times 10^{-7} \text{ cm}^{-1}$$

(in close agreement with the results of Barrow et al. (5,6)).

A comparison of the molecules FeO and FeF (19) is instructive. FeF is known to have a $^6\Delta_i$ ground state which arises from the electron configuration $(4s\sigma)^1 (3d\delta)^3 (3d\pi)^2 (3d\sigma)^1$; in other words the extra electron in FeF goes into the $3d\sigma$ m.o. rather than into $3d\delta$. This

shows the close analogy between FeO and FeF, because the ligand field effect of an F atom is not as great as that of an O atom so that the splitting of the iron 3d manifold is smaller. In FeF Hund's rules apply to the three 3d orbitals and the 4s orbital as a group, producing a high-spin situation, while in FeO Hund's rules apply only to $3d\delta$, $3d\pi$, and $4s\sigma$.

In further laser-induced fluorescence experiments which are not reported here, we have analyzed various sub-bands with $\Omega'' = 0, 1, 2$ and 3 in the orange system of FeO. The regularity of the B'' values leaves no doubt that the lower levels form the other spin-orbit components of the $X^5\Delta_i$ state. The ground state bond length is 1.619 Å, and the spin-orbit intervals are about 190 cm^{-1}.

Chapter 7

Predissociated Rotational Structure in the 2490-Å Band of $^{15}NO_2$

A. Introduction

Slightly predissociated molecular band systems where there is a sizable isotope effect offer the possibility of selective dissociation of one member of a mixture of isotopes. The experimental requirements are a suitable source of radiation which can be tuned to an appropriate wavelength and a scavenging system (chemical or other) which can collect the dissociated products without interference from the undissociated compound. Various experiments of this type have been successfully carried out using narrow-line lasers, for example, on s-tetrazine by Karl and Innes (1) and by Hochstrasser and King (2), and on ICl by Liu et al. (3).

The 2490-Å absorption transition of $NO_2(2^2B_2 - \tilde{X}^2A_1)$ is slightly predissociated (4) and therefore allows the possibility of laser-induced isotope enrichment. For this reason we have studied the corresponding band of $^{15}NO_2$ with a view to identifying those wavelengths where irradiation would selectively dissociate one isotope and permit the separation of ^{14}N and ^{15}N.

Spectroscopically, the 2490-Å band of $^{15}NO_2$ is very similar to that of $^{14}NO_2$, though its origin is shifted 14.5 cm^{-1} to higher energy. An analysis of the quartic centrifugal distortion constants of the upper state has been carried out.

B. Experimental Details

The absorption spectrum of $^{15}NO_2$ in the region 2480 - 2520 Å was photographed in the 23rd order of a 7-m plane grating spectrograph, using Kodak SA-1 plates. The absorption path was 1.85 m, and photo-

graphs were taken with the cell at room temperature and various temperatures up to 200°C. Doppler broadening of the lines becomes appreciable at the higher temperatures, and the highest temperature where useful spectra could be obtained was 120°C. The background continuum was supplied by a 1000-W xenon arc, and exposure times, with the spectrograph slit set to 25 μm, were about 1 hr. Calibration lines were supplied by an iron-neon hollow cathode lamp, the reference wavelengths for which have been given by Crosswhite (5). The plates were measured on a Grant automatic comparator, and reduced to vacuum wave numbers with a four-term polynomial.

C. Analysis of the 2490Å Band of $^{15}NO_2$

The theory of the energy levels of asymmetric top molecules in multiplet electronic states is now fairly well understood (6 - 9). For reference we give the matrix elements required for the NO_2 spectrum in the absence of hyperfine effects:

$$< NK|H|NK > = \frac{1}{2}(B + C)N(N + 1) + [A - \frac{1}{2}(B + C)]K^2$$

$$- \frac{1}{2}[J(J + 1) - N(N + 1) - 3/4][a_o + a\{3K^2/(N(N + 1)) - 1\}$$

$$- nK^4/(N(N + 1))] - \Delta_K K^4 - \Delta_{NK}N(N + 1)K^2 - \Delta_N N^2(N + 1)^2 +$$

$$+ H_K K^6 + H_{KN}K^4 N(N + 1) \dots ;$$

$$< NK \pm 2|H|NK > = \{\frac{1}{2}(B - C) - \frac{1}{4}b[J(J + 1) - N(N + 1) - 3/4]/[N(N + 1)]$$

$$- \delta_N N(N + 1) - \frac{1}{2}\delta_K [K^2 + (K \pm 2)^2]\} \qquad (7.1)$$

$$x [N(N + 1) - K(K \pm 1)]^{\frac{1}{2}}[N(N + 1) - (K \pm 1)(K \pm 2)]^{\frac{1}{2}};$$

$$<N - 1K|H|NK> = (\frac{3}{2}a - \frac{1}{2}nK^2)K[N^2 - K^2]^{\frac{1}{2}}/N;$$

$$<N - 1K \pm 2|H|NK> = \pm \frac{1}{4}b[N(N + 1) - K(K \pm 1)]^{\frac{1}{2}}$$

$$x [N \mp K - 1)(N \mp K - 2)]^{\frac{1}{2}}/N.$$

The basis set for Eq.(7.1)is the type I^r representation case (b) basis $|NJSK>$, where the quantum numbers J and S have been suppressed because the elements are diagonal with respect to them. The coupling scheme (8)

$$\underline{N} + \underline{S} = \underline{J} \tag{7.2}$$

has been used, and the phases are appropriate for the definition of the rotational angular momentum vector $\underline{N}$ as a space-fixed operator rather than a molecule-fixed operator. The quartic centrifugal distortion terms are complete, but only the largest sextic terms have been included. The spin-rotation constants in Cartesian form (10) are related to those of Eq. (7.1) by

$$a_o = - \frac{1}{3} (\varepsilon_{aa} + \varepsilon_{bb} + \varepsilon_{cc}); \quad a = - \frac{1}{6} (2\varepsilon_{aa} - \varepsilon_{bb} - \varepsilon_{cc});$$

$$b = - \frac{1}{2} (\varepsilon_{bb} - \varepsilon_{cc}) \tag{7.3}$$

and η is the leading centrifugal distortion correction to the spin-rotation interaction parameter ε_{aa} (called η_{aaaa} by Dixon and Duxbury (11), η_K by Brown and Sears (12) and Δ_K^S by Cook et al. (13)).

The ground state of $^{15}NO_2$ has not been studied as comprehensively as that of $^{14}NO_2$. The microwave spectrum of NO_2 is very sparse because of the large A rotational constant, and although it has been carefully measured by Bird et al. (14) and Lees et al. (15) the available lines do not carry enough information to determine all the centrifugal distortion parameters required to describe the energy levels to the precision of the optical spectrum. The missing data have been supplied for $^{14}NO_2$ by the high-resolution infrared spectrum (16), but as yet the

infrared data for $^{15}NO_2$ (17-19) are less complete. Even so, the best centrifugal distortion constants for $^{15}NO_2$ are in fact those from the microwave spectrum (14), though, as recognized by Lees et al. (15), they are not particularly good because so few lines are available.

In analyzing the 2490-Å band of $^{15}NO_2$ we proceeded as follows. First we converted the ground-state centrifugal distortion constants (14) from Kivelson and Wilson's τ's to Watson's formalism according to the recipe of Yamada and Winnewisser (20). Next the ground-state energy levels were calculated employing the second-order approximation formula of Cabana et al. (21) for the spin corrections to the rotational energy levels. With the spin parameters written in spherical tensor notation this formula is

$$E^{spin}(J = N \pm 1/2) = \pm 1/2\{(a - a_0 \pm 1/2b\delta_{1,K})N(N \pm 1) - 3aK^2$$
$$+ {_n}K^4 - 9a^2K^2[1 - K^2/(N + 1/2 \pm 1/2)^2]/4B\}/(N + 1/2 \pm 1/2). \quad (7.4)$$

where the term $\pm \frac{1}{2}b\,\delta_{1,K}$ refers to the two asymmetry components of $K_a = 1$, not to the two J components of an (N,K) level. This approximation works very well, since NO_2 is so close to being a prolate symmetric top, and breaks down (22) only where, by accident, a near-degeneracy occurs between levels (N,K) and (N - 1, K + 2). Its advantage is that it permits the rotational energy levels to be calculated using the formalism for a singlet electronic state, where the matrices are half the size of those required for an exact treatment of a doublet state.

At this stage the lines could be assigned by standard combination difference techniques, since there are no perturbations. The band is a

normal asymmetric top type A (parallel) band, with the N and K structures both strongly degraded to the red. The head of the $^{15}NO_2$ 2490-Å band is illustrated in Fig. 7.1 with the corresponding band of $^{14}NO_2$ printed alongside in its correct relative position. The line assignments refer to the lower print, which is the $^{15}NO_2$ spectrum; the $^{14}NO_2$ assignments are not repeated, having been given in Ref. (4). It can be seen that the bands of the two isotopes are quite similar, particularly in the $^qR_0$ head region, but that they are sufficiently different that it is not possible to assign the $^{15}NO_2$ lines by simply comparing the two spectra. The two spin components of the $^qP_1(2)$ line are clearly resolved, and their relative intensities are found to be exactly as in the $^{14}NO_2$ spectrum; this confirms the assignment of the ordering of the $F_1(J = N + 1/2)$ and $F_2 (J = N - 1/2)$ spin component lines made in Ref. (4). The argument goes as follows. The case (b) selection rule $\Delta N = \Delta J$ forbids any satellite branch transitions of the type that can be used in case (a) coupling situations to identify which spin component is which. At very low N, however, the relative intensities of the two spin components of a given line will be noticeably unequal, because the intensities are governed essentially by the number of M_J components in the combining states, or in other words the J values. For the $^qP_1(2)$ line the two components are $J' = \frac{1}{2} - J" = 1\frac{1}{2}$ ($F_2 - F_2$) and $J' = 1\frac{1}{2} - J" = 2\frac{1}{2}$ ($F_1 - F_1$), so that the F_1 component is expected to be stronger. It can be seen in Fig. 7.1 that the stronger line is the long wavelength component. A very weak $J' = 1\frac{1}{2} - J" = 1\frac{1}{2}$ satellite transition is predicted to occur; this should fall between the F_1 and F_2 main branch lines, but has not been observed.
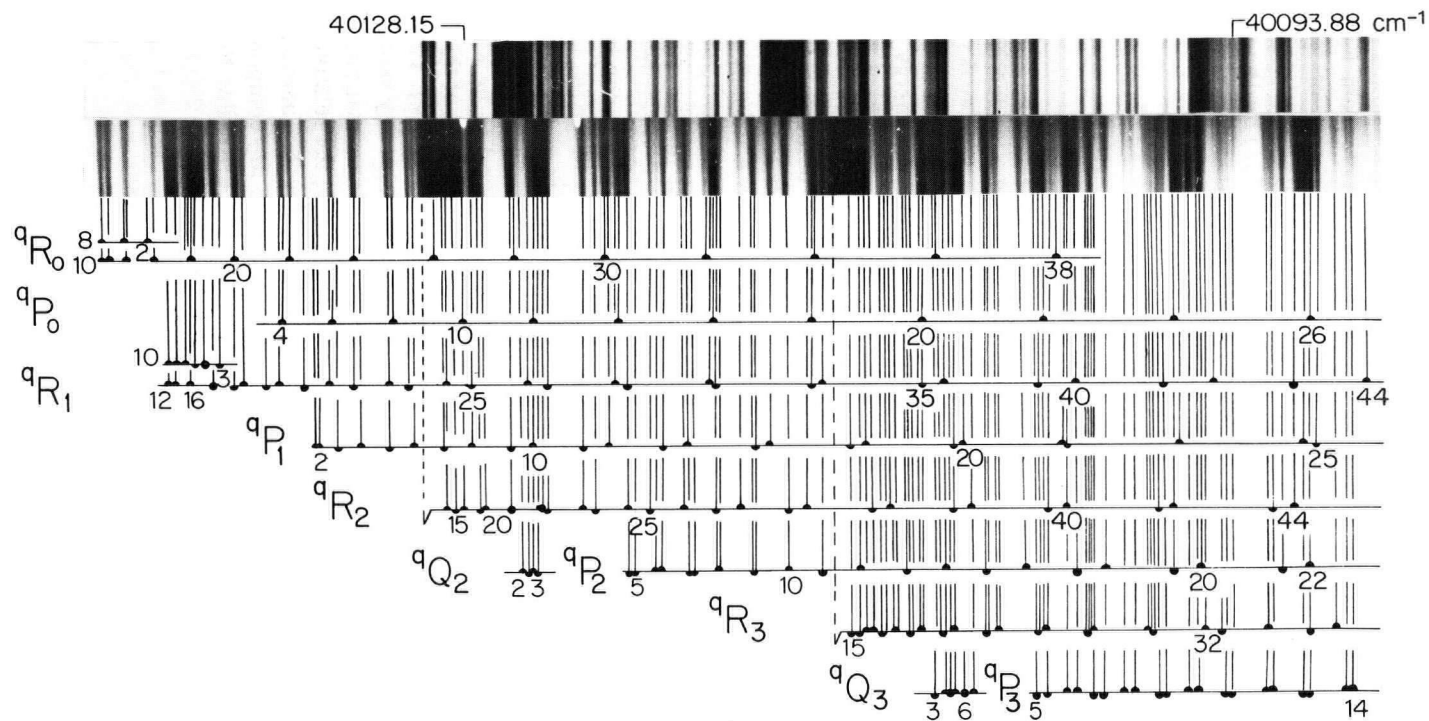
Fig 7.1 Head of the 2490-Å bands ($2^2B_2 - \tilde{X}^2A_1$) of $^{14}NO_2$ (above) and $^{15}NO_2$ (below). The line assignments refer to the $^{15}NO_2$ spectrum.

Figure 7.2 shows the K = 7 and 8 subbands, printed from a plate taken with the gas at 120°C, where the branches run to N values rather higher than in Fig. 7.1. The spectrum is seen to be still quite complex, despite the wide separation of the subbands, but the characteristic large spin doublings of the ^qP branches are clear in the right-hand part of the figure. The K^2 dependence of the spin splitting for constant N can be seen when the splittings for K = 7 and 8 are compared.

The upper-state rotational constants were determined by adding the energies of the unblended lines to the lower-state energies, to obtain the upper-state term values, and fitting these by least squares. The Hamiltonian used for the upper state was the same as that for the lower state. The results are given in Table 7.1. The quartic centrifugal distortion constants of the upper state are very much what would be expected by analogy with $^{14}NO_2$ (4), but the sextic constants are completely different. The reason is that the ground-state Hamiltonian includes no sextic centrifugal distortion, since the microwave data do not allow these constants to be determined. We therefore set all the sextic constants to zero for the ground state, which means that the upper-state sextic constants in Table 7.1 are strictly the differences between the upper- and lower-state sextic distortion constants. When this is appreciated the constants are found to be very much as expected. For instance, in $^{14}NO_2$, Hallin and Merer (4) could only determine the constants H''_K and H'_{KN}, all the others being too small to measure, and they found

$$H'_K - H''_K = (-3.26 \pm 0.46) \times 10^{-6} \text{ cm}^{-1},$$
$$H'_{KN} - H''_{KN} = (-1.85 \pm 1.30) \times 10^{-8} \text{ cm}^{-1}. \tag{7.5}$$
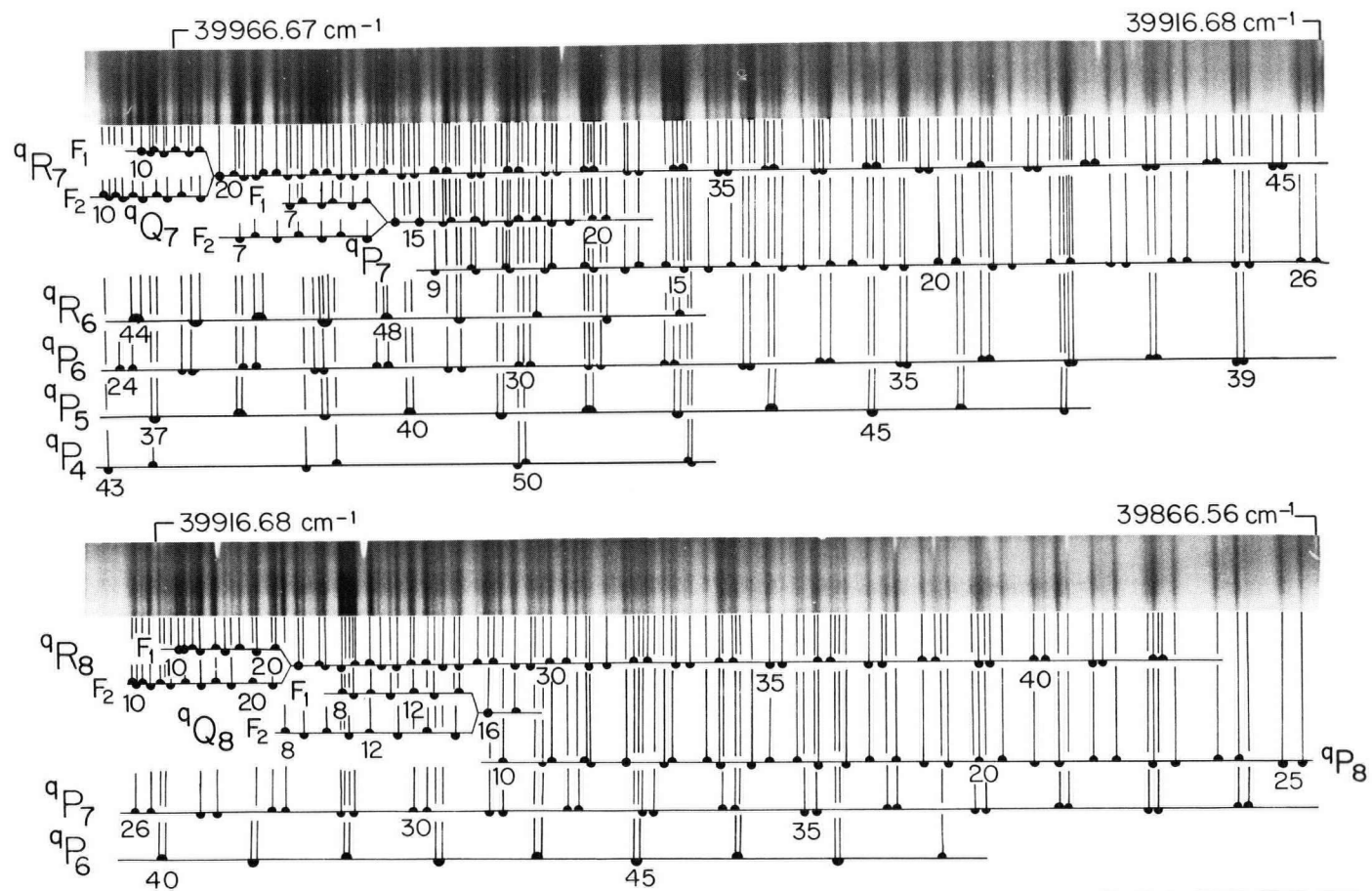
Fig. 7.1 K = 7 and 8 subbands of the 2490-Å band of $^{15}NO_2$ (in the region 2502 - 2508 Å).

Allowing for the mass difference these quantities compare favorably with those in Table 7.1.

We did not attempt to refine the ground-state quartic centrifugal distortion constants in this work, even though they clearly need improvement. The reason is that the most poorly determined microwave constants are precisely those which the parallel selection rules of the electronic transition prevent us from improving. Specifically, the constant Δ_K is probably the least well determined because the microwave results go only to $K = 3$. The electronic spectrum also contains information on the K-stack separations up to $K = 3$ in the form of ^SR branches, but naturally it is far less precise; for $K \geqslant 4$ there are no transitions observed in the electronic spectrum except $\Delta K = 0$ branches. Also the constant Δ_K is difficult to obtain from the electronic spectrum because it is determined from differences between the asymmetry components of the low K stacks, where the lines involved lie in the most crowded region of the spectrum and blending is most severe. A second reason is that because of the predissociation in the upper state the lines are wider than the Doppler width alone.

Because of the difficulties with the ground state we have not been able to obtain as good a fit to the data for $^{15}NO_2$ as Hallin and Merer (4) could for $^{14}NO_2$, even though the data themselves are of comparable quality. The overall standard deviation is 0.032 cm^{-1} for $^{15}NO_2$, which should be compared to 0.025 cm^{-1} for $^{14}NO_2$.[1]

The assigned rotational lines have been collected in Appendix VI .

---

[1] In other words we could perhaps have lowered the standard deviation for $^{15}NO_2$ by refining the ground-state centrifugal distortion but because of the problems described above the improvement would almost certainly have been artificial.

TABLE 7.1

Rotational Constants for the 2490-Å Band of $^{15}NO_2$ (cm^{-1})

	2^2B_2, 000 (upper state)		$\tilde{X}^2A_1$, 000 (ground state)	
T_0	40140.339	± 24	0.00	
A	3.9266	19	7.63047	± 13
B	0.403300	94	0.433735	6
C	0.363946	102	0.409440	6
$10^6 \Delta_K$	460	51	2297	
$10^6 \Delta_{NK}$	13.17	158	-17.69	
$10^6 \Delta_N$	0.439	31	0.2817	
$10^6 \delta_K$	8.8	86	2.704	
$10^6 \delta_N$	0.098	34	0.03189	
$10^6 H_K$	-1.93	42	-	
$10^8 H_{KN}$	-1.9	20	-	
ϵ_{aa}	-0.1724	40	0.1718	
ϵ_{bb}	0		0.000256	
ϵ_{cc}	0		-0.003163	
η	-		-0.000103	
σ	0.032		-	

Notes: Ground state rotational constants from ref. (14), with the quartic centrifugal distortion converted from the τ values, which are

$$\tau_{aaaa} = (-9.12 \pm 0.13) \times 10^{-3} \qquad \tau_{bbbb} = (-1.382 \pm 0.005) \times 10^{-5} \text{ cm}^{-1}$$
$$\tau_{aabb} = (5.87 \pm 0.06) \times 10^{-5} \qquad \tau_{abab} = (8.16 \pm 0.03) \times 10^{-6}$$

Ground state spin constants from ref.(15) except η which was calculated as $\tau_{aaaa} \cdot \epsilon_{aa}/2A$ (11). Uncertainties are three standard deviations, in units of the last significant figure quoted.

D. Conclusion

The 2490-Å bands of both $^{14}NO_2$ (4) and $^{15}NO_2$ are found to be slightly predissociated, and to have essentially the same linewidths. The predissociation lifetime was determined in Ref. (4) to be 42 ± 5 psec. The possibility of selective dissociation of $^{14}NO_2$ in the presence of $^{15}NO_2$, and vice versa, has been explored in this work. The two spectra are compared in Fig. 7.1 It is seen that there would be no difficulty dissociating $^{15}NO_2$ in the presence of $^{14}NO_2$ because the isotope shift of 14.40 cm^{-1} for the $^qR_0$ heads means that many strong $^{15}NO_2$ lines lie in a region where only weak sparse ^SR lines of $^{14}NO_2$ fall. On the other hand, dissociating $^{14}NO_2$ in the presence of $^{15}NO_2$ would require narrow-line lasers specifically tuned to certain wavelengths. The most promising regions appear to be in the heads of the $^qR_1$ and $^qR_2$ branches of $^{14}NO_2$, where many close-lying strong $^{14}NO_2$ lines fall in gaps between the $^{15}NO_2$, $^qP_1$, $^qR_2$, and $^qP_2$ lines. The exact wavelengths can be calculated from the tables of assignments given in Table III for $^{15}NO_2$ and the Appendix to Ref. (4) for $^{14}NO_2$.

Spectroscopically, the 2490-Å band of $^{15}NO_2$ confirms the analysis of the corresponding band of $^{14}NO_2$ in detail, and poses no questions. The need for a more detailed examination of the infrared spectrum of $^{15}NO_2$ is pointed out. It is likely that the resulting changes in the ground-state constants can be transferred directly to the upper-state constants reported in this work, since we have essentially determined the differences between the upper- and lower-state constants in this work. However, it is not impossible that the upper-state constants may need to be reworked if the ground-state changes are considerable, since

the relationship between the two sets is not one-to-one because of the

large changes in the rotational constants on electronic excitation.

Chapter 8

Fourier Transform Spectroscopy of VO;

Rotational Structure in the $A^4\Pi$-$X^4\Sigma^-$

System near 10500 Å

A. Introduction

Vanadium monoxide, VO, is present in considerable amounts in the atmospheres of cool stars, to the extent that its two electronic band systems in the near infra-red are used for the spectral classification of stars of types M7-M9 (1). Both of these systems, A-X near 10500 Å and $B^4\Pi$-$X^4\Sigma^-$ near 7900 Å, were in fact first found in stellar spectra (2,3) before laboratory work, respectively by Lagerqvist and Selin (4) and Keenan and Schroeder (5), proved that VO is the carrier. The purpose of this chapter is to report rotational analyses of the (0,0) and (0,1) bands of the A-X system from high dispersion Fourier transform emission spectra; the A-X system is shown to be another $^4\Pi$-$^4\Sigma^-$ transition.

The $A^4\Pi$ state of VO is found to have quite small spin-orbit coupling, so that the rotational and hyperfine structure follows case (a_β) coupling at low rotational quantum numbers, but is almost totally uncoupled to case $(b_{\beta J})$ coupling at the highest observed quantum numbers. The hyperfine structure caused by the ^{51}V nucleus (I = 7/2) is not resolved in the spectra reported here, but an interesting result is that the hyperfine parameter b for the $A^4\Pi$ state can be estimated from the line shapes at high N values and is found to be essentially the same as in the ground $X^4\Sigma^-$ state. The conclusion is that the $A^4\Pi$ state comes from an electron configuration containing an unpaired $4s\sigma$ electron, as does the ground state.

In contrast to the other excited states of VO the $A^4\Pi$,v = 0 level is unperturbed rotationally; it therefore provides one of the very few examples known where the energy formulae for $^4\Pi$ states can be checked directly against observation.

B. Experimental details

The near infra-red electronic transitions of VO in the region 6000-14000 cm^{-1} were recorded in emission using the 1 meter Fourier Transform spectrometer constructed by Dr. J.W. Brault for the McMath Solar Telescope at Kitt Peak National Observatory, Tucson, U.S.A. The source was a microwave discharge through flowing $VOCl_3$ and helium at low pressures, which was focused directly into the aperture of the spectro-meter. An indium antimonide detector cooled by liquid nitrogen was used, and the resolving power of the spectrometer was set to approximate-ly 800,000. Forty-two interferograms, each taking six minutes to record, were co-added for the final transform. The resulting spectrum, consist-ing of tables of emission intensity against wave number for every 0.013608 cm^{-1}, was processed by a third degree polynomial fitting pro-gramme to extract the positions of the line peaks.

C. Appearance of the spectrum

The spectrum of VO in the near infra-red down to 6000 cm^{-1} consists of the two electronic transitions $B^4\Pi-X^4\Sigma^-$ and $A^4\Pi-X^4\Sigma^-$. The B-X system is very much stronger than the A-X system under our discharge conditions, so that the B-X progressions and sequences mask most of the A-X system except for the (0,0) and (0,1) bands. Even the (0,0) band of the A-X system (which is by far the strongest band) is not free from overlapping B-X structure, which causes some difficulty in the analysis. The main heads of the A-X (0,0) band are illustrated in Fig. 8.1; each of the four sub-bands produces one strong head ($^SR_{43}$, R_3, $^RQ_{21}$ and R_1), and there

VO $A^4\Pi - X^4\Sigma^-$ (0,0)

$^SR_{43}$

9557.83 cm^{-1}

$^RQ_{43}$

R_3

$^RQ_{21}$

R_1

Q_1

9423.49 cm^{-1}

$^4\Pi_{5/2}$ $^4\Pi_{3/2}$ $^4\Pi_{1/2}$ $^4\Pi_{-1/2}$
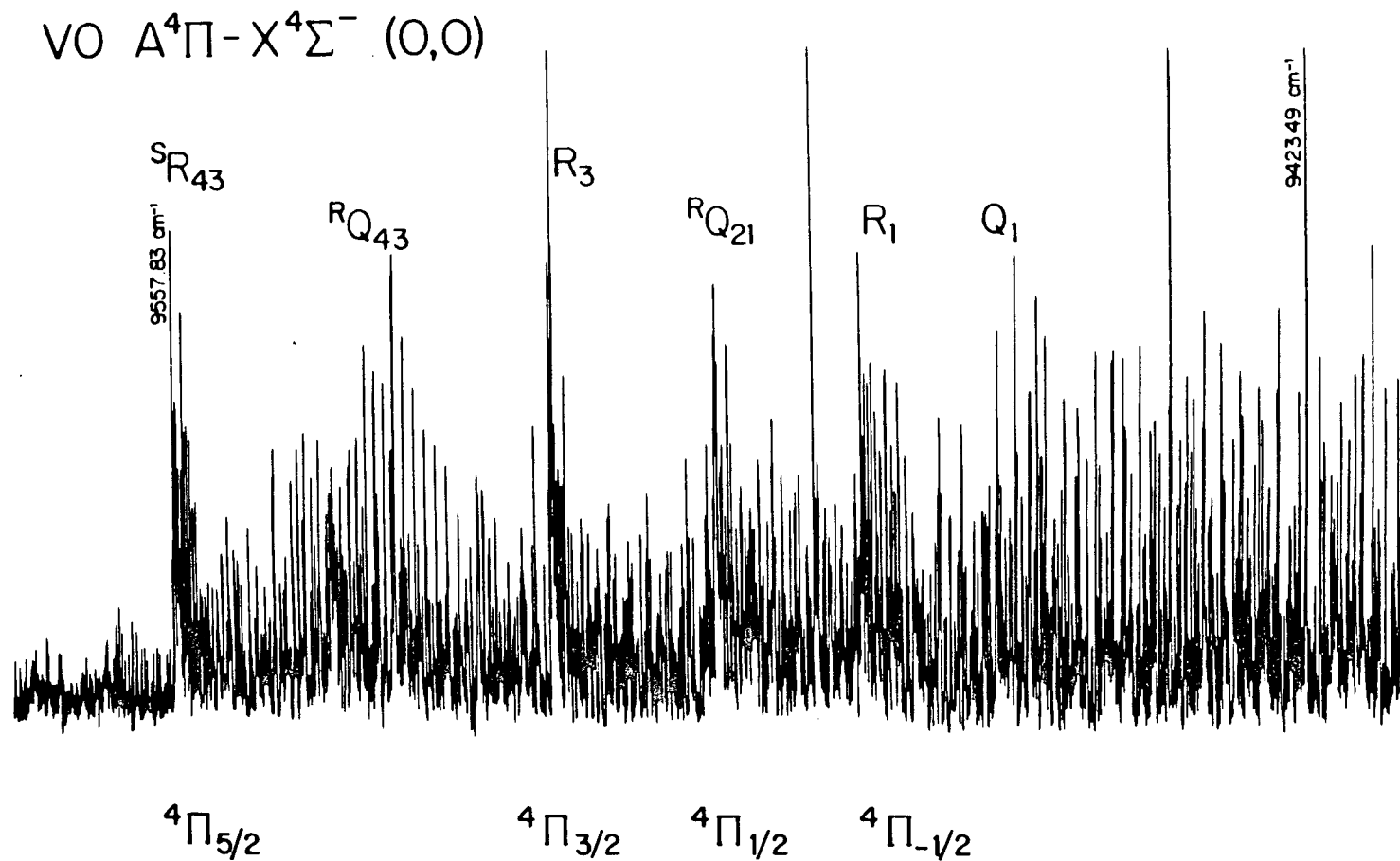
Fig 8.1   Fourier transform spectrum of VO in the region 9410–9570 cm^{-1} showing the heads of the $A^4\Pi - X^4\Sigma^-$ (0,0) band of VO.

is also a less prominent Q_1 head in the $^4\Pi_{-\frac{1}{2}}-^4\Sigma^-$ sub-band. Two other

heads, belonging to the B-X (1,4) band, appear in the region of the

$^4\Pi_{5/2}-^4\Sigma^-$ sub-band; they have not been identified in the Figure, though

their branch structure is readily picked out at higher dispersion.

The A-X (0,1) band is qualitatively similar, though since it is

weaker the background of B-X lines is more troublesome. The A-X (1,0)

band is so heavily overlapped by B-X structure that we have not been

able to analyse it; the $^S R_{43}$ head appears to be at 10503.3 cm^{-1} but even

this is not definite.

D. Energy levels of $^4\Pi$ and $^4\Sigma$ states

Energy levels for $^4\Pi$ electronic states have been considered by a

number of authors (6-11). The most detailed treatment is that of

Féménias (9), who has given a full explanation of how to calculate the

matrix elements for the higher order centrifugal distortion terms.

Detailed analyses of $^4\Pi$ states, against which to test the formulae, are

less common; the best examples come from the spectra of O_2^+ (10) and

NO (12).

$^4\Sigma$ states, on the other hand, are much more numerous, and have been

extensively treated (6,7,9,10,13-17). It will therefore only be necessa-

ry to sketch the Hamiltonian and its derivation, and to give the matrices

we have used.

Following van Vleck (18) we take the rotational Hamiltonian, the

first and second-order spin-orbit interactions and the spin-rotation

interaction, respectively, as

$$H = B(r)(\underset{\sim}{J}-\underset{\sim}{L}-\underset{\sim}{S})^2 + A(r)\underset{\sim}{L}\cdot\underset{\sim}{S} + \frac{2}{3}\lambda(r)(3S_z^2-\underset{\sim}{S}^2) + \gamma(r)(\underset{\sim}{J}-\underset{\sim}{S})\cdot\underset{\sim}{S}. \quad (8.1)$$

The expansion of the parameters A, B, λ and γ, which are functions of the internuclear distance r, in terms of the normal coordinate, produces centrifugal distortion terms, which are conveniently written in operator form as

$$H_{c.d.} = -D(\underset{\sim}{J}-\underset{\sim}{L}-\underset{\sim}{S})^4 + \tfrac{1}{2}A_D[(\underset{\sim}{J}-\underset{\sim}{L}-\underset{\sim}{S})^2, L_zS_z]_+$$
$$+ \frac{1}{3}\lambda_D[(3S_z^2-\underset{\sim}{S}^2), (\underset{\sim}{J}-\underset{\sim}{L}-\underset{\sim}{S})^2]_+ + \tfrac{1}{2}\gamma_D[(\underset{\sim}{J}-\underset{\sim}{L}-\underset{\sim}{S})^2, (\underset{\sim}{J}-\underset{\sim}{S})\cdot\underset{\sim}{S}]_+ \quad (8.2)$$

where $[x,y]_+$ means the anti-commutator $xy + yx$, which is necessary to preserve Hermitian form for the matrices. The Λ-doubling of the $^4\Pi$ state was calculated by setting up the 12x12 matrix for a $^4\Pi$ state interacting with a single $^4\Sigma^-$ state according to the first two terms of eq. (8.1), applying a Wang transformation to convert to a parity basis and treating the elements off-diagonal in Λ by second order perturbation theory. The effect is as if there were an operator

$$H_{LD} = \tfrac{1}{2}(o+p+q)(S_+^2+S_-^2)-\tfrac{1}{2}(p+2q)(J_+S_++J_-S_-)+ \tfrac{1}{2}q(J_+^2+J_-^2) \quad (8.3)$$

acting only within the manifold of the $^4\Pi$ state (11,19). The Λ-doubling parameters (o+p+q), (p+2q) and q are related to matrix elements of the spin-orbit operator, as given in ref. (11). The centrifugal distortion corrections to eq. (8.3) are obtained in the same way that eq. (8.2) is constructed from eq. (8.1). The spin-spin operators $\frac{1}{2}\alpha(r)(S_+^2+S_-^2)$ and $\frac{2}{3}\lambda^{(1)}(r)(3S_z^2-\underset{\sim}{S}^2)$ are incorporated into the terms in (o+p+q) and λ, respectively.

Table 8.1 Matrix elements of the rotational Hamiltonian for a $^4\Pi$ state in case (a) coupling.

	$\lvert -\tfrac{1}{2}\rangle$	$\lvert \tfrac{1}{2}\rangle$	$\lvert \tfrac{3}{2}\rangle$	$\lvert \tfrac{5}{2}\rangle$
$\langle -\tfrac{1}{2}\rvert$	$T_{-\frac{1}{2}} + (B-\tfrac{3}{2}A_D+2\lambda_D)(z+1)$ $-D(z^2+5z+1)$ $\pm\,3(J+\tfrac{1}{2})D_{o+p+q}$	$-\sqrt{3z}[B-\tfrac{1}{2}\gamma-A_D-2D(z+2)]$ $\mp\sqrt{3}[(o+p+q) + (z+2)D_{o+p+q}$ $+\tfrac{1}{2}(2z-1)D_{p+2q}]$	$-\sqrt{3(z-1)}\ [2D(J+\tfrac{1}{2})$ $\mp\tfrac{1}{2}(p+2q)\mp D_{o+p+q}$ $\mp\tfrac{1}{2}(z+1)D_{p+2q}\mp\tfrac{1}{2}(z-2)D_q]$	$\mp\sqrt{(z-1)(z-4)}\ [\tfrac{1}{2}q$ $+\tfrac{3}{4}D_{p+2q} + \tfrac{1}{2}D_q(z-2)]$
$\langle \tfrac{1}{2}\rvert$		$T_{\frac{1}{2}} + (B-\tfrac{1}{2}A_D-2\lambda_D)(z+3)$ $-D(z^2+13z+5)\cdot(J+\tfrac{1}{2})[(p+2q)$ $+3D_{o+p+q} + D_{p+2q}(z+3)+D_q(z-1)]$	$-2\sqrt{z-1}\,[B-\tfrac{1}{2}\gamma-2\lambda_D-2D(z+2)$ $\pm\tfrac{1}{6}(J+\tfrac{1}{2})\{q+\tfrac{7}{2}D_{p+2q}$ $+D_q(z+2)\}]$	$\sqrt{3(z-1)(z-4)}\ [-2D$ $\pm\tfrac{1}{2}D_q(J+\tfrac{1}{2})]$
$\langle \tfrac{3}{2}\rvert$	.		$T_{3/2}+(B+\tfrac{1}{2}A_D-2\lambda_D)(z+1)$ $-D(z^2+9z-15)$ $+(z-1)(J+\tfrac{1}{2})D_q$	$-\sqrt{3(z-4)}\ [B-\tfrac{1}{2}\gamma+A_D$ $-2D(z-2)]$
$\langle \tfrac{5}{2}\rvert$		Symmetric		$T_{5/2}+(B+\tfrac{3}{2}A_D+2\lambda_D)(z-5)$ $-D(z^2-7z+13)$

$z = (J+\tfrac{1}{2})^2$. Upper and lower signs refer to e and f rotational levels respectively.

The basis functions $\lvert J\Omega\rangle$ have been abbreviated to $\lvert \Omega\rangle$

Table 8.2 Matrix elements for spin and rotation in a $^4\Sigma^-$ state

in case (a) coupling .

	$\lvert\tfrac{3}{2}\rangle$	$\lvert\tfrac{1}{2}\rangle$
$\langle\tfrac{3}{2}\rvert$	$2\lambda + Bx - D(x^2+3x)$ $- \tfrac{3}{2}\gamma - 3\gamma_D x$	$-\sqrt{3x}[B-\tfrac{1}{2}\gamma-\gamma_S-\tfrac{1}{2}\gamma_D(x+7\mp\{2J+1\})$ $-2D(x+2)\mp\{J+\tfrac{1}{2}\})]$
$\langle\tfrac{1}{2}\rvert$	symmetric	$-2\lambda + B(x+4)-D[(x+4)^2+7x+4]$ $-\tfrac{7}{2}\gamma-\gamma_D(7x+16)$ $\mp 2[B-\tfrac{1}{2}\gamma-\tfrac{1}{2}\gamma_D(x+11)+\tfrac{3}{2}\gamma_S$ $- 2D(x+4)](J+\tfrac{1}{2})$

$x = (J+\tfrac{1}{2})^2-1$. Upper and lower signs give the $e(F_1$ and $F_3)$ and $f(F_2$ and $F_4)$ levels respectively. The basis functions $\lvert J\Sigma\rangle$ have been written $\lvert\Sigma\rangle$

The resulting Hamiltonian matrices which we have used are given in Tables 8.1 and 8.2 (for $^4\Pi$ and $^4\Sigma$ states respectively). The $X^4\Sigma^-$, $v=0$ parameters were not varied in this work since they have been determined with great precision from the $C^4\Sigma^- - X^4\Sigma^-$ transition using sub-Doppler techniques (17). The parameter γ_S in the $^4\Sigma$ matrix represents the third-order spin-orbit contribution to the spin-rotation interaction (16,17); neither γ_S nor the centrifugal distortion correction γ_D appears in the $^4\Pi$ matrix because they are not needed.

Hyperfine effects have not been considered in Tables 8.1 and 8.2 because the hyperfine structure is not resolved. However, with the large spin and nuclear magnetic moment of ^{51}V ($I = 7/2$), the hyperfine structure is important in determining the details of the branch structure, as will be shown below.

E.   Analysis of the branch structure

Rather surprisingly, the analysis of the $A^4\Pi - X^4\Sigma^-$ bands of VO proved to be remarkably difficult because of unresolved hyperfine structure effects and overlapping sequence bands from the B-X transition. The problem with the hyperfine structure is that only when the hyperfine 'widths' of the combining levels making up a rotational line are the same does the spectrum consist of sharp rotational lines (where the eight hyperfine transitions lie on top of each other). Since the four electron spin components of the ground state have hyperfine widths that differ from one to the next by about 0.2 cm^{-1}, rotational lines with the same upper state which go to different electron spin components of the ground state

have noticeably different line-widths. The broader the line-widths the more the intensity is spread out, and the more the line tends to get lost in the background of overlapping B-X structure. Therefore although a $^4\Pi-^4\Sigma^-$ transition should have 48 branches, most of them are broadened beyond recognition by the hyperfine structure in this case.

There are only two regions of clear branch structure in the (0,0) band. One of these, shown in Fig. 8.2, lies between the two shortest wavelength heads. The obvious branch, later identified as $^RQ_{43}$, could be assigned at once to the F_3 spin component of the ground state because it contains the characteristic internal hyperfine perturbation pattern at N" = 15 discovered by Richards and Barrow (20) in the B-X and C-X systems. This internal hyperfine perturbation is a remarkable occurrence, where the F_2 and F_3 electron spin components (N = J-½ and N = J+½ respectively) would cross at N = 15, because of the particular values of the rotational and spin parameters, were it not for the fact that they differ by one unit in J, and therefore interact through matrix elements of the hyperfine Hamiltonian of the type $\Delta N = \Delta F = 0$, $\Delta J = \pm 1$. Extra lines are induced, and, since the detailed course of the ground state levels is known (17), their positions tell whether a branch containing them has $F_2"$ or $F_3"$, and also give its N-numbering.

Given the numbering of the obvious $F_3"$ branch, the other three F_4' branches marked in Fig. 8.2 could be numbered easily using ground state spin and rotational combination differences. The R_4 and Q_4 branches are hyperfine-broadened, and even though they are intrinsically strong they are by no means obvious in the spectrum. At this stage the lower states of the branches were known, but the nature of the upper state was still
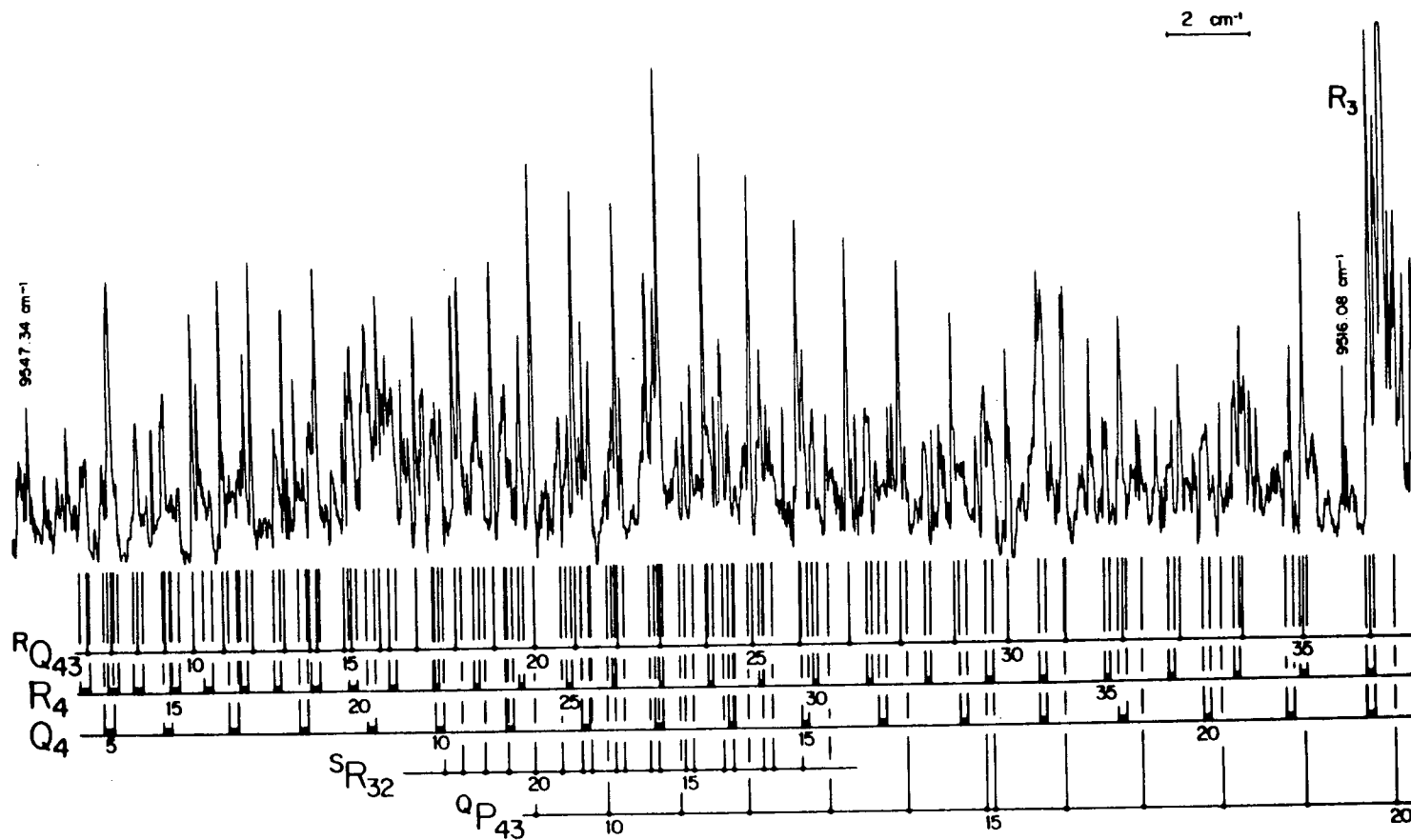
Fig 8.2 Rotational structure in the $A^4\Pi - X^4\Sigma^-$ (0,0) band of VO, showing the F_4' branch structure ($^4\Pi_{5/2}$).

unclear.

The other region of obvious branch structure is the tail of the band, part of which is illustrated in Fig. 8.3. There are at least ten sharp branches in this region, but only eight of them actually belong to the A-X (0,0) band. A further complication is that there are no ground state combination differences connecting any of these eight. The analysis was performed by comparing the (0,0) and (0,1) bands, since the separations between corresponding (N,J) levels of the $X^4\Sigma^-$ v=0 and 1 levels are known from the analysis of the C-X system (21). This method gives at most two possible N-numberings for the branches, but it is less easy to determine the ground state spin component since the intervals are very nearly the same for the four spin components. Eventually all eight of these branches were identified, and assigned to their respective ground state spin components. The resulting pattern can be interpreted as the Q and P main branches of a $^4\Pi-^4\Sigma$ transition where the $^4\Pi$ state is close to case (b) coupling at these high N values, and all four components show Λ-doubling. The analysis is confirmed by the identification of the four R branches, and various weak hyperfine-broadened spin satellite branches.

The Q_4 branch is interesting because it is a sharp branch at the high N values of Fig. 8.3, but hyperfine-broadened at the lower N values of Fig. 8.2. It is possible to follow the Q_4-branch over the complete range of N values, and to see how it changes from broad to narrow fairly quickly in the region N=40-50. The reason for the sudden disappearance of the $^RQ_{43}$ branch near N=35 (see Fig. 8.2) is then clear - the $^RQ_{43}$
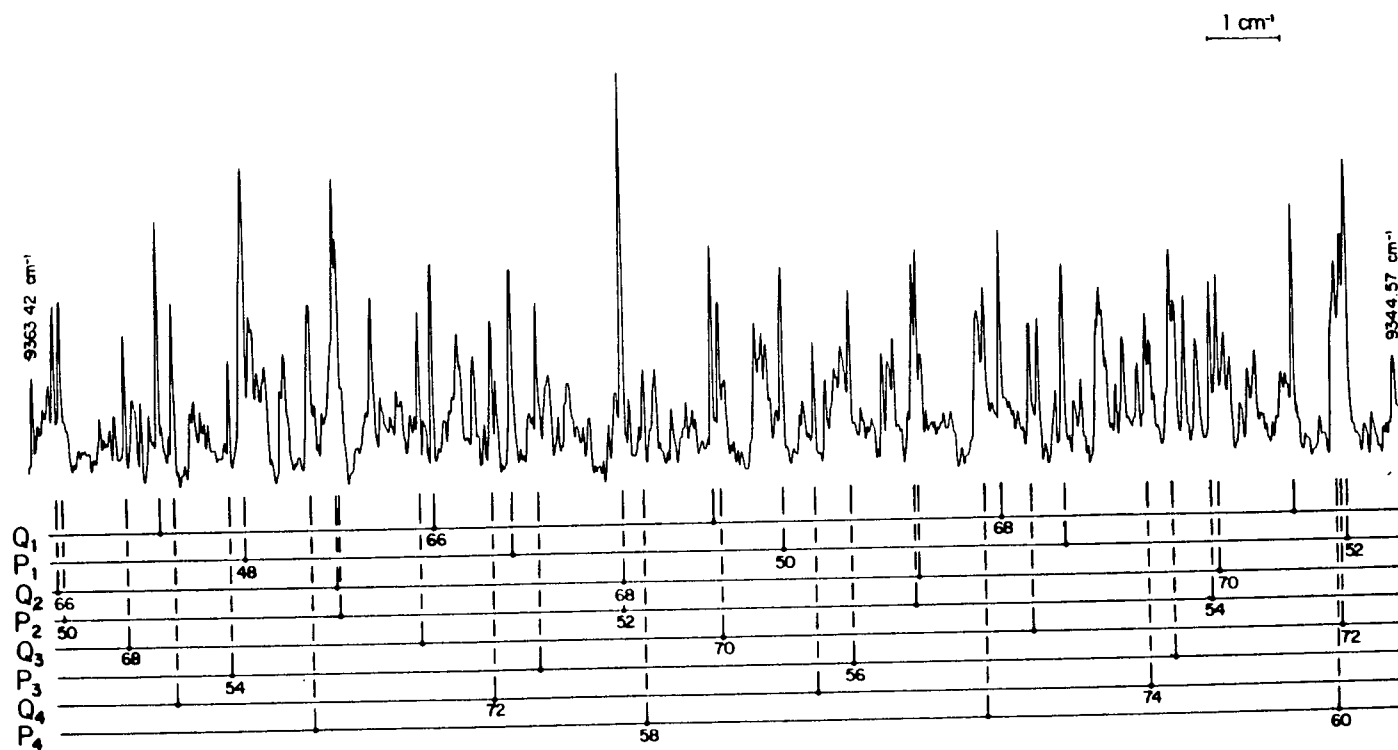
Fig 8.3 High main branch Q and P lines in the tail of the VO $A^4\Pi - X^4\Sigma^-$ (0,0) band.

branch is prominent at low N because the hyperfine structure of the $^4\Pi$ F_4 level is initially the same as that of the $X^4\Sigma^-$ F_3 level, but with increasing N spin-uncoupling changes the $^4\Pi$ hyperfine level pattern until at high N it becomes the same as $X^4\Sigma^-$ F_4; as a result the $^RQ_{43}$ branch becomes broadened. In addition the intensity of $^RQ_{43}$, which is a spin satellite branch that becomes forbidden in a $^4\Pi(b)-^4\Sigma(b)$ transition, must diminish as spin-uncoupling sets in.

What emerges finally is a 'text-book' example of a $^4\Pi_r-^4\Sigma$ transition where the $^4\Pi$ state has quite small spin-orbit coupling so that it changes fairly quickly from case (a) to case (b) coupling. The $^4\Pi$ state is shown to be regular (with a positive spin-orbit coupling constant) because there is no detectable Λ-doubling in the F_4 component ($^4\Pi_{5/2}$) before about N=45, whereas the other three spin components show Λ-doubling effects almost from their first levels. The Λ-doubling and spin-uncoupling patterns are shown qualitatively in Fig. 8.4, where the upper state energy levels, suitably scaled, are plotted against $J(J+1)$. The curvature in the plots of Fig. 8.4 is a consequence of the spin-uncoupling. The assigned lines of the (0,0) and (0,1) bands of the A-X system are given in the Appendix; only the sharp lines are listed, because they are sufficient to determine the upper state constants, and in any case it is often quite difficult to obtain the exact line centres for the hyperfine-broadened branches.

F. Least squares fitting of the data

One of the unexpected effects of the ground state internal hyperfine perturbation is that the F_2'' and F_3'' levels are appreciably shifted from
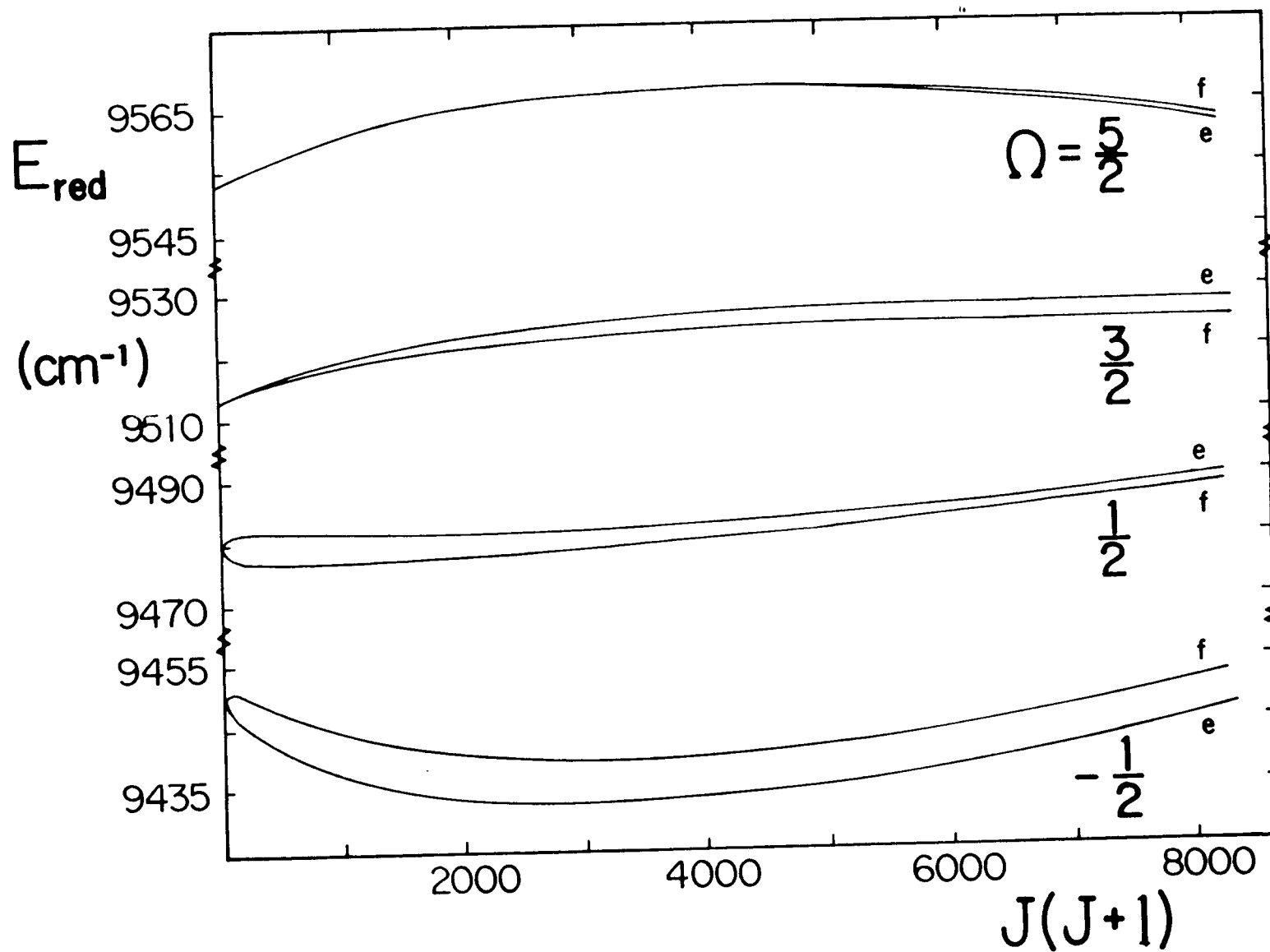
Fig 8.4 Reduced energy levels of the $A^4\Pi$ state of VO plotted against $J(J+1)$. The quantity plotted is the upper state term value less $(0.50865 + 0.00365\Omega)\ (J+\tfrac{1}{2})^2 - 6.7 \times 10^{-7}\ (J+\tfrac{1}{2})^4\ cm^{-1}$.

Table 8.3   Corrections applied to the observed F_2 and F_3 line positions to allow for the internal hyperfine perturbation shifts.

N	F_2	F_3	N	F_2	F_3	N	F_2	F_3
4	-0.030	-0.003	14	-0.079	+0.055	24	+0.029	-0.026
5	-0.031	+0.008	15	±0.080		25	0.027	-0.025
6	-0.031	0.012	16	+0.075	-0.086	26	0.026	-0.024
7	-0.033	0.017	17	0.065	-0.075	27	0.025	-0.022
8	-0.034	0.022	18	0.051	-0.060	28	0.023	-0.021
9	-0.036	0.025	19	0.047	-0.058	29	0.023	-0.020
10	-0.053	0.031	20	0.043	-0.043	30	0.022	-0.019
11	-0.060	0.033	21	0.038	-0.039	31	0.021	-0.018
12	-0.065	0.034	22	0.035	-0.031	32	0.021	-0.018
13	-0.070	0.043	23	0.032	-0.028	33	0.020	-0.017

The corrections were obtained by subtracting the rotational energy calculated in the absence of hyperfine effects from a weighted average of the rotational-hyperfine energies given by a full calculation of the hyperfine structure.

the positions that they would have in the absence of hyperfine structure. Therefore it is necessary to correct all the line positions in the branches involving F_2 or F_3 lower levels for this effect.

It may seem surprising that a hyperfine effect can shift the positions of rotational levels, but the hyperfine matrix element acting between F_2 and F_3 levels with the same N value is about 0.08 cm^{-1}, while the zero-order separation of the F_2 and F_3 levels (which depends on the spin-rotation parameter γ) remains less than 1 cm^{-1} even some distance from the N-value of the internal perturbation. The calculated shifts are given in Table 8.3.

After applying these corrections to the F_2'' and F_3'' branches we fitted the lines directly to the appropriate differences between eigenvalues of the $^4\Pi$ and $^4\Sigma^-$ matrices. No attempt was made to vary the $X^4\Sigma^-$, v=0 parameters in the present work since they have been determined with high precision by the sub-Doppler spectra of (17), where the resolution is a factor of ten higher. Our procedure is therefore equivalent to fitting the term values of the $A^4\Pi$, v=0 state to the eigenvalues of Table 8.1. The (0,1) band was then fitted similarly, but with the $A^4\Pi$ upper state parameters fixed at the values derived from the (0,0) band; the results give essentially the differences between the parameters for $X^4\Sigma^-$ v=0 and v=1.

The final parameters are assembled in Table 8.4. The overall standard deviations listed correspond to unit weighting of all the data; they are not as low as we had expected, but in view of the blending and the unusual line shapes produced by unresolved hyperfine structure effects in some of the branches we see no reason for concern.

Table 8.4 Parmeters derived from rotational analysis of the $A^4\Pi - X^4\Sigma^-$ (0,0) and (1,0) bands of VO in cm^{-1}.

$A^4\Pi$, v = 0		
$T_{5/2}$	9555.500	±0.011 (3σ)
$T_{3/2}$	9512.432	±0.017
$T_{1/2}$	9477.830	±0.023
$T_{-1/2}$	9449.710	±0.021
B	0.516932	±0.000006
$10^7 D$	6.782	±0.010
q	-0.000151	±0.000012
p+2q	-0.01349	±0.00027
o+p+q	2.107	±0.008
γ	0.00383	±0.00010
$10^7 D_q$	0.023	±0.022
$10^7 D_{p+2q}$	-2.32	±0.68
$10^5 D_{o+p+q}$	-4.95	±0.42
λ_D	0.000050	±0.000004

$X^4\Sigma^-$, v = 0		v = 1	
T_0	0	1001.812	±0.011 (3σ)
B	0.546383_3	0.542864	±0.000013
$10^7 D$	6.509	6.54	±0.03
λ	2.0308_7	2.028	±0.002
γ	0.02251_6	0.0226	fixed
$10^5 \gamma_S$	-1	-1	fixed
$10^8 \gamma_D$	5.6	5.6	fixed
	fixed		

Standard deviations (unit weight):- $A^4\Pi$, v = 0: 0.024 cm^{-1}; $X^4\Sigma^-$, v = 1: 0.024 cm^{-1}

Bond lengths: $A^4\Pi$, r_0 = 1.6368 Å; $X^4\Sigma^-$, r_0 = 1.5920 Å, r_e = 1.5894 Å

$(B_e = 0.54814_3, \alpha_e = 0.00351_9 \ cm^{-1})$

G. Discussion

(i) Spin-orbit coupling constants and indeterminacies

Since $^4\Pi$ states are comparatively uncommon it is instructive to see what parameters can be determined in this case, and what happens to the problem of the indeterminacy of some of the parameters in the general case.

Veseth (21) has pointed out how γ and A_D (the spin-rotation interaction and the centrifugal distortion correction to the spin-orbit coupling) cannot be determined separately in a $^2\Pi$ state, and Brown et al (19) have proved this rigorously. Brown et al have also shown that an indeterminacy exists between B, A_D, λ_D and γ for case (a) $^3\Pi$ states, essentially because there are only three effective B-values for the three spin-orbit components, but four parameters to be determined from them. The indeterminacy can be avoided if the levels can be followed to high J values, where case (b) coupling applies, because there is additional information in the effective D-values of the three spin-orbit components. No such indeterminacy occurs for $^4\Pi$ states because there are now four effective B-values to determine the same four parameters; only if higher-order terms such as γ_S (the third-order spin-orbit correction to the spin-rotation interaction (16,17)) are needed will further indeterminacies arise.

It is very clear from our data that A_D is effectively zero for the $A^4\Pi$ state of VO. If A_D is floated the standard deviation increases marginally, and A_D is given as $(4 \pm 12) \times 10^{-6}$ cm^{-1}. Nevertheless if it were not so small it would in principle have been determinable from the data.

Another indeterminacy may arise in the sub-state origins for the components of a multiplet Π state. These origins can be expressed, in terms of the spin-orbit and spin-rotation parameters, as

$$T_\Omega = T_0 + A\Lambda\Sigma + \frac{2}{3} \lambda[3\Sigma^2-S(S+1)] \tag{8.4}$$
$$+ \gamma[\Omega\Sigma-S(S+1)] + \eta\Lambda[\Sigma^3-(3S^2+3S-1)\Sigma/5]$$

where η is the third-order spin-orbit interaction (22,23). From the previous discussion it is seen that for a $^3\Pi(a)$ state only effective values of T_0, A and λ can be determined, but that all five parameters can be determined for a $^4\Pi$ state, because γ can be obtained from the rotational structure.

Because γ has to be determined separately we have written the sub-state origins in Tables 8.1 and 8.4 in the form of T_Ω values. However, it would be entirely equivalent to use expressions derived from eq. (8.4) in the least squares work. Converting from the T_Ω values given in Table 8.4 we have

$$T_0 = 9498.878 \text{ cm}^{-1} \; ; \; A = 35.193 \text{ cm}^{-1}$$
$$\lambda = 1.867 \text{ cm}^{-1} \; ; \; \eta = 0.331 \text{ cm}^{-1} \tag{8.5}$$

It is interesting to see how comparatively large the second-order parameter λ is compared to A. As is well-known (18) the second-order parameter λ includes the diagonal spin-spin interaction, but since the latter cannot be estimated easily it is not possible to say how much of the observed λ is caused by it. The observed λ for the $A^4\Pi$ state is

similar to that for the $X^4\Sigma^-$ state (see Table 8.4), so that its large

size is not unexpected. To our knowledge an accurate value of the

third-order parameter n has only previously been obtained for the level

$v = 4$ of the $^4\Pi_u$ state of O_2^+ (23), though estimates have been made for

the $A^5\Pi$ and $X^5\Pi$ states of CrO (22).

(ii) <u>Λ-doubling parameters</u>

In the approximation where a single $^4\Sigma^-$ state causes the Λ-doubling

in a $^4\Pi$ state the parameters o, p and q are given by

$$o = -\tfrac{1}{2}<^4\Pi|AL_+|^4\Sigma^->^2/\Delta E_{\Pi\Sigma}$$

$$p = -2<^4\Pi|AL_+|^4\Sigma^-><^4\Pi|BL_+|^4\Sigma^->/\Delta E_{\Pi\Sigma} \qquad (8.6)$$

$$q = -2<^4\Pi|BL_+|^4\Sigma^->^2/\Delta E_{\Pi\Sigma}$$

Two approximate relations between the Λ-doubling parameters follow at

once:

$$p/q = A/B \qquad (8.7)$$

and

$$p^2 = 4oq \qquad (8.8)$$

Equation (8.7) should in fact be obeyed quite well no matter what the

states causing the Λ-doubling are because it assumes only that the matrix

elements of AL_+ and BL_+ are in the ratio of A to B; from Table 8.4 we

find

$$(p/q)/(A/B) = 1.26 \qquad (8.9)$$

which is not far from unity. Equation (8.8) on the other hand is not obeyed at all, and the experimental ratio $p^2/4oq$ is -0.13. There are two possible reasons. One is that the off-diagonal spin-spin interaction parameter α (which should be subtracted from the expression for o in eq. (8.6)), is important; the other, which is rather more likely, is that there is a nearby strongly interacting electronic state of different multiplicity. Assuming that the spin-orbit operator is responsible, such a state will have rotation-independent matrix elements with $A^4\Pi$, so that it will contribute to the parameter o, but not to p or q.

As far as we can tell from our spectra the $A^4\Pi$, v=0 level is unperturbed rotationally, and the principal perturbations in $B^4\Pi$ are by another $^4\Sigma^-$ state; however, there is evidence (17) for a $^2\Pi$ state perturbing $C^4\Sigma^-$, v=0 (at 17420 cm^{-1}), which possibly comes from the same electron configuration as $A^4\Pi$ and is a good candidate for causing the effects described.

(iii) Hyperfine structure of the $A^4\Pi$ state

Section E described how the main branches ($\Delta N = \Delta J$) in all four $^4\Pi$-$^4\Sigma^-$ sub-bands become 'sharp' at high N values (where the spin coupling approximates case ($b_{\beta J}$) in both states) although they are often hyperfine-broadened at low N. It has been possible to obtain the approximate hyperfine widths of the four components of $A^4\Pi$ from detailed measurements of the line shapes in the various branches, together with the known hyperfine structure of the ground state (17); the results are shown in

Fig. 8.5. This figure should be considered only as an "artist's impression" because the hyperfine structure is never resolved in the $A^4\Pi-X^4\Sigma^-$ transition, and the deconvolution of the Doppler and hyperfine profiles has not been attempted. The error bars given for the F_2 and F_3 components show that it is relatively futile to try to obtain values for any of the hyperfine parameters except b, but on the other hand the value of b can be obtained with reasonable accuracy.

To understand why only the hyperfine parameter b is determinable we consider the magnetic hyperfine Hamiltonian [24] in detail:

$$H_{mag.hfs} = a\ \underset{\sim}{I}\cdot\underset{\sim}{L} + b\ \underset{\sim}{I}\cdot\underset{\sim}{S} + c\ I_z S_z + \tfrac{1}{2}d(e^{2i\phi}I_-S_- + e^{-2i\phi}I_+S_+) \quad (8.10)$$

In this equation the first term is the interaction between the electron orbital motion and the nuclear spin, the second term is a combination of the Fermi contact interaction and the dipolar interaction, and the last two terms are dipolar interactions, respectively diagonal and off-diagonal in Λ in a signed quantum number basis. The term in d gives rise to different hyperfine structures in the two Λ-doubling components of $^4\Pi_{1/2}$, and its effects can be seen in Fig. 8.5, where there is a definite difference between the hyperfine widths of the F_{2e} and F_{2f} levels up to about J = 50. This difference can be measured fairly accurately because the line widths in the P_2 and Q_2 branches are quite obviously different, though the absolute values of the hyperfine widths are uncertain to the extent of the error bars in Fig. 8.5.

In case (a_β) coupling the diagonal matrix elements (25) of the first three terms of eq. (8.10) are
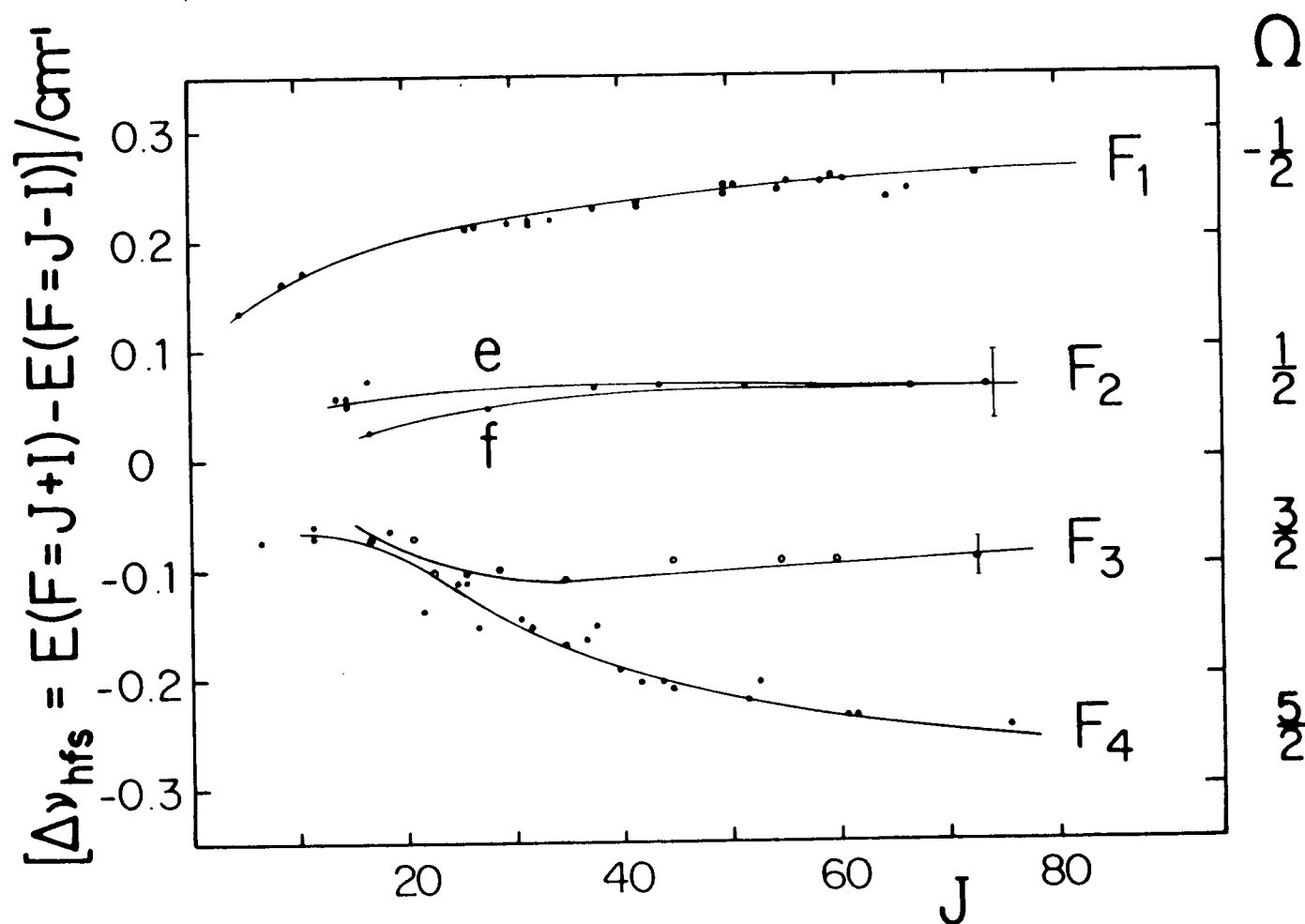
Fig 8.5 Hyperfine widths, $\Delta E_{hfs} = E_{hfs}(F=J+I) - E_{hfs}(F=J-I)$, of the four spin components of the $A^4\Pi$ state of VO, plotted against J. Points are widths calculated from the ground state hyperfine structure and the observed line widths, without correction for the Doppler width.

$$\langle J\Omega\Lambda IF|H_{hfs}|J\Omega\Lambda IF\rangle = [F(F+1)-I(I+1)-J(J+1)]\Omega[a\Lambda+(b+c)\Sigma]/[2J(J+1)]$$

(8.11)

while the d term contributes $\pm d(S+\frac{1}{2})(J+\frac{1}{2})[F(F+1)-I(I+1)-J(J+1)]/[4J(J+1)]$ to the diagonal elements for $\Omega = \frac{1}{2}$ when S is half-integral. The hyperfine widths (in other words the separations of the hyperfine components with $F = J + I$ and $F = J - I$) for a $^4\Pi$ state where $I = 7/2$ are therefore

$$\Delta E_{hfs} = 7(J+\frac{1}{2})\Omega[a+(b+c)\Sigma]/[J(J+1)]$$
$$\pm 7(J+\frac{1}{2})^2 d\delta_{\Omega,\frac{1}{2}}/[J(J+1)]$$

(8.12)

Equation (8.12) implies that the hyperfine widths should decrease as $1/J$ except that there is a J-independent contribution of $\pm 7d$ in the two Λ-components of $^4\Pi_{\frac{1}{2}}$.

In case ($b_{\beta J}$), on the other hand, the diagonal matrix elements of the magnetic hyperfine Hamiltonian are

$$\langle N\Lambda SJIF|H_{hfs}|N\Lambda SJIF\rangle = \frac{[F(F+1)-I(I+1)-J(J+1)]}{4J(J+1)} \left\{ \frac{a\Lambda^2 X(NJS)}{N(N+1)} \right.$$

$$+ bX(JSN) - c\frac{[3\Lambda^2-N(N+1)][3X(SNJ)X(NJS) + 2X(JSN)N(N+1)]}{3N(N+1)(2N-1)(2N+3)}$$

$$\left. \pm d\frac{[3X(SNJ)X(NJS) + 2X(JSN)N(N+1)]}{2(2N-1)(2N+3)} \delta_{|\Lambda|,1} \right\}$$

(8.13)

where $X(xyz) = x(x+1) + y(y+1) - z(z+1)$. It is not so easy to see the J-dependence in these formulae, but order-of-magnitude considerations show that the coefficients of a and c decrease as $1/J$, while the coefficients of b and d are almost independent of J. The hyperfine energy

expressions for $^4\Pi(b)$ states are roughly

$$F_1(J = N+3/2)\ E_{hfs} = -\frac{3}{2}\ (b\pm\tfrac{1}{4}d)\ X(JIF)/(2N+3)$$

$$F_2(J = N+1/2) \qquad -\frac{1}{2}\ (b\pm\tfrac{1}{4}d)\ X(JIF)(2N+9)/[(2N+1)(2N+3)]$$

$$F_3(J = N-1/2) \qquad \frac{1}{2}\ (b\pm\tfrac{1}{4}d)\ X(JIF)(2N-7)/[(2N-1)(2N+1]$$

$$F_4(J = N-3/2) \qquad \frac{3}{2}\ (b\pm\tfrac{1}{4}d)\ X(JIF)/(2N-1)$$

$$(8.14)$$

where the terms in $\pm\tfrac{1}{4}d$ refer to the Λ-doubling components; for $I = 7/2$ the approximate hyperfine widths in the four spin components, in units of $7(b\pm\tfrac{1}{4}d)/2$, are 3,1,-1 and -3, respectively.

Fig. 8.5 shows that the hyperfine patterns in the $A\,^4\Pi$ state of VO, over the range $J = 10$-80, correspond to a spin coupling intermediate between cases (a_β) and $(b_{\beta J})$. As described above, the different hyperfine widths in the F_{2e} and F_{2f} components represent the dipolar d term, but the observed difference is a complicated function of how far the spin-uncoupling has proceeded. The d term should show up again as a small difference between the Q and P branch widths for the high N F_1 and F_4 lines, but this is not observable at our resolution. The high N pattern corresponds to almost pure case $(b_{\beta J})$ coupling, with the parameter b being very nearly the same as in the ground state (hence the 'sharp' main branch lines where the hyperfine components all fall on top of one another). The experimental value of b is

$$b(A\,^4\Pi) = +0.026 \pm 0.002\ cm^{-1} \qquad (8.15)$$

compared to the ground state value $0.02731 \pm 0.00004\ cm^{-1}$ (17).

We have not attempted to obtain values for a, c and d from Fig. 8.5, since the pattern is clearly dominated by the parameter b, with the exact details being governed by the extent of the spin-uncoupling.

The fact that $b(A^4\Pi)$ is closely similar to $b(X^4\Sigma^-)$ indicates that the same $4s\sigma$ electron responsible for the Fermi contact interaction in the ground state is also present in the $A^4\Pi$ state. In single configuration approximation the electron configurations must therefore be

$$X^4\Sigma^- : (4s\sigma)^1(3d\delta)^2$$

$$A^4\Pi : (4s\sigma)^1(3d\delta)^1(4p\pi)^1 \tag{8.16}$$

The configuration given for $A^4\Pi$ also produces a $^4\Phi$ state, which should lie at still lower energy; the chances of observing it appear slim at present since its Λ-value differs by at least 2 units from all the other known states of VO.

Bibliography

Chapter 1

(1) G.C. Dousmanis, T.M. Sanders, Jr., and C.H. Townes, Phys. Rev. 100, 1735-1754 (1955).

(2) H. Spinrad and R.F. Wing, Ann. Rev. Astron. and Astrophys. 7, 249-302 (1969).

(3) P. Toschek in "Spectroscopic sans Largeur Doppler de Systèmes Moléculaires Simples", P13-27, CNRS, Aussois (1973).

(4) N.F. Ramsay "Molecular Beams", Oxford University Press, London (1956).

(5) J.I. Steinfeld and P.L. Houston, "Laser and Coherence Spectroscopy", J.I. Steinfeld ed., Plenum Press, New York (1978).

Chapter 2

(1) A. Carrington, "Microwave Spectroscopy of Free Radicals", Academic Press, London (1974).

(2) P.A.M. Dirac, "The Principle of Quantum Mechanics", Oxford University Press, Oxford (1958).

(3) L.D. Landau and E.M. Lifshitz, "Quantum Mechanics", Pergamon Press (1956).

(4) B.J. Howard and R.E. Moss, Molec. Phys. 19, 433-450 (1970).

(5) B.J. Howard and R.E. Moss, Molec. Phys. 20, 147-159 (1971).

(6) M. Born and K. Huang, "Dynamical Theory of Crystal Lattices", Oxford University Press, London (1954).

(7) R. Renner, Z. Phys., 92, 172-193 (1934).

(8) H.A. Jahn and E. Teller, Proc. Roy. Soc., A161, 220-235 (1937).

(9) E.B. Wilson, Jr., J.C. Decius and P.C. Cross, "Molecular Vibrations", McGraw-Hill, New York (1955).

(10) H.C. Allen, Jr. and P.C. Cross, "Molecular vib-rotors", Wiley, New York (1963).

(11) A.R. Edmonds, "Angular Momentum in Quantum Mechanics", Princeton University Press, Princeton (1974).

(12) M.D. Brink and G.R. Satchler, "Angular Momentum", Clarendon Press, Oxford (1968).

(13) J.M. Brown and B.J. Howard, Molec. Phys. 31, 1517-1525 (1976).

(14) R.S. Mulliken, Phys. Rev. 59, 873-889 (1941).

(15) L. Eyges, "The Classical Electromagnetic Field", Addison-Wesley, London (1972).

(16) Thomas, Nature, 107, 514 (1926).

(17) K. Kayama and J.L. Baird, J. Chem. Phys. 46, 2604-2618 (1967).

(18) J.H. Van Vleck, Rev. Mod. Phys. 23, 213-229 (1951).

(19) K.E. Hallin, Ph.D. Thesis, University of British Columbia (1977).

(20) R.S. Henderoon, Phys. Rev. 100, 723-729 (1955).

(21) R.A. Frosch and H.M. Foley, Phys. Rev. 88, 1337-1349 (1952).

(22) G.C. Dousmanis, Phys. Rev. 97, 967-970 (1955).

(23) C.H. Townes and A. Schawlow, "Microwave Spectroscopy", Dover, New York (1975).

(24) E.U. Condon and G.H. Shortley, "Theory of Atomic Spectra", Cambridge University Press, Cambridge (1970).

(25) A. Messiah, "Quantum Mechanics", Vol. I and II, Wiley, Amsterdam (1958).

(26) N.F. Ramsey, "Nuclear Moments", John Wiley & Son Inc., New York (1955).

(27) H.H. Nielsen, Rev. Mod. Phys. 23, 90-136 (1951).

(28) C.E. Soliverez, J. Phys. C, 2, 2161-2174 (1969).

(29) C. Bloch, Nuclear Physics, 6, 329-347 (1958).

(30) T.A. Miller, Mol. Phys. 16, 105-120 (1969).

(31) K.F. Freed, J. Chem. Phys. 45, 4214-4241 (1966).

(32) B.L. Silver, "Irreducible Tensor Methods", Academic Press, London (1976).

(33) M.E. Rose, "Elementary Theory of Angular Momentum:, John Wiley and Sons Inc., (1967).

(34) G. Racah, Phys. Rev., 62, 431-462 (1942).

(35) U. Fano and G. Racah, "Irreducible Tensorial Sets", Academic Press, New York (1959).

(36) G. Herzberg, "Spectra of Diatomic Molecules", D. van Nostrand Company Inc., New York (1950).

(37) J.K.G. Watson, J. Chem. Phys., 46, 1935-1949 (1967).

(38) K.E. Hallin and A.J. Merer, J. Mol. Spectrosc. 65, 163-166 (1977).

(39) I.C. Bowater, J.M. Brown and A. Carrington, Proc. R. Soc. Lond. A333, 265-288 (1973).

(40) W.T. Raynes, J. Chem. Phys. 41, 3020-3032 (1964).

(41) R.F. Curl and J.L. Kinsey, J. Chem. Phys. 35, 1758-1765 (1961).

(42) J.M. Brown and A.J. Merer, J. Mol. Spectrosc. 74, 488-494 (1979).

(43) J.T. Hougen, J. Chem. Phys. 36, 519-534 (1962).

(44) J.K.G. Watson, Molec. Phys. 19, 465-487 (1970).

(45) J.M. Brown, I. Kopp, C. Malmberg and B. Rydh, Physica Scripta, 17, 55-67 (1978).

Chapter 3

1. R.A. Frosch and H.M. Foley, Phys. Rev. 88, 1337-1349 (1952).
   G.C. Dousmanis, Phys. Rev. 97, 967-970 (1955).

2. E. Fermi, Z. Physik 60, 320 (1930).

3. C.H. Townes and A.L. Schawlow, "Microwave Spectroscopy", McGraw-Hill, New York (1955).

4. T.M. Dunn, in "Molecular Spectroscopy-Modern Research", eds. K.N. Rao and C.W. Mathews, pp. 231-257, Academic Press, New York (1972).

5. A.S-C.Cheung, R.C. Hansen and A.J. Merer, J. Mol. Spectrosc. 91, in press (1982).

6. J.T.Hougen, Canad. J. Phys. 40, 598-606 (1962).

7. J.M.Brown and D.J. Milton, Mol. Phys. 31, 409-422 (1976).

8. J.M. Brown, E.A. Colbourn, J.K.G. Watson and F.D. Wayne, J. Mol. Spectrosc. 74, 294-318 (1979).

9. T.A. Miller, Mol. Phys. $\underline{16}$, 105-120 (1969).

10. G. Herzberg, "Spectra of Diatomic Molecules", 2nd ed., Van Nostrand Inc., Princeton, N.J. (1950).

11. A.R. Edmonds, "Angular Momentum in Quantum Mechanics", Princeton University Press, Princeton (1974).

12. R.W. Martin and A.J. Merer, Canad. J. Phys. $\underline{51}$, 125-143 (1973).

13. I. Kopp and J.T. Hougen, Canad. J. Phys. $\underline{45}$, 3581-2596 (1967). L. Klynning, B. Lindgren and N. Åslund, Ark. Fys. 30, 141 (1965).

14. J.M. Brown and B.J. Howard, Mol. Phys. $\underline{31}$, 1517-1525 (1976).

15. D.M. Brink and G.R. Satchler, "Angular Momentum", 2nd ed., Clarendon Press, Oxford (1968).

16. Landolt-Börnstein, Zahlenwerte und Funktioner Group I, Vol. III (H. Appel) "Numerical tables of the Wigner 3-j, 6-j and 9-j coefficients", Springer-Verlag, Berlin (1968).

17. I.C. Bowater, J.M. Brown and A. Carrington, Proc. Roy. Soc. (London) $\underline{A333}$, 265-288 (1973).

18. J.M. Brown and A.J. Merer, J. Mol. Spectrosc. $\underline{74}$, 488-494 (1979).

19. A. Carrington, P.N. Dyer and D.H. Levy, J. Chem. Phys. $\underline{47}$, 1756-1763 (1967).

20. E.U. Condon and G.H. Shortley, "The Theory of Atomic Spectra", Cambridge University Press, Cambridge (1970).

Chapter 4

1. H. Walther, ed., "Laser Spectroscopy of Atoms and Molecules", Topics in Applied Physics, Vol. 2, Springer-Verlag, Heidelberg (1976).

2. K. Shimoda, ed., "High Resolution Laser Spectroscopy", Topics in Applied Physics, Springer-Verlag, Heidelberg (1976).

3. V.S. Lotokhov and V.P. Chebotaev, "Principle of Non-linear Laser Spectroscopy", Springer-Verlag, Heidelberg (1977).

4. S. Haroche, J.C. Pebay, Payroula, T.W. Hänsch and S.E. Harris, eds. "Laser Spectroscopy". Lecture Notes in Physics, Vol. 43, Springer-Verlag, Heidelberg (1975).

5. J.I. Steinfeld and P.L. Houston in "Coherence and Laser Spectroscopy", J.I. Steinfeld, ed., Plenum Press, New York (1979).

6. A. Szoke and A. Javan, Phys. Rev. Letters, $\underline{10}$, 521-524 (1963).

7. W.E. Lamb Jr., Phys. Rev. $\underline{A134}$, 1429-1450 (1964).

8. C. Freed and A. Javan, Appl. Phys. Letters, $\underline{17}$, 53-56 (1970).

9. M.S. Sorem and A.L. Schawlow, Opt. Comm. $\underline{5}$, 148-151 (1972).

10. K. Shimoda and T. Shimizu, "Progress in Quantum Electronics", Vol. 2, J.H. Sanders and S. Stenholm, eds., Pergamon, Oxford (1972).

11. R.H. Pantell and H.E. Puthoff, "Fundamentals of Quantum Electronics", Wiley, New York (1969).

12. W.R. Bennett, Jr., Phys. Rev. $\underline{126}$, 580-593 (1962).

13. T.W. Hänsch, M.D. Levenson and A.L. Schawlow, Phys. Rev. Letters, $\underline{26}$, 946-949 (1971).

14. M.S. Sorem, T.W. Hänsch and A.L. Schawlow, Chem. Phys. Letters, $\underline{17}$, 300-302 (1972).

15. A. Muirhead, K.V.L.N. Sastry, R.F. Curl, J. Cook and F.T. Tittel, Chem. Phys. Letters, $\underline{24}$, 208-211 (1974).

16. R.S. Lowe, H. Gerhardt, W. Dillenschneider, R.F. Curl and F.K. Tittel, J. Chem. Phys. $\underline{70}$, 42-49 (1979).

17. G. Herzberg, "Molecular Spectra and Molecular Structure", Vol. 1, "Spectra of Diatomic Molecules", Van Nostrand Reinhold, New York (1950).

18. R.A. Gottscho, P.S. Weiss and R.W. Field, J. Mol. Spectrosc. $\underline{82}$, 283-309 (1980).

Chapter 5

1. H. Spinrad and R.F. Wing, Ann. Rev. Astron. and Astrophys. $\underline{7}$, 249-302, (1969).

2. G.P. Kuiper, W. Wilson and R.J. Cashman, Ap. J. $\underline{106}$, 243-256 (1947).

3. A. Lagerqvist and L -E. Selin, Ark. Fys. $\underline{11}$, 429-430 (1957).

4. A.S-C. Cheung, A.W. Taylor and A.J. Merer, J. Mol. Spectrosc., submitted for publication.

5. P.C. Keenan and L.W. Schroeder, Ap. J. 115, 82-88 (1952).

6. D. Richards and R.F. Barrow, Nature 217, 842 (1968).

7. P.C. Mahanti, Proc. Phys. Soc. 47, 433-445 (1935).

8. A. Lagerqvist and L-E. Selin, Ark. Fys. 12, 553-568 (1957).

9. D. Richards and R.F. Barrow, Nature 219, 1244-1245 (1968).

10. P.H. Kasai, J. Chem. Phys. 49, 4979-4984 (1968).

11. R.A. Frosch and H.M. Foley, Phys. Rev. 88, 1337-1349 (1952).

12. W.H. Hocking, A.J. Merer and D.J. Milton, Canad. J. Phys. 59, 266-270 (1981).

13. M.S. Sorem and A.L. Schawlow, Optics Comm. 5, 148-151 (1972).

14. M. Dulick, P.F. Bernath and R.W. Field, Canad. J. Phys. 58, 703-712 (1980).

15. J.M. Brown, H. Martin and F.D. Wayne, Chem. Phys. Lett. 55, 67-70 (1978).

16. S. Gerstenkorn and P. Luc, "Atlas du spectre d'absorption de la molécule d'Iode", Editions du CNRS, Paris, France 1978; S. Gerstenkorn and P. Luc, Rev. Phys. Appl. 14, 791-794 (1979).

17. J.H. Van Vleck, Rev. Mod. Phys. 23, 213-227 (1951).

18. C.H. Townes and A.L. Schawlow, "Microwave Spectroscopy", McGraw-Hill, New York (1955).

19. I.C. Bowater, J.M. Brown and A. Carrington, Proc. Roy. Soc. London A 333, 265-288 (1973).

20. W. Gordy and R.L. Cook, "Microwave Molecular Spectra", Wiley-Interscience, New York (1970).

21. A.R. Edmonds, "Angular Momentum in Quantum Mechanics", Princeton Univ. Press, Princeton, N.J. (1960).

22. Landolt-Börnstein, Zahlenwerte und Funktionen Group I, Vol. III, "Numerical tables of the Wigner 3-j, 6-j and 9-j coefficients", Springer-Verlag, Berlin (1968).

23. M. Mizushima, "The Theory of Rotating Diatomic Molecules", John Wiley and Sons, New York (1975).

24. R.M. Gordon and A.J. Merer, Canad. J. Phys. 58, 642-656 (1980).

25. J.M. Brown and D.J. Milton, Mol. Phys. 31, 409-422 (1976).

26. A.S-C. Cheung and A.J. Merer, Mol. Phys., submitted for publication.

27. A. Budó, Z. Phys. 105, 73-80 (1937).

28. A. Budó and I. Kovács, Hung. Acta. Phys. 1, 7-14 (1948).

29. T. Nevin, Phil. Trans. Roy. Soc. (London) 237, 471-507 (1938).

30. B. Kleman and E. Werhagen, Ark. Fys. 6, 399-405 (1953).

31. R.D. Verma, Canad. J. Phys. 40, 586-597 (1962).

32. J.T. Hougen, Canad. J. Phys. 40, 598-606 (1962).

33. R.W. Martin and A.J. Merer, Canad. J. Phys. 51, 634-643 (1973).

34. R.F. Barrow in "Données Spectroscopiques relatives aux Molécules Diatomiques", B. Rosen ed., Pergamon Press, Oxford, England (1970).

35. M.S. Sorem, T.W. Hänsch and A.L. Schawlow, Chem. Phys. Lett. 17, 300-302 (1972).

36. A. Carrington, P.N. Dyer and D.H. Levy, J. Chem. Phys. 47, 1756-1763 (1967).

37. I. Kóvacs, "Rotational Structure in the Spectra of Diatomic Molecules", Adam Hilger Ltd., London, 1969.

38. A.S-C. Cheung, R.C. Hansen, A.M. Lyyra and A.J. Merer, J. Mol Spectrosc. 86, 526-533 (1981).

39. B.R. McGarvey, J. Phys. Chem. 71, 51-67 (1967).

40. A.J. Freeman and R.E. Watson, "Magnetism", Vol. IIA, G.T. Rado and H. Suhl, ed., Academic Press Inc., New York, (1965).

41. G. Herzberg, "Spectra of Diatomic Molecules", 2nd ed., Van Nostrand Company Inc., Princeton, N.J. (1950).

Chapter 6

1. P.C. Engelking and W.C. Lineberger, J. Chem. Phys. <u>66</u>, 5054-5058 (1977).

2. T.C. De Vore and T.W. Gallaher, J. Chem. Phys. <u>70</u>, 4429-4431 (1979).

3. D.W. Green, G.T. Reedy, and J.G. Kay, J. Mol. Spectrosc. <u>78</u>, 257-266 (1979).

4. R.K. Dhumwad and N.A. Narasimham, Proc. Indian Acad. Sci. <u>64</u>, 283-290 (1966).

5. R.F. Barrow and M. Senior, Nature (London) <u>223</u>, 1359 (1969).

6. S.M. Harris and R.F. Barrow, J. Mol. Spectrosc. <u>84</u>, 334-341 (1980).

7. R.W.B. Pearse and A.G. Gaydon, "The Identification of Molecular Spectra", 3rd ed., Chapman & Hall, London, 1965.

8. J.B. West and H.P. Broida, J. Chem. Phys. <u>62</u>, 2566-2574 (1975).

9. P.S. Bagus and H.J.T. Preston, J. Chem. Phys. <u>59</u>, 2986-3002 (1973).

10. S.P. Walch and W.A. Goddard III, unpublished results quoted as Ref. 4 of (1).

11. H.H. Michels, Unpublished results quoted in Ref. 6.

12. W. Weltner, Jr., Ber. Bunsenges, Phys. Chem. <u>82</u>, 80-89 (1978).

13. M.S. Sorem and A.L. Schawlow, Optics Comm. 5, 148-151 (1972).

14. S. Gerstenkorn and P. Luc, "Atlas du spectre d'Absorption de la Molécule d'Iode". Editions du CNRS, Paris, France 1978; S. Gerstenkorn and P. Luc, Rev. Phys. Appl. <u>14</u>, 791-794 (1979) and H.M. Crosswhite, J. Res. Natl. Bur. Stand., Sect. A, <u>79</u>, 17 (1975).

15. T.M. Dunn, in "Physical Chemistry, An Advanced Treatise, Vol. V" (H. Eyring, Ed.), Chap. 5, Academic Press, New York.

16. R.M. van Zee, C.M. Brown, K.J. Zeringue, and W. Weltner, Jr., Accts. Chem. Res. <u>13</u>, 237-242 (1980).

17. W.H. Hocking, M.C.L. Gerry, and A.J. Merer, Canad. J. Phys. <u>57</u>, 54-68 (1979).

18. W.H. Hocking, A.J. Merer, D.J. Milton, W.E. Jones, and G. Krishnamurty, Canad. J. Phys. <u>58</u>, 516-533 (1980).

19. B. Pouilly, J. Schamps, D.J.W. Lumley, and R.F. Barrow, J. Phys. <u>B 11</u>, 2281-2287, 2289-2299 (1978).

Chapter 7

1. R.R. Karl and K.K. Innes, Chem. Phys. Lett. 36, 275-279 (1975).

2. R.M. Hochstrasser and D.S. King, J. Amer. Chem. Soc. 98, 5443-5450 (1976).

3. D.D-S. Liu, S. Datta, and R.N. Zare, J. Amer. Chem. Soc. 97, 2557-2558 (1975).

4. K-E. J. Hallin and A.J. Merer, Can. J. Phys. 54, 1157-1171 (1976).

5. H.M. Crosswhite, J. Res. Nat. Bur. Stand. Sect. A 79, 17-69 (1975).

6. J.H. van Vleck, Rev. Mod. Phys. 23, 213-227 (1951).

7. W.T. Raynes, J. Chem. Phys. 41, 3020-3032 (1964).

8. I.C. Bowater, J.M. Brown and A. Carrington, Proc. Roy. Soc. London A 333, 265-288 (1973).

9. K-E.J. Hallin, Y. Hamada, and A.J. Merer, Can. J. Phys. 21, 2118-2127 (1976).

10. C.C. Lin, Phys. Rev. 116, 903-910 (1959).

11. R.N. Dixon and G. Duxbury, Chem. Phys. Lett. 1, 330-332 (1967).

12. J.M. Brown and T.J. Sears, Mol. Phys. 34, 1595-1610 (1977).

13. J.M. Cook, G.W. Hills and R.F. Curl, J. Chem. Phys. 67, 1450-1461 (1977).

14. G.R. Bird, J.C. Baird, A.W. Jache, J.A. Hodegeson, R.F. Curl, A.C. Kunkle, J.W. Bransford, J. Rastrup-Andersen, and J. Rosenthal, J. Chem. Phys. 40, 3378-3390 (1964).

15. R.M. Lees, R.F. Curl, and J.G. Baker, J. Chem. Phys. 45, 2037-2040 (1966).

16. A. Cabana, M. Laurin, C. Pépin, and W.J. Lafferty, J. Mol. Spectrosc. 13-27 (1976).

17. M.D. Olman and C.D. Hause, J. Mol. Spectrosc. 26, 241-253 (1968).

18. R.E. Blank, M.D. Olman, and C.D. Hause, J. Mol. Spectrosc. 33, 109-118 (1970).

19. R.E. Blank and C.D. Hause, J. Mol. Spectrosc. 34, 478-486 (1970).

20. K. Yamada and M. Winnewisser, Z. Naturforsch. 31a, 131-138 (1976).

21. A. Cabana, M. Laurin, W.J. Lafferty, and R.L. Sams, Can. J. Phys. 53, 1902-1926 (1975).

22. W.J. Lafferty, private communication.

Chapter 8

1. H. Spinrad and R.F. Wing, Ann. Rev. Astron. and Astrophys. 7, 249-302 (1969).

2. G.P. Kuiper, W. Wilson and R.J. Cashman, Ap. J. 106, 243-250 (1947).

3. J.J. Nassau, G.B. van Alleda and P.C. Keenan, Ap. J. 109, 333-336 (1949).

4. A. Lagerqvist and L-E. Selin, Ark. Fys. 11, 429-430 (1957).

5. P.C. Keenan and L.W. Schroeder, Ap. J. 115, 82-88 (1952).

6. A. Budó and I. Kóvacs, Phys. Zeitschr. 45, 122-126 (1944).

7. I. Kóvacs, "Rotational Structure in the Spectra of Diatomic Molecules", Adam Hilger Ltd., London 1969.

8. L.Veseth, Phys. Scripta 12, 125-128 (1975).

9. J-L. Féménias, Can. J. Phys. 55, 1733-1774 (1977).

10. D.L. Albritton, A.L. Schmeltekopf, W.J. Harrop, R.N. Zare and K. Czarny, J. Mol. Spectroscopy 67, 157-184 (1977); P.C. Cosby, J-B. Ozenne, J.T. Moseley and D.L. Albritton, J. Mol. Spectroscopy 79, 203-235 (1980); A. Carrington, P.G. Roberts and P.J. Sarre, Mol. Phys. 35, 1523-1535 (1978).

11. J.M. Brown and A.J. Merer, J. Mol. Spectroscopy 74, 488-494 (1979).

12. P.L. Radloff and P.A. Freedman, Mol. Phys. 37, 1633-1638 (1979); P.A. Freedman and P.L. Radloff, J. Mol. Spectroscopy 88, 225-227 (1981).

13. A. Budó, Z. Phys. 105, 73-80 (1937).

14. J.T. Hougen, Canad. J. Phys. 40, 598-606 (1962).

15. R.W. Martin and A.J. Merer, Canad. J. Phys. 51, 634-643 (1973).

16. J.M. Brown and D.J. Milton, Mol. Phys. 31, 409-422 (1976).

17. A.S-C. Cheung, R.C. Hansen and A.J. Merer, J. Mol. Spectroscopy, accepted for publication August 1981.

18. J.H. van Vleck, Phys. Rev. 23, 213-227 (1951).

19. J.M. Brown, E.A. Colbourn, J.K.G. Watson and F.D. Wayne, J. Mol. Spectroscopy 74, 294-318 (1979).

20. D. Richards and R.F. Barrow, Nature 219, 1244-1245 (1968).

21. L. Veseth, J. Mol. Spectroscopy 38, 228-242 (1971).

22. W.H. Hocking, A.J. Merer, D.J. Milton, W.E. Jones and G. Krishnamurty, Canad. J. Phys. 58, 516-533 (1980).

23. J.M. Brown, private communication; J.M. Brown, D.J. Milton, J.K.G. Watson, R.N. Zare, D.L. Albritton, M. Horani and J. Rostas, J. Mol. Spectroscopy, submitted for publication.

24. R.A. Frosch and H.M. Foley, Phys. Rev. 88, 1337-1349 (1952); G.C. Donsmanis, Phys. Rev. 97, 967-970 (1955).

25. A. Carrington, P.N. Dyer and D.H. Levy, J. Chem. Phys. 47, 1756-1763 (1967); J.M. Brown, I. Kopp, C. Malmberg and B. Rydh, Physica Scripta 17, 55-67 (1978); C.H. Townes and A.L. Schawlow "Microwave Spectroscopy" McGraw-Hill, New York (1955).

26. I.C. Bowater, J.M. Brown and A. Carrington, Proc. Roy. Soc. (London) A 333, 265-288 (1973).

Appendices

(A1) J.H. van Vleck, Rev. Mod. Phys., 23, 213-227 (1951).

(A2) J.A.R. Coope, J. Math. Phys. 11, 1591-1612 (1970).

(A3) A. Carrington, D.H. Levy and T.A. Miller, Advan. Chem. Phys. 18, 149-248 (1970).

(A4) J. Jerphaguon, D. Chemla and R. Bonneville, Advan. in Phys., 27, 609-650 (1971).

(A5) A.R. Edmonds, "Angular Momentum in Quantum Mechanics", Princeton University Press, Princeton (1974).

(A6) B.L. Silver, "Irreducible Tensor Methods", Academic Press, London (1976).

(A7) M.D. Brink and G.R. Satchler, "Angular Momentum", Clarendon Press, Oxford (1968).

(A8) T.M. Dunn, in "Physical Chemistry, An Advanced Treatise, Vol. V", (H. Eyring, Ed.), Chapter 5, Academic Press, New York (1972).

(A9) C.J. Cheetham and R.F. Barrow, Adv. High Temp. Chem., $\underline{1}$, 7 -41(1967).

(A10) R.M. Van Zee, C.M. Brown, K.J. Zeringne, and W. Weltner, Jr., Accts. Chem. Res. $\underline{13}$, 237 -242(1980).

Appendix I

Transformation between Cartesian Tensors

and Spherical Tensors

. This appendix gives the tranformation between cartesian and spherical tensor components for operators of up to second rank, and outlines some problems that arise when angular momenta referred to different axis systems commute in different ways.

In practice, it is not always necessary to formulate every. interaction in spherical form; for example, the electron spin-rotation interaction can be written conveniently in cartesian form (A1). However for uniformity all terms in the Hamiltonian will be written in spherical tensor form in this thesis.

Tensors of rank 0 are scalars, and are the same in cartesian and spherical form. First rank tensors (i.e. vectors) can be expressed either in a cartesian basis $|i>$ with $i=\{X,Y,Z\}$ or in a spherical basis $|1,\mu>$ with $\mu = \{-1,0,1\}$. The unitary transformation $<i|\ell,\mu>$ between the two bases is

	$\|1,1>$	$\|1,0>$	$\|1,-1>$
$\|X>$	$-(2)^{-\frac{1}{2}}$	0	$(2)^{-\frac{1}{2}}$
$\|Y>$	$-i(2)^{-\frac{1}{2}}$	0	$-i(2)^{-\frac{1}{2}}$
$\|Z>$	0	1	0

$$(A.I.1)$$

i.e. for the components of a vector T.

$$T_1^1 = -(2)^{-\frac{1}{2}}(T_X + i\, T_Y)$$

$$T_0^1 = T_Z$$

$$T_{-1}^1 = (2)^{-\frac{1}{2}}(T_X - i\, T_Y)$$

$$(A.I.2)$$

It is implicit in (A.I.1) that cartesian components satisfy the commutation relations with the "normal" sign of i,

$$[T_X, T_Y] = T_X T_Y - T_Y T_X = +iT_Z \qquad (A.I.3)$$

The transformation of second-rank tensors from cartesian to spherical form can be performed in a two step process. Starting from a second-rank cartesian tensor (whose elements are $T_{i_1 i_2}$) one first changes the cartesian coordinates into spherical coordinates through a product of unitary transformations $<i|\ell,\mu>$. This results in a reducible spherical tensor, which is reduced by the well-known properties of the Clebsch-Gordan coefficients to give the irreducible spherical tensors T_m^J (A 2, A 4).

$$T_m^J = <J m | 1 \ 1 \ \mu_1 \ \mu_2> <1, \mu_1 | i_1> <1, \mu_2 | i_2> T_{i_1 i_2} \qquad (A.I.4)$$

where $<J m | 1 \ 1 \ \mu_1 \ \mu_2>$ is the usual Clebsch-Gordan coefficient, which is related to the Wigner 3-j symbols by

$$<J m | 1 \ 1 \ \mu_1 \ \mu_2> = (-1)^m (2J+1)^{\frac{1}{2}} \begin{pmatrix} 1 & 1 & J \\ \mu_1 & \mu_2 & -m \end{pmatrix} \qquad (A.I.5)$$

Substituting numerical values for the 3-j symbols, and using (A.I.1), a second rank cartesian tensor can be decomposed into a sum of spherical tensors of ranks 0, 1 and 2,

$$T^1 \times T^1 = T^0 + T^1 + T^2 \qquad (A.I.6)$$

The explicit expressions are

$$T_0^0 = - (3)^{-\frac{1}{2}} \{T_{XX} + T_{YY} + T_{ZZ}\}$$

$$T_0^1 = i (2)^{-\frac{1}{2}} \{T_{XY} - T_{YX}\}$$

$$T_{\pm 1}^1 = \frac{1}{2} \{(T_{ZX} - T_{XZ}) \pm i (T_{ZY} - T_{YZ})\}$$

$$T_0^2 = (6)^{-\frac{1}{2}} \{2T_{ZZ} - T_{XX} - T_{YY}\}$$

$$T_{\pm 1}^2 = \mp (\frac{1}{2}) \{(T_{XZ} + T_{ZX}) \pm i (T_{YZ} + T_{ZY})\}$$

$$T_{\pm 2}^2 = \frac{1}{2} \{(T_{XX} - T_{YY}) \pm i (T_{XY} + T_{YZ})\}$$

(A.I.7)

In molecular spectroscopy we must distinguish between space-fixed and molecule-fixed operators. Tensor components defined in terms of axes mounted on the molecule, which are denoted by x, y and z, have the sign of i in the commutation relations reversed (A 1), i.e.

$$[T_x, T_y] = -i T_z$$

(A.I.8)

Components of molecule-fixed tensor operators will transform differently from cartesian to spherical form. For components of a molecule-fixed vector T (A 3):

$$T_1^1 = - (2)^{-\frac{1}{2}}(T_x - i T_y)$$

$$T_0^1 = T_z$$

$$T_{-1}^1 = (2)^{-\frac{1}{2}}(T_x + i T_y)$$

(A.I.9)

For second rank tensors, only T_0^1 and $T_{\pm 1}^1$ are different from (A.I.7)

$$T_0^1 = - (2)^{-\frac{1}{2}} \{T_{xy} - T_{yx}\}$$

$$T_{\pm 1}^1 = - \frac{1}{2} \{(T_{zx} - T_{xz}) \pm i (T_{zy} - T_{yz})\}$$

(A.I.10)

Appendix II

The Derivation of the Nuclear spin -

Electron spin Dipolar Interaction

Matrix Elements in case $(b_{\beta J})$ coupling

This Appendix gives a derivation of the matrix elements of

$$H_{ns-es} = - \frac{(10)^{\frac{1}{2}}}{R^3} g \, \mu_B \, g_N \, \mu_N \, T^1(I) \cdot T^1(S,c^2) \qquad (A.II.1)$$

in the case $(b_{\beta J})$ basis (i.e. $|\, \eta \quad N \, K \, S \, J \, I \, F >$) given as eq. (2.144) in Chapter 2.

Matrix elements can only be evaluated when the operator and the relevant parts of the wavefunctions are in the same reference frame, i.e. either both in the molecule-fixed axis system (q) or in the space fixed axis system (p). Our procedure will be to expand the Hamiltonian in the first instance as a space-fixed operator, so that irreducible tensor methods can be applied in their standard form, and then those parts that are physically appropriate are referred to the molecule-fixed axis system by means of the rotation matrix eq. (2.110).

The operator H_{ns-es} is a scalar product of two commuting tensor operators because $\underset{\sim}{I}$ and $\underset{\sim}{S}$ are in different spin spaces. Therefore, from Edmonds' eq. (7.1.6) (A5)

$$< \eta \, N' \, K' \, S' \, J' \, I' \, F' \, M_F' \,|\, H_{ns-es} \,|\, \eta \, N \, K \, S \, J \, I \, F \, M_F >$$

$$= - (10)^{\frac{1}{2}} g \, \mu_B \, g_N \, \mu_N \, \delta_{F'F} \, \delta_{M_F' M_F} (1)^{I+J+F} \begin{Bmatrix} F & J' & I' \\ 1 & I & J \end{Bmatrix}$$

$$< I' \,||\, T^1(I) \,||\, I > < \eta \, N' \, K' \, S' \, J' \,||\, \frac{T^1(S,c^2)}{R^3} \,||\, \eta \, N \, K \, S \, J >$$

$$\qquad\qquad (A.II.2)$$

where the reduced matrix elements are with respect to the space-fixed axis system. $< I' \,||\, T^1(I) \,||\, I >$ can now be evaluated directly, because,

in case $(b_{\beta J})$, the nuclear spin I is quantized in the space-fixed axis system, as is the operator $T^1(I)$.

Therefore by eq. (2.109)

$$< I' \parallel T^1(\underline{I}) \parallel I > = \delta_{I'I} [I(I+1)(2I+1)]^{\frac{1}{2}} \qquad (A.II.3)$$

The operator $T^1(\underline{S},C^2)$, in the second reduced matrix element, is a compound tensor operator constructed from simpler commuting operators; by using Edmonds' eq. (7.1.5) (A5),

$$< n\ N'\ K'\ S'\ J' \parallel \frac{T^1(\underline{S},C^2)}{R^3} \parallel n\ N\ K\ S\ J > = (3)^{\frac{1}{2}}[(2J+1)(2J'+1)]^{\frac{1}{2}}$$

$$< S' \parallel T^1(\underline{S}) \parallel S > < n\ N'\ K' \parallel \frac{C^2}{R^3} \parallel n\ N\ K > \begin{Bmatrix} N' & N & 2 \\ S' & S & 1 \\ J' & J & 1 \end{Bmatrix} \qquad (A.II.4)$$

Again for a case $(b_{\beta J})$ coupling scheme the electron spin S is quantized in the space-fixed axis system, so that, for the matrix elements

$$< S' \parallel T^1(\underline{S}) \parallel S > = \delta_{S'S} [S(S+1)(2S+1)]^{\frac{1}{2}} \qquad (A.II.5)$$

The second-rank spherical harmonic C^2 is defined in the molecule-fixed axis system, but so far its matrix elements have been reduced with respect to the space-fixed system. The transformation from space-fixed to molecule-fixed axes is carried out by means of the rotation matrix D,

$$C^2 = \sum_q D^{(2)*}_{\cdot q} (\omega)\ C^2_q \qquad (A.II.6)$$

where ω represents the three Euler angles $(\alpha\beta\gamma)$.

$D^{(2)*}_{.q}(\omega)$ is the rotation matrix with no reference to the space-fixed components, and its reduced matrix element is defined by eq. (A.II.17).

When this is substituted into the reduced matrix element we obtain

$$< n \; N' \; K' \; || \; \frac{C^2}{R^3} \; || \; n \; N \; K > \; = \; \sum_q < n \; | \; \frac{C_q^2}{R^3} \; | \; n >$$

$$< N' \; K' \; || \; D^{(2)*}_{.q}(\omega) \; || \; N \; K > \qquad (A.II.7)$$

where $< n \; | \; \frac{C_q^2}{R^3} \; | \; n >$ is an experimentally determinable parameter, which will be redefined as

$$T_q^2(C) \; = \; < n \; | \; \frac{C_q^2}{R^3} \; | \; n > \qquad\qquad (A.II.8)$$

Lastly, we must calculate $< N' \; K' \; || \; D^{(2)*}_{.q}(\omega) \; || \; N \; K >$

which is the reduced matrix element of $< N' \; K' \; M' \; | \; D^{(2)*}_{pq}(\omega) \; | \; N \; K \; M >$. We will first evaluate $< N' \; K' \; M' \; | \; D^{(2)*}_{pq}(\omega) \; | \; N \; K \; M >$ and then apply the Wigner-Eckart Theorem (A5) to get its reduced matrix element.

Since

$$| \; N \; K \; M > \; = \; \left[\frac{2N+1}{8\pi^2} \right]^{\frac{1}{2}} D^{(N)*}_{MK}(\omega) \qquad (A.II.9)$$

and its complex conjugate is

$$< N' \; K' \; M' \; | \; = \; \left[\frac{2N'+1}{8\pi^2} \right]^{\frac{1}{2}} D^{(N')}_{M'K'}(\omega) \qquad (A.II.10)$$

the relationship between $D*$ and D is (A7)

$$D_{pq}^{(k)*}(\omega) = (-1)^{p-q} D_{-p\ -q}^{(k)}(\omega) \qquad \text{(A.II.11)}$$

Therefore,

$$< N'\ K'\ M'\ |\ D_{pq}^{(k)*}\ |\ N\ K\ M > = \frac{[(2N'+1)(2N+1)]^{\frac{1}{2}}}{8\pi^2}$$

$$\cdot\ (-1)^{p-q}\ (-1)^{M-K} \int D_{M'K'}^{(N')}(\omega)\ D_{-p\ -q}^{(k)}(\omega)\ D_{-M-K}^{(N)}\ d\Omega$$

$$\text{(A.II.12)}$$

Using the relationship in Silver (A6) p. 43, we have

$$< N'\ K'\ M\ |\ D_{pq}^{(k)*}(\omega)\ |\ N\ K\ M > = (-1)^{p-q}\ (-1)^{M-K}\ [(2N'+1)(2N+1)]^{\frac{1}{2}}$$

$$\begin{pmatrix} N' & k & N \\ M' & -p & -M \end{pmatrix} \begin{pmatrix} N' & k & N \\ K' & -q & -K \end{pmatrix} \qquad \text{(A.II.13)}$$

The pair of 3-j symbols in (A.II.13) will be non-zero only if they satisfy the conditions

$$M' + (-p) + (-M) = 0$$

and

$$K' + (-q) + (-K) = 0\ ; \qquad \text{(A.II.14)}$$

Also with the use of symmetry properties of the 3-j symbol, we finally obtain

$$< N' K' M' | D_{pq}^{(k)*} (\omega) | N K M >$$

$$= (-1)^{M'-K'} [(2N'+1)(2N+1)]^{\frac{1}{2}} \begin{pmatrix} N' & k & N \\ -M' & p & M \end{pmatrix} \begin{pmatrix} N' & k & N \\ -K' & q & K \end{pmatrix} \quad \text{(A.II.15)}$$

Applying the Wigner-Eckart Theorem, we find

$$< N' K' M' | D_{pq}^{(k)*} (\omega) | N K M > = (-1)^{N'-M'} \begin{pmatrix} N' & k & N \\ -M' & p & M \end{pmatrix}$$

$$< N' K' || D_{.q}^{(k)*} (\omega) || N K > \quad \text{(A.II.16)}$$

Therefore,

$$< N' K' || D_{.q}^{(k)*} || N K > = (-1)^{N'-K'} [(2N'+1)(2N+1)]^{\frac{1}{2}}$$

$$\begin{pmatrix} N & k & N \\ -K' & q & K \end{pmatrix} \quad \text{(A.II.17)}$$

with the special case of k=2

$$< N' K' || D_{.q}^{(2)*} || N K > = (-1)^{N'-K'} [(2N'+1)(2N+1)]^{\frac{1}{2}} \begin{pmatrix} N' & 2 & N \\ -K' & q & K \end{pmatrix} \quad \text{(A.II.18)}$$

Combining eqs (A.II.2), (A.II.3), (A.II.4), (A.II.5), (A.II.7), (A.II.8) and (A.II.18) we finally get

$$\langle \eta \, N' \, K' \, S \, J' \, I \, F \, | \, H_{ns-es} \, | \, \eta \, N \, K \, S \, J \, I \, F \rangle$$

$$= -(30)^{\frac{1}{2}} g \, \mu_B \, g_N \, \mu_N \, (-1)^{J+I+F} \begin{Bmatrix} I & J' & F \\ J & I & 1 \end{Bmatrix}$$

$$[I(I+1)(2I+1)S(S+1)(2S+1)]^{\frac{1}{2}} \, [(2J'+1)(2J+1)(2N'+1)(2N+1)]^{\frac{1}{2}}$$

$$\begin{Bmatrix} N' & N & 2 \\ S & S & 1 \\ J' & J & 1 \end{Bmatrix} \sum_q (-1)^{N'-K'} \begin{pmatrix} N' & 2 & N \\ -K' & q & K \end{pmatrix} T_q^2(C)$$

$$(A.II.19)$$

which completes the derivation.

Appendix III

Derivation of the matrix elements of the

operator $\sum_{i>j} T^1(\underset{\sim}{I}) \cdot T^1[T^3\{T^1(\underset{\sim}{S}) \cdot T^2(\underset{\sim}{s}_i, \underset{\sim}{s}_j)\}, C^2]/r_{ij}^3$

in a Hund's case $(b_{\beta J})$ basis

We begin by applying eqs. (7.1.5) and (7.1.6) of Edmonds (A5) to reduce the general form of the matrix elements of eq. (3.25) in Chapter 3,

$$\sum_{i>j} T^1(\underline{I}) \cdot T^1[T^3\{T^1(\underline{S}), T^2(\underline{s}_i,\underline{s}_j)\}, C^2]/r_{ij}^3 ,$$

set up in a Hund's case $(b_{\beta J})$ basis:

$$< n \; N \; \Lambda S \; J \; I \; F \; | \; \sum_{i>j} T^1(\underline{I}) \cdot T^1[T^3\{T^1(\underline{S}),T^2(\underline{s}_i,\underline{s}_j)\}, C^2]/r_{ij}^3 \; | \; n'N' \; \Lambda' \; S \; J'I \; F>$$

$$= (-1)^{I+J'+F} \begin{Bmatrix} F & J & I \\ 1 & I & J' \end{Bmatrix} < I \; || \; T^1(\underline{I}) \; || \; I > \times (3)^{\frac{1}{2}} \; [(2J+1)(2J'+1)]^{\frac{1}{2}} .$$

$$\begin{Bmatrix} N & N' & 2 \\ S & S & 3 \\ J & J' & 1 \end{Bmatrix} \sum_{i>j} < S \; || \; T^3\{T^1(\underline{S}) \cdot T^2(\underline{s}_i,\underline{s}_j)\} \; || \; S> < n \; N \; \Lambda \; || \; \frac{C^2}{r_{ij}^3} \; || \; n'N' \; \Lambda'>$$

$$\text{(A.III.1)}$$

The scaled spherical harmonic C^2 is defined in molecule-fixed axes, so we need to project it into molecule-fixed axes according to

$$C^2 = \sum_q D^{(2)*}_{.q} (\omega) \; C^2_q \qquad \text{(A.III.2)}$$

where ω stands for the Euler angles of the rotation. The reduced matrix element of C^2/r_{ij}^3 then becomes

$$\sum_{i>j} < n \; N \; \Lambda \; || \; C^2/r_{ij}^3 \; || \; n' \; N' \; \Lambda' > = \sum_q < N \; \Lambda \; || \; D^{(2)*}_{.q} (\omega) \; || \; N' \; \Lambda' >$$

$$\times \sum_{i>j} < n \; | \; C^2_q/r_{ij}^3 \; | \; n' >$$

$$= \sum_q (-1)^{N-\Lambda}[(2N+1)(2N'+1)]^{\frac{1}{2}} \begin{pmatrix} N & 2 & N' \\ -\Lambda & q & \Lambda' \end{pmatrix} \; T^2_q(C) \qquad \text{(A.III.3)}$$

In our case $\Lambda = \Lambda' = 0$, so that $q = 0$. There will be just one experimental parameter $T_0^2(C)$, which will be proportional to b_S.

Next we break up the reduced matrix element of the electron spin tensor product in eq. (A.III.1) using Edmonds' eq. (7.1.1):

$$\sum_{i>j} < S \mid\mid T^3\{T^1(S)\cdot T^2(\underset{\sim}{s}_i,\underset{\sim}{s}_j)\} \mid\mid S > = (7)^{\frac{1}{2}} (-1)^{2S+3} \begin{Bmatrix} 1 & 2 & 3 \\ S & S & S \end{Bmatrix}$$

$$[S(S+1)(2S+1)]^{\frac{1}{2}} \times \sum_{i>j} < S \mid\mid T^2(\underset{\sim}{s}_i,\underset{\sim}{s}_j) \mid\mid S > \qquad (A.III.4)$$

where we have eliminated the sum over states with total spin S' because

$$< S \mid\mid T^1(\underset{\sim}{S}) \mid\mid S' > = [S(S+1)(2S+1)]^{\frac{1}{2}} \delta_{SS'} \qquad (A.III.5)$$

The tensor product in eq. (A.III.4) appears in the matrix elements of the dipolar electron spin-spin interaction and the Λ-doubling parameter o; with Edmonds' eq. (7.1.1) again we find

$$< S \mid\mid T^2(\underset{\sim}{s}_i,\underset{\sim}{s}_j) \mid\mid S > = (5)^{\frac{1}{2}} \sum_{S'}(-1)^{2S+2} \begin{Bmatrix} 1 & 1 & 2 \\ S & S & S' \end{Bmatrix} < S \mid\mid T^1(\underset{\sim}{s}_i) \mid\mid S' >$$

$$< S' \mid\mid T^1(\underset{\sim}{s}_j) \mid\mid S > \qquad (A.III.6)$$

The triangle rules on the 6-j symbol limit S' to S or $S\pm1$, but $S' = S+1$ is physically impossible, so that the tensor product becomes

$$< S \; || \; T^2(\underset{\sim}{s}_i, \underset{\sim}{s}_j) \; || \; S > \; = \; (2) \quad (-1)^{2S} \left[\begin{Bmatrix} 1 & 1 & 2 \\ S & S & S\text{-}1 \end{Bmatrix} < S \; || \; T^2(\underset{\sim}{s}_i) \; || \; S\text{-}1 > \right.$$

$$< S\text{-}1 \; || \; T^1(\underset{\sim}{s}_j) \; || \; S > \; + \begin{Bmatrix} 1 & 1 & 2 \\ S & S & S \end{Bmatrix} < S \; || T^1(\underset{\sim}{s}_i) \; || \; S >$$

$$\left. < S \; || \; T^2(\underset{\sim}{s}_j) \; || \; S > \right] \qquad \qquad \text{(A.III.7)}$$

To evaluate the reduced matrix elements of $\underset{\sim}{s}_i$ and $\underset{\sim}{s}_j$ we define the coupling scheme

$$\underset{\approx}{S} = \sum_i \underset{\sim}{s}_i = \underset{\sim}{s}_1 + \underset{\sim}{s}_2 + \cdots \underset{\sim}{s}_i = \underset{\sim}{s}_1 + \underset{\sim}{S}_a \qquad \qquad \text{(A.III.8)}$$

Then, by Edmonds' eq. (7.1.7)

$$< S' \; || \; T^1(\underset{\sim}{s}_i) \; || \; S > \; = \; (-1)^{s_1 + S_a + S + 1} \left[(2S+1)(2S'+1) \right]^{\frac{1}{2}} \begin{Bmatrix} s_1 & S' & S_a \\ S & S & 1 \end{Bmatrix}$$

$$< s_1 \; || \; T^1(\underset{\sim}{s}_1) \; || \; s_1 > \qquad \qquad \text{(A.III.9)}$$

where $< s_1 \; || \; T^1(\underset{\sim}{s}_i) \; || \; s_1 > \; = \; [s_1(s_1+1)(2s_1+1)]^{\frac{1}{2}} = (3/2)^{\frac{1}{2}}$, following eq. (A.III.5), since $s_1 = \frac{1}{2}$. Using the definition $\underset{\sim}{S}_a = \underset{\sim}{S} - \underset{\sim}{s}_1$, and substituting for the Wigner coefficient, we obtain

$$< S \; || \; T^1(\underset{\sim}{s}_1) \; || \; S > \; = \; \frac{1}{2}[(S+1)(2S+1)/S]^{\frac{1}{2}} \qquad \qquad \text{(A.III.10)}$$

which is a general expression holding for all $\underset{\sim}{s}_i$ and

$$< S\text{-}1 \; || \; T^1(\underset{\sim}{s}_1) \; || \; S > \; = \; -\frac{1}{2} \, [(2S-1)(2S+1)/S]^{\frac{1}{2}}$$

$$= \; - < S \; || \; T^1(\underset{\sim}{s}_1) \; || \; S\text{-}1 > \qquad \qquad \text{(A.III.11)}$$

For the off-diagonal reduced matrix elements of the other spins we need to extend the coupling scheme:

$$\underline{S} = \underline{s}_1 + \underline{s}_2 + \underline{s}_b, \quad \text{or} \quad \underline{S}_a = \underline{s}_2 + \underline{s}_b \tag{A.III.12}$$

Then

$$< S\text{-}1 \; || \; T^1(\underline{s}_2) \; || \; S > \; = \; (-1)^{S_1+S_a+S+1} \; [(2S+1)(2S-1)]^{\frac{1}{2}} \begin{Bmatrix} S_a & S\text{-}1 & s_1 \\ S & S_a & 1 \end{Bmatrix}$$

$$< S_a \; || \; T^1(\underline{s}_2) \; || \; S_a > \tag{A.III.13}$$

Now $\underline{S}_a$ still represents a coupled basis as far as electron 2 is concerned, so that

$$< S_a \; || \; T^1(\underline{s}_2) \; || \; S_a > \; = \; (-1)^{S_a+S_b+s_2+1} \; (2S_a+1) \begin{Bmatrix} s_2 & S_a & S_b \\ S_a & s_2 & 1 \end{Bmatrix}$$

$$< s_2 \; || \; T^1(\underline{s}_2) \; || \; s_2 > \tag{A.III.14}$$

which gives the results

$$< S\text{-}1 \; || \; T^1(\underline{s}_2) \; || \; S > \; = \; \frac{1}{2}[(2S+1)/\{S(2S-1)\}]^{\frac{1}{2}}$$

$$= - < S \; || \; T^1(\underline{s}_2) \; || \; S\text{-}1 > \tag{A.III.15}$$

We can now return to eq. (A.III.7), and substituting the new expressions just obtained, we get

$$< S \; || \; T^2(\underline{s}_i,\underline{s}_j) \; || \; S > \; = \; [(S+1)(2S+1)(2S+3)/\{24\,S(2S-1)\}]^{\frac{1}{2}} \tag{A III.16}$$

We need the sum, $\sum\limits_{i>j} < S \parallel T^2(s_i,s_j) \parallel S >$, for eq. (A.III.4), which is

equivalent to multiplying eq. (A.III.16) by $S(2S-1)$ since each pair of

electrons is counted once only; this gives

$$\sum_{i>j} < S \parallel T^2(\underset{\sim}{s}_i,\underset{\sim}{s}_j) \parallel S > = [(2S-1)2S(2S+1)(2S+2)(2S+3)/24]^{\frac{1}{2}}$$

$$= \frac{1}{2} < S \parallel T^2(\underset{\sim}{S},\underset{\sim}{S}) \parallel S > \qquad (A.III.17)$$

Finally, substituting into eq. (A.III.4) we find

$$\sum_{i>j} < S \parallel T^3 \{T^1(\underset{\sim}{S}), T^2(\underset{\sim}{s}_i,\underset{\sim}{s}_j)\} \parallel S >$$

$$= [(2S-2)(2S-1)2S(2S+1)(2S+2)(2S+3)(2S+4)/640]^{\frac{1}{2}} \qquad (A.III.18)$$

so that

$$< n \ N \ \Lambda \ S \ J \ I \ F | \sum_{i>j} T^1(\underset{\sim}{I}) \cdot T^3\{T^1(\underset{\sim}{S}) \cdot T^2(\underset{\sim}{s}_i,\underset{\sim}{s}_j) , C^2]/r_{ij}^3 | n´ \ N´ \ \Lambda´ \ S´ \ J´ \ I \ F >$$

$$= \left(\frac{3}{640}\right)^{\frac{1}{2}} (-1)^{I+J´+F} \begin{Bmatrix} F & J & I \\ 1 & I & J´ \end{Bmatrix} [I(I+1)(2I+1)]^{\frac{1}{2}}$$

$$[(2J+1)(2J´+1)(2N+1)(2N´+1)]^{\frac{1}{2}} \times \sum_q (-1)^{N-\Lambda} \begin{pmatrix} N & 2 & N´ \\ -\Lambda & q & \Lambda´ \end{pmatrix} \begin{Bmatrix} N & N´ & 2 \\ S & S & 3 \\ J & J´ & 1 \end{Bmatrix}$$

$$[(2S-2)(2S-1)(2S)(2S+1)(2S+2)(2S+3)(2S+4)]^{\frac{1}{2}} \ T_q^2(C) \qquad (A.III.19)$$

Where q, Λ and $\Lambda´$ are zero this becomes equivalent to eq. (3.20) in chapter 3,

with

$$T_0^2(C) = \frac{10}{3} (14)^{\frac{1}{2}} b_S \qquad (A.III.20)$$

The useful results from the derivation are the general forms for the electron spin reduced matrix elements, (A.III.10), (A.III.11), (A.III.15) and (A.III.17).

Appendix IV

Wigner 9-j symbols needed for the $\underset{\sim}{I},\underset{\sim}{S}$ dipolar

interaction and the third-order isotropic

hyperfine interaction

$$\begin{Bmatrix} N & N & 2 \\ S & S & 1 \\ J & J & 1 \end{Bmatrix} = \frac{3X(NSJ)X(NJS) + 2X(SJN) \; N(N+1)}{[30(2N-1)2N(2N+1)(2N+2)(2N+3).S(S+1)(2S+1).J(J+1)(2J+1)]^{\frac{1}{2}}}$$

where $X(abc) = a(a+1) + b(b+1) - c(c+1)$

$$\begin{Bmatrix} N & N & 2 \\ S & S & 1 \\ J-1 & J & 1 \end{Bmatrix} = - \frac{[N(N+1) + 3S(S+1) - 3J^2][(N+J-S)(N+S-J+1)(J+S-N)(J+S+N+1)]^{\frac{1}{2}}}{[15(2N-1)2N(2N+1)(2N+2)(2N+3).S(S+1)(2S+1).(2J-1)2J(2J+1)]^{\frac{1}{2}}}$$

$$\begin{Bmatrix} N-2 & N & 2 \\ S & S & 1 \\ J+1 & J & 1 \end{Bmatrix} = - \frac{[(J+S+N+1)(N+S-J)(N+J-S)(J+S-N+1)(N+S-J-2)(N+S-J-1)(J+S-N+2)(J+S-N+3)]^{\frac{1}{2}}}{[10(2N-3)(2N-2)(2N-1)2N(2N+1).S(S+1)(2S+1).(2J+1)(2J+2)(2J+3)]^{\frac{1}{2}}}$$

$$\begin{Bmatrix} N-2 & N & 2 \\ S & S & 1 \\ J & J & 1 \end{Bmatrix} = - \frac{[(J+S+N+1)(N+S-J)(N+J-S)(J+S-N+1)(N+S+J)(N+J-S-1)(N+S-J-1)(J+S-N+2)]^{\frac{1}{2}}}{[20(2N-3)(2N-2)(2N-1)2N(2N+1).S(S+1)(2S+1).J(J+1)(2J+1)]^{\frac{1}{2}}}$$

$$\begin{Bmatrix} N-2 & N & 2 \\ S & S & 1 \\ J-1 & J & 1 \end{Bmatrix} = - \frac{[(J+S+N+1)(N+S-J)(N+J-S)(J+S-N+1)(N+S+J)(N+J-S-1)(N+S+J-1)(N+J-S-2)]^{\frac{1}{2}}}{[10(2N-3)(2N-2)(2N-1)2N(2N+1).S(S+1)(2S+1).(2J-1)2J(2J+1)]^{\frac{1}{2}}}$$

$$\begin{Bmatrix} N & N & 2 \\ S & S & 3 \\ J & J & 1 \end{Bmatrix} = \frac{12\{2X(JSN)X(SNJ)[5N(N+1)-2] + 2X(NJS)S(S+1)[2X(SNJ)-1] - 5X(NJS)X(SNJ)X(JSN) \\ -4X(SNJ)J(J+1) - 4X(JSN)N(N+1)S(S+1)\}}{[105(2N-1)2N(2N+1)(2N+2)(2N+3).2J(2J+1)(2J+2).(2S-2)(2S-1)2S(2S+1)(2S+2)(2S+3)(2S+4)]^{\frac{1}{2}}}$$

where $X(abc) = a(a+1) + b(b+1) - c(c+1)$

$$\begin{Bmatrix} N & N & 2 \\ S & S & 3 \\ J-1 & J & 1 \end{Bmatrix} = \frac{2[6(N+S+J+1)(J+S-N)(N+J-S)(N+S-J+1)]^{\frac{1}{2}}}{[35(2N-1)2N(2N+1)(2N+2)(2N+3).(2J-1)2J(2J+1).(2S-2)(2S-1)2S(2S+1)(2S+2)(2S+3)(2S+4)]^{\frac{1}{2}}} \times$$

$$\times \{[5N(N+1) + S(S+1) - 5(J-1)(J+1) - 13/2][N(N+1) + S(S+1)$$

$$- (J-1)(J+1) - 3/2] - 4N(N+1)S(S+1) + 3(J-1/2)(J+1/2)\}$$

$$\begin{Bmatrix} N-2 & N & 2 \\ S & S & 3 \\ J-1 & J & 1 \end{Bmatrix} = -\frac{2[(N+S+J)(N+S+J+1)(N+S+J-1)(N+J-S-2)(N+J-S-1)(N+J-S)(N+S-J)(J+S-N+1)]^{\frac{1}{2}}}{[35(2N-3)(2N-2)(2N-1)2N(2N+1).(2J-1)2J(2J+1).(2S-2)(2S-1)2S(2S+1)(2S+2)(2S+3)(2S+4)]^{\frac{1}{2}}} \times$$

$$\times [5J(J+1) + 5N(N+1) - S(S+1) - 10N(J+1) + 2]$$

$$\begin{Bmatrix} N-2 & N & 2 \\ S & S & 3 \\ J & J & 1 \end{Bmatrix} = \frac{4[(N+S+J)(N+S+J+1)(N+S-J)(N+S-J-1)(N+J-S-1)(N+J-S)(J+S-N+1)(J+S-N+2)]^{\frac{1}{2}}}{[70(2N-3)(2N-2)(2N-1)2N(2N+1).2J(2J+1)(2J+2).(2S-2)(2S-1)2S(2S+1)(2S+2)(2S+3)(2S+4)]^{\frac{1}{2}}} \times$$

$$\times [5J(J+1) - 5N(N+1) + S(S+1) + 2(5N-1)]$$

$$\begin{Bmatrix} N-2 & N & 2 \\ S & S & 3 \\ J+1 & J & 1 \end{Bmatrix} = -\frac{2[(J+S-N+3)(J+S-N+2)(J+S-N+1)(N+S-J)(N+J-S)(N+J+S+1)(N+S-J-2)(N+S-J-1)]^{\frac{1}{2}}}{[35(2N-3)(2N-2)(2N-1)2N(2N+1).(2J+1)(2J+2)(2J+3).(2S-2)(2S-1)2S(2S+1)(2S+2)(2S+3)(2S+4)]^{\frac{1}{2}}} \times$$

$$\times [5J(J+1) + 5N(N+1) - S(S+1) + 10NJ + 2]$$

Appendix V

Molecular Orbital Description of

the First-row Transition Metal Monoxides

This appendix gives a molecular orbital description of the first-row transition metal oxides. In this approach the molecules are formally represented as $M^{2+} O^{2-}$ and the splitting of the degenerate d orbitals of the M^{2+} ion by the ligand field of the O^{2-} ion is considered (A8). The relative stabilities of high-spin or low spin states will depend on the size of this ligand field splitting (A9).

A typical molecular-orbital energy level diagram for a first-row transition metal monoxide is presented in Fig. A.V.1. The relative positions of the $3d\delta$ and $4s\sigma$ orbitals in these oxides vary as the atomic number increases, as a result of the screening effect created by the electrons. Therefore Fig. A.V.1 represents only one way of writing this molecular-orbital energy level sequence, as found in ScO and TiO, for example.

The ground state electronic configurations and term symbols that have been determined for the transition metal oxides (A8, A10) are

Sc O	$(4s\sigma)^1$	$^2\Sigma^+$
TiO	$(4s\sigma)^1 (3d\delta)^1$	$^3\Delta_r$
VO	$(43\sigma)^1 (3d\delta)^2$	$^4\Sigma^-$
CrO	$(4s\sigma)^1 (3d\delta)^2 (3d\pi)^1$	$^5\Pi_r$
MnO	$(4s\sigma)^1 (3d\delta)^2 (3d\pi)^2$	$^6\Sigma^+$
FeO	$(4s\sigma)^1 (3d\delta)^3 (3d\pi)^2$	$^5\Delta_i$
CuO	$(4s\sigma)^2 (3d\delta)^4 (3d\pi)^3$	$^2\Pi_i$
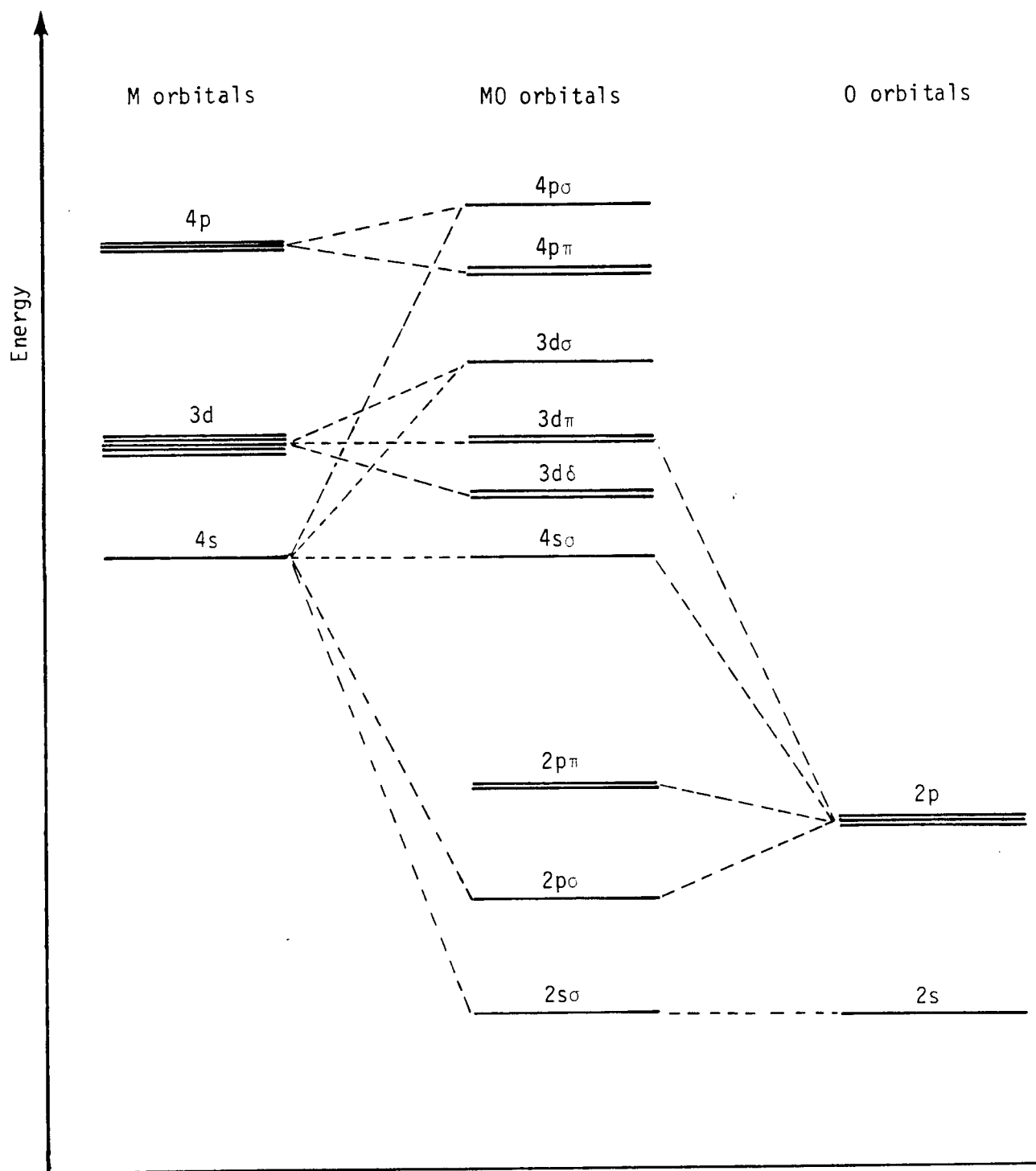
Fig A. V . 1   Relative orbital energies in a general transition-metal

monoxide molecule, MO.

Appendix VI

Tables of assigned lines

This Appendix contains the rotational line assignments on which the results of this thesis are based. The abbreviations used have meanings as follows:

* indicates a blended line

} indicates multiple line assignments for a given rotational transition

( ) indicates the line assignment is uncertain

- indicates a line is expected but has not been observed

p indicates the line is perturbed.

TABLE I   ROTATIONAL LINES ASSIGNED OF THE $C^4\Sigma^-$ - $X^4\Sigma^-$ (0,0) BAND OF VO

BRANCH	J"	F'-F"	F"=J"-7/2	F=J-5/2	F=J-3/2	F=J-1/2	F=J+1/2	F=J+3/2	F=J+5/2	F=J+7/2
N=-1 R1(-1)	0.5	1							-	17422.3960
		0							17422.6435*	-
RQ21(-1)FE	0.5	1							424.7946	
		0							424.7657*	424.6161
		-1								424.5847*
N= 0 R1(0)	1.5	0					-	17423.2760		
P1(0)	1.5	-1						-	17422.4357*	17422.2735
		0						422.5170	422.3751*	
		1					17422.5758	-		
R2(0)	0.5	1							-	422.9294
PQ12(0)EF	0.5	1							420.4331	
		0							420.4952*	420.5507
		-1								420.6116
N= 1 R1(1)	2.5	1			-	-	-	17423.8571	17423.7646*	17423.6589
P1(1)	2.5	-1						-	420.9413	420.8177*
		0					17421.0956	421.0096	420.9015*	
R2(1)	1.5	1						422.6854	422.6779	422.6718
P2(1)	1.5	1							420.3914	420.4420
		-1						420.3814*	420.4246*	
N= 2 R1(2)	3.5	1	17424.6441*	17424.6288*	17424.5994*	17424.5545*	17424.5020	17424.4336	17424.3508	17424.2540
		0						424.4514	-	-
P1(2)	3.5	-1		-	-	419.7263	419.6699	419.5987	419.5111	419.4076
		0			419.7569	419.7113	419.6500	419.5757*	419.4815*	
R2(2)	2.5	1						-	422.7955	422.7605
P2(2)	2.5	-1						-	417.9737	417.9324
R3(2)	1.5	1					-	420.8046	420.7608	420.7084
		0						-	420.7637*	-
RQ43(2)FE	1.5	0						-	-	419.2124
		-1						419.1927	419.2260	-
N= 3 R1(3)	4.5	1	17425.1708	17425.1478*	17425.1122	17425.0679	17425.0127	17424.9461	17424.8682	17424.7795
P1(3)	4.5	-1	-	-	-	418.2437	418.1876	418.1191	418.0386	417.9451
		0	-	-	418.2762	418.2288	-	-	423.0844*	423.0314
R2(3)	3.5	1	-				-	416.2622*	416.2255	416.1796
P2(3)	3.5	-1		-	-	-	416.2441		-	
		0			-	416.2974	-			
R3(3)	2.5	1			421.6615	421.6483*	-	-	421.6055*	421.5935*
		0			-	421.6521		-		
P3(3)	2.5	-1					-	414.6489*	-	414.5950*
R4(3)	1.5	1					-	423.0193	423.0218*	423.0218*
PQ34(3)EF	1.5	0							- .	417.4442

TABLE I (CONTINUED)

BRANCH	J"	F'-F"	F"=J"-7/2	F=J-5/2	F=J-3/2	F=J-1/2	F=J+1/2	F=J+3/2	F=J+5/2	F=J+7/2
N= 4 R1(4)	5.5	1	17425.6131*	17425.5847	17425.5474	17425.5001	17425.4452	17425.3802	17425.3057	17425.2215
P1(4)	5.5	-1	416.7986*	416.7734*	416.7366	416.6905	416.6346	416.5686	416.4920	416.4053
		0	-	416.7628*	416.7245	416.6765*	416.6176	416.5487*	-	
R2(4)	4.5	1	-	-	-	423.4934*	423.4796	423.3872	423.3652	423.3504*
RQ32(4)	4.5	1	-	-	-	-	-	423.4573	423.4261	
P2(4)	4.5	-1	-	414.6593*	414.6489*	414.6349*	414.6167*	414.5889*	414.5551*	414.5059
R3(4)	3.5	1	-	-	-	-	-	-	-	422.3534
P3(4)	3.5	-1		-	413.4042	413.3946*	413.3898	413.3807*	413.3743*	413.3713
		0		-	413.3995	413.3920	413.3827	-	-	
PQ23(4)	3.5	-1	-	-	-	-		413.5095	413.4989	413.4850
		0	-	-	-	-	-	-		413.4614
R4(4)	2.5	1	-	-	-	-	-	-	424.3073	424.3527
P4(4)	2.5	-1		-	-	-	-		415.2546*	415.3016
N= 5 R1(5)	6.5	1	17425.9648	17425.9313*	17425.8922	17425.8442	17425.7887	17425.7255	17425.6529*	17425.5738
P1(5)	6.5	-1	415.1702	415.1395	415.1004	415.0531	414.9970	414.9323	414.8594	414.7781
R2(5)	5.5	1	-	-	-	-	-	423.6966	423.6723	423.6463
RQ32(5)	5.5	1	-	-	-	-	-	-	423.7488*	
P2(5)	5.5	-1	412.9848*	412.9776	412.9689	412.9577	412.9394	412.9137	412.8776	412.8190
		0					412.9528	412.9325*	412.9002*	412.8102
PO32(5)	5.5	-1	-	-	-	-	-	-	-	422.9153
R3(5)	4.5	1	-	-	-	-	-	422.8330*	422.8330*	422.8383
RS23(5)	4.5	1		411.9873	411.9820	411.9769*	411.9707*	411.9677*	411.9689*	411.9769*
P3(5)	4.5	-1							412.0513	412.0453
PQ23(5)	4.5	-1								
R4(5)	3.5	1	425.0202	425.0323	425.0539*	425.0794	425.1178	425.1623	425.2146	425.2754
P4(5)	3.5	-1					414.1441	414.1891	414.2424	414.3045
		0	-	-	-	414.1574	-	-		
N= 6 R1(6)	7.5	1	17426.2207	17426.1828*	17426.1427	17426.0954	17426.0393	17425.9771	17425.9069	17425.8300
P1(6)	7.5	-1	413.4495	413.4156	413.3743*	413.3260	413.2702	413.2072	413.1364*	413.0574
R2(6)	6.5	1	424.0326	-	424.0013	423.9826	423.9621	423.9400*	423.9126*	423.8819*
P2(6)	6.5	-1	411.2497*	411.2454*	411.2402*	411.2268	411.2135*	-	411.0930	411.0756
PO32(6)	6.5	-1	411.1994*	-	411.1754	411.1573	411.1377	-	411.1536	
R3(6)	5.5	1	-	-	423.2582	-	423.3383	423.3440	-	-
RS23(6)	5.5	1	410.4471	410.4398	410.4329	410.4254*	410.4204*	410.4204*	-	410.4958*
P3(6)	5.5	-1		410.4812	-	-	-	-	410.4240	410.4355
PQ23(6)	5.5	-1	425.6393*	425.6558*	425.6823*	425.7173	425.7599	425.8088*	425.8668	425.9313*
R4(6)	4.5	1	-	-	412.7606	412.7931	412.8337*	412.8845*	412.9427*	413.0090
P4(6)	4.5	-1	-	-	-	412.8040	-	412.9002*	412.9608	

TABLE I (CONTINUED)

	BRANCH	J"	F'-F"	F"=J"-7/2	F=J-5/2	F=J-3/2	F=J-1/2	F=J+1/2	F=J+3/2	F=J+5/2	F=J+7/2
N= 7	R1(7)	8.5	1	17426.3805	17426.3446*	17426.2991	17426.2491	17426.1936	17426.1318	17426.0634	17425.9890
	P1(7)	8.5	-1	411.6312	411.5950	411.5529*	411.5032	411.4475*	411.3850*	411.3160	411.2402
	R2(7)	7.5	1	424.1946	424.1800*	424.1639	424.1471*	424.1253	424.1018	424.0743	424.0396
	P2(7)	7.5	-1	409.4051*	409.3903*	409.3735	409.3552	409.3347	409.3117	409.2858	409.2571
	PO32(7)	7.5	-1	409.4418*	409.4418*	409.4384	409.4292	409.4152	-	409.3636	
	R3(7)	6.5	1	423.6267	423.6324	423.6377	423.6422	423.6480	423.6552*	423.6645	423.6774
	P3(7)	6.5	-1	408.7877	408.8013	408.8085	408.8136	408.8189	408.8249	408.8312	408.8386*
	PQ23(7)	6.5	-1		408.7660	408.7554*	408.7488*	408.7449*	408.7449*	408.7488*	408.7618
	R4(7)	5.5	1	426.0828	426.1077	426.1358	426.1740	426.2203	426.2722	426.3321	426.3986*
	P4(7)	5.5	-1	-	-	411.2497	411.2869	411.3325	411.3850*	411.4451*	411.5120
N= 8	R1(8)	9.5	1	17426.4376	17426.3985	17426.3540	17426.3038	17426.2489	17426.1872	17426.1198	17426.0471
	P1(8)	9.5	-1	409.7154	409.6764	409.6334	409.5827	409.5273	409.4651	409.3989*	409.3240
	R2(8)	8.5	1	424.2666	424.2540	424.2389	424.2192*	424.2010*	424.1756	424.1471	424.1102
	RQ32(8)	8.5	1	-	-	-	-	424.3428	424.3251	424.3005	
	P2(8)	8.5	-1	407.5051*	407.4902	407.4744	407.4560	407.4357	407.4121	407.3842	407.3495
	PO32(8)	8.5	-1	407.5605*	407.5605*	407.5549	407.5476	407.5349	407.5151	407.4869	
	R3(8)	7.5	1	-	-	-	-	423.8465	423.8556*	423.8660*	423.8819
	P3(8)	7.5	-1	407.0122	407.0188	407.0261*	407.0301*	407.0375	407.0453	407.0545	407.0677
	PQ23(8)	7.5	-1	-	-	-	-	406.9432*	406.9496*	406.9647	
	R4(8)	6.5	1	426.3808*	426.4079*	426.4428	426.4842	426.5311	426.5842	426.6445	426.7098*
	P4(8)	6.5	-1	409.5310*	409.5560	409.5886	409.6290*	409.6764*	409.7297	409.7896	409.8563

FROM HERE ON ALL THE LINES HAVE DELTA F EQUAL TO DELTA N

BRANCHES LABELLED RQ32, PO32, RS23 AND PQ23 ARE INDUCED
BY INTERNAL HYPERFINE PERTURBATIONS

TABLE I (CONTINUED)

BRANCH	J"	F"=J"-7/2	F=J-5/2	F=J-3/2	F=J-1/2	F=J+1/2	F=J+3/2	F=J+5/2	F=J+7/2
N= 9 R1(9)	10.5	17426.3957	17426.3542	17426.3091	17426.2584	17426.2031	17426.1427	17426.0762	17426.0052*
P1(9)	10.5	407.6953	407.6570*	407.6107	407.5606	407.5051	407.4432	407.3768	407.3041
R2(9)	9.5	424.2448	424.2333	424.2192*	424.2010	424.1813	424.1579	424.1272*	424.0869*
P2(9)	9.5	405.5092	405.4956	405.4809	405.4640	405.4436	405.4203	405.3907	405.3516
PO32(9)	9.5	405.5876*	405.5876*	405.5831	405.5763*	405.5639	405.5457	405.5180*	
R3(9)	8.5			423.9205	423.9249	423.9314*	423.9400*	423.9527	423.9714
P3(9)	8.5	405.1270	405.1317	405.1366	405.1420	405.1491	405.1573	405.1687	405.1855*
PQ23(9)	8.5					405.0368*	405.0368*	405.0424	405.0578*
R4(9)	7.5	426.5492	426.5802	426.6174	426.6603	426.7098*	426.7631*	426.8231	426.8886
P4(9)	7.5	407.7252	407.7555	407.7913	407.8334	407.8824	407.9368	407.9970	408.0636
N=10 R1(10)	11.5	17426.2491	17426.2083	17426.1627	17426.1113	17426.0554	17425.9963	17425.9313	17425.8609
P1(10)	11.5	405.5765*	405.5349	405.4894	405.4386	405.3828	405.3216	405.2566	405.1855
R2(10)	10.5	424.1253*	424.1150	424.1018*	424.0869*	424.0674*	424.0437	424.0135	423.9678
RQ32(10)	10.5							424.2132	
P2(10)	10.5	403.4155		403.3894	403.3747	403.3548*	403.3317	403.3015	403.2570
PO32(10)	10.5		403.5190	403.5167	403.5092	403.4994	403.4813	403.4537	
R3(10)	9.5			423.8959	423.9002*	423.9067	423.9149*	423.9314*	423.9493
P3(10)	9.5	403.1321*	403.1343	403.1386	403.1432	403.1506	403.1583*	403.1707	403.1899
PQ23(10)	9.5					403.0118	403.0165*	403.0218	403.0373
R4(10)	8.5	426.5960	426.6301	426.6689	426.7130	426.7631*	426.8168	426.8776*	426.9419
P4(10)	8.5	405.8008	405.8341	405.8719	405.9161	405.9655	406.0200	406.0807	406.1457
N=11 R1(11)	12.5	17426.0025	17425.9602	17425.9136	17425.8609*	17425.8065	17425.7471	17425.6823	17425.6131
P1(11)	12.5	403.3551*	403.3125	403.2651*	403.2147	403.1583*	403.0993	403.0344	402.9647
R2(11)	11.5	423.9091	423.9002*	423.8878	423.8725	423.8556*	423.8322*	423.8015	423.7488
RQ32(11)	11.5						424.0509		
P2(11)	11.5	401.2233	401.2132*	401.2017	401.1872	401.1695	401.1467	401.1153	401.0628*
PO32(11)	11.5			401.3506	401.3455	401.3356	401.3192	401.2919	
R3(11)	10.5	423.7610*	423.7610*	423.7610*	423.7646*	423.7705	423.7782	423.7928	423.8146
P3(11)	10.5	401.0289*	401.0289*	401.0313*	401.0343	401.0398	401.0483*	401.0622*	401.0825*
PQ23(11)	10.5				400.8881*	400.8825*	400.8825*	400.8879*	400.9062
R4(11)	9.5	426.5266	426.5629	426.6031	426.6488	426.6989*	426.7540	426.8140	426.8776*
P4(11)	9.5	403.7575	403.7923	403.8321	403.8775	403.9279	403.9827	404.0429	404.1076

TABLE I (CONTINUED)

BRANCH	J"	F"=J"−7/2	F=J−5/2	F=J−3/2	F=J−1/2	F=J+1/2	F=J+3/2	F=J+5/2	F=J+7/2
N=12 R1(12)	13.5	17425.6529	17425.6089	17425.5618	17425.5103	17425.4546	17425.3953	17425.3312	17425.2630
P1(12)	13.5	401.0290	400.9863	400.9389	400.8880*	400.8324	400.7730	400.7085	400.6400
R2(12)	12.5	423.5900*	423.5834	423.5742	423.5618	423.5459	423.5251	423.4934	423.4297
RQ32(12)	12.5					423.7784*	423.7646*	423.7386	
P2(12)	12.5	398.9331*	398.9258	398.9163	398.9038	398.8876	398.8652*	398.8345	398.7714
PO32(12)	12.5			399.0869*	399.0839*	399.0767	399.0611	399.0341	
R3(12)	11.5	423.5195*	423.5195*	423.5195*	423.5195*	423.5251*	423.5327	423.5459*	423.5684
RS23(12)	11.5					423.3000*	423.3000*	423.3058	423.3229
P3(12)	11.5	398.8174*	398.8174*	398.8174*	398.8174*	398.8225*	398.8304*	398.8426*	398.8652*
PQ23(12)	11.5		398.6655*	398.6556	398.6481*	398.6426*	398.6426*	398.6481	398.6655*
R4(12)	10.5	426.3447*	426.3808*	426.4240	426.4699	426.5209	426.5761	426.6354	426.6989*
P4(12)	10.5	401.6059	401.6428	401.6840	401.7298	401.7809	401.8358	401.8955	401.9594
N=13 R1(13)	14.5	17425.1974	17425.1535	17425.1058	17425.0539	17424.9983	17424.9392	17424.8757*	17424.8090
P1(13)	14.5	398.6036	398.5600	398.5124	398.4607	398.4051	398.3457	398.2823	398.2145
R2(13)	13.5			423.1612*	423.1525	423.1373*	423.1169*	423.0875	423.0077
RQ32(13)	13.5				423.3980	423.3915*	423.3793	423.3559*	
P2(13)	13.5	396.5417	396.5375*	396.5316*	396.5205	396.5061	396.4879*	396.4576*	396.3771*
PO32(13)	13.5			396.7235*	396.7235*	396.7178*	396.7039	396.6798	
R3(13)	12.5						423.1717*	423.1849	423.2075
RS23(13)	12.5		422.9492*				422.9187	422.9236	422.9390
P3(13)	12.5	396.4995*		396.4922*	396.4922*	396.4941*	396.4995	396.5108	396.5313*
PQ23(13)	12.5		396.3220	396.3088*	396.2992*	396.2915*	396.2890*	396.2937*	396.3088*
R4(13)	11.5	426.0492	426.0900	426.1317	426.1794	426.2302	426.2851	426.3447*	426.4079*
P4(13)	11.5	399.3410	399.3792	399.4217	399.4687	399.5199	399.5750	399.6345	399.6982
N=14 R1(14)	15.5	17424.6399	17424.5947	17424.5470	17424.4950	17424.4397	17424.3809	17424.3177	17424.2517
P1(14)	15.5	396.0721	396.0277	395.9798	395.9282	395.8717	395.8127	395.7498	395.6832
R2(14)	14.5	422.6502*	422.6502*	422.6473	422.6401	422.6294	422.6130	422.4420	422.4831
RQ32(14)	14.5	422.8875	422.9006*	422.9055*	422.9081	422.9055*	422.8961	422.7309	
P2(14)	14.5	394.0504*	394.0504*	394.0465	394.0394	394.0282	394.0112	393.8404*	393.8815
PO32(14)	14.5	394.2455	394.2557	394.2613*	394.2637*	394.2613*	394.2509	394.0857	
R3(14)	13.5	422.7179	422.7089	422.7034	422.6999*	422.6999*	422.7034	422.7130	422.8765
RS23(14)	13.5		422.4708	422.4544	422.4420*	422.4323	422.4293*	422.4301	422.5875
P3(14)	13.5	394.0738	394.0651	394.0590*	394.0558*	394.0558*	394.0590*	394.0683	394.2311
PQ23(14)	13.5		393.8695	393.8527	393.8404*	393.8308*	393.8268*	393.8279*	393.9859
R4(14)	12.5	425.6465	425.6861	425.7305	425.7780	425.8300	425.8849	425.9436	426.0052
P4(14)	12.5	396.9664	397.0059	397.0496	397.0964	397.1482	397.2029	397.2622	397.3252

TABLE I (CONTINUED)

BRANCH	J"	F"=J"-7/2	F=J-5/2	F=J-3/2	F=J-1/2	F=J+1/2	F=J+3/2	F=J+5/2	F=J+7/2
N=15 R1(15)	16.5	17423.9774	17423.9314*	17423.8819*	17423.8318*	17423.7782*	17423.7178	17423.6552	17423.5900
P1(15)	16.5	393.4373	393.3923	393.3440	393.2926	393.2367	393.1780	393.1154	393.0491
R2(15)	15.5	422.0307*	422.0346*	422.0346*	422.0307*	421.8254*	421.8254*	421.8317*	421.8553
RQ32(15)	15.5	422.2928	422.3051*	422.3145*	422.3201*	422.1221*	422.1304*	422.1409*	
P2(15)	15.5	391.4571*	391.4613*	391.4613*	391.4571*	391.2517*	391.2517*	391.2584*	391.2819
PO32(15)	15.5	391.6741	391.6886	391.6979*	391.7042*	391.5082*	391.5120*	391.5248*	
R3(15)	14.5	422.1572	422.1409*	422.1304*	422.1241	422.1221*	422.3201*	422.3145*	422.3008
RS23(15)	14.5		421.8808	421.8601	421.8441	421.8317*	422.0231	422.0108	421.9899
P3(15)	14.5	391.5414	391.5251*	391.5144	391.5079	391.5062*	391.7042*	391.6979*	391.6835
PQ23(15)	14.5		391.3080	391.2872	391.2710	391.2584*	391.4496	391.4363	391.4140*
R4(15)	13.5	425.1339	425.1745	425.2190	425.2670	425.3194	425.3746	425.4333	425.4955
P4(15)	13.5	394.4824	394.5229	394.5672	394.6150	394.6662	394.7214	394.7802	394.8423
N=16 R1(16)	17.5	17423.2103	17423.1650*	17423.1161*	17423.0636	17423.0077*	17422.9492	17422.8875*	17422.8222
P1(16)	17.5	390.6994	390.6537	390.6051	390.5520	390.4967	390.4379	390.3760	390.3105
R2(16)	16.5	421.3102	421.3187*	421.3225	421.1213	421.1124	421.1089	421.1114	421.1239
RQ32(16)	16.5	421.5926*	421.6101	421.6234*	421.6234*	421.4321*	421.4312*	421.4334	421.4422
P2(16)	16.5	388.7643	388.7737*	388.7771*	388.5781	388.5674	388.5634	388.5668*	388.5786*
PO32(16)	16.5	389.0035	389.0228	389.0359*	388.8451*	388.8451*	388.8451*	388.8506*	
R3(16)	15.5	421.4901	421.4625	421.4472	421.4375*	421.6324*	421.6339*	421.6324*	421.6234*
RS23(16)	15.5		421.1816	421.1567	421.1366	421.3225	421.3168	421.3071	421.2929
P3(16)	15.5	388.9030	388.8755	388.8601	388.8506*	389.0451*	389.0451*	389.0451*	389.0361*
PQ23(16)	15.5		388.6365	388.6111	388.5913	388.7771*	388.7720*	388.7630*	388.7478*
R4(16)	14.5	424.5127	424.5545*	424.5994	424.6482	424.7000	424.7548	424.8131	424.8757*
P4(16)	14.5	391.8910	391.9326	391.9779	392.0258	392.0776	392.1327	392.1914	392.2528
N=17 R1(17)	18.5	17422.3389	17422.2928*	17422.2434	17422.1916*	17422.1360*	17422.0772	17422.0158	17421.9509
P1(17)	18.5	387.8556	387.8094	387.7610	387.7082	387.6532	387.5944	387.5330	387.4677
R2(17)	17.5	420.4920	420.3419	420.3203	420.3035	420.2914	420.2844	420.2835	420.2900
RQ32(17)	17.5	420.7930	420.6537	420.6415	420.6333	420.6302*	420.6302*	420.6347*	
P2(17)	17.5	385.9744	385.8251	385.8034	385.7864	385.7730*	385.7672*	385.7672*	385.7730*
PO32(17)	17.5	386.2348	386.0954	386.0833*	386.0756*	386.0717*	386.0717*	386.0756*	
R3(17)	16.5	420.7171	420.6730	420.8177*	420.8332	420.8452*	420.8495*	420.8495*	420.8452*
RS23(17)	16.5		420.3712	420.5050	420.5112*	420.5128*	420.5112*		
P3(17)	16.5	386.1586	386.1145	386.2584	386.2742	386.2860*	386.2910*	386.2910*	386.2860*
PQ23(17)	16.5		385.8547	385.9877*	385.9944*	385.9944*	385.9944*		
R4(17)	15.5	423.7831*	423.8253	423.8725*	423.9205*	423.9714	424.0278	424.0869*	424.1471
P4(17)	15.5	389.1906	389.2326	389.2788	389.3274	389.3794	389.4343	389.4926	389.5539

TABLE I (CONTINUED)

BRANCH	J"	F"=J"-7/2	F=J-5/2	F=J-3/2	F=J-1/2	F=J+1/2	F=J+3/2	F=J+5/2	F=J+7/2
N=18 R1(18)	19.5	17421.3628	17421.3158	17421.2668	17421.2143	17421.1590	17421.1009	17421.0382*	17420.9757
P1(18)	19.5	384.9112	384.8647	384.8157	384.7630	384.7081	384.6495	384.5880*	384.5235
R2(18)	18.5	419.4485	419.4176	419.3941	419.3761	419.3623	419.3525*	419.3508*	419.3508*
RQ32(18)	18.5	419.7711	419.7501	419.7362	419.7263*	419.7209	419.7196		
P2(18)	18.5	382.9627	382.9313	382.9081	382.8900	382.8760	382.8664*	382.8664*	382.8664*
PO32(18)	18.5	383.2442	383.2230	383.2089	383.1998	383.1937*	383.1937*	383.1937*	
R3(18)	17.5	419.8368	419.8957*	419.9219	419.9397	419.9524	419.9611*	419.9611*	419.9611*
RS23(18)	17.5		419.5738	419.5899	419.5987*	419.6014*	419.6014*	419.5987*	419.5899*
P3(18)	17.5	383.3101	383.3695	383.3952	383.4133	383.4246	383.4346*	383.4346*	383.4346*
PQ23(18)	17.5		383.0879	383.1041	383.1123*	383.1159*	383.1159*	383.1123*	383.1041*
R4(18)	16.5	422.9454	422.9889	423.0350	423.0844	423.1373	423.1920	423.2502*	423.3116*
P4(18)	16.5	386.3846	386.4274	386.4739	386.5231	386.5750	386.6299	386.6885	386.7494
N=19 R1(19)	20.5	17420.2835*	17420.2359	17420.1861	17420.1336	17420.0784	17420.0204	17419.9611*	17419.8957*
P1(19)	20.5	381.8741	381.8273	381.7781	381.7247	381.6702	381.6121	381.5509	381.4869
R2(19)	19.5	418.4159	418.3845	418.3603	418.3412	418.3250	418.3151	418.3083*	418.3083*
RQ32(19)	19.5	418.7595	418.7363	418.7211					
P2(19)	19.5	379.9597	379.9278	379.9038	379.8846	379.8697	379.8588	379.8520*	379.8520*
PO32(19)	19.5	380.2616	380.2397	380.2255	380.2147	380.2086	380.2041*	380.2041*	
R3(19)	18.5	418.8511	418.8991	418.9255	418.9442	418.9579	418.9674	418.9732*	418.9732*
RS23(19)	18.5		418.5566	418.5725	418.5823	418.5879			
P3(19)	18.5	380.3537	380.4022	380.4287	380.4469	380.4613	380.4705	380.4759*	380.4759*
PQ23(19)	18.5		380.1004	380.1166	380.1260*	380.1312*	380.1312*	380.1312*	
R4(19)	17.5	421.9999	422.0439	422.0907	422.1409*	422.1924*	422.2477	422.3051*	422.3663
P4(19)	17.5	383.4733*	383.5173*	383.5637*	383.6133*	383.6656*	383.7203*	383.7785*	383.8390*
N=20 R1(20)	21.5	17419.0980	17419.0506	17419.0007	17418.9477	17418.8930	17418.8350	17418.7745	17418.7114*
P1(20)	21.5	378.7066*	378.6594*	378.6094*	378.5567*	378.5020*	378.4442*	378.3833*	378.3195*
R2(20)	20.5	417.2740*	417.2433	417.2190	417.1993	417.1832	417.1710	417.1627	417.1597
P2(20)	20.5	376.8502	376.8187	376.7945	376.7747	376.7585	376.7467	376.7382	376.7349
PO32(20)	20.5	377.1723	377.1508	377.1355	377.1246	377.1175*	377.1175*	377.1175*	
R3(20)	19.5	417.7591*	417.8001	417.8265	417.8458	417.8603	417.8708	417.8776	417.8804
RS23(20)	19.5			417.4531	417.4626				
P3(20)	19.5	377.2922	377.3337	377.3598	377.3792	377.3940	377.4047	377.4119	377.4139
PQ23(20)	19.5		377.0124	377.0286	377.0384	377.0453*	377.0453*	377.0453*	377.0453*
R4(20)	18.5	420.9476	420.9920	421.0382*	421.0891	421.1412	421.1962	421.2538	421.3140
P4(20)	18.5	380.4530	380.4975	380.5446	380.5942	380.6465	380.7018	380.7596	380.8199

TABLE I (CONTINUED)

	BRANCH	J"	F"=J"-7/2	F=J-5/2	F=J-3/2	F=J-1/2	F=J+1/2	F=J+3/2	F=J+5/2	F=J+7/2
N=21	R1(21)	22.5	17417.8084	17417.7604	17417.7108	17417.6585	17417.6027	17417.5452	17417.4840	17417.4214
	P1(21)	22.5	375.4483	375.4005	375.3508	375.2980	375.2429	375.1850	375.1239	375.0609
	R2(21)	21.5	416.0261*	415.9954	415.9707	415.9508	415.9332	415.9209*	415.9117	415.9060
	P2(21)	21.5	373.6304	373.6007	373.5765	373.5561	373.5393	373.5261	373.5170*	373.5117*
	PO32(21)	21.5	373.9745*	373.9547*	373.9386*					
	R3(21)	20.5	416.5598	416.5967	416.6221	416.6414	416.6572	416.6687	416.6766	416.6808
	P3(21)	20.5	374.1254	374.1620	374.1864	374.2066	374.2217	374.2333	374.2407	374.2449
	PQ23(21)	20.5			373.8357	373.8445*				
	R4(21)	19.5	419.7864	419.8315	419.8790	419.9288	419.9816	420.0367	420.0941	420.1538
	P4(21)	19.5	377.3269	377.3716	377.4188	377.4689	377.5216	377.5767	377.6343	377.6939
N=22	R1(22)	23.5	17416.4131	17416.3655*	17416.3149	17416.2622	17416.2071	17416.1493	17416.0890	17416.0261*
	P1(22)	23.5	372.0866	372.0390	371.9888	371.9363	371.8810	371.8231	371.7627	371.7001
	R2(22)	22.5	414.6701	414.6407	414.6167	414.5950	414.5787	414.5652	414.5551*	414.5478
	P2(22)	22.5	370.3084	370.2783	370.2540	370.2336	370.2164	370.2029	370.1921	370.1852
	R3(22)	21.5	415.2546*	415.2884	415.3130	415.3323	415.3480	415.3601	415.3690	415.3747
	P3(22)	21.5	370.8570	370.8907	370.9158	370.9349	370.9512	370.9633	370.9721	370.9768
	R4(22)	20.5	418.5155	418.5611	418.6093	418.6592	418.7114*	418.7669	418.8240	418.8834
	P4(22)	20.5	374.0930	374.1376	374.1864*	374.2356	374.2883	374.3432	374.4008	374.4601
N=23	R1(23)	24.5	17414.9127	17414.8649	17414.8148	17414.7617	17414.7067	17414.6490	17414.5889	17414.5261
	P1(23)	24.5	368.6174	368.5700	368.5193	368.4668	368.4112	368.3536	368.2936	368.2307
	R2(23)	23.5	413.2101*	413.1815	413.1576*	413.1364*	413.1193	413.1047	413.0941	413.0858
	P2(23)	23.5	366.8756	366.8473	366.8227	366.8021	366.7850	366.7702	366.7594	366.7513
	R3(23)	22.5	413.8440	413.8744	413.8990	413.9178*	413.9343	413.9471	413.9570	413.9632
	P3(23)	22.5	367.4704	367.5018	367.5261	367.5453	367.5610	367.5736	367.5847	367.5900
	R4(23)	21.5	417.1301	417.1758	417.2239	417.2740*	417.3271	417.3822	417.4392	417.4986
	P4(23)	21.5	370.7522	370.8021	370.8500	370.9004	370.9528	371.0078	371.0652	371.1248
N=24	R1(24)	25.5	17413.3091	17413.2612	17413.2101*	17413.1576*	17413.1029	17413.0448	17412.9848	17412.9225
	P1(24)	25.5	365.0467	364.9974	364.9473	364.8941	364.8390	364.7817	364.7214	364.6597
	R2(24)	24.5	411.6444	411.6158	411.5923	411.5718*	411.5529*	411.5395	411.5272	411.5181
	P2(24)	24.5	363.3486	363.3211	363.2967	363.2763	363.2590	363.2439	363.2316	363.2233
	R3(24)	23.5	412.3285	412.3578	412.3811	412.4005	412.4165	412.4300	412.4401	412.4486
	P3(24)	23.5	363.9938	364.0237	364.0484	364.0667	364.0829	364.0952	364.1064	364.1131
	R4(24)	22.5	415.6102	415.6568	415.7052	415.7557	415.8084	415.8633	415.9209*	415.9793
	P4(24)	22.5	367.2973	367.3437	367.3915	367.4423	367.4948	367.5498	367.6070	367.6665

TABLE I (CONTINUED)

	BRANCH	J"	F"=J"-7/2	F=J-5/2	F=J-3/2	F=J-1/2	F=J+1/2	F=J+3/2	F=J+5/2	F=J+7/2
N=25	R1(25)	26.5	17411.6003	17411.5496*	17411.5013	17411.4475*	17411.3930	17411.3342*	17411.2744	17411.2135*
	P1(25)	26.5	361.3685	361.3203	361.2696	361.2169	361.1617	361.1043	361.0444	360.9832
	R2(25)	25.5	409.9726	409.9457	409.9216	409.9010	409.8834	409.8681	409.8563*	409.8462
	P2(25)	25.5	359.7140	359.6871	359.6631	359.6412	359.6241	359.6089	359.5962	359.5868
	R3(25)	24.5	410.7053	410.7350	410.7582	410.7770	410.7933	410.8069	410.8168	410.8255
	P3(25)	24.5	360.4086	360.4364	360.4601	360.4788	360.4946	360.5083	360.5187	360.5260
	R4(25)	23.5	413.7716	413.8183	413.8664	413.9178*	413.9675	414.0231	414.0790	414.1377
	P4(25)	23.5	363.7398	363.7864	363.8355	363.8855	363.9385	363.9938	364.0504	364.1097
N=26	R1(26)	27.5	17409.7867	17409.7376	17409.6870	17409.6334*	17409.5793	17409.5219	17409.4623	17409.3989*
	P1(26)	27.5	357.5880	357.5393	357.4889	357.4363	357.3808	357.3247	357.2632	357.2025
	R2(26)	26.5	408.1940	408.1678	408.1439	408.1222	408.1048	408.0894	408.0758	408.0658
	P2(26)	26.5	355.9693	355.9432	355.9192	355.8979	355.8802	355.8654	355.8519	355.8414
	R3(26)	25.5	408.9786	409.0060	409.0278	409.0470*	409.0633	409.0773	409.0887	409.0975
	P3(26)	25.5	356.7132	356.7397	356.7622	356.7818	356.7974	356.8120	356.8232	356.8310
	R4(26)	24.5	412.5748	412.6189	412.6679	412.7181	412.7710	412.8256	412.8823	412.9407
	P4(26)	24.5	360.0464	360.0932	360.1422	360.1916	360.2455	360.3009	360.3567	360.4159
N=27	R1(27)	28.5	17407.8654	17407.8178	17407.7659	17407.7129	17407.6570*	17407.6010	17407.5417	17407.4796
	P1(27)	28.5	353.7048	353.6554	353.6044	353.5510	353.4960	353.4387	353.3795	353.3181
	R2(27)	27.5	406.3112	406.2847	406.2614	406.2405	406.2221	406.2068	406.1934	406.1826
	P2(27)	27.5	352.1217	352.0955	352.0720	352.0521	352.0333	352.0184	352.0041	351.9934
	R3(27)	26.5	407.1429*	407.1683	407.1904	407.2097	407.2261	407.2399	407.2529	407.2611
	P3(27)	26.5	352.9143	352.9409	352.9635	352.9824	352.9985	353.0122	353.0246	353.0325
	R4(27)	25.5	410.7125	410.7613	410.8086	410.8598	410.9125	410.9671	411.0236	411.0822*
	P4(27)	25.5	356.0296)	356.0755)	356.1244)	356.1751)	356.2278)	356.2819)	356.3368)	356.3975)
			357.0774)	357.1235)	357.1718)	357.2203)	357.2722)	357.3251)*	357.3808)*	357.4365)*
N=28	R1(28)	29.5	17405.8412	17405.7925	17405.7418	17405.6887	17405.6336	17405.5763	17405.5180	17405.4560
	P1(28)	29.5	349.7179	349.6673	349.6184	349.5651	349.5105	349.4534	349.3943	349.3326
	R2(28)	28.5	404.3237	404.2968	404.2743	404.2538	404.2345	404.2193	404.2050	404.1940
	P2(28)	28.5	348.1768	348.1511	348.1279	348.1069	348.0893	348.0727	348.0584	348.0478
	R3(28)	27.5	405.2016	405.2276	405.2497	405.2680	405.2848	405.2991	405.3113	405.3216*
	P3(28)	27.5	349.0140	349.0402	349.0619	349.0813	349.0974	349.1117	349.1235	349.1332
	R4(28)	26.5	408.7915	408.8388*	408.8880	408.9392	408.9922	409.0470*	409.1033	409.1619
	P4(28)	26.5	352.6560	352.7039	352.7523	352.8039	352.8564	352.9114	352.9668	353.0246

TABLE I (CONTINUED)

	BRANCH	J"	F"=J"-7/2	F=J-5/2	F=J-3/2	F=J-1/2	F=J+1/2	F=J+3/2	F=J+5/2	F=J+7/2
N=29	R1(29)	30.5	17403.7129	17403.6637	17403.6126	17403.5595	17403.5050	17403.4471	17403.3888*	17403.3270
	P1(29)	30.5	345.6249	345.5754	345.5240	345.4717	345.4164	345.3592	345.3002	345.2397
	R2(29)	29.5	402.2290	402.2034	402.1802	402.1599	402.1420	402.1259	402.1115	402.1001
	P2(29)	29.5	344.1137	344.0888	344.0653	344.0443	344.0265	344.0088	343.9958	343.9847
	R3(29)	28.5	403.1559*	403.1806	403.2021	403.2208	403.2379	403.2526*	403.2652*	403.2745
	P3(29)	28.5	345.0052*	345.0289*	345.0510*	345.0705*	345.0869*	345.1011*	345.1125	345.1233
	R4(29)	27.5	406.7729	406.8206	406.8698	406.9213	406.9743	407.0301	407.0850	407.1429*
	P4(29)	27.5	348.6240	348.6707	348.7200	348.7715	348.8234	348.8790	348.9348	348.9929
N=30	R1(30)	31.5	17401.4781	17401.4296	17401.3777	17401.3240	17401.2694	17401.2133*	17401.1535	17401.0926
	P1(30)	31.5	341.4290	341.3784	341.3275	341.2746	341.2198*	341.1630	341.1043	341.0430*
	R2(30)	30.5	400.0305	400.0048	399.9825	399.9614	399.9432	399.9268	399.9129	399.9011
	P2(30)	30.5	339.9561	339.9308	339.9074	339.8869	339.8687	339.8522	339.8382	339.8263
	R3(30)	29.5	401.0027	401.0274*	401.0481*	401.0630*	401.0825*	401.0976	401.1108	401.1213
	P3(30)	29.5	340.8908	340.9153	340.9360	340.9555	340.9717	340.9856	340.9991	341.0087
	R4(30)	28.5	404.6556	404.7029	404.7523	404.8040	404.8570	404.9113	404.9683	405.0259
	P4(30)	28.5	344.5278	344.5751	344.6252	344.6753	344.7291	344.7839	344.8401	344.8988
N=31	R1(31)	32.5	17399.1419	17399.0922	17399.0407	17398.9876	17398.9329*	17398.8760	17398.8180*	17398.7564
	P1(31)	32.5	337.1277	337.0787	337.0272	336.9743	336.9197	336.8630	336.8029	336.7424
	R2(31)	31.5	397.7282	397.7029	397.6802	397.6598	397.6416	397.6249	397.6106	397.5985
	P2(31)	31.5	335.6900	335.6655	335.6424	335.6214	335.6034	335.5869	335.5719	335.5595
	R3(31)	30.5	398.7457	398.7714*	398.7905	398.8101*	398.8253*	398.8401*	398.8533	398.8652*
	P3(31)	30.5	336.6717	336.6967	336.7176	336.7347	336.7519	336.7668	336.7796	336.7899
	R4(31)	29.5	402.4313	402.4791	402.5290	402.5801	402.6340	402.6876	402.7440	402.8017
	P4(31)	29.5	340.3376	340.3844	340.4346	340.4861	340.5395	340.5945	340.6499	340.7087
N=32	R1(32)	33.5	17396.7000*	17396.6500	17396.5992	17396.5453*	17396.4879*	17396.4334	17396.3765*	17396.3140*
	R2(32)	32.5	395.3172	395.2915	395.2689	395.2488	395.2300	395.2136	395.1984	395.1856
	R3(32)	31.5	396.3814*	396.4037	396.4246	396.4442	396.4611*	396.4763*	396.4879*	396.4995
	R4(32)	30.5	400.1058	400.1537	400.2033	400.2546	400.3080	400.3630	400.4192	400.4771
	P4(32)	30.5	336.0468	336.0944	336.1466	336.1955	336.2494	336.3046	336.3605	336.4186
N=33	R1(33)	34.5	17394.1558	17394.1064	17394.0570	17394.0020	17393.9468	17393.8899	17393.8278	17393.7712
	P1(33)	34.5	328.2193	328.1706	328.1188	328.0660	328.0101	327.9533	327.8947	327.8338
	R2(33)	33.5	392.8034	392.7786	392.7560	392.7352	392.7169	392.6994	392.6848	392.6720
	P2(33)	33.5	326.8487	326.8245	326.8019	326.7813	326.7628	326.7462	326.7311	326.7193
	R3(33)	32.5	393.9114	393.9343	393.9553	393.9740	393.9907	394.0056	394.0190	394.0303*
	P3(33)	32.5	327.9225	327.9461	327.9665	327.9857	328.0012	328.0167	328.0298,	328.0414
	R4(33)	31.5	397.6763	397.7242	397.7739	397.8249	397.8779	397.9326	397.9885	398.0466

TABLE I (CONTINUED)

	BRANCH	J"	F"=J"-7/2	F=J-5/2	F=J-3/2	F=J-1/2	F=J+1/2	F=J+3/2	F=J+5/2	F=J+7/2
N=34	R1(34)	35.5	17391.5145*	17391.4678*	17391.4167*	17391.3651	17391.3107	17391.2544	17391.1970	17391.1373
	P1(34)	35.5	323.6086	323.5598	323.5072	323.4522*	323.3998	323.3428	323.2840	323.2235
	R2(34)	34.5	390.1826	390.1584	390.1358	390.1145*	390.0962	390.0795	390.0641	390.0511
	P2(34)	34.5	322.2716	322.2475	322.2252	322.2044	322.1866	322.1694	322.1547	322.1412
	R3(34)	33.5	391.3347	391.3574	391.3781	391.3967	391.4140	391.4286	391.4419	391.4537
	P3(34)	33.5	323.3887	323.4127	323.4318	323.4522	323.4676	323.4824	323.4961	323.5072
	R4(34)	32.5	395.1372	395.1856	395.2345	395.2862	395.3397	395.3941	395.4503	395.5081
	P4(34)	32.5	327.1620	327.2106	327.2604	327.3119	327.3652	327.4199	327.4760	327.5336
N=35	R1(35)	36.5	17388.6951	17388.6471	17388.5970	17388.5449	17388.4914	17388.4361	17388.3793	17388.3202
	P1(35)	36.5	318.8962	318.8456*	318.7943*	318.7424	318.6866	318.6314	318.5723	318.5120
	R2(35)	35.5	387.4764	387.4518	387.4288	387.4074	387.3870	387.3695	387.3535	387.3388
	P2(35)	35.5	317.5879	317.5639	317.5410	317.5211	317.5016	317.4851	317.4690	317.4571
	R3(35)	34.5	388.6511	388.6738	388.6951	388.7128	388.7297	388.7459	388.7583	388.7643*
	P3(35)	34.5	318.7509	318.7731	318.7943*	318.8121	318.8290	318.8456*	318.8589	318.8694
	R4(35)	33.5	392.4938	392.5423	392.5924	392.6441	392.6973	392.7519	392.8075	392.8655
	P4(35)	33.5	322.5611	322.6098	322.6605	322.7121	322.7645	322.8193	322.8759	322.9325
N=36	R1(36)	37.5	17385.7700)	17385.7339)	17385.6984)	17385.6587)	17385.6131	17385.5654	17385.5116	17385.4568
			385.9101)	385.8716)	385.8360)	385.8034)				
	P1(36)	37.5	314.1003	314.0457	313.9988	313.9479	313.8926	313.8370	313.7801	313.7207
	R2(36)	36.5	384.6143	384.5880	384.5679	384.5476	384.5286	384.5116	384.4966	384.4825
	P2(36)	36.5	312.8120	312.7874	312.7647	312.7453	312.7271	312.7109	312.6943	312.6808
	R3(36)	35.5	385.8616	385.8840	385.9040	385.9226	385.9395	385.9547	385.9687	385.9803
	P3(36)	35.5	314.0165	314.0376	314.0505	314.0778	314.0941	314.1088	314.1225	314.1350
	R4(36)	34.5	389.7428	389.7914	389.8419	389.8933	389.9462	390.0008	390.0572	390.1145
	P4(36)	34.5	317.8555*	317.9042*	317.9539*	318.0065*	318.0594*	318.1140*	318.1709*	318.2275*
N=37	R1(37)	38.5	17382.9005	17382.8523*	17382.7993	17382.7461	17382.6914	17382.6349	17382.5766	17382.5167
	P1(37)	38.5	309.1084	309.0605	309.0095	308.9571	308.9046	308.8491	308.7927	308.7342
	R2(37)	37.5	381.6934	381.6702	381.6476	381.6274	381.6088	381.5917	381.5758	381.5623
	P2(37)	37.5	307.9339*	307.9089	307.8856	307.8646	307.8450	307.8264	307.8100	307.7972
	R3(37)	36.5	382.9668	382.9890	383.0093	383.0279	383.0445	383.0601	383.0740	383.0879
	P3(37)	36.5	309.1624	309.1845	309.2034	309.2228	309.2391	309.2547	309.2690	309.2810
	R4(37)	35.5	386.8887	386.9366	386.9871	387.0387	387.0922	387.1466	387.2024	387.2598
	P4(37)	35.5	313.0558	313.1056	313.1552	313.2070	313.2598	313.3151	313.3697	313.4288*

TABLE I (CONTINUED)

	BRANCH	J"	F"=J"-7/2	F=J-5/2	F=J-3/2	F=J-1/2	F=J+1/2	F=J+3/2	F=J+5/2	F=J+7/2
N=38	R1(38)	39.5	17379.8342	17379.7841	17379.7323	17379.6785	17379.6241	17379.5671	17379.5087	17379.4491
	P1(38)	39.5	304.0095)	303.9787)	303.9481)	303.9030)	303.8586)	303.8098	303.7575	303.7020
			304.1553)	304.1168)	304.0800)	304.0458)	304.0142)			
	R2(38)	38.5	378.6378	378.6140*	378.5923	378.5719	378.5526*	378.5356	378.5207	378.5059*
	P2(38)	38.5	302.9061	302.8835	302.8599	302.8397	302.8216	302.8037	302.7895	302.7741
	R3(38)	37.5	379.9630*	379.9852	380.0054	380.0239	380.0405	380.0561	380.0701	380.0826
	P3(38)	37.5	304.2041	304.2260	304.2461	304.2647	304.2811	304.2967	304.3105	304.3233
	R4(38)	36.5	383.9286	383.9778	384.0281	384.0806	384.1333	384.1880	384.2434	384.3011
	P4(38)	36.5	308.1335	308.1829	308.2344	308.2841	308.3370	308.3920	308.4480	308.5054
N=39	R1(39)	40.5	17376.6630	17376.6130	17376.5610	17376.5077	17376.4533	17376.3962	17376.3384	17376.2783
	P1(39)	40.5	298.9842	298.9340	298.8820	298.8289	298.7735	298.7172	298.6588	298.5996
	R2(39)	39.5	375.4894	375.4660	375.4439	375.4234		375.3880*	375.3725	375.3577*
	P2(39)	39.5	297.8052	297.7808	297.7597	297.7394	297.7206	297.7040	297.6886	297.6739
	R3(39)	38.5	376.8533	376.8749	376.8943	376.9136	376.9302	376.9452	376.9596	376.9724
	P3(39)	38.5	299.1469	299.1683	299.1887	299.2070	299.2241	299.2398	299.2540	299.2660
	R4(39)	37.5	380.8613	380.9104	380.9610	381.0125	381.0656	381.1202	381.1758	381.2334
	P4(39)	37.5	303.1179*	303.1653*	303.2166*	303.2680*	303.3217*	303.3765*	303.4321*	303.4894*
N=40	R1(40)	41.5	17373.3860	17373.3362	17373.2838	17373.2300	17373.1754	17373.1196	17373.0610	17373.0014
	P1(40)	41.5	293.7550	293.7053	293.6565	293.5998	293.5456	293.4895	293.4307	293.3713
	R2(40)	40.5	372.2370	372.2132	372.1918	372.1706	372.1524	372.1348	372.1194	372.1054
	P2(40)	40.5	292.6033	292.5783	292.5572	292.5368	292.5176	292.5000	292.4846	292.4716
	R3(40)	39.5		373.6518	373.6712	373.6902	373.7074	373.7225	373.7367	373.7496
	P3(40)	39.5	293.9824	294.0026	294.0237	294.0412	294.0581	294.0735	294.0877	294.0998
	R4(40)	38.5	377.6885*	377.7369*	377.7869*	377.8395*	377.8932*	377.9483*	378.0039*	
	P4(40)	38.5	297.9912	298.0398	298.0914	298.1428	298.1961	298.2505	298.3058	298.3638
N=41	R1(41)	42.5	17370.0064	17369.9561	17369.9046	17369.8508	17369.7962	17369.7406	17369.6815	17369.6225
	P1(41)	42.5	288.4225	288.3720	288.3207	288.2666	288.2120	288.1553	288.0974	288.0362
	R2(41)	41.5	368.8754	368.8523	368.8294	368.8092	368.7898	368.7737	368.7579	368.7435
	R3(41)	40.5	370.2947	370.3162	370.3367	370.3548	370.3720	370.3880	370.4027	370.4150
	P3(41)	40.5	288.7093	288.7305	288.7504	288.7689	288.7862	288.8017	288.8156	288.8283
	R4(41)	39.5	374.4071	374.4601*	374.5069	374.5585	374.6130	374.6674	374.7226	374.7800
	P4(41)	39.5	292.7646	292.8127	292.8636	292.9153	292.9686	293.0240	293.0794	293.1374

TABLE I (CONTINUED)

	BRANCH	J"	F"=J"-7/2	F=J-5/2	F=J-3/2	F=J-1/2	F=J+1/2	F=J+3/2	F=J+5/2	F=J+7/2
N=42	R2(42)	42.5			17365.3637	17365.3429	17365.3243	17365.3067	17365.2915	17365.2772
	R3(42)	41.5						366.9103	366.9263*	366.9405*
	R4(42)	40.5	17371.0271	17371.0761	371.1248*	371.1781	371.2315	371.2873	371.3423	371.3995
N=43	R2(43)	43.5	17361.8357*	17361.8137*	17361.7913*	17361.7699*	17361.7512*	17361.7341*	17361.7173*	17361.7020*
	R4(43)	41.5	367.5270*		367.6300*	367.6825*	367.7360*			
N=44	R4(44)	42.5	17363.8522*	17363.8988*	17363.9533*	17364.0137*	17364.0829*	17364.1654*	17364.2492*	
N=45	R3(45)	44.5	17356.2819*	17356.2946	17356.3135	17356.3368*	17356.3516	17356.3697	17356.3860	17356.4005*
	R4(45)	43.5	360.2333*	360.2842*	360.3365*	360.3859*	360.4369*	360.4945*	360.5497*	360.6047*
N=46	R3(46)	45.5	17352.3349*	17352.3554*	17352.3746*	17352.3941*	17352.4104*	17352.4266*	17352.4420*	17352.4566*
	R4(46)	44.5	356.3162*	356.3712*	356.4214*	356.4712*	356.5224*	356.5745*	356.6271*	356.6818*
N=47	R3(47)	46.5	17348.3506*	17348.3727*	17348.3906*	17348.4097*	17348.4257*	17348.4426*	17348.4567*	17348.4712*
	R4(47)	45.5	352.5050*	352.5545*	352.6060*	352.6598*	352.7089*	352.7649*	352.8203*	352.8764*
N=48	R4(48)	46.5	17348.4856	17348.5354	17348.5862	17348.6383	17348.6909	17348.7462	17348.8022	17348.8585

TABLE II   ROATIONAL LINES ASSIGNED IN THE $\Omega'=4-\Omega''=4$ BANDS OF FEO

5819 Å BAND (V"=0)   (CONTINUED)

J"	R	Q	P
4	17180.200	17176.120	
5	79.990	75.091	17171.011
6	79.582	73.859	68.962
7	78.982	72.435	66.710
8	78.184	70.808	64.261
9	77.201	68.994	61.618
10	76.035	66.989	58.781
11	74.686	64.798	55.756
12	73.163	62.432	52.545
13	71.472	59.888	49.156
14	69.598	57.161	45.593
15	67.579	54.284	41.848
16	65.402	51.243	37.949
17	63.074	48.045	33.889
18	60.591	44.701	29.670
19	57.979	41.196	25.307
20	55.227	37.565	20.783
21	52.373	33.800	16.135
22	49.350	29.926	11.347
23	46.215	25.881	06.446
24	42.957	21.731	01.397
25	39.560	17.446	17096.228
26	36.161	13.045	90.936
	35.998		
	35.872		
27	32.458		85.511
	32.401		
28	28.647		80.071
			97.912
			79.791
			74.342
29	34.282		74.287
	33.530		
	24.630		
30	27.118		68.503
	26.551		
	20.309		
	20.198		
	18.924		
	18.424		
31	21.284		71.985
	20.604		71.356
	14.160		62.454
	13.915		

J"	R	P
32	17116.479	17062.915
	15.763	62.349
	07.427	56.106
		55.996
		54.719
		55.051
33	12.542	55.051
	11.271	54.373
	10.355	47.928
		47.685
34	09.723	48.223
	06.897	47.503
	06.504	39.161
	04.860	
35	06.067	42.261
	03.175	40.983
	02.461	40.072
	00.992	
36	17098.961	37.411
	98.114	34.588
	96.782	34.194
		32.548
37	94.656	31.747*
	93.698	28.842
	92.564	28.131
		26.653
38	90.083	22.603
	89.206	21.759
	88.219	
39	85.148	16.272
	84.516	15.331
	83.566	14.187
40	82.393	09.690
	81.173	08.809
	79.536	07.824
41	77.289	02.737*
	76.289	02.105
	74.416	01.158
42	72.432	16997.965
	71.677	96.744
	68.655	95.111

TABLE II (CONTINUED)

	5583 Å BAND (V"=0)			6230 Å BAND (V"=2)		
J"	R	Q	P	R	Q	P
4	17906.063	17901.406			16168.326	
5	06.544	00.943		16173.531*	67.954*	
6	06.977	00.437		74.032	67.484	16161.879
7	07.278	17899.798	17893.272	74.463*	66.991*	60.470
8	07.543*	99.138	91.639	74.795*	66.410	58.922
9	07.676*	98.310	89.897	75.079*	65.748	57.348
10	07.676*	97.408	88.137*	75.288*	64.010	55.686
11	07.676*	96.446*	86.188	75.460*		53.922*
12	07.543*		84.203	75.460*		52.151
13	07.358		82.143	75.460*		50.265
14	07.089		79.992	75.460*		48.310
15	06.728		77.748	75.288*		46.309
16	06.285		75.441	75.079*		44.234
17	05.740		73.055*	74.795*		42.082
18	05.150		70.545	74.463*		39.872
19	04.706		68.075	74.316 P		37.582
20	03.827		65.336	73.729		35.242
21	02.958		62.864	73.192		33.079 P
22	02.059		59.946	72.608		30.484
23	01.071		57.055	71.970		27.948
24	00.009		54.098	71.264		25.360
25	17898.834		51.074	70.464		22.717
26	97.913		47.991	69.735		20.009
27	96.446*		44.795*	68.874		17.201
28	–		41.624	67.954*		14.473
29	–		38.325	66.991*		11.610
30	92.225		34.957	65.971		08.691
31	90.699		31.527	64.897		05.732
32	89.094		28.022	63.773		02.701
33	87.395		24.469	62.576		16099.647
34	85.661		20.838	61.343		96.521
35	83.746		17.114	59.962		93.329
36	81.787		13.353	58.538 P		90.100
37	79.664		09.405	56.969		86.725
38	77.623		05.424	55.497		83.292 P
39	75.441*		–	53.922*		79.764*
40	73.197*		17797.218	52.286		76.307
41			93.009*	50.582		72.708
42			88.670*	48.789		69.098
43				47.052		65.406
44				44.077		61.639

TABLE III   ROTATIONAL LINES ASSIGNED IN 2491 Å BAND OF 15NO2

N	K=0		K=1		K=2		
	QR11+QR22	QP11+QP22	QR11+QR22	QP11+QP22	QR11+QR22	QQ11	QQ22
2	40142.352			(a)		40125.275*	40125.804*
3			40139.202*	(40133.798*)		124.992*	125.392*
4	143.300*	40136.441*	139.857*	132.880*		124.682*	124.992*
5			(139.857*)	131.621*		124.429*	124.682*
6	144.025*	134.013*	140.649	130.479*		123.951	
7			140.280*	(129.055*)		123.526	
8	144.360*	131.431	141.131*	(127.869*)	40129.819*		
9			140.280*	126.164*	130.029*		
10	144.360*	128.403	141.456*	124.992*	129.819*		
11			140.037*	122.864*	129.942*		
12	144.025	124.992*	141.366*	121.884*	129.363*		
13			139.394*	119.294	129.639		
14	143.232*	121.293	141.131*	118.336	(128.673*)		
15			138.422*	115.327	129.146*		
16	142.035	117.081*	140.450*	114.569	127.641*		
17			137.079	111.012*	128.430*		
18	140.450*	112.630*	139.394*	110.401*	126.164*		
19			135.336	106.251*	127.463*		
20	138.422*	107.733*	138.079	106.096*	124.566*		
21			133.153*	101.324*	126.164*		
22	135.978	120.428*	136.346*	101.324*	122.376		
23			130.737	095.915*	124.682*		
24	133.135*	096.610*	134.161*	096.128*	199.914		
25			127.869*	090.145	122.864*		
26	129.774*	090.466*	131.696*	090.743*	117.081*		
27			124.566*	083.891*	120.999*		
28	126.164*	083.891	128.754*	084.878*	113.901*		
29			120.999*	077.372*	118.600		
30	121.976	076.861	125.275*	(076.861*)	110.401*		
31			117.081*	070.521*	115.931		
32	117.471	069.474*	121.378	071.702*	106.410*		
33			112.630*	063.217*	112.894*		
34	122.630*	061.624*	117.081*	064.458*	102.025		
35			107.733*	055.460*	109.357*		
36	107.513*		112.211*	056.733*	097.279*		
37			102.608*	(047.583*)	105.614*		
38	101.851		106.915*	048.529*	092.179*		
39			097.083*	039.021	101.324*		
40	095.915*		100.992*	039.857*	086.597*		
41			091.035*	030.114*	074.219*		
42	089.466*		094.723	030.673*			
43			084.878*	020.993*			
44			088.045				

(a) 40135.000 (F2) ; 40134.790 (F1)

TABLE III (CONTINUED)

	K=2		K=3					
N	QP11	QP22	QR11	QR22	QQ11	QQ22	QP11	QP22
3					40106.600*	40107.513*		
4					106.410*			
5	40120.619	40120.999*			106.096*	106.600*	40102.159*	40102.781*
6	119.294*	119.621*			105.614*	106.096*	100.992*	101.660*
7	118.117	118.336*				105.614*	099.745*	100.319*
8		116.777*					098.400	098.762
9		115.327*					097.083*	097.279*
10		113.901*		40111.937*			095.433*	095.915*
11		112.211*	(40111.547*)	111.868*			093.879	094.173
12		110.585*					092.179*	092.454
13		108.733*	111.216*	111.547*			090.466*	090.743*
14		107.208*	111.012*	111.216*			088.680	088.881
15		104.988*	110.585*	110.800*			086.697*	086.884*
16		103.495	110.243*	110.410*			084.878	084.878*
17		(100.992*)	109.600*	109.771			082.858*	082.858*
18		099.601*	109.176*	109.357*			080.777*	080.777*
19		096.465*	108.381*	108.540*				(078.653*)
20		095.433*	107.733*	107.978*				076.326*
21		091.714	(106.727*)	106.915*				(073.646*)
22		090.996*	106.251*	106.410*				071.620*
23		086.597*	104.988*	105.026				068.933*
24		086.422*		104.585				066.709*
25		081.188*		102.781*				063.635*
26		081.489*		102.428*				061.509*
27		075.340		(100.319*)				058.165
28		076.326*		(100.319*)				056.084
29		069.145*		097.578*				052.262*
30		070.986*		(097.727*)				050.478*
31		062.636		094.471				046.064*
32		065.063*		095.123*				044.589*
33		055.675*		090.996*				039.597*
34		059.070		092.316*				038.627*
35		(048.520*)		087.162*				032.810*
36		052.556*		(089.431*)				032.496*
37		040.745*		083.091*				025.654
38		045.794*		086.141*				026.080
39		032.600*		(078.653*)				
40		038.309*		082.652*				019.504
41		024.180		073.646				010.282
42		030.553*		079.011*				(012.480)
43		015.342*		068.396*				002.060*
44		022.553*		075.005*				005.490*

TABLE III (CONTINUED)

		K=4						K=5	
N	QR11	QR22	QQ11	QQ22	QP11	QP22		QR11	QR22
4			40080.777*	40082.103*					
5			080.641*	081.489*					
6			080.224*		40074.216	40075.017*			
7			079.639*	(080.443*)	072.900	073.665*			
8				079.639*	071.645*	072.100*			
9				078.998	069.984	070.514*		(40053.769*)	40054.347*
10	40086.141*	40086.697*			068.392	068.933*		053.577*	(054.347*)
11	(086.141*)	086.597*			066.709*	067.209		053.488*	054.105*
12	085.911*	086.422*			065.071*	065.411		053.204*	053.879*
13	085.791	(086.141*)			(063.236*)	(063.643*)		052.929*	053.483*
14	085.439*	085.791*			061.280*	061.607*		052.572*	(053.100*)
15	(085.110*)	085.439*			059.284	059.626		052.044*	052.573*
16	084.668*	(085.110*)			057.201	057.568		051.539	052.044*
17	084.049*	084.426			055.111	055.427*		050.910*	051.450*
18	083.522	083.891*			052.912*	053.146*		050.275*	050.625*
19	082.858*	083.091*			050.621*	050.903		049.508*	049.907
20	082.103	082.378			048.239*	048.545*		(048.552*)	049.037*
21	081.188*	081.489*			045.785*	046.087		047.733*	048.169*
22	080.443*	080.641*			043.341*	043.556		046.765*	047.120
23	079.415	079.639			040.760*	040.945		045.775*	(046.064*)
24	(078.352*)	(078.651*)			038.090	038.308*		044.600*	044.843*
25	077.372*	077.421*			035.398	035.562		043.357	043.558*
26	(076.326*)	076.326*			032.618*	032.711*		042.052	042.355
27	074.848*	075.005*			029.756*	029.913		040.767*	040.947*
28	073.646*	073.930*			026.778*	026.964*		039.277*	(039.575*)
29	072.096*	072.096*			023.816*	023.994*		037.741	(038.091*)
30	(070.868*)	070.867*			020.656*	020.816*		036.151	036.353
31	069.041*	069.145*			017.619*	017.168		034.470	034.747
32	067.732	067.989*			014.234*	(014.402*)		032.718*	032.923*
33	065.675	065.798*			(011.093*)	011.288*		030.947*	037.162*
34	(064.458*)	064.458*			007.572*	007.716*		029.004	029.304*
35	(062.013*)	062.215			004.466	004.588		027.114*	027.278*
36	060.696	060.886			39997.485*	39997.637*		023.047*	
37		058.165*			993.206	993.360*		020.827*	020.941*
38					(990.450*)			018.490*	018.764*
39		053.908*			985.641			016.101	016.301
40		052.916*			982.935*			013.921*	
41		(049.503*)			977.739			011.250*	
42		048.714*			975.337				
43		(044.611*)			969.587*				
44		(044.404*)			967.676*				
45		039.310*							

TABLE III (CONTINUED)

	K=5				K=6			
N	QQ11	QQ22	QP11	QP22	QR11	QR22	QQ11	QQ22
5		40049.498*					40008.137*	40010.061*
6	40047.583*	048.927*	40042.962	40044.394*			007.802*	009.252*
7	047.119*	048.242*	041.861*	042.962			007.280*	008.594*
8	046.589*	047.583*	040.469*	041.436			006.614*	007.718*
9	046.064*	046.760*	038.993*	039.849*			005.344*	006.977*
10		(046.064*)	037.541	038.310	40014.237*	40015.344*	005.045*	006.041*
11		045.134*	035.927	036.625	014.237*	015.344*		055.045*
12			034.256	034.946	014.237*	015.042		
13			032.533*	033.132	013.910*	014.722		
14			030.670*	031.242	013.594*	014.370*		
15			028.761	029.303	013.214*	013.911		
16			026.780*	027.278	012.709*	(013.594*)		
17			024.712	025.200	012.188*	012.850		
18			022.550*	023.037	011.492*	012.187*		
19			020.365	020.818*	010.841*	011.492*		
20			018.009	018.479*	010.062*	010.704*		
21			015.653	016.089	009.252*	009.806		
22			013.212*	013.594*	008.411*	008.841		
23			010.704*	011.095	007.300*	007.719*		
24			008.143*	008.411*	006.227*	006.619		
25			005.475*	005.79)	005.049	005.477*		
26			002.664	002.946*	003.799	004.135		
27			39999.907*	000.148	002.503*	002.917*		
28			997.035	39999.258	000.992*	001.465		
29			994.013*	(994.337*)	39999.628*	39999.908*		
30			990.972*	991.249*	998.078*	998.377		
31			987.816	988.106*	996.526*	996.789		
32			984.542*	984.892	994.687	995.015		
33			981.330	981.573*	992.942*	993.208*		
34			977.963	978.224	990.990*	(991.249*)		
35			974.529	974.782	(989.052*)	989.419*		
36			971.107*	971.245*	987.083	987.414*		
37			(967.486*)	967.665*	985.097	985.339*		
38			963.885*	964.024*	982.941*	983.147*		
39			960.073*		980.616	980.949*		
40			(956.280*)	956.585	978.224*	978.558*		
41			952.389*	952.675*	975.899*	976.232*		
42			948.504*	948.798*	973.493	973.790*		
43			944.538*		970.887*	(971.222*)		
44			936.308*	(940.763*)	968.272*	968.618*		
45			932.294*		965.596*	(965.956*)		

TABLE III (CONTINUED)

	K=6				K=7			
N	QP11	QP22	QR11	QR22	QQ11	QQ22	QP11	QP22
7	(40002.057)	40004.055*			39961.699			
8	000.994*	002.508			961.152*			
9	39999.630*	000.996*	39968.287*	39969.911*		39962.228*	(39962.665*)	39955.374*
10	998.080*	39999.353	(968.176*)	969.773*	959.831	961.354	952.1311*	953.764*
11	996.528*	997.644	968.176*	969.590*		960.420*	950.523*	951.987*
12	994.866*	995.915	968.008*	969.306*	958.105*	959.473*	948.813*	950.253
13	993.210*	994.018*	967.860*	969.116*	957.152*		947.110	948.491*
14	991.251*	992.190	967.630*	968.619*	956.009*	957.158	945.261*	946.481*
15	989.421	990.260	967.137*	968.176*	954.808*	956.009*	943.398	944.528*
16	987.416*	988.110	966.668	967.669*	953.677*		941.407	942.442
17	985.341*	986.070	966.153	967.137*	952.400*	953.321*	939.312	940.285
18	983.148*	983.863	965.592*	966.410*	951.042*	(951.706*)	937.146	938.129*
19	980.951*	981.577*	964.804*	965.592*	949.503	950.268*	934.936*	935.782
20	978.560	979.257	964.023*	964.804*	947.950*	948.809*	932.570	933.414
21	976.237	976.836	963.123*	963.886*			930.209	931.026
22	973.791	974.361	962.226	926.948*			927.751*	928.478
23	971.231*	971.789	961.147	961.844			925.180	925.862
24	968.618*	969.117*	960.079	960.728*			922.523	923.211
25	965.953*	966.411*	958.903*	959.467*			919.814	920.434
26	963.122*	(963.646*)	957.567	958.141			916.980*	917.606*
27	960.409*	960.729	956.279	956.776			914.164*	914.743*
28	957.390	957.818	954.809*	955.368			911.174*	911.671*
29	954.375	954.810*	953.307	953.769			908.102*	908.643*
30	951.296	951.703	951.702*	952.207			904.998*	905.635*
31	948.148*	948.500*	950.044	950.527*			901.799	(902.386)
32	944.876*	945.266*	(948.352*)	948.817*			898.509	898.990*
33	941.507*	941.913	946.485*	946.982*			895.190	895.614*
34	938.177*	938.497*	944.532*	944.974*			891.724*	892.235*
35	934.773*	934.942*	942.581	943.012			888.171*	888.780*
36	931.153	931.487	940.554	940.938			884.580	885.150*
37	927.606*	(927.822*)	938.358*	938.807			881.021*	881.392
38	923.912	924.181	936.230*	936.534			877.121	877.690*
39	920.095	920.440*	933.810	934.250			(873.340*)	873.763
40	916.240*	916.519*	931.491*	931.861			869.536*	869.950*
41	912.355*	912.525*	928.996	929.450			(865.460)	865.918
42	908.370*	908.640*	926.540	926.910			861.481*	861.888*
43	904.285*		923.917*	924.191*			(857.293*)	857.752*
44	900.053*		921.199	921.634				
45			918.461*	918.847*				
46			915.587*	916.007*				
47	887.213							
48				910.029				

TABLE III (CONTINUED)

| N | K=8 | | | | | | K=9 | |
	QR11	QR22	QQ11	QQ22	QP11	QP22	QR11	QR22
8			39908.637*	39911.177*				
9			908.116*	910.327*				
10	(39915.775*)	39917.809*	907.382*	909.426	39899.633*	39901.792*		
11	915.777*	917.613*	906.574	908.371*	(898.143*)	900.051*		
12	(915.680*)	917.285	905.638*	907.382*	896.395	898.152	39856.807	(39858.468*)
13	(915.530*)	916.991*	904.703*	906.238*	894.720	896.402*	856.506*	858.468*
14	915.110	916.520*	903.581*	(904.973*)	892.907	894.380	856.130*	857.755*
15	914.746*	916.012	902.394*	903.783	890.979	892.239*	855.524*	857.165*
16	914.166*	915.480*	901.203*	902.394*	888.945	890.234	854.999*	856.506*
17	913.710	(914.750*)			886.872	888.181*	854.391	(855.699*)
18	913.073	914.170*			(884.714)	885.881	853.607	854.999*
19	912.347	913.391			882.472	883.570	852.927*	854.075
20	911.564*	912.527			880.120	881.162*	851.936*	853.036*
21	910.583*	(911.677*)			877.690	878.725	850.898*	852.014*
22	909.656	910.587			875.208	876.170	849.730*	850.898*
23	908.645*	909.428*			872.626	873.540	848.727*	849.730*
24	907.376*	908.369*			869.948	870.841	847.360*	848.437*
25	906.241*	907.042			(867.218)	868.052	846.086*	847.050*
26	904.980*	905.641*			864.370	865.214	844.596	845.625*
27	903.586*	904.283			861.473	862.236	843.126*	844.155*
28	902.100*	902.815			858.502*	859.246	841.601	842.446*
29	900.535*	901.212*			855.516*	856.133	839.897*	840.768*
30	898.991*	899.650*			852.231*	852.968	838.179*	838.938*
31	897.240	897.898			849.156*	849.620*	(836.216*)	837.153
32	895.433*	896.074			(845.626*)	846.394	834.425*	835.297*
33	893.576	894.185*			(824.431*)	(843.899*)	(832.573*)	833.203
34	891.748*	892.243*			838.929*	839.499*	830.372*	831.129
35	889.597	890.238*			825.298*	835.931*	828.263*	828.968
36	887.451	888.185*			831.692	832.346*	826.058*	826.786
37	885.294	885.884*			827.981	828.563	823.797*	824.339*
38	882.870*	883.573*			824.226*	824.785	(821.207*)	821.907
39	880.656*	881.166*			820.274*	820.782	818.759*	819.503*
40	878.279	878.728*			816.338*	816.838*	816.347*	816.836*
41	875.749	876.181*			812.287*	812.916*	(813.624*)	
42	(873.081)	(873.549*)						
43					804.034	804.524		

TABLE III (CONTINUED)

K=9

N	QQ11	QQ22	QP11	QP22
9	39849.434	39852.236*		
10	848.727	851.251	39841.011*	39843.711*
11	(848.049*)	850.256	839.487*	841.841
12	847.050*	849.162*	837.908*	940.030*
13	846.086	848.049*	836.071*	838.179*
14	844.956*	846.863	834.335*	836.216*
15	843.828*	845.625*	832.330*	834.122*
16		844.155	830.358*	832.017
17	841.281*		827.263	829.849
18	839.897*	841.281*	826.039	827.549
19			823.794	825.184
20	836.745		821.450	822.772
21	835.098*		818.999	820.284
22			(816.357*)	817.685
23			813.834	815.027
24			811.166	812.274
25			808.417	809.470
26			805.573	806.605
27			802.628	803.615
28			799.674	800.585
29			796.518	797.428
30			793.366	794.188
31			(789.925)	790.988
32			786.722	787.526
33			783.367*	784.139
34			779.807*	780.503
35			776.219	776.966
36				

SRO	SR1
F1+F2	F1+F2

ASYMMETRY
INDUCED

SRO F1+F2	SR1 F1+F2
40158.837*	40167.552*
158.357	166.174
157.768	164.740
157.045	162.971*
156.279*	161.020
155.211	158.837*
154.156	156.279*
152.727	153.706
151.229	150.834
149.580	147.680*
147.685*	
145.550	

TABLE IV   ASSIGNED ROTATIONAL LINES OF THE   A $^4\Pi$ - X $^4\Sigma^-$ (0,0) BAND OF VO

N	P1	Q1	R1	P2	Q2	R2	P3	Q3
8		9463.781*						
9		9464.329						
10		9464.857						
11								
12		9465.522*						
13			9475.676*					
14	9445.053		9476.479*					9499.634*
15	9443.808		9477.192*	9459.359				9498.535)
								98.348)
16	9442.432*	9465.573*	9477.857*	9457.662	9479.218			9497.349)
								97.147)
17	9441.077	9465.484*	9478.474*	9455.897	9478.572*			9496.124
18	9439.591	9464.989*	9478.989*	9454.010	9477.857*			9494.847
19	9438.053	9464.642	9479.453*	9452.210*	9477.042			9493.540
20	9436.339*	9464.051	9479.817*	9450.217*	9476.164			9492.169
21	9434.673	9463.383*	9480.116*	9448.210*	9475.195			9490.751
22	9432.846*	9462.702*	9480.343*	9446.150*	9474.189			9489.272*
23	9430.936*	9461.873*	9480.501	9444.080	9473.095			9487.782*
24	9428.994*	9460.968*	9480.626*	9441.903	9471.922	9493.023	9462.440	9486.195*
25	9426.963	9460.014*	9480.626*	9439.537*	9470.674	9492.829	9459.841	9484.581
26	9424.883*	9459.029*	9480.572*	9437.343	9469.360	9492.616	9457.208	9482.915
27	9422.725*	9457.860*	9480.343*	9434.997*	9467.977	9492.253	9454.513	9481.180
28	9420.476*	9456.680*	9480.116*	9432.560	9466.521	9491.868*	9451.765	9479.411
29	9418.133	9455.394*	9479.817*	9430.044	9464.989	9491.414	9448.978*	9477.573
30	9415.714	9454.010	9479.453*	9427.502	9463.383*	9490.920*	9446.052*	9475.676
31	9413.245	9452.588	9478.989*	9424.883*	9461.723	9490.334*	9443.213	9473.750
32	9410.705*	9451.041	9478.474*	9422.199	9460.014*	9489.693	9440.251	9471.748*
33	9408.076	9449.435	9477.857*	9419.535*	9458.218	9488.950*	9437.235	9469.707
34	9405.384	9447.786	9477.192*	9416.649	9456.360	9488.220	9434.157	9467.606
35	9402.600*	9446.052*	9476.479*	9413.773	9454.426	9487.380*	9431.023	9465.448*
36	9399.787	9444.214	9475.676*	9410.834	9452.434*	9486.472*	9427.851	9463.238*
37	9396.867	9442.319	9474.779	9407.808	9450.382	9485.578	9424.644*	9460.968*
38	9393.899	9440.361	9473.838	9404.777	9448.237	9484.483*	9421.311	9458.634
39	9390.879*	9438.324	9472.819	9401.649	9446.052*	9483.415*	9417.932	9456.247
40	9387.752	9436.218	9471.748	9398.462	9443.808	9482.232	9414.516*	9453.812
41	9384.577	9434.042	9470.590	9395.189	9441.491	9481.006	9411.067*	9451.317*
42	9381.333	9431.796	9469.360*	9391.881	9439.113	9479.723	9407.538	9448.764
43	9378.035*	9429.482	9468.058	9388.488	9436.667	9478.358	9403.951*	9446.150*
44	9374.641	9427.096	9466.708	9385.048	9434.157	9476.932*	9400.301	9443.492
45	9371.193	9424.644	9465.275	9381.535*	9431.588	9475.503	9396.600	9440.773
46	9367.675	9422.120	9463.781	9377.964*	9428.948	9473.898*	9392.844	9437.992
47	9364.110	9419.535	9462.220	9374.325	9426.253	9472.292*	9389.018	9435.145
48	9360.455*	9416.869*	9460.587*	9370.603	9423.490*	9470.590*	9385.143	9432.255
49	9356.743	9414.154	9458.895	9366.856	9420.660	9468.870*	9381.213	9429.303
50	9352.965	9411.366	9457.132	9363.009	9417.755	9467.046	9377.203	9426.295

TABLE IV (CONTINUED)

N	P1	Q1	R1	P2	Q2	R2	P3	Q3
51	9349.124	9408.512	9455.313	9359.144	9414.818	9465.175	9373.172	9423.236
52	9345.218	9405.596	9453.403	9355.179	9411.812	9463.238*	9369.059	9420.106
53	9341.248	9402.600*	9451.458	9351.164	9408.719	9461.240	9364.889	9416.869*
54	9337.209	9399.548	9449.435*	9347.089	9405.596*	9459.180	9360.665	9413.659
55	9333.103	9396.427	9447.330*	9342.949	9402.396	9457.047	9356.385	9410.379
56	9328.940	9393.239	9445.170	9338.733*	9399.145	9454.856	9352.043	9407.024
57	9324.708	9389.992	9442.940	9334.482	9395.812	9452.588*	9347.637	9403.604
58	9320.412	9386.677	9440.648	9330.137*	9392.429	9450.273*	9343.180	9400.126
59	9316.061*	9383.295	9438.324*	9325.763*	9388.982	9447.863*	9338.663	9396.600*
60	9311.634	9379.847*	9435.887*	9321.306	9385.467*	9445.437	9334.087*	9393.001
61	9307.134	9376.340	9433.386	9316.793	9381.901	9442.940*	9329.456	9389.348
62	9302.600	9372.771	9430.837		9378.277	9440.361*	9324.756	9385.643
63	9297.979*	9369.130	9428.212		9374.573	9437.712	9320.012*	9381.901*
64	9293.298	9365.424	9425.497		9370.820	9434.997*	9315.194*	9378.035
65	9288.569	9361.658	9422.785		9366.984	9432.233*	9310.325*	9374.158
66	9283.764	9357.811*	9419.979		9363.124	9429.386	9305.433*	9370.209
67	9278.906	9353.937			9359.184	9426.454*	9300.415*	9366.201
68	9273.976	9349.976			9355.179	9423.490*	9295.368	9362.139
69	9268.980	9345.925			9351.123		9290.247	9358.013
70	9263.925	9341.849			9346.994			9353.827
71	9258.810	9337.715			9342.808			9349.565
72		9333.503			9338.563			9345.277
73		9329.220*			9334.248			9340.922
74		9324.885			9329.879			9336.500
75		9320.490			9325.454			9332.017
76		9316.024			9320.963			
77		9311.484			9316.410			
78		9306.899			9311.793			
79		9302.240						
80		9297.529						
81		9292.724						
82		9287.905						
83		9282.998						
84		9278.036						
85		9273.010						
86		9267.920						
87		9262.779						
88		9257.507						

TABLE IV (CONTINUED)

N	R3	P4	Q4	R4
51	9478.859	9386.394	9438.425	9491.584
52	9476.779	9382.035	9435.104	9489.272*
53	9474.642	9377.667*	9431.705	9486.908
54	9472.422	9373.172	9428.260	9484.483*
55	9470.167	9368.694	9424.770	9482.031
56	9467.836	9364.110*	9421.213	9479.453*
57	9465.448*	9359.534	9417.620	9476.932*
58	9463.006	9354.888	9413.962	9474.295*
59	9460.511	9350.189	9410.254	9471.619
60	9457.860*	9345.365*	9406.486	9468.870*
61	9455.913*	9340.672*	9402.664	9466.090
62	9452.588*	9335.757	9398.791	9463.238*
63	9449.857	9330.827	9394.869	9460.345*
64	9447.071*	9325.819	9390.879*	9457.417*
65	9444.214*	9320.823	9386.844	9454.361*
66	9441.311*	9315.761	9382.762	9451.291*
67			9378.609	9448.164*
68			9374.407	9444.980*
69			9370.143	9441.740*
70			9365.828	9438.442*
71			9361.447	9435.088*
72			9357.012	9431.676*
73			9352.527	9428.207*
74			9347.977	
75			9343.379	9421.117*
76			9338.733*	9417.452
77			9334.000	9413.773*
78			9329.228*	
79			9324.393	9406.190
80			9319.494	9402.337*
81			9314.542	9398.380
82			9309.530	9394.382
83			9304.461	9390.303
84			9299.336	9386.202
85			9294.143	9382.035*
86			9288.901	9377.794
87			9283.597	
88			9278.224	
89			9272.797	
90			9267.312	
91			9261.786	

N	PQ13	SR32
4	9448.699	
5	9448.303	
6	9447.863*	
7	9447.330*	
8	9446.731	
9		
10	9445.276	
11	9444.427	
12	9443.497*	
13		
14		9531.011
15		9531.956
16		9532.856
17		9533.688
18		9534.481
19		9535.213
20		9535.880*
21		9536.525
22		9537.105
23		9537.649*
24		9538.104

TABLE IV (CONTINUED)

N	R3	P4	Q4	R4	QP43	RQ43	SR43
4							9552.881
5							9553.306
6						9546.923*	9553.904
7						9546.320*	9554.335
8						9545.672*	9554.829*
9						9545.003*	9555.197*
10						9544.291*	9555.563*
11					9532.315	9543.567	9555.897
12					9530.485*	9542.805	9556.205
13					9528.632	9542.020	9556.476
14					9526.736	9541.188*	9556.712*
15					9525.020)	9540.533)	9556.930)
					24.806)*	40.311)*	57.183)
16	9515.097					9539.649	9557.314
17	9514.934				9521.083	9538.740	9557.465
18	9514.842				9519.094	9537.793	9557.583*
19	9514.596				9517.073*	9536.841	9557.705*
20	9514.365					9535.880	9557.795*
21	9514.067				9512.963*	9534.857	9557.823*
22	9513.716				9510.867	9533.818	9557.823*
23	9513.335				9508.741	9532.750	9557.823*
24	9512.830				9506.581	9531.644	9557.795*
25	9512.313				9504.387	9530.485*	9557.705*
26	9511.738				9502.169*	9529.314	9557.583*
27	9511.148*				9499.901	9528.121	9557.428
28	9510.446				9497.616*	9526.880	9557.231
29	9509.703					9525.597	9556.997
30	9508.911	9467.217*				9524.274	9556.712*
31	9508.062	9463.781*				9522.908	9556.404
32	9507.159	9460.348*				9521.514	9556.057
33	9506.199	9456.809*				9520.077	
34	9505.178	9453.282*				9518.593	
35	9504.100	9449.685		9521.901*		9517.073*	
36	9502.964	9446.052		9520.250*		9515.501*	
37	9501.772	9442.436*	9480.116*	9518.718*		9513.899*	
38	9500.521	9438.691	9477.400*	9517.073*		9512.223*	
39	9499.205	9434.928*	9474.642	9515.406*		9510.534*	
40	9497.835	9431.146	9471.922	9513.716*			
41	9496.408	9427.349	9469.112	9511.923*			
42	9494.918	9423.490*	9466.306	9510.126*			
43	9493.376	9419.535*	9463.383*	9508.293*			
44	9491.777	9415.536	9460.445*	9506.331			
45	9490.103	9411.499	9457.464*	9504.387*			
46	9488.378	9407.446	9454.426*	9502.375*			
47	9486.591	9403.330	9451.317*	9500.323			
48	9484.752	9399.199	9448.172	9498.213			
49	9482.838	9395.007	9444.985	9496.028*			
50	9480.877	9390.728	9441.746	9493.844*			

TABLE IV   (CONTINUED)   (0,1) BAND OF VO A-X SYSTEM

N	P1	Q1	R1	P2	Q2	Q3	R3	RQ43	SR43
7		8461.506						8544.072*	8553.232
8		8462.320						8543.503*	8553.720*
9		8462.959						8542.869	8554.122
10		8463.595					8513.337*	8542.216	8554.542
11		8463.987					8513.525	8541.537	8554.940*
12		8464.292*					8513.756	8540.840	8555.340
13		8464.613*					8513.980*	8540.112	8555.639
14		8464.803*					8514.053*	8539.560)*	8555.959)
15		8464.919*						39.365)	56.162)
16		8464.919*	8477.084					8538.798	8556.449*
17		8464.855	8477.814*				8514.250*	8537.999	8556.724
18		8464.613	8478.389*					8537.192	8556.993
19		8464.292*	8479.046*				8514.053*	8536.370	8557.238
20		8463.840	8479.541*		8475.833*		8513.980*	8535.543	8557.439*
21	8434.525*	8463.421*	8479.963*		8475.026	8490.470*	8513.865	8534.672	8557.641
22	8432.863*	8462.815*	8480.331*		8474.157	8489.268*	8513.712	8533.786	8557.804*
23	8431.115	8462.084*	8480.658*		8473.223*	8487.849*	8513.413	8532.876	8557.954*
24	8429.321*	8461.374*	8480.859*		8472.214	8486.513*	8513.122	8531.937	8558.079*
25	8427.481*	8460.532*	8481.059*		8471.153	8485.040	8512.779	8530.988	8558.191*
26	8425.521	8459.660*	8481.167*		8470.004	8483.568	8512.406	8529.946	8558.245*
27	8423.567	8458.726*	8481.167*		8468.819	8482.041	8511.969	8528.969	8558.245*
28	8421.507	8457.703*	8481.167*	8433.667*	8467.559	8480.446	8511.447*	8527.933	8558.245*
29	8419.354*	8456.629	8481.059*	8431.333*	8466.220	8478.824	8510.936*	8526.799	8558.245*
30	8417.136	8455.449	8480.859*	8429.051	8464.855	8477.152	8510.384	8525.732	8558.191*
31	8414.913*	8454.250	8480.658*	8426.561*	8463.421*	8475.437		8524.611*	8558.079*
32	8412.544	8452.951*	8480.331*	8424.102	8461.918*	8473.668	8509.075	8523.419	8557.945*
33		8451.563	8479.936*	8421.635	8460.353	8471.847*	8508.329	8522.211*	8557.724
34	8407.787	8450.131	8479.541*	8419.000	8458.726*	8470.004*	8507.557	8520.976*	
35	8405.228*	8448.638	8479.046*	8416.433	8457.053	8468.075	8506.725		
36	8402.670*	8447.049	8478.540	8413.759*	8455.312	8466.112	8505.850		
37	8399.992	8445.450	8477.896	8410.979	8453.513	8464.098	8504.909		
38	8397.276*	8443.744	8477.229	8408.184	8451.675	8462.034	8503.915*		
39	8394.513	8441.988		8405.313	8449.673	8459.929	8502.894		
40	8391.710	8440.163	8475.677	8402.448*	8447.776	8457.779	8501.811		
41	8388.844*	8438.273	8474.812	8399.438	8445.734*	8455.565	8500.665		
42	8385.855	8436.320	8473.879	8396.420	8443.656	8453.326	8499.478		
43	8382.857	8434.312		8393.343	8441.510	8451.014	8498.230		
44	8379.777	8432.241		8390.246*	8439.315	8448.638*	8496.933		
45	8376.656	8430.107		8387.006	8437.062	8446.261	8495.604		
46	8373.467	8427.908		8383.782	8434.750	8443.806*	8494.171		
47	8370.208*	8425.658		8380.458	8432.390	8441.306*	8492.729		
48	8366.915	8423.336		8377.098	8429.956	8438.748	8491.237		
49	8363.533	8420.961		8373.671	8427.481	8436.145	8489.672		
50		8418.516			8424.948	8433.486	8488.069		

TABLE IV (CONTINUED)

N	Q1	Q2	Q3
51	8416.033	8422.356	8430.781
52	8413.479	8419.694	8428.033*
53	8410.854	8417.016	8425.215
54	8408.184	8414.253	8422.356
55	8405.466	8411.454	8419.444
56	8402.670*	8408.579	
57	8399.819	8405.669	
58	8396.900	8402.670*	
59	8393.945	8399.654	
60	8390.943	8396.560	
61	8387.855	8393.442	
62	8384.722*	8390.246*	
63	8381.622	8387.006	
64	8378.287	8383.782	
65	8374.797	8380.458	
66	8371.622	8377.098*	